# PERFORMANCE EVALUATION OF ENCASED STONE COLUMN SUPPORTED EMBANKMENTS WITH GEOSYNTHETIC MATERIALS AS BASAL REINFORCEMENT

Thesis

Submitted in partial fulfilment of the requirements for the degree of

**DOCTOR OF PHILOSOPHY**

by

**VIBHOOSHA. M. P**
**(CV16F19)**



**DEPARTMENT OF CIVIL ENGINEERING**

**NATIONAL INSTITUTE OF TECHNOLOGY KARNATAKA**

**SURATHKAL, MANGALURU – 575 025**

**DECEMBER, 2021**

# PERFORMANCE EVALUATION OF ENCASED STONE COLUMN SUPPORTED EMBANKMENTS WITH GEOSYNTHETIC MATERIALS AS BASAL REINFORCEMENT

Thesis

Submitted in partial fulfilment of the requirements for the degree of
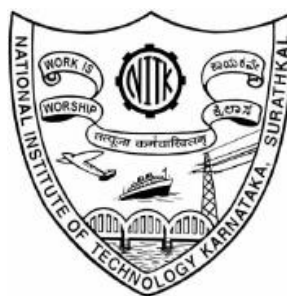
**DOCTOR OF PHILOSOPHY**

by

**VIBHOOSHA. M. P**
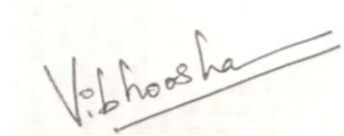**(CV16F19)**

Under the Guidance of
**Dr. Sitaram Nayak**
**Dr. Anjana Bhasi**



**DEPARTMENT OF CIVIL ENGINEERING**

**NATIONAL INSTITUTE OF TECHNOLOGY KARNATAKA**

**SURATHKAL, MANGALURU – 575 025**

**DECEMBER, 2021**

# DECLARATION

I hereby *declare* that the Research Thesis entitled **"Performance Evaluation of Encased Stone Column Supported Embankments with Geosynthetic Materials as Basal Reinforcement"** which is being submitted to the **National Institute of Technology Karnataka, Surathkal** in partial fulfilment of the requirements for the award of the Degree of **Doctor of Philosophy** in **Civil Engineering**, is a *bonafide* report of the research work carried out by me. The material contained in this Research Thesis has not been submitted to any University or Institution for the award of any degree.

**Vibhoosha. M. P.**
Register No. 165017CV16F19
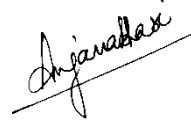Department of Civil Engineering

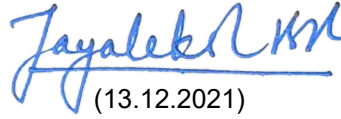Place: NITK Surathkal

Date: 07-12-2021

# CERTIFICATE

This is to certify that the Research Thesis entitled **"Performance Evaluation of Encased Stone Column Supported Embankments with Geosynthetic Materials as Basal Reinforcement"** submitted by **Mrs. Vibhoosha. M. P.** (Register Number: **165017CV16F19**) as the record of the research work carried out by her, is accepted as the Research Thesis submission in partial fulfilment of the requirements for the award of degree of Doctor of Philosophy.


Dr. Sitaram Nayak
(Research Guide)
Professor
Department of Civil Engineering
NITK Surathkal

Dr. Anjana Bhasi
(Research Guide)
Assistant Professor
Department of Civil Engineering
NIT Calicut


(13.12.2021)

Dr. B. R Jayalekshmi
(Chairman-DRPC)
Head of the Department
Department of Civil Engineering
NITK Surathkal
Professor and Head
Department of Civil Engineering
National Institute of Technology Karnataka, Surathkal
Mangalore - 575 025, Karnataka, INDIA

# ACKNOWLEDGEMENT

# ABSTRACT

Lithomargic clay is extensively found along the Konkan belt in peninsular India and serves as a foundation for most structures. The reduction in strength under saturated conditions makes lithomargic clay problematic, causing many engineering problems such as uneven settlements, erosion, slope failures, and foundation problems. The effect of column configuration (i.e., equivalent number of columns with reduced diameter for the same surface area) on the performance of lithomargic clay reinforced with geogrid encased stone columns, and the basal geogrid layer was studied. The investigations were performed both experimentally through small-scale models and finite element analyses. The results were compared with the performance of lithomargic clay reinforced with ordinary and encased stone columns.

A single geogrid encased stone column with a basal geogrid layer improved the load-carrying capacity of lithomargic clay by 180%. In contrast, the percentage increment in a group of three geogrid encased stone columns with a basal geogrid layer having the same surface area was 210%. It was also observed that the geogrid encasement of stone columns reduced the maximum column bulging by 38%. In comparison, geogrid encased stone columns along with basal geogrid layer reduced the bulging by 82% compared to ordinary stone columns.

Geocells are a superior form of reinforcement due to their cost-effectiveness and three-dimensional confining properties. Numerical modeling of geocell is always challenging due to its three-dimensional honeycomb structure. The limitations of the equivalent composite approach (ECA) led to the recent development of full 3D numerical models, which consider geocell-infill material interaction. The present work discusses the time-dependent performance of geocell reinforced encased stone column supported embankment considering the actual 3D nature of geocells using the finite element program ABAQUS. Parametric studies were carried out to study the stress transfer mechanism, vertical deformation of the foundation soil, arching behavior, and stress-strain variation inside the geocell pockets. It is found from the analyses that with the provision of a geocell layer on top of Geosynthetic Encased Stone Columns (GESC), the stress concentration ratio improved by 47% at the end of consolidation compared to

GESC alone. Also, with geocell-sand mattresses, an 80% reduction in foundation surface settlement is observed. Analysis results showed that the arching behavior is not predominant in geocell reinforced columnar structures. The proposed model's numerical results show an overestimation of stress concentration ratio and bearing capacity by ECA.

The geocell-sand mattress reduced the vertical settlement of foundation soil due to the embankment construction by 80%. The vertical settlement reduction was 78% and 79% for single and two-basal geogrids, respectively. The basal geogrids and geocell-sand mattress decreased the bulging of the stone columns, and the maximum bulging was visible at a depth of 3.5 D in both cases, where D is the diameter of stone columns. 69% reduction in the lateral bulging occurred in GESC than the ordinary stone column when a single basal layer was placed. The reduction is 52% and 54% for two basal layers and geocell, respectively. When the geocell-sand mattress was placed, almost 80% of the stone column bulging occurred by the end of the embankment construction. Among the various infill materials analyzed, the aggregates were the best suited considering stress concentration ratio and vertical settlement. The mobilized tensile stress in geocell due to embankment loading was maximum for aggregates and minimum for quarry dust.

Multiple layers of geosynthetic can be replaced by a single layer of geocell, considered to be a superior form of reinforcement because of the three-dimensional confinement offered to the infill material. The proposed system from this research work encased stone columns with geocells as basal reinforcement at the embankment base, serves like a Geosynthetic Reinforced Piled Embankment System (GRPES).

Time-dependent analyses on encased stone columns supported basal geogrid reinforced embankment were carried out using the developed full 3D model. Compared to an unreinforced embankment, 87% reduction in lateral deformation near the toe was observed for GESC+ One basal layer at the end of consolidation, and 90% reduction in the lateral deformation was obtained when two layers of geogrids (stiffness equivalent to that of a single layer) was provided at the base. In multiple basal geogrids, the tensile force at the top layers was less compared to the bottom layers. The variation of stress reduction ratio with embankment height from different analytical methods and 3D numerical model for the encased stone column with single basal geogrid follows the

same trend. Among the different design methods, Guido et al. (1987), Low et al. (1994), and Abusharar et al. (2009) significantly under-predicted the stress reduction ratio. Terzaghi's method (1943) and BS 8006 (2010) exhibited a closer range of Stress Reduction Ratio values than that from full 3D analysis for low height embankments. These methods over-predicted the tensile force in the basal reinforcement. 3D column analysis gave lesser tensile forces compared to full 3D analyses. Guido et al. (1987) method shows good agreement with full 3D results for basal geogrid tension compared to other methods.

# CONTENTS

# LIST OF FIGURES

vii

ix

# LIST OF TABLES

# ABBREVATIONS

| | |
|---|---|
| AR | Arching Ratio |
| ECA | Equivalent Composite Approach |
| FEM | Finite Element Method |
| GESC | Geogrid Encased Stone Column |
| GESC+ BASAL GEOGRID | Encased Stone Columns with a Horizontal Layer of Geogrid on the Top |
| GESC+GEOCELL | Geogrid Encased Stone Column with Geocell as Basal Reinforcement |
| GESC+ One basal layer | Encased Stone Columns with Single Layer of Horizontal Geogrid on the Top |
| GESC+ Two basal layers | Encased Stone Columns with Two Layers of Horizontal Geogrid on the Top |
| GRPES | Geosynthetic Reinforced Piled Embankment Systems |
| IF | Improvement Factor |
| MCC | Modified Cam Clay Model |
| OSC | Ordinary Stone Column |
| SCR | Stress Concentration Ratio |
| SRR | Stress Reduction Ratio |
| UCS | Unconfined Compression Strength |

# SYMBOLS

$\sigma_{rs}$      Radial stress acting on the stone column

$\sigma_{rc}$      Radial stress of the surrounding clay

R      Radius of the stone column

u      Depth to the top of geocell layer below the footing

$h_c$      Height of geocell mattress

b      Maximum geocell width

d      Pocket size of geocell

B      Footing width

$D_f$      Embedment depth of footing

$b_1$      Width of single cell

$\varepsilon_a$      Axial strain of soil at failure

$\varepsilon_c$      Circumferential strain of soil at failure

$D_o$      Initial diameter of geocell pocket (m)

$D_1$      Diameter of the sample at an axial strain of $\varepsilon_{a,}$(m)

$\sigma_1$      Normal stress (kPa)

$\sigma_3$      Cell pressure (kPa)

$\Delta\sigma_3$      Additional confining pressure developed (kPa)

$C_r$      Apparent cohesion (kPa)

$K_r$      Dimensionless modulus parameters of geocell-sand mattress

$K_u$      Dimensionless modulus parameters of unreinforced sand

$E_g$      Young's modulus of geocell-reinforced sand

$P_a$      Atmospheric pressure (kPa)

n      Modulus exponent of unreinforced soil

$p_s$      Bearing capacity of unreinforced foundation soil

$P_{rs}$      Bearing capacity of reinforced foundation soil bed

| | |
|---|---|
| $\Delta P_1$ | The contribution of vertical dispersion effect on bearing capacity |
| $\Delta P_2$ | The contribution of membrane effect on bearing capacity |
| $b_n$ | Width of the uniform load $p_s$ |
| $\theta$ | Dispersion angle of geocell reinforcement |
| T | Tensile strength geosynthetic material |
| $\alpha$ | Horizontal angle of tensile force T |
| [k] | Element stiffness matrix |
| {u} | Nodal displacement vector |
| {f} | Nodal force vector |
| $\pi_{t+\Delta t}$ | nodal pore pressure vector |
| $v_{n_{t+\Delta t}}$ | seepage forces on the boundary. |
| $[\Phi]$ | The matrix governing the dissipation of pore fluid |
| $f_{t+\Delta t}$ | Applied load terms |
| $N_u$ | shape functions for displacements |
| $N_\pi$ | shape functions for pore pressures |
| $\{a^e\}$ | Vector of nodal displacements for a particular element |
| $\{\varepsilon\}$ | Strain vector |
| [L] | Interaction term between the soil, and pore fluid |
| [B] | Matrix for axisymmetric conditions |
| [C] | Constitutive matrix relating the stresses and strains |
| $E$ | Young's modulus (kPa) |
| $v$ | Poisson's ratio |
| $\tau_f$ | Shear stress at failure |

| | |
|---|---|
| $\sigma_f$ | Effective normal stress |
| c | Cohesion |
| $\Phi$ | Internal friction angle of soil |
| $p'$ | Mean effective stress |
| q | Shear stress |
| $p'_c$ | Preconsolidation pressure |
| M | Critical state stress ratio |
| $\lambda$ | Logarithmic hardening constant for plasticity |
| $C_c$ | Compression index |
| $\kappa$ | Logarithmic bulk modulus for elastic material behavior |
| $C_s$ | Swelling index |
| $d\varepsilon_\upsilon^p$ | Plastic volumetric strain increment |
| $d\varepsilon_s^p$ | Plastic shear strain increment |
| $d\varepsilon_s^e$ | Elastic shear strain increment |
| $d\varepsilon_s$ | Total shear strain increment |
| $d\varepsilon_\upsilon$ | Total volumetric strain increment |
| $d\varepsilon_\upsilon^e$ | Elastic volumetric strain increment |
| $d\varepsilon_\upsilon^p$ | Plastic volumetric strain increment |
| S | Center to center spacing of stone columns |
| $R_e$ | Effective radius of unit cell |
| k | Permeability(m/day) |
| $e_0$ | Initial void ratio |
| $a_o$ | Initial yield surface size |

| | |
|---|---|
| φ | Dilation angle |
| D | Diameter of the stone column |
| h | Depth of the stone column |
| $\tau_{crit}$ | Critical shear stress |
| μ | Friction coefficient |
| δ | Interface friction angle |
| Δs | Foundation surface settlement |
| H | Embankment height |
| $\gamma_e$ | Unit weight of embankment fill |
| $q_s$ | Surcharge applied on the surface of the embankment |
| $\sigma_s$ | Stress in the soil |
| $K_p$ | Passive earth pressure coefficient |
| $E_c$ | Elastic modulus of stone column |
| $E_s$ | Elastic modulus of surrounding soil |
| w | Distance along the geocell width |
| P | load carried by the pile |
| $E_f$ | Pile efficacy |
| $K_p$ | Passive earth pressure coefficient |
| $\sigma_h$ | Horizontal stress |
| $K_0$ | Earth pressure coefficient at rest |
| $a$ | Width of pile cap |
| $a_c$ | Arching Coefficient |
| $S_{3D}$ | Stress reduction ratio |

| | |
|---|---|
| $s$ | Center to center spacing of piles |
| $\sigma_p$ | Vertical stress on the column |
| $\sigma_s$ | Vertical stress on the geosynthetic layer |
| $P_0$ | Uniform pressure applied on the geosynthetic layer |
| $P_c$ | Arched vertical stress per unit length at the top of the conduit/pile |
| t | Maximum vertical displacement of the foundation soil midway between the pile caps |
| $J$ | Tensile stiffness of the geosynthetic |
| $h_1$ | Depth of the foundation soil |
| $\sigma_v$ | Average vertical stress per unit length at the top of the conduit/pile |
| $W_{Tn}$ | The distributed load on the reinforcement |

# CHAPTER 1

# INTRODUCTION

## 1.1  GENERAL

The ever-accelerating urbanization and industrialization always demanded the augmentation of construction processes and activities irrespective of the nature of soil present. Those areas where the subsoil conditions are notably poor pose serious challenges before the geotechnical engineers. The evolution of different techniques for improving the properties and behavior of soil arises from these challenges. The selection of methods is based on various parameters like soil type, design requirement of structures, etc.

Ground modification techniques should increase subsoil strength and stress-strain modulus and a reduction in compressibility and susceptibility to liquefaction. The selection of a method depends on soil formation, soil characteristics, availability of backfill material, cost, and experience in the past.

## 1.2  GROUND MODIFICATION TECHNIQUES

The various ground modification techniques include

- Replacement of problematic soils
- Adding various admixtures
- Use of geosynthetic products
- Dynamic compaction or vibration
- Accelerated consolidation
- Columnar systems

### a. Replacement of problematic soils

If the depth of problematic soil is less, around 2 to 3 m, the soil is excavated and replaced by good quality soil suitable for construction.

### b. Adding various admixtures

If the depth of problematic soil is more than 3 m, treating the soil with suitable admixtures is economical. Fly ash, lime, cement, etc., are commonly used chemicals for modification. The admixtures are mixed with the soil, and the engineering properties are altered suitably.

### c. Use of geosynthetic products

Soil reinforcement is popular worldwide because of its simplicity and economic aspects (Vidal 1969; Binquet and Lee 1975). Load-bearing elements with good tensile strength and stiffness are embedded in the soil as reinforcements. Though the soil is weak in tension, substantial tensile stress acting on the soil can be taken up by these reinforcing materials. Straws, reeds, bamboo, etc., were used as soil reinforcements in the beginning.

The effective use of geosynthetic products as reinforcement has been identified since the 1970s. Geosynthetic products are usually manufactured from polymeric materials like HDPE. Different forms of reinforcement, like planar, bars, strips, etc., were effective as soil reinforcements (Jones 1996).

### d. Dynamic compaction or vibration

This method applies to any granular soil. Here, problematic in-situ soil is densified and rearranged to a greater depth by repeated application of high-intensity impacts. It is a rapid process and results in increased shear strength and reduced permeability of the soil.

### e. Accelerated consolidation

To construct any structure in clayey soils, it is essential to accelerate the consolidation process by reducing drainage path length. Methods like preloading, stage construction, vertical sand drains, prefabricated vertical drains, vacuum-assisted consolidation, etc., are used to achieve it, although these are highly expensive and consume time for consolidation.

*f. Columnar systems*

Columnar systems such as concrete piles, timber piles, soil-cement columns, stone columns have been extensively used to support structures on problematic ground conditions. Plain concrete piles with horizontal layers of geosynthetic at the embankment base are very efficient in controlling total and differential settlements. It is a quick construction process as there is no waiting time for consolidation. For flexible and lightly loaded structures, lime columns or stone columns are ideal ground reinforcement. The stone columns are best suited for soft clay soils, peat and cohesive deposits, and silty soils.

Among the different columnar systems, stone columns have been widely used to reinforce soft soils and increase the foundation soil's bearing capacity. Stone columns have been successfully applied for structures like liquid storage tanks, earthen embankments, raft foundations, etc., where a relatively large settlement can be tolerated by the structure. The stone column is preferred among other methods as it gives the advantage of reduced settlement, decreased liquefaction potential of the ground, and also accelerated consolidation settlements due to reduction in the drainage paths. Another significant merit of the stone column technique is the simplicity of its construction method. Stone columns continue to gain popularity today due to the considerable savings in cost and time that they can offer over conventional piling solutions in many circumstances.

## 1.3   STONE COLUMN TECHNIQUE

The stone column (also called granular pile) is nothing but a vertical column element formed below the ground level with compacted and uncemented stone fragments or gravels. The technique has been used since the 1950s for improving both cohesive soils and silty sands (Barksdale and Bachus 1983). These columns considerably improve the vertical load carrying capacity and shear resistance in the soil mass. Stone column construction involves the partial replacement of unsuitable subsurface soils (usually 15 to 35 percent) with a compacted vertical column of stone that usually completely penetrates the weaker strata. The presence of the column creates a composite material of lower overall compressibility and higher shear strength than the native soil.

Confinement is provided by the lateral stress of the surrounding soft soil, which increases the stiffness of the stone column. Upon application of vertical stress at the ground surface, the stone and the soil move downward together, resulting in the concentration of stress within the stone column, primarily due to the column being stiffer than the soil.

Stone column systems in soft, compressible soils are somewhat like pile foundations, except that pile caps, structural connections, and deep penetration into underlying firm strata are not required. Stone columns are more compressible, and when loaded, the stone columns deform by bulging into the subsoil strata and distribute the stresses at the upper portion of the soil profile rather than transferring the stresses into a deeper layer, unlike in the case of pile foundation, thereby causing the soil to support it. If installed in loose sands, Stone columns minimize the likelihood of liquefaction of these deposits due to earthquakes because they tend to dilate while shearing and dissipate the excess pore pressures generated (Mitchell and Huber 1985). The granular column materials with higher permeability accelerate the consolidation settlement and thereby minimize the post-construction settlement. Moreover, in situ stress conditions get improved due to the installation of the stone columns.

Significance of stone columns in India:

- The method of installing stone columns (RAMMING) does not require any skilled labour.
- Stone column installation is economically very feasible-no high cost is required to execute the installation in the field.

### 1.3.1 Load bearing Mechanism of Stone Columns

The load-bearing mechanism of the stone column can be explained by employing lateral bulging of columns into the surrounding soil. The stone column distributes vertical load to the soil by shear stresses at the column-soil interface and the end bearing at the bottom of the column. Due to the vertical loading, the aggregates start bulging, and significant vertical compression occurs in the column. The compression and lateral movement of aggregates together increase the stress in the surrounding soil. Thus, the passive resistance offered by the soil provides confinement for the stone column. The

lateral confinement is more due to the increased overburden pressure at deeper depths, and thus the bulge formation is less. The maximum bulging was visible at a depth of four times the diameter of the stone column (Greenwood 1970; Hughes and Withers 1975).

## 1.4 GEOSYNTHETIC ENCASED STONE COLUMNS (GESC)

All traditional design of the stone column considers the undrained shear strength value $Cu>15kN/m^2$ (Greenwood and Kirsch 1983). Hence, the soil with an undrained shear strength value of less than 15 $kN/m^2$ demands a new technique. The problem can be solved by confining the compacted sand or gravel column in a high-modulus geosynthetic encasement. Van Impe (1985) proposed the concept of encasing the stone column by wrapping it with geotextile. Fig 1.1 shows the schematic diagram of the geosynthetic encased stone column. Among various methods of enhancing the load capacity of the stone columns, encasing the column with geosynthetic would be an ideal form since it also offers other benefits as follows (Alexiew et al. 2005),

- Additional lateral confinement
- Making the stone column act as a semi-rigid element enabling the load transfer to deeper depths.
- Preventing the lateral squeezing of stones into surrounding soft clays, thereby minimizing the loss of stones.
- Enabling a higher degree of compaction compared to the conventional stone columns.
- Promoting the vertical drainage function of the column by acting as a good filter.
- Preserving the frictional properties of the aggregates.
- Increasing the shear resistance of the stone column.

### 1.4.1 Load Bearing Mechanism of Geosynthetic Encased Stone Columns

Stone columns installed in very soft clay were observed with excessive bulging due to the very low lateral confinement pressure offered by the surrounding soil. In such situations, the stone column itself derives additional confinement from the geosynthetic encasement provided. The lateral movement of aggregates causes hoop tension in the

geosynthetic encasement, which along with the passive resistance, offers all-around confinement to the stone column. Lateral confinement increases the stiffness of the stone column and reduces the lateral bulging by redistributing the stresses into deeper depths.

The radial stress acting on the stone column, $\sigma_{rs}$, is induced by the radial stress of the surrounding clay, $\sigma_{rc}$, and the hoop tension, T, in the geosynthetic encasement as shown in Fig 1.1 below,

i.e,

$$\sigma_{rs} = \sigma_{rc} + T/R \tag{1.1}$$

Where R is the radius of the stone column. The second term can be viewed as the additional radial stress due to the geosynthetic encasement.
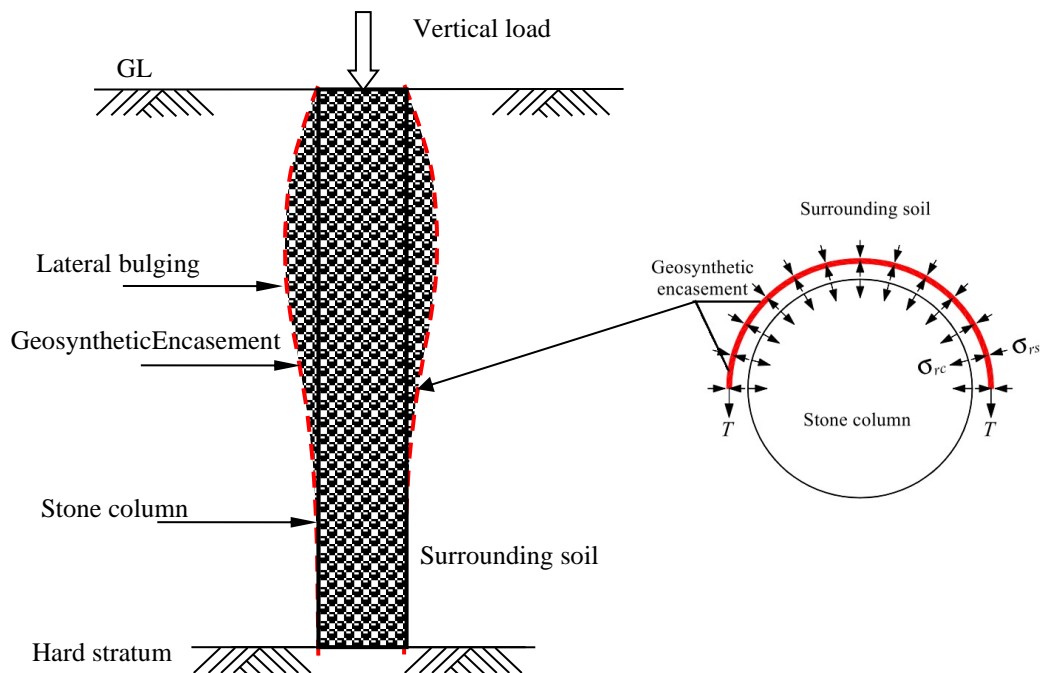


Fig 1.1 Schematic diagram of geosynthetic encased stone column (Based on Zhang and Zhao 2014)

## 1.5 GEOCELLS

Another popular technique in India is three-dimensional geocells as an effective soil reinforcement technique for improving soft subgrade behavior. With regards to the effectiveness, the more attractive are cellular systems owing to their 3-dimensional (3D) structure compared to planar geosynthetic reinforcements (Mhaiskar and Mandal 1996; Tafreshi et al. 2013). Geocell is a honeycomb structured polymeric cellular

6

system connected by joints (Bush et al. 1990). Combining two parts- "geo" means soil or earth, and "cell" means a cellular type of shape for infill material such as soil, the word geocell is formed.

The three-dimensional honeycomb structure of geocell offers more lateral confinement to the infill soil resulting in improved load carrying capacity. This led to the widespread use of geocells for different geotechnical applications like pavements, foundations, embankments, slope protection, erosion control, etc. The geocells enclose weaker materials like soil, stones, etc., and their 3D structure provides all-around confinement. The combination of geocell and the fill material, which acts as a reinforced composite, is characterized by improved stiffness and strength to unreinforced soil. The composite system also ensures better distribution of the vertical load to a wider area by preventing lateral material spread. Fig. 1.2 shows the confinement effect of geocells on soils.

Geocells exist in various dimensions, and facia colours suiting different project needs, materials used are eco-friendly and offer high strength to weight ratio and durability. Studies have shown that geocells offer an enhancement in structure reliability and life, high degree of protection for the impermeable layers, cost-effectiveness compared to other products, serves as a working platform and saves construction time, enhances the soil bearing capacity and facilitates gradual settlements and reduces lateral deformations, functions as embankment base with improved stiffness and rigidity enhancing the stability (Latha 2000; Pokharel et al. 2010; Dash and Bora 2013; Sitharam and Hegde 2013; Tafreshi et al. 2013; Hegde and Sitharam 2015a). The long term performance of the resin which is used to make the geocell and the additives added, should be appropriately tested. Also, quality control must be assured to handle, store, and install geocells in the field (IGS 2018).

## 1.5.1 History of Geocells

For the smooth movement of military vehicles over weak subgrade, studies were carried out by U. S. Army Engineer Waterways Experiment Station on various soil reinforcement methods in the late 1970s (Webster and Watkins 1977; Webster 1979). Webster and Watkins (1977) placed different types of materials such as crushed stone, wire gabions with rock, sand confinement system, pervious polyester fabric, and coated

nylon membrane as base reinforcement over clay subgrade in unpaved roads and compared the rut depth after traffic loading with that oTf the unreinforced base. The studies concluded that the sand base course reinforced by isolated plastic tubes performed better than the conventional base course with crushed stones. Square-shaped grids filled with sand, called "grid cell confinement systems," were developed after this study. Laboratory experiments (Rea and Mitchell 1978; Webster 1979) were conducted to investigate different parameters such as material, size, and shape of the grid, subgrade stiffness, sand-grid layer thickness, properties of sand, compactive effort, loading, etc. that can affect the performance of reinforced soil. Analytical formulas were developed based on the experimental results to predict the capacity of the reinforced base course (Mitchell et al. 1979) by considering different failure modes. Initially, paper and aluminum were used to make grid cells, and later Webster (1979) suggested plastic as grid material due to the many drawbacks of these materials. Polymeric materials, generally known as "geocell," were introduced in the cellular confinement system in the 1980s. Later, materials like HDPE (high-density polyethylene), which has low-temperature flexibility, came into being (Pokharel et al. 2010; Yang et al. 2010).

### 1.5.2 Reinforcement Mechanism of Geocells

The three-dimensional honeycomb structure of geocells confines the soil present in the pockets. The applied load will induce pressure inside each cell of the geocell. Induced pressure causes lateral movement of the confined soil, which will exert pressure on the geocell walls. Thus, deformation of the geocell membrane takes place. Due to the circumferential deformation, the stress in the geocell membrane gets mobilized, and therefore confinement pressure of soil increases (Bathurst and Karpurapu 1993). The three-dimensional confinement restricts the lateral movement of the infill soil that results in a more stable and stiffer composite structure. This triaxial state of confinement results in increased shear strength and resistance to deformation. This imparts the lateral resistance mechanism. The interlocking and frictional resistance between the surrounding soil and geocell wall also leads to higher load carrying capacity.

Many researchers reported that, due to the shear and bending rigidity, the behaviour of geocell soil system is similar to a foundation beam or flexible slab foundation which can carry both bending and membrane stresses (Dash et al. 2001a, 2007; Sitharam et al. 2007; Mehdipour et al. 2013). Dash et al. (2007) observed that the geocell mattress behaves as a flexural member and by increasing the thickness of the mattress deep beam behavior becomes predominant. Zhang et al. (2010) proposed three different mechanisms for geocell reinforced systems, such as lateral restrain (confinement), stress dispersion, and membrane action. This approach approximated the geocell-reinforced-soil as a 'layer with higher flexural rigidity'. They found that the modulus and the height of the geocell contribute to the rigidity of the geocell-reinforced-soil. The interconnected pockets provide all-round confinement to in-filled soil and behaves as a semi-rigid composite slab. It redistributes the applied load to a wider area with lesser intensity to improve the load-bearing capacity of underlying soil (vertical stress dispersion effect/wide slab mechanism). The semi-rigid-slab configuration improves the performance by resisting differential settlement of concerned structure and generates membrane resistance. The deflection of geocell due to the vertical loading, generates additional tensile force transferring more load to the columnar inclusions beneath the geocell (membrane effect). Overall, the mechanism of geocell-reinforcements can be discretized as 'confinement', 'membrane action', and 'stress distribution'. All the above three mechanisms together contribute towards the bearing capacity increment due to the placement of geocell reinforcement.



Fig. 1.2 Confinement of soil using geocell

## 1.6 SCOPE AND OBJECTIVES OF THE RESEARCH WORK

As more and more land becomes subject to urban and industrial development, good construction sites are difficult to find. Different techniques to improve the marginal foundation soil become a necessity. The geotechnical engineers are challenged by the presence of different problematic soils with varied engineering characteristics. In the present work, Lithomargic clay, which is widely available at the Konkan belt of peninsular India, Assam, and West Bengal, is considered for the experimental work. The road and railway embankment construction over lithomargic clay pose many engineering challenges due to reduced strength under saturated conditions. The use of columnar systems like concrete piles, stone columns, and soil-cement columns beneath the embankment can improve the bearing capacity and settlement characteristics of lithomargic clays. Among these techniques, the stone column method is preferred because of its cost-effectiveness, ease of construction, reduced consolidation time and decreased liquefaction potential of the ground.

Stone columns are suited for various soils, ranging from loose sands to soft compressible clays. Applications of stone columns include support to embankments, liquid storage tanks, raft foundations, and other low-rise structures. The stone columns are popular in India because of two main reasons. Firstly, installing stone columns does not require any skilled labour-any layman to do the job. Secondly, installation is fast and economical.

The suitability of the method is decided by the undrained shear strength of the surrounding soil. For very soft clays, stone columns, not being restrained by the surrounding soil, cause excessive bulging of the columns, and the soft clay particles are squeezed into the voids of the aggregates (Murugesan and Rajagopal 2009). Excessive bulging of stone columns led to the encasement of columns. Encasement of the stone column imparts additional confinement to the columns and increases the column's increased stiffness. Encasement prevents the loss of stones into the surrounding soft clay and preserves the drainage and frictional properties of the stone aggregates. To avoid damage to the geosynthetic encasement, only moderate compaction of the stone columns is carried out during installation. This, coupled with the geosynthetic strain during loading, can cause relatively large settlements. There is also the possibility of

10

shear deformations near the embankment toe, which can be critical for large height embankments.

Hence, this research work proposes the concept of using encased stone column supported embankments with a horizontal layer of geosynthetic material (planar and 3-dimensional geocell) as reinforcement. This could reduce the vertical settlements and also prevent the lateral spreading of soil. Thus, the whole system may serve like a Geosynthetic Reinforced Piled Embankment System (GRPES). GRPES is a popular ground improvement technique in European countries to construct structures with strict settlement criteria. Conceptually GRPES is equivalent to a piled raft system. The present investigation is aimed to explore the time-dependent behavior of geosynthetic reinforced embankments supported on encased stone columns and compare the results with the performance of GRPES reported in the literature.

Based on the literature review and identified research gap, the following objectives are proposed for the research work

1. To carry out typical laboratory model tests in the unit cell to study the following aspects,
   i.   The behavior of a single encased stone column (with and without a horizontal layer of geogrid) installed in lithomargic clay subjected to vertical loading.
   ii.  The behavior of a group of encased stone columns with the equivalent area as that of a single column (with and without a horizontal layer of geogrid) installed in lithomargic clay subjected to vertical loading.
2. To develop simplified numerical models (2-d axisymmetric, 3-d Column) and examine their accuracy regarding experimental data and case studies reported in the literature.
3. To investigate the time-dependent behaviour of the system modeled as a unit cell by carrying out axisymmetric and 3D column analyses.
4. To investigate the time-dependent behaviour of the overall system by carrying out full three-dimensional finite element analyses.

5. Interpretation of the results from experimental and numerical studies and comparison of the proposed system with the performance of Geosynthetic Reinforced Piled Embankment Systems (GRPES).

## 1.7   ORGANIZATION OF THE THESIS

This thesis contains seven chapters. Following the introduction to the research topic in this chapter, a comprehensive literature review of the geocells, lithomargic clay and encased stone column supported embankments is made in the second chapter to understand the state-of-the-art in this area.

The third chapter describes the finite element analysis procedures used for the solution of the problem. This chapter also discusses the various numerical models used in the study and the validation of the models with respect to the case studies reported in the literature.

The details of various materials used in experimental investigation, the test setup, and the test procedure are included in the fourth chapter. The validation of the developed models with respect to experimental data is also given in this chapter.

The fifth chapter describes the numerical investigations performed to study the time-dependent behavior of geosynthetic reinforced encased stone column supported embankments. Parametric studies using the axisymmetric and 3D Column models are discussed. The proposed system was compared with the performance of Geosynthetic Reinforced Piled Embankment Systems (GRPES) from the obtained results.

In chapter six, full three-dimensional analyses of geosynthetic reinforced encased stone column supported embankment are described. Comparison of numerical results with the available design methods is also carried out.

The seventh chapter summarises the entire research work performed in this thesis and lists the conclusions drawn from this research work. A brief note on the scope for further research on this topic is presented.

# CHAPTER 2

# LITERATURE REVIEW

## 2.1 GENERAL

A comprehensive review of relevant literature on ground improvement techniques using encased stone columns and geocell has been carried out in this chapter. The research publications are classified based on experimental, numerical, and analytical studies.

Geocells are a superior form of reinforcement due to their cost-effectiveness and three-dimensional confining properties. Numerical modeling of geocell is always challenging due to its three-dimensional honeycomb structure. Most of the available works of literature are based on laboratory model studies and numerical modeling using the equivalent composite approach (ECA). The critical review on the topic led to identifying the research gap and scope for current research work.

## 2.2 STUDIES ON GEOCELL

Many researchers tried to explain the reinforcing mechanism of geocells based on their experimental and numerical studies. Predominantly, geocell reinforcements were used to support loads besides improving the performance of soft soil.

### 2.2.1 Installation of Geocell Mattress in the Field

Bush et al. (1990) described the procedure for construction and installation of geocells in the field. Geocells are manufactured by the thermal welding of geosynthetics. It can be constructed from planar geotextiles and geogrid in the field. Different types of readymade geocells are also available. Based on the design requirements, they can be suitably selected and stretched in the ground as a geocell mattress.

Before geocell mattress construction, the ground has to be cleared and leveled. After that, basal geotextile material is laid on the ground by keeping minimum overlapping distance between adjacent rolls. Over the basal layer, another geogrid sheet is placed in a transverse direction with one end stitched to the bottom layer. The

13

transverse member is rotated about the stitched end to make it vertical and temporarily tensioned with the help of timber posts. The procedure is repeated to cover the entire area. Another layer of geogrid was positioned between two transverse members, and it connected with a transverse sheet with hooked steel bars known as bodkin joints (Carroll Jr. and Curtis 1990; Simac 1990). The bodkin joints form the cellular structure, and a suitable material is filled inside the pockets.

### 2.2.2 Applications of Geocell

Yadav et al. (2014) reviewed different applications of geocell in the field of geotechnical engineering. They reported the mechanism, field installation, and the various applications of geocell reinforcement. Geocells have been used for different structures such as embankment, foundation, reinforced wall, slope stability, and erosion control. They also mentioned the necessity of further studies to evaluate the application of geocells in other fields. Dhane et al. (2015) discussed the importance of geocells in the civil engineering field from the studies conducted by various researchers. They reported different applications and basic mechanisms of geocells and confirmed the cost-effectiveness and versatility of geocells.

#### a. *Waste Containment System*

Geosynthetic products in waste containment systems as liners, cover systems, leachate collection systems, cut-off wall systems, etc., became common practice (Giroud and Cazzuffi 1989; Koerner 1990; Daniel and Bowders 1996; Rowe 1998). Many researchers reported the application of geocells in waste conatinement system (Zornberg and Christopher 1999; Rawat et al. 2010; Zhao and Karim 2018). Hendricker et al. (1998) and Bouazza et al. (2002) investigated the effectiveness of geocell mattresses as a cover system for hazardous waste containment systems in southern California. They reported that using stiffness, geocells could distribute loads to a wider area, and also chemical compatibility of geocells proved its stress resistance to the waste exposure.

#### b. *Pavement and Road Construction*

Many researchers have stated the successful application of geocell mattresses in road construction and pavements (Rajagopal et al. 2014; Pokharel et al. 2015). The ability

of geocells to transfer vertical stresses to a wider area makes construction possible even over soft soil subgrade. Moreover, they raise the modulus of the layer, thereby lowering the surface deflection.

The suitability of geocell in Asphalt pavement was investigated by Thakur and Han (2012) and reported their enhanced performance compared to unreinforced base layers. Emersleben and Meyer (2008) enumerated that the presence of geocell layer in the gravel base reduces the vertical stresses on the subgrade to around 30 percent of traffic load.

### c. Foundation

In the present scenario, the construction of a foundation over weak, soft soils is highly challenging. The construction of foundations can be done either by conventional methods like piles, rafts, or improving soil properties. Also, geosynthetic materials were used to stabilize the weak soil deposits (Alawaji 2001; Basudhar et al. 2007; Sitharam and Sireesh 2004). Compared to unreinforced soil base, footing on geocell reinforced soil exhibits higher bearing capacity and reduced settlement. 3D confinement action of geocells forms a rigid composite with a higher load-bearing capacity (Latha et al. 2008; Latha et al. 2009; Latha and Somwanshi 2009; Hegde and Sitharam 2013, 2015a, 2017). Many researchers have substantiated it through laboratory model tests over different types of footings (Mandal and Gupta 1994; Dash et al. 2001a; Sitharam and Sireesh 2005, 2006; Sitharam et al. 2007; Sireesh et al. 2009; Pokharel et al. 2010; Dash 2012; Sitharam and Hegde 2013).

### d. Embankment

Embankment construction over weaker subgrades suffers several flaws, either during pre-construction (incapability of the soils to support the construction equipment) or post-construction (excessive settlement of the weaker soil after construction). Considering the problems mentioned above, the usual remedial actions involve removing the topsoil and their replacement with stronger and stiffer material. But the method of removal and replacement is suitable only for thickness 2 to 3 m. If soft soil thickness is more, other ground improvement techniques like chemical treatment or soil reinforcement will be effective and economical.

The unique features of geocells, like their ability to act as a stiff, rigid base and incoming load distribution to a wider area, make it suitable for countering the inconveniences faced during the construction of embankments over soft soil. Johnson (1982), Bush et al. (1990), Zheng et al. (2009), Zhang et al. (2010), and Latha (2011) have reported the successful application of geocells in embankment construction.

### e. Railway

Many studies were conducted on geosynthetic reinforced railway ballast (Indraratna et al. 2006, 2013, 2015; Sireesh et al. 2013; Biabani et al. 2016b). Indraratna et al. (2006) assessed the performance of geosynthetic stabilized ballast in the coastal region of Australia and confirmed the suitability and cost-effectiveness of the reinforcement. The geocell confinement of railway ballast displayed a significant reduction of the vertical deformations, which enabled low-quality material to be used as ballast. Leshchinsky and Ling (2012) verified the effectiveness of geocell reinforcement through numerical modeling. From the studies, they found out that geocells effectively confines ballast and thus reduces vertical deformation.

### f. Slope Protection and Erosion Control

Vegetation is the usual method adopted for slope stability and erosion control. But in steep slopes and high rainfall areas, this method fails to bind the soil particles as a single entity. In such cases, geocells can be used as reinforcement (Boyle and Robertson 2007). They can retain the soil particles by retarding the surface runoff and subsequently controlling soil erosion. Many researchers studied the confining effect of geocells in soil erosion control and slope stability. Mehdipour et al. (2013) considered both bending, and membrane stresses in geocell and modeled geocell as a beam element. They found out that the main parameters of geocell reinforcement responsible for the decrease in the lateral displacements and the increased factor of safety of the slopes were bending moment and tensile strength. Geocell reinforcements mainly control the advancing of failure surfaces and reallocate the loads over a wider area and provide slope stability.

### g. Reinforced Walls

Ling et al. (2009), Chen et al. (2013), Soude et al. (2013), Latha and Manju (2016) reported the use of geocells in retaining structures. Ling et al. (2009) found out that geocell reinforced walls can resist earthquake loading to some extent. The confining effect of geocells was responsible for the performance improvement, and it also prevents the structure from collapse.

### h. Box Culverts

Successful application of geocells in the construction of box culverts was reported by Gupta and Somnath (1994) in Bombay. A marine clay layer of 6 m was reported in the site. First tubular gabions resting on a hard mooram layer were constructed. Over the gabion layer, a geocell mattress was placed. With this arrangement, considerable improvement in the load carrying capacity of the clay bed was obtained.

### 2.2.3 Effect of Different Parameters on the Geocell Reinforcement Performance

The influence of the various parameters on the response of Geocell reinforcement for supporting foundations and the construction of embankments was briefly reviewed in the following sections. The properties of geocells and properties of native and infill soil count for the performance of reinforcement. The effect of various geocell parameters is summarised below.

### i. Properties of Geocell

### a. Geocell dimensions

Cell height and width are the two parameters that are used to express the geocell dimensions. According to Rea and Mitchell (1978), optimum footing diameter is 1.5 to 2.0 times cell width, and optimum cell height to cell width ratio was 2.25, above which considerable improvement was not observed. Based on laboratory experiments, Mitchell et al. (1979) proved that the geocell height to width ratio was between 2 to 3.

Dash et al. (2001a) performed laboratory model tests on strip footings supported by geocell sand beds with additional planar reinforcement, as shown in Fig. 2.1. Poorly graded river sand and 35 x 35 mm biaxial geogrid were used to test plane strain conditions.
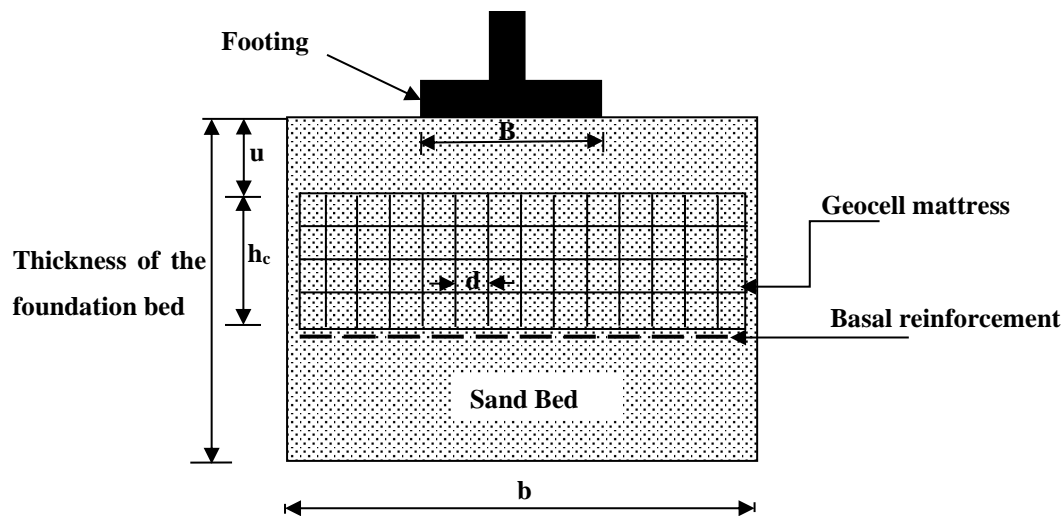
Fig. 2.1 Schematic view of strip footing supported by geocell reinforced foundation bed (After Dash et al. 2001a)

Effect of parameters such as i) height of the geocell layer ($h_c$) and ii) placement position of planar reinforcements was studied by keeping the pocket size of geocells (d), the width of the geocell layer (b), and depth to the top of the geocell layer from the base of the footing (u) constant. The pressure-settlement response for different widths and heights of geocell mattresses are depicted in Fig. 2.2 and Fig. 2.3. Beyond ($h_c/ B$) ratio 2 and (b/B) ratio 4, bearing capacity change is marginal, where h and b are geocell mattress height and width, B is the footing width.

The test results concluded that the presence of basal geogrid under geocell mattress increases the load carrying capacity of the footing. But the effect of planar geogrid becomes marginal at large heights of geocell mattresses. Maximum performance increment was obtained for geocell height which is twice the footing width.
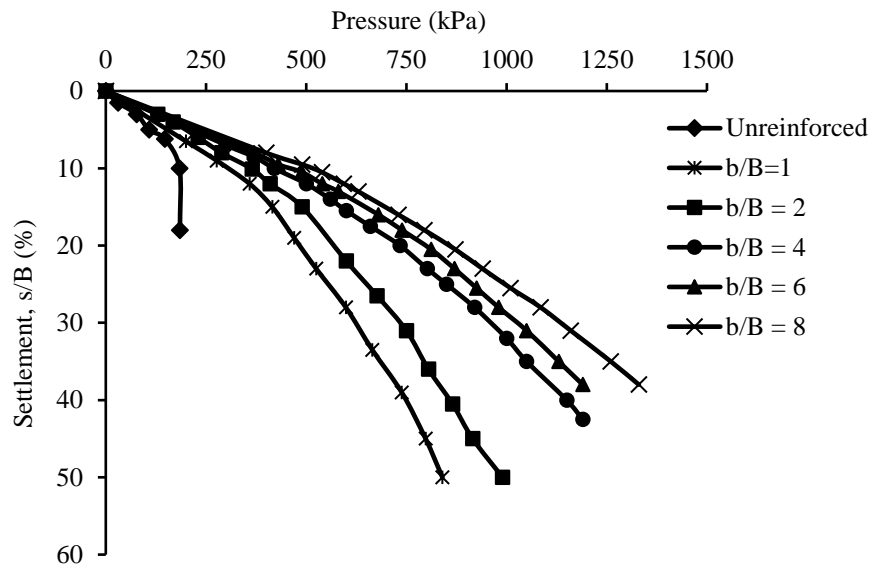
Fig. 2.2 Pressure-settlement response for different width of geocell mattress (After Dash et al. 2001a)
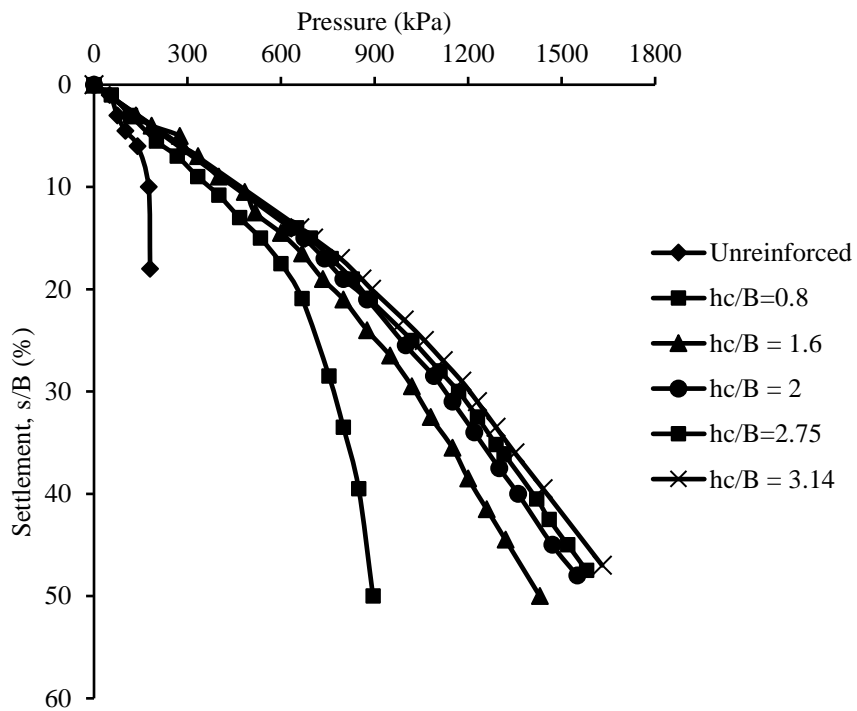


Fig. 2.3 Pressure-settlement response for different height of geocell mattress (After Dash et al. 2001a)

In continuation to the above studies, they varied the following parameters-formation of the geocell mattress, pocket-size of geocells (d), the height of geocell layer ($h_c$), the width of the geocell mattress (b), depth to the top of the geocell layer below the footing (u), the relative density of soil and type of reinforcement used to form the geocell. It was observed that, though the sand filled in the cell pockets fails, the geocell mattress act as a beam due to its shear and bending rigidity and support footing.

Geocell reinforcement enabled the soil to resist failures even at a settlement equal to 50% of the footing width and load as high as eight times the ultimate bearing capacity of the unreinforced sand. From Fig. 2.2 and Fig. 2.3, the maximum performance can be obtained with geocell height equal to twice the footing width, geocell layer width around four times the footing width, top of geocell mattress at a depth of 0.1B from the bottom of the footing, and by filling the geocells with denser soils. Based on the experimental works on geocell reinforced circular footing, the maximum performance of foundation in load carrying was observed for geocell layer width equal to the diameter of footing (Dash et al. 2003).

The ratio of geocell height to geocell diameter, known as the aspect ratio, is a primary factor contributing to the performance of the geocell layer. A higher aspect ratio results in improved bearing capacity of geocell-supported embankments, and the improvement is less significant when the aspect ratio is greater than unity (Latha and Rajagopal 2007). Flexural strength of geocells increases with increased cell height to cell width ratio (Tang and Yang 2013).

When the height of the geocell increases, the number of bodkin joint layers also increases, which in turn makes the geocell mattress a semi-rigid slab with high rigidity (Dash et al. 2001a; Dash et al. 2007). Thus, the load can be distributed to a wider area, and the overall performance of the structure improves (Hegde and Sitharam 2015a).

### b.    *Pattern of Arrangement*

Pokharel et al. (2010) performed lab tests on single geocell reinforced bases in the pavement. They found out that a circular-shaped one has higher stiffness and bearing capacity compared to an elliptical-shaped geocell. Chen et al. (2013) also reported that

the highest apparent cohesion was induced by circular-shaped geocells and lowest by hexagonal shape.

Transverse and diagonal geogrids were arranged in different patterns and connected by Bodkin joints to form geocells. Chevron pattern and diamond pattern are more popular among the different patterns and are shown in Fig. 2.4. Chevron pattern was more efficient than the diamond pattern of arrangement (Dash et al. 2001b; Rai 2010). The number of joints per area is more for the Chevron pattern. Thus, the bending and shearing rigidity is more. Higher rigidity geocell pattern helps to distribute large loads uniformly to the soft foundation soils.
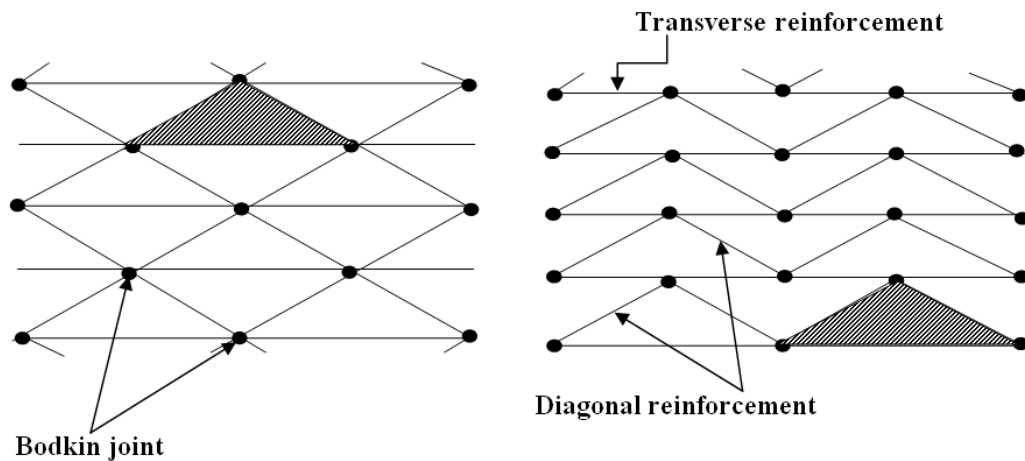


Fig. 2.4 Various geocell configurations (a) handmade geocell diamond pattern and (b) handmade geocell chevron pattern (After Dash et al. 2003)

## c.  *Pocket Size of Geocells*

Though the actual shape of the geocell is triangular, pocket size is expressed in terms of equivalent diameter.  To allow for axial symmetry conditions, the triangular area is transformed into a circle of the same cross-sectional area to get the equivalent diameter. The behavior of reinforced foundation beds is highly dependent on the pocket size of geocells.

Rai (2010) reported that a smaller pocket size geocell gives better performance. Confinement per unit volume is more for smaller size pockets, which results in bearing capacity improvement (Hegde and Sitharam 2015b). As per Dash et al. (2003) and Rai (2010), optimum pocket size was identified as 0.8 times the footing diameter.

21

### d.    *Properties of Geocell Material*

Properties of geogrid from which geocell has been formed have a major influence on the reinforced system's performance. The orientation of geogrid ribs and stiffness were some of the significant parameters. Compared to diamond openings, the square or rectangular openings geogrid give better performance improvement. Also, reinforced foundation bed bearing capacity increases with an increase in geocell elastic modulus (Hegde and Sitharam 2015b). It is explained as a higher elastic modulus of geocell material exerts higher confining pressure on infill soil, leading to bearing capacity increment.

Compared to confined geocell, unconfined geocell has lower stiffness and higher ultimate load capacity (Pokharel et al. 2010). In plate load tests, the geocell that is fully embedded in the sand is referred to as confined geocell, and which is exposed to air is termed as unconfined.

### ii.  Soil parameters

### a.    *Interface Friction angle*

Textured geocells were found to perform better than smooth-walled geocells as the textured surface provided a higher degree of frictional interaction between the geocell wall and the infill material.  The increase in the friction angle caused only a marginal increment in the load carrying capacity for the reinforced foundation bed (Hegde and Sitharam 2015b).

### b.    *Properties of Infill Soil*

Granular soils are preferred over cohesive soils as geocell fill material since the confinement effect is more significant in these soils, which leads to a reduction in settlement (Latha and Rajagopal 2007). The relative density of infill material was directly affecting the bearing capacity of footing (Rai 2010; Dash et al. 2001b). Maximum efficiency of geocell can be obtained with denser infill soil.

### c.    *Embedment Depth*

Davarifard and Tafreshi (2015) conducted plate load tests on a multi-layered geocell reinforced bed in the field. Most of the experimental works related to geocell

reinforcement have been carried out for surface footings, and only a few have considered embedment depth of footing. The influence of the embedment depth on the load carrying capacity of the footing was investigated through a large-scale model test on embedded square footing. It was observed that the bearing capacity of the footing increased proportionally with an increase in embedment depth ratio ($D_f/B$) [$D_f$ is the embedment depth; B is the footing width].

### d. *Properties of Native soil*

The properties of subsoil influence the performance of the geocell reinforced foundation. The stiffness of the foundation bed is a major factor that determines the percentage of improvement obtained through geocell reinforcement. Higher stiffness subgrade provides more support against settlement to geocell soil composite, which results in reduced membrane resistances and less improvement factor (Biswas et al. 2016). Also, geocell reinforcement is more effective in soft clay beds than sand beds (Hegde and Sitharam 2013).

### iii. Review of the optimum parameters of geocell for maximum performance

Various researchers have reported optimum parameters of geocell mattress which gives the maximum performance and above which improvement is marginal as summarised in Table 2.1. The different parameters of the geocell mattress were expressed in terms of either footing diameter or width depends upon type footing.

Properties of geocell as well as infill soil influence the performance of the reinforced foundation system. Various factors like height of the geocell mattress, width of the geocell mattress, pocket-size of geocell, the placement depth below the footing, the pattern of formation, density of infill soil, properties of geosynthetic material from which geocell has formed, etc. have discussed in this section to obtain optimum parameters for effective and economical design, and construction of geocell reinforced system. The type of construction, economy, type of subgrade, stiffness, etc., affects the quantification of improvement. Geocells can be effectively used as reinforcement both in the case of clay as well as the sand bed.

Table 2.1 Summary of optimum parameters of geocells for maximum performance

| Sl No. | Reference | Application | Optimum Parameters | | | Pattern |
|---|---|---|---|---|---|---|
| | | | $h_c$ | b | u | |
| 1 | Rea and Mitchell (1978) | Circular footing | $2.25b_1$ | - | - | Square shaped opening |
| 2 | Mandal and Gupta (1994) | Strip footing | 1.5B | - | - | Hexagonal shaped pocket |
| 3 | Mhaiskar and Mandal (1996) | Rectangular footing | 0.625B | 3.4B | 0 | - |
| 4 | Dash et al. (2001b) | Strip footings | 2B | 4B | 0.1B | Chevron pattern |
| 5 | Dash et al. (2003) | Circular footing | 2.1D | 5D | 0.1D | Chevron pattern |
| 6 | Dash et al. (2004) | Strip footing | 2B | 4B | 0.1B | Chevron pattern |
| 7 | Latha et al. (2006) | Strip footing | 2.75B | 6B | 0.1B | Chevron pattern |
| 8 | Sitharam et al. (2007) | Circular footing | 2.4D | 4.9D | 0 | Chevron pattern |
| 9 | Sireesh et al. (2009) | Circular footing | 1.8D | 4.9D | 0.05D | Chevron pattern |
| 10 | Tafreshi and Dawson (2010) | Strip footing | 1.5-2B | 4.2B | 0.1B | - |
| 11 | Rai (2010) | Circular footing | 0.8D | 6.67D | 0.1D | Chevron pattern |
| 12 | Biswas et al. (2016) | Circular footing | 1.15D | 6.67D | 0.1D | Chevron pattern |
| 13 | Davarifard and Tafreshi (2015) | Square footing | 0.2D | 5D | 0.2D | - |

($h_c$= height of geocell mattress, b= width of geocell mattress, $b_1$ = width of single cell, u= depth of placement below footing)

Based on previous studies, it can be concluded that the most effective geocell reinforced foundation was obtained with Chevron pattern with 0.8D pocket size, 0.1D

placement depth, (4-6) D of geocell width and (1.5-2) D of geocell height, denser infill soil, and textured geocell material, where D is the footing diameter same values can be used for strip footing also by replacing footing diameter by footing width.

### 2.2.4 Design Aspects of Geocell

Geocell was designed as an equivalent material with cohesion greater than the infill soil and friction angle the same as that of the infill. Membrane stress in the geocell walls confines the soil particles, which results in apparent cohesion in the soil. The geocell membrane stress caused additional confining stress ($\Delta\sigma_3$), which was given by (Henkel and Gilbert 1952),

$$\Delta\sigma_3 = \frac{2M\varepsilon_c}{D_1}\frac{1}{1-\varepsilon_a} = \frac{2M}{D_0}\frac{1-\sqrt{1-\varepsilon_a}}{1-\varepsilon_a} \qquad (2.1)$$

where    $\varepsilon_a$ = axial strain of soil at failure

$\varepsilon_c$ = circumferential strain of soil at failure

$D_0$ = initial diameter of geocell pocket.

$D_1$ = diameter of the sample at an axial strain of $\varepsilon_a$,

M = modulus of the membrane, obtained from the load-strain curves of
wide-width tensile strength test on geogrids.

Bathurst and Karpurapu (1993) conducted triaxial compression tests on a single cell reinforced granular soil sample. Construction of Mohr circle for both reinforced and unreinforced soil and apparent cohesion estimation is shown in Fig. 2.5. Because of the confinement effect of geocell, cell pressure $\sigma_3$ increased to ($\sigma_3 + \Delta\sigma_3$) and normal stress $\sigma_1$ increased to $\sigma^r_1$.

Rajagopal et al. (1999) conducted a triaxial test on a single cell, and multi-cell reinforced sand samples and concluded that among different samples, a more accurate value of apparent cohesion was obtained for samples with at least three interconnected cells. The apparent cohesion induced by the geocell layer (Rajagopal et al. 1999) was given as,

$$C_r = \frac{\Delta\sigma_3\sqrt{K_p}}{2} \qquad (2.2)$$

here $K_p$ is the passive earth pressure coefficient and $\Delta\sigma_3$ is the additional confining stress due to the geocell membrane stress. This apparent cohesion was added with the original cohesion of infill soil to get the cohesive strength of the reinforced layer.
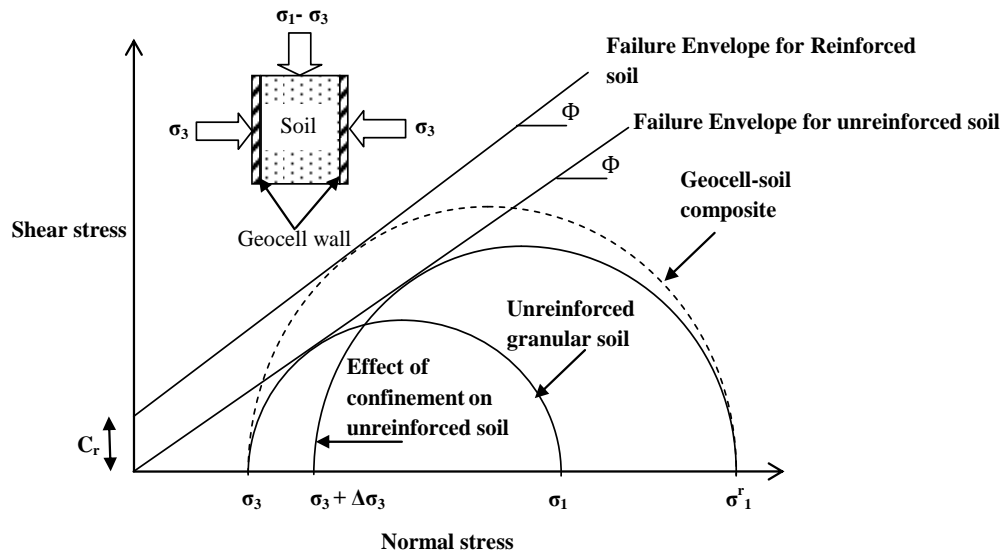


Fig. 2.5 Mohr circles for both reinforced and unreinforced soil and apparent cohesion estimation (After Bathurst and Karpurapu 1993)

Mitchell et al. (1979) carried out the first analytical work on geocell reinforced soil. Analytical solutions were developed to obtain the base course load carrying capacity reinforced with the grid cell. The method considered different types of failures such as (a) bearing capacity, (b) bending, (c) durability failure, (d) excessive rutting, (e) cell penetration of subgrade (f) cell bursting (g) cell wall buckling. Due to the complex structure of geocell and the stress-dependent nature of sand stiffness, estimating the modulus of geocell is difficult. Latha (2000) proposed an empirical relation between modulus numbers of soil,

$$K_r = K_e + 200M^{0.16} \tag{2.3}$$

where $K_r$ and $K_e$ are the modulus number of geocell-soil composite and unreinforced soil, respectively. Young's modulus parameter ($K_e$) is the modulus number in the hyperbolic model (Duncan and Chang 1970), and M corresponds to the tensile stiffness of the geocell material.

The equivalent stiffness of geocell reinforced soil is a function of the stiffness of unreinforced soil, the secant modulus of geocell material, and an interaction parameter in the case of multiple cells. A nonlinear empirical equation to express Young's modulus of geocell-reinforced sand ($E_g$) is given by (Latha 2000; Rajagopal et al. 2001),

$$E_g = P_a \left[ K_u + 200M^{0.16} \right] \left( \frac{\sigma_3}{P_a} \right)^n \tag{2.4}$$

here, $P_a$ = atmospheric pressure in kPa, M = secant modulus of geocell material in kN/m [corresponding to the average strain of 2.5% in the load elongation curve of geocell material], $\sigma_3$ = confining pressure in kPa, $K_u$ = Young's modulus parameter of the unreinforced sand, n= Modulus exponent of unreinforced soil that determines the rate of variation of $E_g$ with $\sigma_3$.

Various design methods for geocell-supported embankments include the slip line method (Jenner et al. 1988), a method based on Bishop's slope stability analysis (Latha et al. 2006), and a method based on plane strain finite element analysis (Latha 2011). Jenner et al. (1988) considered a plastic bearing failure of embankments, which can be expected for embankments with a width more than four times the foundation soil depth. With the help of a non-symmetric slip line field, the contribution of geocell in bearing capacity was determined. The construction of a slip line makes this method complex.

Koerner (1998) proposed a method for bearing capacity estimation based on the plastic limit equilibrium mechanism. He observed that the shear strength between geocell and infill soil was responsible for the strength improvement and considered the geocell as a soil layer with improved strength parameters due to the confinement.

Latha et al. (2006) developed a computer program based on Bishop's slope stability method to design geocell reinforced embankments. In this method, the geocell layer was treated as a soil layer with additional cohesion due to confinement. Input parameters were slope geometry, depth of foundation soil, the height of geocell, shear strength parameters of soil and geocell layer, foundation soil properties, pore pressure coefficients, and surcharge pressure on the embankment crest. If all the parameters are known, slope stability analysis can be carried out with the trial height of the geocell

27

layer to get its cohesive strength corresponding to the required safety factor. After getting the cohesion value, the modulus of geocell for a particular geocell size and axial strain can be determined by back-calculation.

Later Zhang et al. (2010) proposed a bearing capacity calculation method for the geocell-supported embankments on soft foundation soil. They considered three functional aspects of the geocell layer, which are (a) lateral resistance effect, (b) vertical stress dispersion effect as shown in Fig. 2.6, and (c) membrane effect as in Fig 2.7. The increase in bearing capacity can be obtained by summing up all three mechanisms.

### a.  *Lateral resistance effect*

The shear strength between the geocell wall and the infill soil imparts the lateral resistance component, as shown in Fig. 2.6.

### b.  *Vertical stress dispersion effect*

Wider distribution of load can be possible because of the three-dimensional structure of geocells which improves the load carrying capacity of foundation soil. The interconnected cells from a panel that acts as a slab and redistributes the applied load. This is known as the vertical stress dispersion effect. Due to the vertical dispersion effect, the load per unit area increases from $p_s$ to $p_r$, as shown in Fig. 2.6. The contribution of vertical dispersion effect on bearing capacity $\Delta P_1$ is given by,

$$\Delta p_1 = \frac{2h_c \tan\theta}{b_n} p_s \tag{2.5}$$

Here, $h_c$ and $\theta$ are the height and the dispersion angle of geocell reinforcement, respectively, $b_n$= width of the uniform load $P_s$.

### c.  *Membrane effect*

Due to the loading, the geocell deflects and generates additional tension force. This force reduces pressure on the foundation soil, decreases the vertical deformation, and increases the bearing capacity. The membrane effect is due to the vertical component of the mobilized tensile strength (Zhao et al. 2009). The contribution of membrane effect on bearing capacity $\Delta P_2$ is given by,

$$\Delta p_2 = \left( \frac{2T \sin \alpha}{b_n} \right) \quad (2.6)$$

Here,   T = tensile strength geosynthetic material.

α = Horizontal angle of tensile force T as shown in Fig. 2.7

$b_n$= width of the uniform load $p_s$ as shown in Fig. 2.6

The sum of the above mechanisms gives the bearing capacity increment due to the placement of geocell reinforcement, and the increment in bearing capacity($\Delta p$) was added with the bearing capacity of unreinforced foundation soil($p_s$) to get the bearing capacity of reinforced foundation soil bed ($P_{rs}$).

$\Delta p$ = vertical stress dispersion effect + membrane effect = $\Delta p_1 + \Delta p_2$

$$P_{rs} = p_s + \Delta p = p_s + \Delta p_1 + \Delta p_2 = p_s + \frac{2h_c \tan \theta}{b_n} p_s + \left( \frac{2T \sin \alpha}{b_n} \right) \quad (2.7)$$

For larger settlements, the method proposed by Zhang et al. (2010) showed better results than Koerner's method.
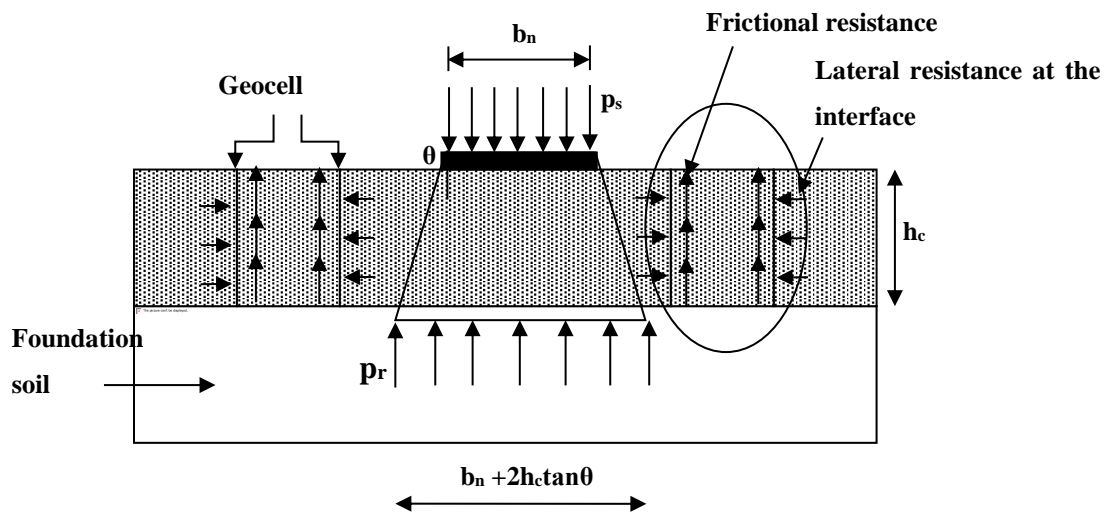


Fig. 2.6 Schematic diagram of lateral resistance effect and vertical stress dispersion effect (After Zhang et al. 2010)
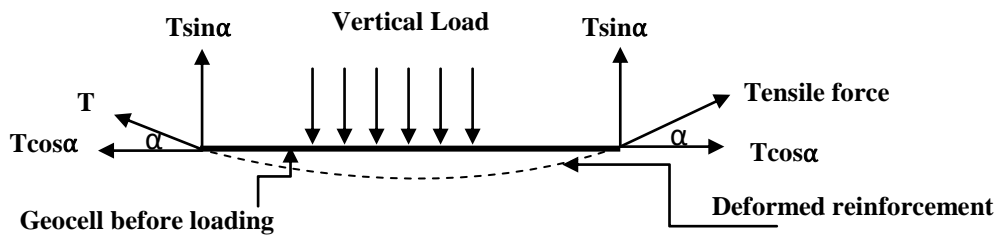
Fig. 2.7 Membrane effect in the reinforcement (After Zhang et al. 2010)

### 2.2.5 Experimental Studies on Geocell Reinforced Soil

Based on various experimental studies conducted by many researchers, the behavior of geocell reinforced soil was analyzed. In geotechnical engineering, conventional building materials are effectively replaced by geosynthetic products in various aspects. They made the following conclusions from their review studies,

    a. The efficiency of reinforcement decreases with an increase in the height and width of geocell.

    b. The optimum width of a cellular mattress in the sand is five times the footing width.

    c. Geocell reinforcement is more efficient than planar reinforcement in settlement reduction and load carrying capacity.

    d. Compared to unreinforced footing, geocell-supported footings have very little mobilized shear stress ratio.

Mitchell et al. (1979) conducted model laboratory tests on footings resting on sand beds with square-shaped paper grid cells as reinforcement. The influence of parameters such as diameter and height of geocells were investigated. The experimental results concluded that the substantial increment in elastic modulus of soil could be obtained with geocell reinforcement.

Dash et al. (2004) conducted laboratory model tests to compare the performance of different geosynthetic materials as reinforcements in sand beds under a strip footing. They considered geocell, planar biaxial polypropylene geogrid, and randomly distributed mesh elements as reinforcing materials. Plain strain condition was maintained for testing. The experimental results concluded that geocells were the most effective reinforcement among different geosynthetic materials. Geocell reinforced soil

was able to resist failures at settlement values equal to about 45% of footing width and the applied load equal to eight times the ultimate capacity of the unreinforced soil, while geogrid reinforced soil was able to withstand settlement of around 15% of the footing width and a load equalling four times the ultimate capacity of the unreinforced soil.

Zhou and Wen (2008) studied the problematic soft soil condition for the foundation of the Qin-Shen Railway (from Qinhuangdao to Shenyang) in China. The laboratory model test results showed that the provision of geocell reinforced cushion improves the subgrade reaction coefficient corresponds to 30cm diameter plate ($K_{30}$) by 3000% and reduces deformation by 44%.

Sireesh et al. (2009) examined the effect of geocell sand mattress provided over clay subgrade with voids. Influence of various parameters such as the thickness of unreinforced sand layer above clay bed, width and height of the geocell mattress, the relative density of the infill soil in the geocells, and influence of basal geogrid were studied through laboratory model tests. Clay subgrade was prepared by using natural silty clay of low plasticity (CL). The circular footing was used for loading. Biaxial geogrid with square shape aperture opening size of 0.035 x 0.035 m in chevron pattern was used to form geocells and cell pockets filled with poorly graded sand (SP). From the test results, it was clear that the provision of a geocell mattress improves the load carrying capacity and reduces the settlement of clay subgrade with the void. Geocells are effective only when it spreads beyond the void to a distance equal to the diameter of the void. The load carrying capacity of the foundation is directly proportional to geocell width, geocell layer height, the density of infill soil. Performance improves with an increase in geocell width only up to a value of 4.9 times footing diameter. The critical height of the geocell layer was found to be 1.8 times footing diameter, beyond which performance reduces. If geocell reinforcement were provided with basal geogrid in the granular soil layer overlying soft subgrade with the void, a 3.4-fold improvement in performance could be obtained. The overall load carrying capacity of the footing with reinforced foundation increased by about 40 times compared to clay subgrade with void alone.

Pokharel et al. (2010) investigated the factors such as elastic modulus of geocell, type of the geocell, the thickness, embedment of the geocell and the infill material

quality, etc. the performance of single geocell reinforced bases in the pavement. Plate load tests were conducted on a single geocell under static load with two types of infill material. It was observed that higher stiffness and bearing capacity was exhibited by circular-shaped geocell compared to elliptical-shaped geocell and by geocells with higher elastic modulus. Also, compared to confined geocell, unconfined geocell has lower stiffness and higher ultimate load capacity.

Tafreshi and Dawson (2010) carried out laboratory model tests on strip footing supported on the reinforced sand bed. Experiments were conducted using geocells and geotextiles of the same characteristics as reinforcements, and their performances were compared. Parameters such as reinforcement width, the number of planar layers of geotextile, and the height of the geocell below the footing base were also studied. It was concluded that with the increase of these parameters, the efficiency of reinforcement decreases. They suggested optimum depth of topmost geocell layer as 0.1 times footing width. They confirm the suitability of geocell over conventional planar geosynthetic materials. Also, they pointed out the necessity of large-scale field tests to identify the actual behavior in the field.

Chen et al. (2013) examined the confining effect of geocell reinforced sand by both triaxial compression tests and theoretical analysis. The effect of various parameters such as shape, size, number of cells, sample size, etc., on the behavior of samples were also studied. It was found that the confining effect of geocells was influenced by the size and shape of the geocell, cell pressure, and multiple cell effect. The highest apparent cohesion was induced by circular-shaped geocells and lowest by hexagonal shape among circular, rectangular, and hexagonal cross-sections. Lower confining pressure makes the reinforcement more effective. They also concluded that the sample behaves like a stiff column under axial compression at higher confining pressure.

Dash and Bora (2013) conducted a series of strain-controlled experiments to understand the behavior of foundation beds reinforced by stone column-geocell mattresses. They found out that the composite system is more efficient than other planar reinforcement systems. Clay with low plasticity (CL) was used as the foundation bed, and poorly graded crushed granite aggregates of size 2-10 mm were used to form the

stone columns. The diameter of the geocell was taken as 0.8D (where D is the diameter of footing) and followed the chevron pattern. The load-bearing capacity of soft clay beds improved by 3.7 times when stone columns alone were used, and 7.8 times improvement was observed with geocell alone. But the combined system improved the load carrying capacity by 10.2 times. The use of a stone column-geocell system also increased the stiffness of the clay bed, which resulted in the reduction of footing settlement. Maximum performance improvement was observed with stone column length and spacing as five times and 2.5 times the column diameter. Also, the critical height of the geocell mattress was identified as the diameter of footing, above which the improvement was less significant.

Biswas et al. (2016) carried out several model studies on geocell-supported embankments with and without basal reinforcements. A scale factor of 10 and a side slope of 1H: 1V was assumed for testing. 50 mm x 50 mm geocells with height 25 mm and diamond pattern were used. The test results revealed that geocell-supported embankments have more bearing capacity than the unreinforced embankments and geogrid-supported embankments. A non-dimensional term called improvement factor, $I_f$ was introduced, is the ratio between pressure over embankment and reinforcement to that without reinforcement. The provision of basal reinforcement below geocells increases the improvement factor.

Tafreshi et al. (2015) conducted a cyclic plate load test on unreinforced one and two layers of geocell reinforced soil beds. They used a circular plate of diameter 300 mm for the test. It is observed that the surface settlement decreases with an increase in the number of geocell layers. Also, the vertical spacing between geocells and optimum depth of the first layer was obtained as 0.2 times plate diameter.

Pancar (2016) evaluated the suitability of geocell and geotextile reinforcement for pavement in clayey subgrade with optimum moisture content and higher water contents through plate load test. They examined eight different cases with optimum moisture content as high as 25% and water content as high as 35%. Test results were summarised, and they confirmed the efficiency of geocells over geotextiles in bearing capacity improvement and further observed that the combination of these two materials

gave the most effective soil reinforcement. Also, it was found that to keep highway standards, water content should be kept optimum in this treatment.

Lekshmi et al. (2016) put forward an alternative method to reduce the base thickness of pavements due to aggregates' unavailability. Plate load tests were carried out in the laboratory for unreinforced and geocell reinforced base layers under repeated loading. Permanent and resilient deformations have been examined from the results. It was observed that the geocell reinforced layer offered greater resilience than the unreinforced layer. Thus, they confirmed the suitability of the geocell layer in unpaved roads as it reduced deformation by reinforcing the unbound aggregates, thereby reducing the thickness of the base layer. Also, for predicting permanent deformation in the base layer due to a higher number of cycles, they proposed a numerical model.

### 2.2.6  Numerical Studies on Geocell Reinforced Soil

Most of the early researchers adopted Equivalent Composite Approach for modeling geocells. Equivalent composite approach, ECA (Bathrust and Knight 1998; Latha 2000; Latha and Somwanshi 2009; Mehdipour et al. 2013; Hegde and Sitharam 2015a) uses 2D framework for modeling. In this approach, geocell reinforced soil was modeled as a composite material with the equivalent parameters determined by Equations (2.1), (2.2), (2.3), and (2.4). Though ECA is simple, it is unrealistic to model a 3-dimensional honeycomb structure as a two-dimensional soil layer. Also, the ECA model cannot accurately simulate the interaction between geocell and infill material responsible for the development of additional load-bearing capacity. Duncan- Chang model was commonly used to simulate stress dependency of infill soil. The shortcomings of ECA led to the advancement in the three-dimensional modeling of geocell with the help of many 3D software like FLAC 3D, ABAQUS, etc. Mhaiskar and Mandal (1996) modeled axisymmetrically the geocell- soil composite system using ANSYS 3D. Eight noded isoparametric solid elements with anisotropic and plasticity capabilities were used to model geocell and clay subgrade. The geocell reinforced sand layer was modeled as an isotropic, elastic-perfectly plastic, non-dilatant material, and Drucker Prager yield criterion was applied. But here also, the stress-strain relationship of the soil-geocell composite system could not be modeled properly.  So, the geocell layer was considered as a soil layer with equivalent stiffness.

Han et al. (2008) may be the first researcher to model geocell and soil separately in a three-dimensional workspace. By modeling geocell and the soil separately, the confining effect of geocell on the infill, interface friction between geocell and the infill, contribution of geocell on strength improvement of the reinforced composite, etc. be evaluated. They studied the behavior of single-cell reinforced sand under vertical loading and modeled single-cell geocell as a square box in FLAC 3D software, as shown in Fig. 2.8. The model adopted was Mohr-Coulomb for soil and linearly elastic membrane model for geocell. Since the Mohr-Coulomb model does not consider the stress dependency of soil, bearing capacity increment due to geocell cannot be stimulated in the modeling.
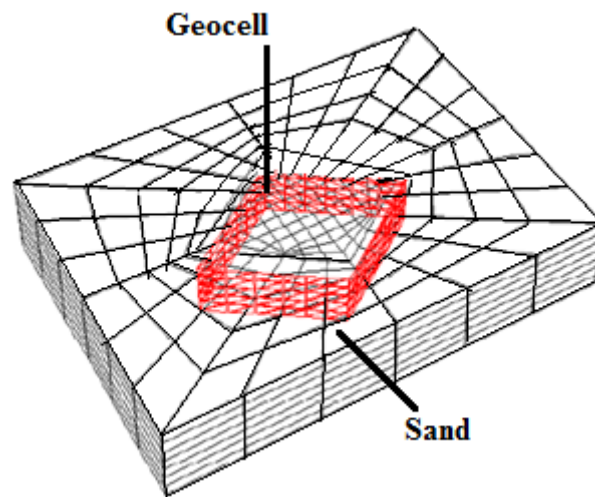


Fig. 2.8 Numerical model of single-cell reinforced sand (Han et al. 2008)

Yang et al. (2010) proposed a three-dimensional model for geocell reinforced soil. Geocell and infill soil was modeled separately using FLAC 3D, and the results were checked with plate load test results. 80 cm x 80 cm x 60 cm test box was used for experiments. A single cell was used to reinforce a 12 cm thick sand layer, and a 15cm diameter steel plate was used for loading. The Duncan and Chang model was used to model the fill material to account for stress dependency. Nowadays, manufacturers use stronger and stiffer polymers for making geocells. Thus, a thin geocell strip can carry a considerable bending load. Therefore, the geocell was modeled by the linearly elastic plate elements, carrying both membrane and bending stress. The actual shape of the

geocell can be simulated by using the digitization of photographs taken from the top of the geocell.

A sinusoidal curve approximated the curvature of the digitized geocell. The axisymmetric model was used with vertical and horizontal movements restrained. At the joint of geocell, special boundary conditions were applied for soil. The compaction effect was considered by keeping the lateral earth pressure coefficient, $k_0$, as 1. To simulate circular loading, velocity boundary was applied on the top of the sand layer.

Chen et al. (2013) proposed a numerical model for analyzing the behavior of geocell reinforced retaining structures. They have used the finite difference program FLAC for analysis. The stability and the deformation of the retaining structures were examined using the proposed model. For different soils, backfill, foundation soil, and geocell reinforced soils, a non-linear elastic stress-strain relationship with Mohr-Coulomb yield criteria was adopted. They did not model the geocell and infill separately, instead of that apparent cohesion was considered for modeling geocell reinforced soil. Cable elements were used to model different interfaces, such as the reinforced zone interface with backfill and foundation bed. Two-dimensional analysis using finite difference program FLAC 2D was carried out to study the stability of geocell reinforced slopes (Mehdipour et al. 2013). The geocell was modeled with the two-dimensional beam element that can carry both membrane and bending stress and with three degrees of freedom at each end node.

After reporting the limitations of ECA, Hegde and Sitharam (2015a and b, 2017) proposed a new modeling approach by considering the actual shape of geocells. Geocell and infill material were modeled separately with different constitutive models. The numerical model of the geocell reinforced sand bed was validated with the plate load test results obtained from the laboratory. They digitized the photograph of an expanded single cell to get the actual curvature, and with deduced coordinates and numerical analyses were carried out in FLAC 3D. The linear elastic geogrid element was used to model the geocell. The elastic-perfectly plastic Mohr-Coulomb model was used for foundation, and the infill soil and the geocell-infill soil interface were linearly modeled with the Mohr-Coulomb yield criterion. The bottom boundary was fully constrained from movement, and the horizontal movement was restrained for side boundaries. They

36

modeled four different cases: (i) unreinforced foundation bed (ii) geogrid reinforced (iii) geocell reinforced and (iv) geocell and geogrid. Fig. 2.9 shows the three-dimensional models adopted for the four cases. It was observed that a combination of geogrid and geocell increased the bearing capacity of the soil, which led to a decreased settlement of the footing.
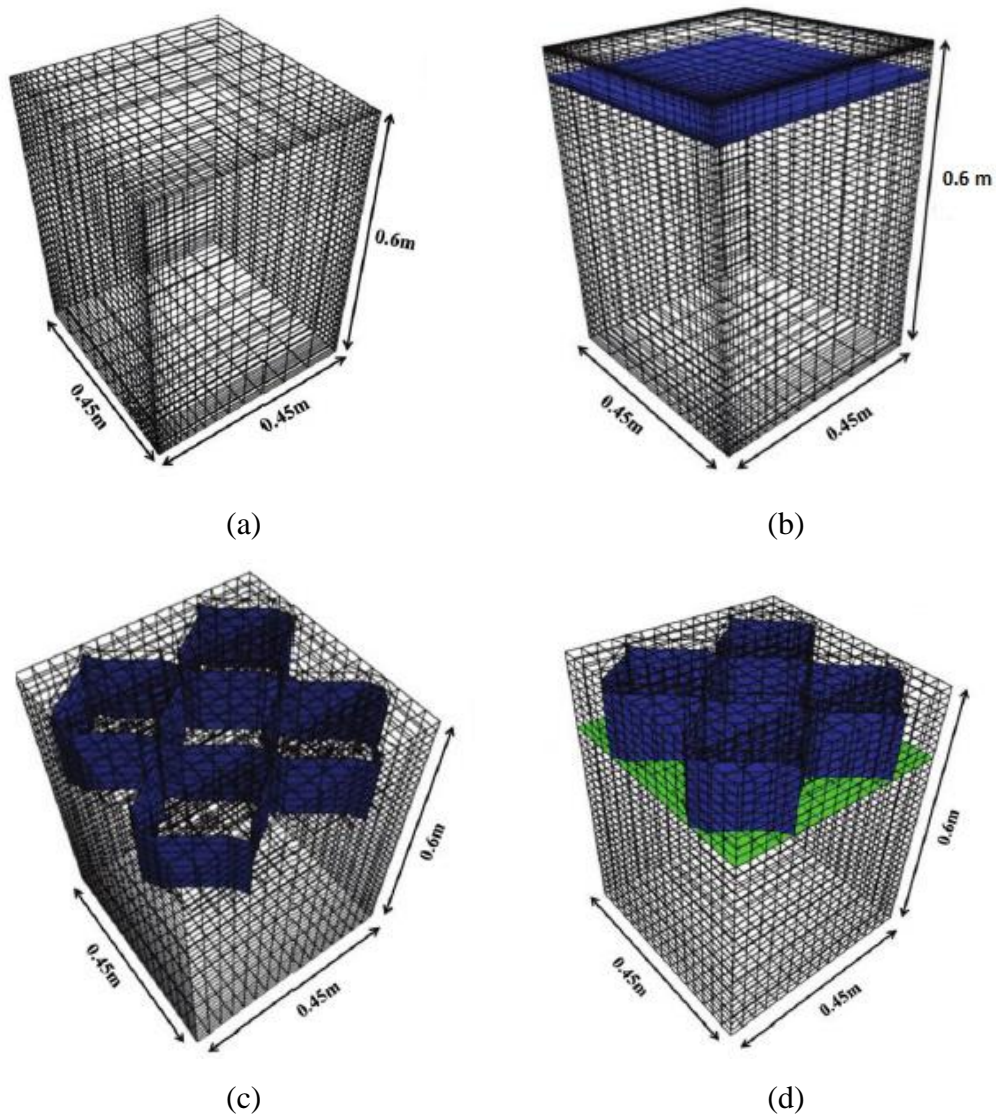


Fig. 2.9 3D model of unreinforced and reinforced foundation bed (a) unreinforced (b) geogrid reinforced (c) geocell reinforced and (d) geocell and geogrid reinforced (Hegde and Sitharam 2005(b))

The combination of geocell and geogrid gave the maximum performance improvement among the four cases. The geogrid helps in accumulating stresses above

the geogrid and thus transferring lesser stress intensity to the subgrade. Whereas in geocells, the stresses are horizontally spread to the wider area and shallower depth. Though this 3D numerical modeling is more accurate than the ECA approach, the anisotropic behavior of the sand bed was not considered in the modeling.

Biabani et al. (2016a) studied the effectiveness of geocell reinforced soil as subballast, which is subjected to cyclic loading, with the help of a numerical model developed in ABAQUS. The numerical results were compared with the large-scale prismoidal triaxial experiment and concluded that the numerical model of geocell reinforced subballast was able to successfully predict the deformations under cyclic loading in both vertical and lateral directions. For the numerical modeling, suitable material properties and boundary conditions were selected, the elastoplastic material with non-associative behavior for sub-ballast and linear elastic- perfectly plastic material for geocell mattress. The hexagonal shape was used to model geocell, as shown in Fig. 2.10. The movement was fully restricted at the bottom, and the lateral displacement was constrained in the direction parallel to tracks ($\varepsilon_2 = 0$). Both monotonic load and cyclic load were superimposed at different confining pressures to simulate the loading condition. The model in ABAQUS has 9380 elements, and 12624 nodes and eight noded reduced integration elements (C3D8R) were used for analyses.
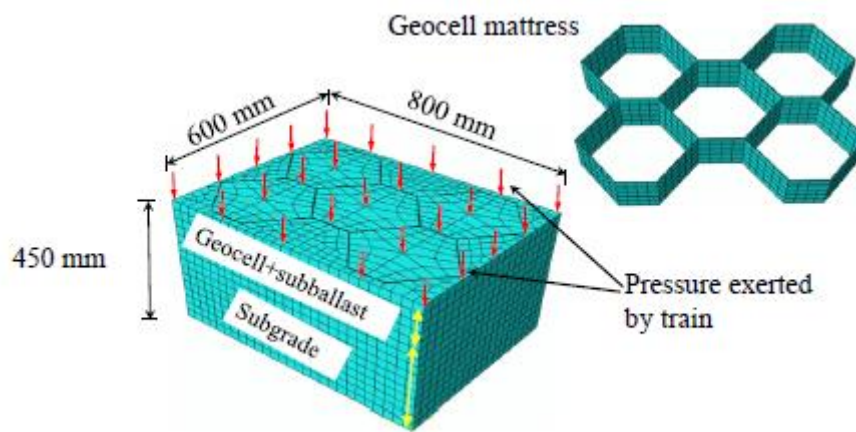


Fig. 2.10 3D modeling of geocells as hexagonal shaped pockets (Biabani et al. 2016a)

## 2.3   STUDIES ON LITHOMARGIC CLAY

The lithomargic clay is usually whitish, yellowish, or pinkish. Physical, chemical, and biological weathering of Alumino Silicate source rocks leads to residual laterite bauxite deposits via clay mineral formation stage. The clay mineral formation stage leads to lithomargic clay, which lies between the underlying parent rock and the formed laterite layer (Momade and Gawu 2009). The chemical constitution of lithomargic clay is mainly of Alumina and Kaolinite. The main drawback of these soils is the drastic reduction in strength with the rise in moisture content, making them highly prone to erosion (Ramesh and Nanda 2007). This increased shearing tendency will have a drastic effect on the foundations laid over them.

Shankar and Suresha (2006) investigated the behavior of lithomargic clay by varying the water content through a road construction project. Based on soaked and unsoaked UCC sample tests, Ramesh et al. (2011) inferred that the addition of Neyveli ash improves the strength properties of shedi soil around 18 times. Nayak and Sarvade (2012) found out that the quarry dust and cement effectively improve the shear strength and hydraulic parameters of lithomargic clay. Shankar et al. (2012) confirmed the application of sand and coir for the stabilization of lithomargic clay through their experimental investigations. The addition of suitable high plasticity binding material will improve the plasticity characteristics of lithomargic clay (Andrews et al. 2014).

Nayak et al. (2014) conducted laboratory tests to evaluate the performance of granular columns installed in dispersive soils. Based on the test results, they found out that the improvement in load carrying capacity and reduction in vertical settlement can be achieved by granular columns.  Stone columns improve drainage and the relative density of surrounding soil (Selcuk and Kayabali 2015). Darshan et al. (2017) found out that granulated blast furnace slag (GBFS) and cement effectively improves the geotechnical properties of lithomargic clay. Thomas et al. (2019) conducted hole erosion tests on lithomargic clay to study the erosion characteristics.

## 2.4 STUDIES ON ENCASED STONE COLUMNS

As already discussed, the concept of wrapping stone columns was first introduced by VanImpe (1985). Numerous experimental and numerical studies on soft clay soils showed that confining the individual stone columns with geosynthetic encasement improves its strength and stiffness considerably (Murugesan and Rajagopal 2007; Gniel and Bouazza 2009; Khabbazian et al. 2010; Yoo 2010; Keykhosropur and Imam 2012; Dash and Bora 2013; Fattah et al. 2016; Castro 2017; Mazumder et al. 2018). Also, the provision of horizontal layers of reinforcement at the ordinary stone column top reduces the bulging, which improves the performance in soft soils (Arulrajah et al. 2009; Lo et al. 2010; Debnath and Dey 2017). The combined use of columnar systems and multiple layers of reinforcement is widespread due to the effectiveness in load transfer, which reduced the total and differential settlement (Han and Gabr 2002; Bhasi and Rajagopal 2015).

### 2.4.1 Unit Cell Concept

Stone Columns are usually arranged in a triangular or a square grid pattern in the field. For experimental/analyses purpose, it is convenient to consider a single column and the associated tributary area of soil surrounding the column forming a unit cell (Fig. 2.11a). The tributary area can be a square ('square grid') or hexagonal ('triangular grid') and can be closely approximated as an equivalent circle having the same plan area (Fig. 2.11b).

Many researchers have used the unit cell approach with the approximation mentioned above to evaluate the performance of stone columns (Shahu et al. 2000; Raithel and Kempfert 2002; Murugesan and Rajagopal 2007; Ambily and Gandhi 2007; Malarvizhi and Ilamparuthi 2008; Yoo and Kim 2009; Castro 2017). Among the different patterns of stone column arrangement, the equilateral triangular pattern is more commonly used in the field since the coverage area of a single column is more than that in the square pattern (IS: 15284-2003).

### 2.4.2 Experimental Studies on Encased Stone Columns

Malarvizhi and Ilamparuthi (2004) conducted experimental investigations on stone columns with three different types of geosynthetics as encasement. It was observed that

the ultimate bearing capacity of unreinforced clay bed was improved by 2 to 3 times by encased stone columns. The bearing capacity improvement was directly proportional to the stiffness of geosynthetics. Murugesan and Rajagopal (2007) performed laboratory model tests and numerical analyses on encased stone columns and reported the benefits of the geosynthetic encasement.



(a)



(b)
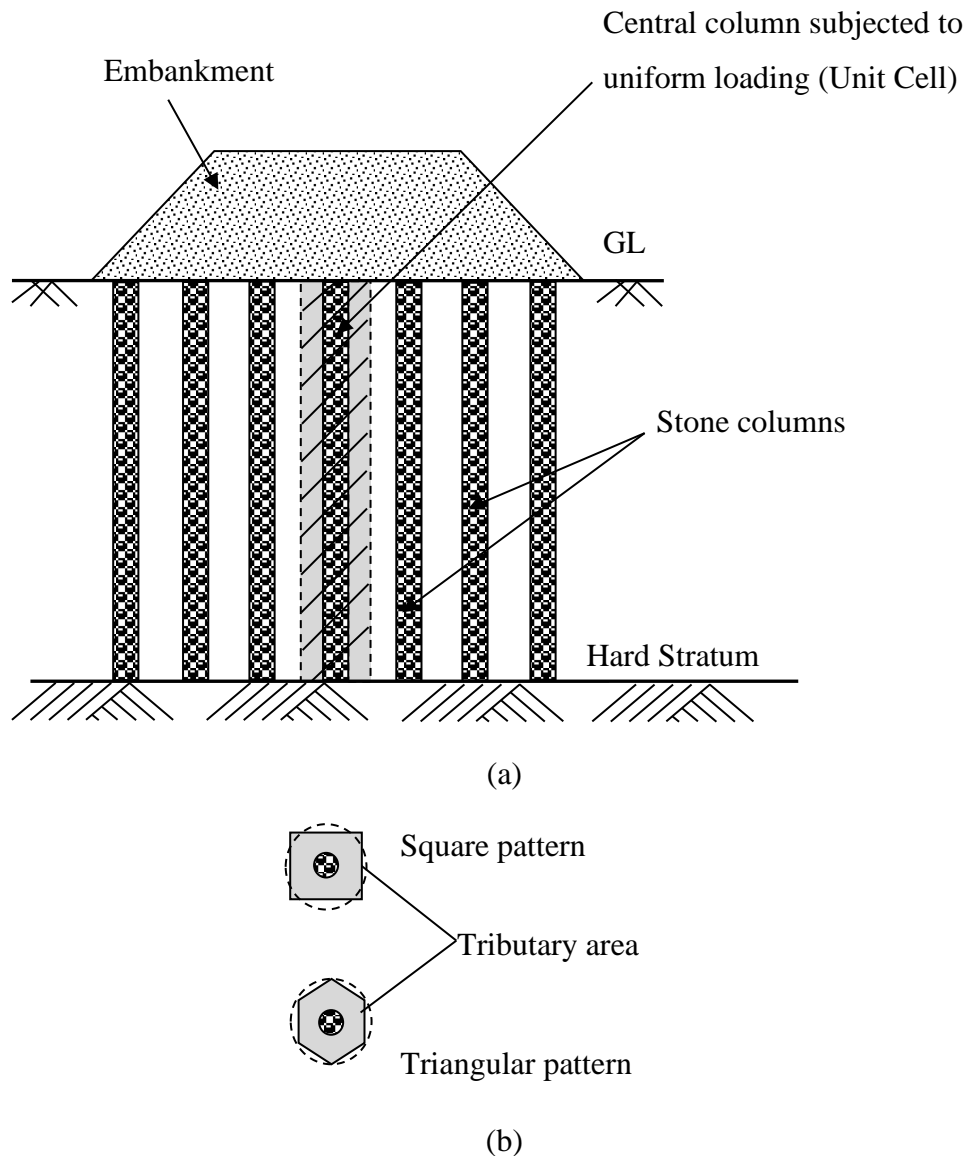
Fig. 2.11 Arrangement of stone columns in field (a) unit cell concept and (b) tributary area around the stone column and the equivalent circle

Debnath and Dey (2017) conducted series of laboratory model tests on an unreinforced sand bed (USB) and a geogrid-reinforced sand bed (GRSB) placed over a

41

group of vertically encased stone columns (VESC) floating in soft clay, and their numerical simulations were conducted. A steel tank of plan dimensions 1000 mm x 1000 mm and height 1000 mm was used for the test. All columns for the group tests were constructed in the clay bed with encasement and sand bed at the top. A rigid steel plate was used to apply the footing load. Three-dimensional numerical simulations were performed using a finite element package ABAQUS 6.12. In the finite element analysis, geogrid and geotextile were modeled as elastoplastic material.

The load carrying capacity of encased stone columns can be further increased by providing a geogrid reinforced sand bed over it. From the results, it is clear that, compared to unreinforced clay beds, an 8.45-fold increase in bearing capacity was observed with the provision of a geogrid reinforced sand bed over vertically encased stone columns. The optimum thickness of the unreinforced sand bed and the geogrid reinforced sand bed was found to be 0.2 times and 0.15 times the diameter of the footing. A considerable decrease in bulging of columns was also noticed by providing a geogrid reinforced sand bed over the encased stone column. Both the improvement factor and stress concentration ratio of the encased stone column with geogrid reinforced sand bed showed an increasing trend with an increase in the settlement. It was observed that the optimum length of stone columns and the optimum depth of encasement of the group of floating encased stone columns with the geogrid reinforced sand bed are six times and about three times the diameter of the column, respectively.

Chen et al. (2015) conducted large-scale triaxial tests on ordinary stone columns and uniaxial tests on geotextile encased stone columns. In soft soils where surrounding soil pressure is low, especially in the top section, the stone columns may be close to a uniaxial compression state. The uniaxial compression strength controls the bearing capacity of the stone columns. The test results show that the uniaxial compressive strength of the encased stone columns is affected mainly by the tensile strength of the encasing geotextiles. The stress-strain curves of the encased stone columns under uniaxial loading conditions are nearly linear before failure, which is similar to the tensile behavior of the geotextiles.

Das and Deb (2018) conducted laboratory model tests and three-dimensional (3D) numerical analysis (using FLAC3D) on stone column–improved ground under

embankment loading. In the numerical analysis, the stone column and the sand embankment were represented with the Mohr-Coulomb model, whereas the modified Cam-clay model was used for the soft clay. It was observed that to ensure no differential settlement on the embankment surface, a minimum embankment height of 2 times the clear spacing between the stone columns is necessary. The maximum lateral deformation of the stone column was observed at approximately 2.5 times the diameter of the column from the top.

Hamidi and Lajevardi (2018) conducted laboratory tests on stone columns with various gravels, such as mixed gravels with steel fibers, different distributions, and particle shapes. Stone columns with a gravel mattress on top and encased by ordinary geotextile were also tested. They observed that using the mattress, geotextile, and steel-fiber reinforcements enhances the load-carrying capacity of columns.

### 2.4.3   Numerical Studies on Encased Stone Columns

Castro (2017) carried out, set of systematic 2D and 3D finite element analyses to check the performance of groups of encased stone columns beneath a rigid footing. Based on the numerical analyses, he concluded that, if the area replacement ratio, i.e., area of the columns over the area of the footing, and the ratio of encasement stiffness to column diameter are kept constant, the column arrangement (both number of columns and column position) has a small influence on the settlement reduction achieved with the treatment.

He also proposed a new simplified approach to study groups of encased stone columns, converting all the group columns beneath the footing in just one central column with an equivalent area and encasement stiffness. The simplified model for fully encased columns in a homogeneous soil is used to conclude that, for settlement reduction, there is a column critical length of around two or three times the footing width.

Deb and Behera (2017) developed a mathematical formulation to determine the consolidation rate of stone column-improved ground due to radial flow, considering a change in the permeability and compressibility of soft soil during the equal strain approach. He observed that the degree of consolidation due to change in stress

concentration ratio and diameter ratio reduces when variable soil properties are considered. Depending on the soil properties, the time required to achieve a 90% degree of consolidation increases or decreases by around 50%–100%.

Mehmet (2017) studied the settlement behavior of a geosynthetic-reinforced and geosynthetic-encased stone column supported embankment on soft soil. Numerical analyses were carried out using a PLAXIS 2D-2012 finite element model to investigate the effect of reinforcement and encasement on the vertical displacement of stone columns and soft soil. An axisymmetric finite element unit cell model with fifteen-nodded triangular elements was used for the analysis. The stone column and the embankment fill were modeled using a linear elastic perfectly plastic model with Mohr-Coulomb failure criterion and soft soil using a Cam Clay model. The geosynthetics used for both basal reinforcement and encasement were modeled as linear elastic material with axial stiffness.

From the analysis results, they concluded that, with the help of base reinforcement, a significant settlement reduction of soft soil could be obtained. The stiffness of the reinforcement does not have a considerable effect on the settlement behavior of GEC.

Benmebarek et al. (2017) carried out numerical analyses using Plaxis 2D code in axisymmetric model to evaluate the influence of stone column installation effects on the loading–settlement performance of circular footing supported by a small group of columns. By considering both effective horizontal stresses and soil stiffness improvements due to column installation, more settlement improvement is obtained, and the improvement is more pronounced for high footing loading.

## 2.5 SUMMARY

After reviewing various works reported in the literature, the following limitations and future scope in studies related to geocell reinforced soil are listed.

In the present construction scenario, these cellular confinement systems have a wide variety of geotechnical applications. The three-dimensional honeycomb shape of geocells contributes to the load carrying capacity and stiffness of the structure, and also surface characteristics play a major role in the strength improvement. So there is a need

to accurately model geocells and to study the suitability of using different elements available in various software programs by considering the actual stress-strain response of geocells under loading. Giving actual field conditions and stress state in the analysis makes it possible for geotechnical practitioners to implement the field results without scaling directly.

Even though numerous time-dependent studies on the individual use of encased stone columns and geocells on embankment construction are available, limited reviews are available on the combined application of encased stone columns and geocells. Most of the early researchers adopted the equivalent composite approach method for numerical analysis, where two-dimensional modeling was done by considering geocell reinforced soil as an equivalent soil layer with modified parameters obtained from either theoretical calculations or experimental works. Few researchers modeled geocell and infill soil separately using the appropriate constitutive models. A review of numerical studies has shown a lack of models like Modified Cam Clay (MCC), which can model volume changes in soft soils more realistically than Mohr-Coulomb or Drucker Prager. In this research, geocell-sand mattress's effectiveness as a load transfer platform in encased stone column supported embankment was investigated by carrying out time-dependent 3D coupled analyses. Also the geocell and infill soil modeled separately using the appropriate constitutive models and Modified Cam Clay (MCC) is used for foundation soil.

# CHAPTER 3

# FINITE ELEMENT TECHNIQUES

## 3.1 GENERAL

The finite element method (FEM) is a powerful analysis tool that can handle various problems in geotechnical engineering. The complexity in material behavior, such as nonlinear stress-strain relationships, non-homogeneity, etc., and different hydraulic boundary conditions of soils can be easily simulated by this method. The mathematical solutions for various field problems were based on simplified assumptions which are not appropriate for real soil behavior. In such situations, numerical methods are identified as the best option to obtain acceptable solutions.

In this chapter, the fundamentals of finite element techniques, equilibrium equations, constitutive models, analysis techniques, details of the numerical model developed for the present investigation, and validation of the numerical model against published literature are described.

## 3.2 FINITE ELEMENT METHOD (FEM)

The fundamental concept of the finite element method is the discretization and assembling of finite elements. The whole body of structure to be analyzed is divided into tiny components called elements in the finite element method. Nodes connect these elements at the common boundaries. The elements can be one, two, or three-dimensional. These finite elements are analyzed individually to get the equations and then combined to formulate the solutions for the whole body. To obtain the full features of FEM analyses, the material properties, constitute equations, and boundary conditions are to be correctly defined and modeled.

The step by step procedure involved in FEM analyses is given below,

*a. Discretisation of the Domain*: The first step in the FEM analyses is discretizing the domain or the whole body, which is to be analysed into sub-regions or finite elements, as shown in Fig 3.1. These finite elements are interconnected by discrete points known

as nodes. The nodes are equally spaced if the physical structure has uniform geometry, material properties, and loading conditions. On the other hand, a non-uniform spacing of nodes is observed in a discontinuity in the domain. Though a small, larger number of elements increases the accuracy of the final solution, the computation time will be more in such cases. The number of elements is chosen based on the accuracy required, element size, and computational time. The displacements at the nodal points due to the applied load are the primary unknowns.



FEM

Domain                                                    Mesh
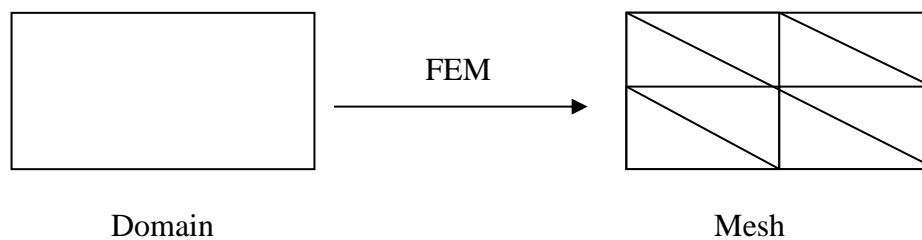
Fig 3.1 Discretisation of the domain

*b. Selection of Interpolation Functions*: After discretization, the next step is selecting a simple function to approximate the solution of each finite element. These functions are called interpolation/approximating functions or displacement functions. Generally, polynomials are selected as interpolation functions since it is the simplest form of a continuous function. The accuracy of the results can be improved by increasing the order of polynomials. Polynomials with infinite order give the exact solution. With finite order, it corresponds to approximate results. The polynomial function should maintain continuity along the boundary of elements.

*c. Derivation of the Stiffness Matrix:* A set of equilibrium equations for each element is obtained based on any one of the following principles; the variational principle of mechanics, principle of minimum potential energy, or principle of virtual work. From the set of equations obtained, the load-displacement relationship is established between the stiffness of the element, the load applied, and the displacements as,

$$[k]\{u\} = \{f\} \tag{3.1}$$

The equilibrium equations are written in matrices as in Equation 3.1 at the element level. In the equation, [k] is the element stiffness matrix consisting of the coefficients of the equilibrium equation derived from the material and the geometrical properties of

48

the element, representing the resistance of the element to deformation when subjected to loading. {u} is the nodal displacement vector, and {f} is the nodal force vector. Since the material properties are defined for individual elements, it is possible to account for non-homogeneity by assigning different material properties for different parts without much additional computational effort. This equation can be solved mathematically by the matrix inversion method.

*d. Assembling the element equations:* The overall or global stiffness matrix is formed for the whole body from the individual stiffness matrices for various elements. Assembling the individual stiffness matrix is based on the nodal connectivity that ensures the displacements at a node to be the same for all the elements connected to that node. The overall equilibrium equation is then written as,

$$[K]\{U\} = \{f\} \tag{3.2}$$

All the terms are as Equation 3.1 but for the whole body, i.e., global equilibrium equations.

*e. Imposing Boundary Restraints:* The global equilibrium equations will show singularity and cannot be solved until a sufficient number of boundary restraints are applied to the system to remove rigid body modes. In the global equations, the necessary boundary restraints are imposed by appropriate modifications in the equilibrium equations.

*f. Solutions for the Unknown Displacements:* The equations are solved for the unknown displacements. In linear equilibrium problems, it is directly solved by matrix techniques. For nonlinear problems, the desired solutions are obtained iteratively by a sequence of steps, each involving modifying the stiffness matrix and load vector.

*g. Computation of Element Stresses and Strains:* In general, the strains are computed as the derivatives of the displacements within the element. Then the stresses in the element are calculated from the strains using an appropriate constitutive equation.

### 3.2.1 Advantages of FEM

- A wide variety of engineering problems can be solved, such as; Solid Mechanics, Dynamics, Heat problems, Fluids, and Electrostatic problems

- The actual behavior of soil by considering the complex geometry can be analyzed
- Complicated boundary conditions and loading can be handled

### 3.2.2 Disadvantages of FEM

- The solutions obtained are approximate, not exact
- Since the finite element method makes a large amount of data, electronic computation is inevitable

## 3.3 FINITE ELEMENT SCHEME OF THE PRESENT STUDY

When the foundation soil is subjected to embankment weight, excess pore pressures develop and the soil undergoes initial settlement. The pore water then flows from regions of higher excess pore pressure to regions of lower excess pore pressure. As this dissipation takes place, foundation soil settles and finally reaches a final settlement. This process was first investigated by Terzaghi (1925) for one dimensional condition. The real soil behaviour is time related with the pore pressure response dependent on soil permeability, the rate of loading and the hydraulic boundary conditions. To account for such behaviour, it is necessary to combine the equations governing the deformation of the soil due to loading. Such a theory is called ***coupled***, as it essentially couples pore fluid flow and stress strain behaviour together. This results in both displacement and pore fluid pressure degrees of freedom at the nodal points. If the soil skeleton is rigid, the soil cannot deform and the coupled equations reduce to the steady state seepage equations. Biot (1941) extended Terzaghi's theory to three dimensional conditions for a more generalised condition in which both the displacements and the pore pressures are coupled and the constitutive relations include the compressibility of the fluid. The global equilibrium equations are modified to,

$$\begin{bmatrix} k & L \\ L^T & -\Phi\Delta t \end{bmatrix} \begin{Bmatrix} u_{t+\Delta t} \\ \pi_{t+\Delta t} \end{Bmatrix} = \begin{Bmatrix} f_{t+\Delta t} \\ v_{n_{t+\Delta t}} \end{Bmatrix} \tag{3.3}$$

Here, [k] is the stiffness matrix of the soil, [L] is the interaction term between the soil, and pore fluid, [Φ] is the matrix governing the dissipation of pore fluid, $u_{t+\Delta t}$

is the nodal displacement vector, $\pi_{t+\Delta t}$ is the nodal pore pressure vector, $f_{t+\Delta t}$ consists of the incrementally applied load terms and $v_{n_{t+\Delta t}}$ consists of load term corresponding to seepage forces on the boundary.

## 3.4 INTERPOLATION POLYNOMIALS (SHAPE FUNCTIONS)

The values of the displacement computed at the nodes approximate the values at non-nodal points (any point within the element) by interpolating the nodal values.

$$\{u\} = \sum N_{u_i} a_i^e = \left[ N_{u_i}, N_{u_j}, ...... \right] \begin{Bmatrix} a_i \\ a_j \\ . \end{Bmatrix} = [N_u]\{a^e\} \qquad (3.4)$$

where $\{u\}$ is the displacement vector at any point (x,y), $[N_u]$ is the shape function matrix which represents the variation of the quantities, in this case, displacements across an element, and $\{a^e\}$ is the vector of nodal displacements for a particular element. For a continuum divided into elements in two-dimensional space with two displacement degrees of freedom at node 1, the different displacement vectors can be written as follows,

$$\{u\} = \begin{Bmatrix} u(x,y) \\ v(x,y) \end{Bmatrix} \qquad \{a_i\} = \begin{Bmatrix} u_i \\ v_i \end{Bmatrix} \qquad (3.5)$$

For a coupled element, $[N_\pi]$ is the pore fluid pressure interpolation function matrix, similar to $[N_u]$. If an incremental pore fluid pressure degree of freedom is assumed at each node of every consolidating element, $[N_\pi]$ is the same as the matrix of displacement shape functions $[N_u]$. Consequently, pore fluid pressures vary across the element in the same fashion as the displacement components. The variation can be achieved only by having a pore fluid pressure degree of freedom at the corner nodes (Fig. 3.2). This will result in the $[N_\pi]$ matrix having contributions only from the corner nodes, differing from $[N_u]$.



Displacement DOF

Displacement + Pore fluid pressure DOF
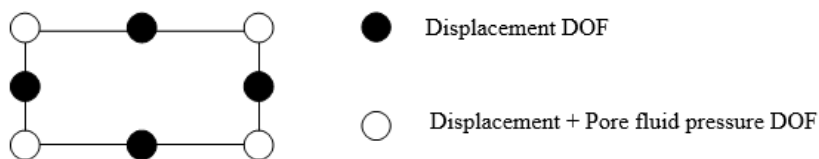
Fig. 3.2 Coupled pore pressure element

For a six-noded triangular element, pore fluid pressure degrees of freedom are available only at the three apex nodes. In the case of a 20 noded three-dimensional element, pore pressure degrees of freedom are available at the eight corner nodes.

## 3.5 COMPUTATION OF STRAINS

The strains are obtained as the first derivatives of displacements for small strain problems. Once the nodal displacements are computed, the strains at any point can be obtained as follows,

$$\{\varepsilon\} = [L]\{u\} \tag{3.6}$$

here, $[L]$ is a matrix of a suitable linear operator. Using Equation 3.4 for the displacements, the strains within an element can be written as,

$$\{\varepsilon\} = [L]\{u\} = [L][N_u]\{a^e\} = [B]\{a^e\} \tag{3.7}$$

The matrix $[B]$ is defined as the product of $[L]$ and $[N_u]$ matrices. Problems in which the geometry, loadings, boundary conditions, and materials are symmetric with respect to the vertical axis can be modeled using axisymmetric idealization. An additional strain in the circumferential direction ($\varepsilon_\theta$- hoop strain) is considered, and the strain vector is written as follows,

$$\varepsilon = \begin{Bmatrix} \varepsilon_r \\ \varepsilon_z \\ \varepsilon_\vartheta \\ \varepsilon_{rz} \end{Bmatrix} = \begin{Bmatrix} \dfrac{\partial u}{\partial r} \\ \dfrac{\partial v}{\partial z} \\ \dfrac{u}{r} \\ \dfrac{\partial u}{\partial z} + \dfrac{\partial v}{\partial r} \end{Bmatrix} \tag{3.8}$$

The $[B]$ matrix for axisymmetric conditions can be written as follows,

$$[B] = [L][N_u] = \begin{bmatrix} \dfrac{\partial N_{u_1}}{\partial r} & 0 & \dfrac{\partial N_{u_2}}{\partial r} & 0 & .... \\[2ex] 0 & \dfrac{\partial N_{u_1}}{\partial y} & 0 & \dfrac{\partial N_{u_2}}{\partial y} & .... \\[2ex] \dfrac{N_{u_1}}{r} & 0 & \dfrac{N_{u_2}}{r} & 0 & .... \\[2ex] \dfrac{\partial N_{u_1}}{\partial y} & \dfrac{\partial N_{u_1}}{\partial r} & \dfrac{\partial N_{u_2}}{\partial y} & \dfrac{\partial N_{u_2}}{\partial r} & .... \end{bmatrix} \tag{3.9}$$

## 3.6   COMPUTATION OF STRESSES

The stresses $\{\sigma\}$ are computed from the strains as follows,

$$\{\sigma\} = [C]\{\varepsilon\} \tag{3.10}$$

here, [C] is the constitutive matrix relating the stresses and strains, $\{\varepsilon\}$ is the strain vector. The constitutive matrix/ material stiffness matrix determining the material stress-strain behavior is given as:

$$C = \frac{E}{(1-2v)(1+v)} \begin{bmatrix} 1-v & v & v & 0 & 0 & 0 \\ v & 1-v & v & 0 & 0 & 0 \\ v & v & 1-v & 0 & 0 & 0 \\ 0 & 0 & 0 & \dfrac{1}{2}-v & 0 & 0 \\ 0 & 0 & 0 & 0 & \dfrac{1}{2}-v & 0 \\ 0 & 0 & 0 & 0 & 0 & \dfrac{1}{2}-v \end{bmatrix} \tag{3.11}$$

where $E$ and $v$ are Young's modulus and Poisson's ratio, respectively.

## 3.7   CONVERGENCE CRITERIA FOR ELEMENTS

The numerical solution of a finite element method converges to an exact solution under certain circumstances (Melosh 1961; Johnson and McLay 1968; Bathe 2006). The increase in the degrees of freedom and finer subdivision of the finite element mesh will not always converge. The displacement fields should satisfy the below-mentioned criteria;

- The displacement function should be continuous within the element. This can be achieved by selecting polynomials as shape functions.

- The approximate function should provide inter-element compatibility upto the degree required by the problem. In other words, the approximate function is selected so that the nodal displacement between the adjacent nodes is the same.

- The displacement model should consider the rigid body motion of the model. The nodal displacement corresponds to rigid body motion cause zero strain and zero nodal forces. The shape function should not permit the straining of an element to occur under rigid body motion. The constant term in the polynomial function accounts for the constant strain state.

- When the finite element is subdivided into an infinitesimal size, the strain rate is approximately constant throughout the model. That is, they are isotropic for generalized coordinates. The shape of the displacement function is constant irrespective of the change in the local coordinate system.

## 3.8   NUMERICAL INTEGRATION TECHNIQUES

To develop the finite element equations, the ordinary/partial differential equations must be restated in an integral form called the weak form. A weak form of the differential equations is equivalent to the governing equation and boundary conditions, i.e. the strong form. When computing integrals over general domains, numerical methods are used. The simplest of these procedures are the trapezoidal and Simpson's rules for the integration of areas. These integration rules are exact for linear and cubic functions, respectively. For the evaluation of higher-order functions, many sampling points have to be considered to minimize the errors. The major drawback of these procedures is that the number of sampling points cannot be decided prior to obtaining the exact value of the integrand.

The integration technique popularly used in finite element is Gauss quadrature. The entire integration range is divided into small segments and Gauss quadrature is applied to each segment. Gauss quadrature uses the function values evaluated at a number of interior points and corresponding weights to approximate the integral by a weighted sum. For n sampling points, there are 2n unknowns, so the order of

polynomials that can be integrated exactly with n sampling points is 2n-1. Reduced integration uses a lesser number of Gaussian coordinates when solving the integral. The more Gaussian coordinates, the more accurate the results will be.

## 3.9    CONSTITUTIVE MODELLING

The actual stress-strain behavior of soil can be modeled with constitutive relationships in the finite element method. The various factors that depend upon constitutive relationships are density, water content, drainage conditions, strain or creep conditions, duration of loading, stress histories, confining pressure, etc. Different constitutive models available for modeling the soil are linear elastic, non-linear elastic, hyperelastic, bilinear, hyperbolic, Rarnberg Osgood model, Drucker-Prager model, Cap model, Cam Clay model, Modified Cam Clay model, soft soil creep model, strain hardening model, hysteretic model, etc.

Elastic strains are developed when an elastic material is subjected to loading. The elastic strains are estimated by Hooke's law which is based on elasticity theory. The material recovers to undeformed conditions upon removal of external loading. But in the case of plastic material, on the removal of load, the elastic strains are recovered, whereas plastic strains are irreversible. The estimation of plastic strains is based on plasticity theory.

The behavior of materials like concrete, soil, and polymer, which, when subjected to load, exceeds the elastic limit, is evaluated based on plasticity theory. So, in the field of geotechnical engineering, plasticity models are of greater importance. A plasticity model consists of (1) a yield criterion that predicts whether the material should respond elastically or plastically due to a loading increment, (2) a strain-hardening rule that controls the shape of the stress-strain response during plastic straining, and (3) a plastic flow rule that determines the direction of the plastic strain increment caused by a stress increment.

In the present investigation, the Mohr-Coulomb model and Modified Cam Clay model were used to describe the stress-strain behavior of sand and soft soil. The details of constitutive models are given below.

### 3.9.1 Mohr-Coulomb Model

Mohr-Coulomb model is an elastic- perfectly plastic model used to model soil behavior. Fig. 3.3 (a) shows that in the general stress state, the Mohr-Coulomb model behaves linearly in the elastic range, with two defining parameters from Hooke's law (Young's modulus, E and Poisson's ratio, $\nu$). In stress space the boundary of the yield criterion defines a surface, the so-called yield surface. A yield surface is generally a convex, smooth, closed surface in stress space that bounds stress states that can be reached without initiating plastic strains. As a matter of convenience, the yield surface is mathematically represented by a scalar yield function f = 0 that is taken as the yield criterion. If f < 0, the stress state lies inside the yield surface and corresponds to purely elastic response. Finally, the condition f > 0 represents inaccessible states. For Mohr-Coulomb model, the two parameters that define the failure criteria are the friction angle ($\phi$) and cohesion (c). Dilatancy angle ($\psi$) describes the flow rule, which models a realistic irreversible change in volume due to shearing.

The general equation for the constitutive model is as follows,

$$\tau_f = c + \sigma_f \tan\phi$$

(3.12)

Where $\tau_f$ is the shear stress at failure, $\sigma_f$ is the effective normal stress, c and $\phi$ are the shear parameters of the soil.

The Mohr–Coulomb yield surface is a cone with a hexagonal cross section in three-dimensional deviatoric stress space as shown in Fig. 3.3(b).



(a)                                          (b)
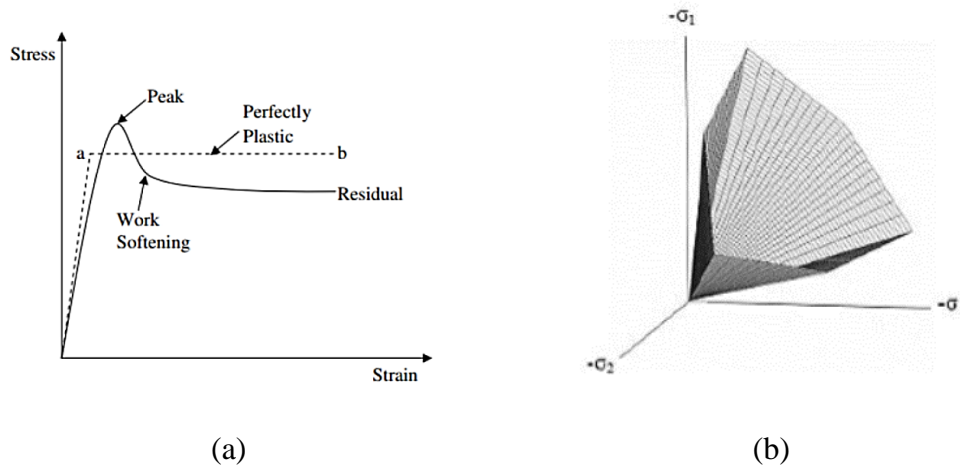
Fig. 3.3 Mohr-Coulomb model (a) stress-strain graph and (b) yield surface in principal stress space (Ti et al. 2009)

56

The Mohr-Coulomb model has several limitations also. The model works well in drained conditions, but the effective stress path significantly varies with the observations for undrained materials. Hence, it is preferable to use undrained shear parameters in the case of undrained analysis. The stiffness behavior before reaching the local shear is poorly modeled in the Mohr-Coulomb model. Also, for perfect plasticity, the Mohr-Coulomb model does not include the strain hardening or softening effect.

### 3.9.2 Modified Cam Clay Model (MCC)

The soft soil behavior can be modeled using the Modified Cam Clay model (MCC) developed by researchers at the Cambridge University based on critical state theory. The main features of the model are the use of an elastic model (either linear elasticity or the porous elasticity model, which exhibits an increasing bulk elastic stiffness as the material undergoes compression) and for the inelastic part of the deformation a particular form of yield surface with associated flow and a hardening rule that allows the yield surface to grow or shrink. A key feature of the model is the hardening/softening concept, which is developed around the introduction of a "critical state" surface. It is defined as the locus of effective stress states where unrestricted, purely deviatoric, plastic flow of the soil skeleton occurs under constant effective stress.

The basic assumption of the model is that when a soil sample is consolidated under isotropic conditions, the void ratio; e is varied linearly as a function of the logarithm of effective stress, $p'$. Also, the unloading and reloading behavior of soil in the e- $\log p'$ plane represents straight lines that are more realistic for normally consolidated clays. The yield surface of the MCC model in the $p'$-q plane forms an ellipse, as shown in Fig. 3.4. The yield surface equation is given by,

$$\frac{q^2}{p'^2} + M^2\left(1 - \frac{p'_c}{p'^2}\right) = 0 \tag{3.13}$$

where, $p'_c$ is the pre-consolidation pressure and this parameter controls the hardening behavior of soil, M is the slope of the critical state line, $p'$ is the mean effective stress and q is the shear stress.
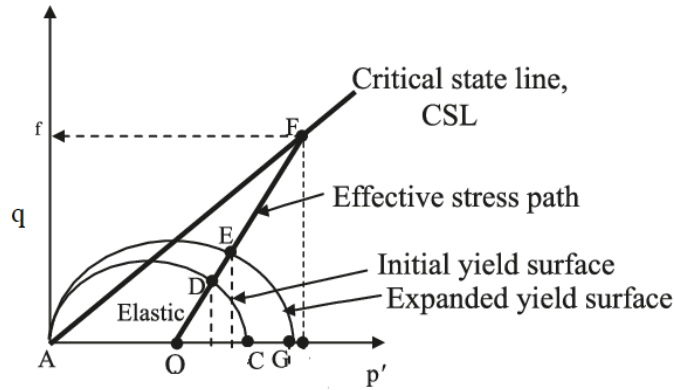
Fig 3.4 Yield surface of a modified Cam clay model in the q–p′ plane.

The soil is elastic till the stress state ($p′$, q) touches the yield surface, and after that, the soil exhibits plasticity properties. The input parameters for the MCC model are,

*a.* *Critical state stress ratio* (M)

The slope M of the critical state line is calculated from the internal friction angle ϕ obtained from the undrained triaxial test using the equation below,

$$M = \frac{6\sin\phi}{3-\sin\phi}$$
(3.14)

*b.* *Logarithmic hardening constant for plasticity* (λ)

The slope λ, of loading curve at e- $\ln p′$ plane is an important parameter of the MCC model and is related to compression index, $C_c$ obtained the one-dimensional compression tests in the oedometer by the following equation,

$$\lambda = \frac{c_c}{\ln 10} = \frac{c_c}{2.3}$$
(3.15)

*c.* *Logarithmic bulk modulus for elastic material behavior* (κ)

The slope κ of reloading line at e- $\ln p′$ plane is related to swelling index, $C_s$ as follows,

$$\kappa = \frac{c_s}{\ln 10} = \frac{c_s}{2.3}$$
(3.16)

### 3.9.2.1    *Modified Cam Clay Model formulations*

Roscoe and Burland (1968) assumed that the work done on a soil specimen by a load $(q, p')$ is given by,

$$dW = p'd\varepsilon_v^p + qd\varepsilon_s^p \qquad (3.17)$$

$d\varepsilon_\upsilon^p$ is the plastic volumetric strain increment and $d\varepsilon_s^p$ is the plastic shear strain increment. The associated flow rule is defined as,

$$\frac{d\varepsilon_v^p}{d\varepsilon_s^p} = \frac{M^2 - \eta^2}{2\eta} \qquad (3.18)$$

where $\eta = q/p'$ and $\eta = M$ when $q = q_f$, $p' = p_f'$ (at failure)

If the plastic volumetric strain increment is $d\varepsilon_\upsilon^p$, the elastic volumetric strain increment is $d\varepsilon_\upsilon^e$, the plastic shear strain increment is $d\varepsilon_s^p$ and the elastic shear strain increment is $d\varepsilon_s^e$; the total volumetric strain $(d\varepsilon_\upsilon)$ increment and total shear strain increment $(d\varepsilon_s)$ is given as,

$$d\varepsilon_v = d\varepsilon_v^e + d\varepsilon_v^p \qquad (3.19)$$

$$d\varepsilon_s = d\varepsilon_s^e + d\varepsilon_s^p \qquad (3.20)$$

The critical state theory assumes that $d\varepsilon_s^e = 0$. Thus $d\varepsilon_s = d\varepsilon_s^p$. Since all these equations were given in incremental forms, the load must be applied in small increments to get the corresponding strain increment. Volumetric and shear strain increments are found out using the following equations (Desai and Siriwardane1984), The plastic volumetric strain increment, $d\varepsilon_\upsilon^p$ is,

$$d\varepsilon_v^p = \frac{\lambda - \kappa}{1+e}\left(\frac{dp'}{p'} + \frac{2\eta d\eta}{M^2 + \eta^2}\right) \qquad (3.21)$$

The elastic volumetric strain increment, $d\varepsilon_\upsilon^e$ is,

$$d\varepsilon_v^e = \frac{\kappa}{1+e}\frac{dp'}{p'} \qquad (3.22)$$

Thus, the total volumetric strain increment $d\varepsilon_\upsilon$ is found by the equation,

$$d\varepsilon_v = \frac{\lambda}{1+e}\left(\frac{dp'}{p'} + \left(1 - \frac{\kappa}{\lambda}\right)\frac{2\eta d\eta}{M^2 + \eta^2}\right) \qquad (3.23)$$

The total shear strain $d\varepsilon_s$ is,

$$d\varepsilon_s = d\varepsilon_s^p = \frac{\lambda\text{-}\kappa}{1\text{+}e}\left(\frac{dp'}{p'} + \frac{2\eta d\eta}{M^2\text{+}\eta^2}\right)\frac{2\eta}{M^2\text{-}\eta^2} \qquad (3.24)$$

Comparing Eqns 3.24 and 3.23,

$$d\varepsilon_s = d\varepsilon_s^p = d\varepsilon_v \frac{2\eta}{M^2\text{-}\eta^2} \qquad (3.25)$$

## 3.10  FINITE ELEMENT PROGRAM USED IN THIS STUDY

The finite element program used in the present study was ABAQUS/CAE (2016). ABAQUS software can analyze both simple linear problems and complex non-linear structure problems. Also, the software is ideal for stress-pore pressure coupled analysis. The program has no built-in unit systems. So, the user must specify consistent units throughout the analysis process. Table 3.1 shows the SI unit system followed in the present study.

Table 3.1 Unit system used in the present study

| Quantity | SI | SI (mm) |
|----------|-----|---------|
| Length | m | mm |
| Force | N | N |
| Mass | kg | Tone ($10^3$ kg) |
| Time | s | s |
| Stress | Pa (N/m$^2$) | Mpa (N/mm$^2$) |
| Energy | J | mJ ($10^{-3}$ J) |
| Density | Kg/m$^3$ | tonne/mm$^3$ |

## 3.11  CASE STUDY CONSIDERED

A case study of geosynthetic encased stone column supported embankment reported by Yoo and Kim (2009) was used for modeling purposes. They have compared different finite element approaches for modeling an embankment constructed over a geosynthetic-encased stone column-reinforced ground.  The three models developed for the simulation were; an axisymmetric unit cell model, a 3D column model, and a full 3-dimensional model. The analysis of the stone column-supported embankment problem is truly a three-dimensional problem. Though the analyses give accurate results, carrying out full 3-dimensional analyses requires high computer memory and

60

analysis time. 2D analyses being computationally less intensive and the results comparable to full three-dimensional analyses, are widely used to model actual field problems (Yoo and Kim 2009; Khabbazian et al. 2010; Bhasi and Rajagopal 2015).When it comes to 2-dimensional axisymmetric analyses, even though the 2-d models cannot completely represent the realistic conditions, they are found to give sufficiently accurate results (Yoo and Kim 2009), which can be used for preliminary studies.

The embankment is 45 m wide and 6 m high, and it is constructed over a 10 m deep clay layer reinforced with 0.8 m diameter geosynthetic encased stone columns (GESC). The embankment geometry is shown in Fig. 3.5. The stone columns were placed in a square pattern at 2.4 m c/c spacing (S), giving an area replacement ratio of approximately 9.0 %. The groundwater level was set at the top of the clay layer. The stiffness of the geosynthetic material used for encasement was 2500 kN/m.
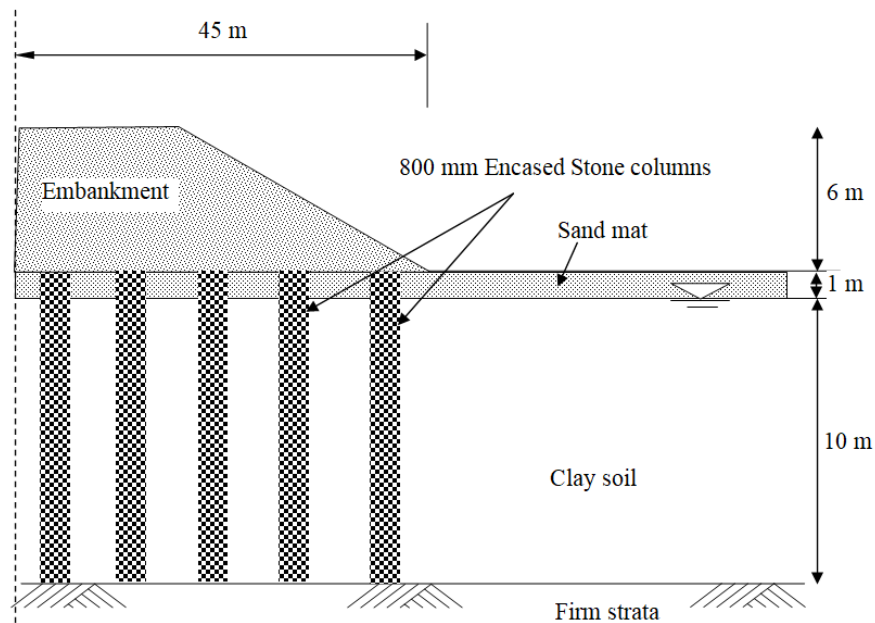


Fig. 3.5 Cross-section of GESC supported embankment (Based on Yoo and Kim 2009)

### 3.11.1 Models developed for the analyses

Three modeling approaches were considered a) an axisymmetric unit cell, b) a 3D Column model, and (3) a Full three-dimensional model.

*Unit Cell Concept*

Stone columns are usually arranged in a triangular or a square grid pattern, as shown in Fig. 3.6. For analysis purposes, it is convenient to consider a single stone column and the associated tributary area of the soil surrounding the stone column, as illustrated in Fig.3.6. Although the tributary area forms a square or regular hexagon around the stone column, it can be closely approximated as an equivalent circle having the same plan area. For a square pattern of column arrangement, the equivalent circle has an effective radius ($R_e$) of $0.564S$. For an equilateral triangle pattern, it is $0.525S$, where $S$ is the center-to-center spacing of the stone column.



|     |     |
| :-: | :-: |
| (a) | (b) |
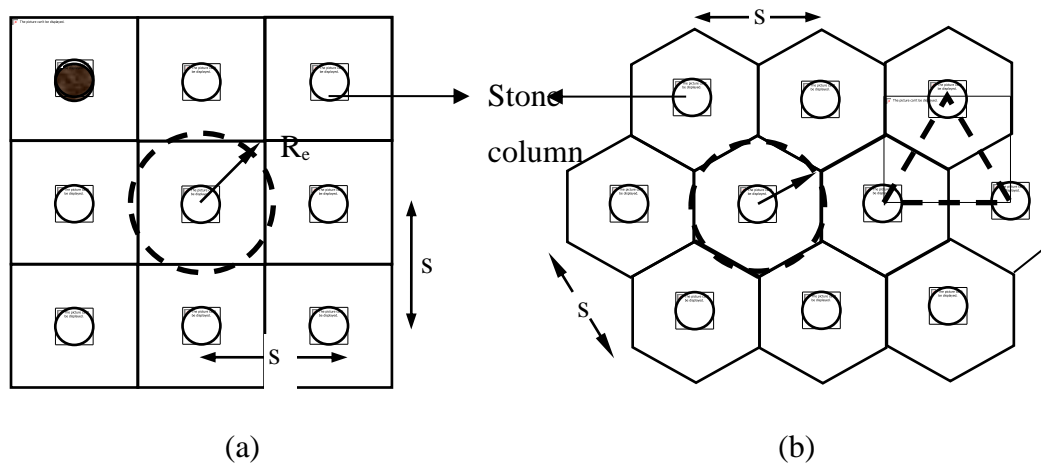
Fig. 3.6 Arrangement of stone columns in the field (a) square layout and (b) triangular layout

A unit cell approach represents the interior portion of an embankment away from the influence of side slopes. In the present study, for the 2-dimensional axisymmetric model, the diameter of the unit cell that corresponds to an area ratio of 9% was taken (Fig. 3.7 (a)), and a square portion with an area equal to that of the unit cell area was considered for the 3D column model (Fig. 3.7 (b)).
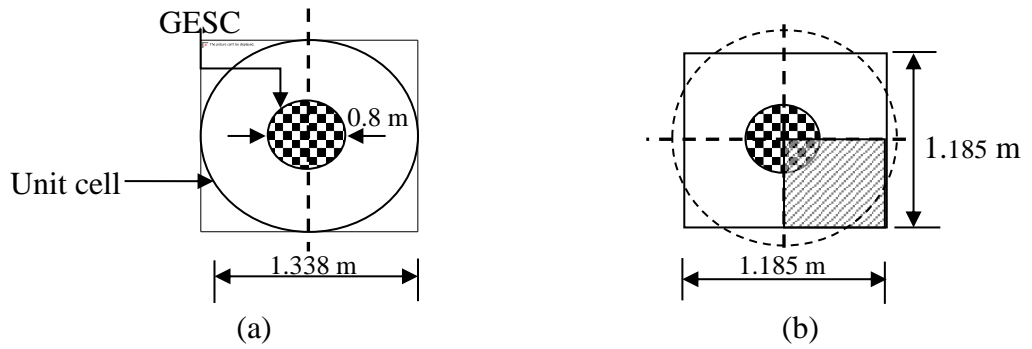
Fig. 3.7 Representation area for analyses (a) axisymmetric and (b) 3D column

Due to the symmetry, only one-quarter of the unit cell was modeled for axisymmetric and 3D column models. The developed models are shown in Figs. 3.8 (a) - (e).



(a)                                                         (b)
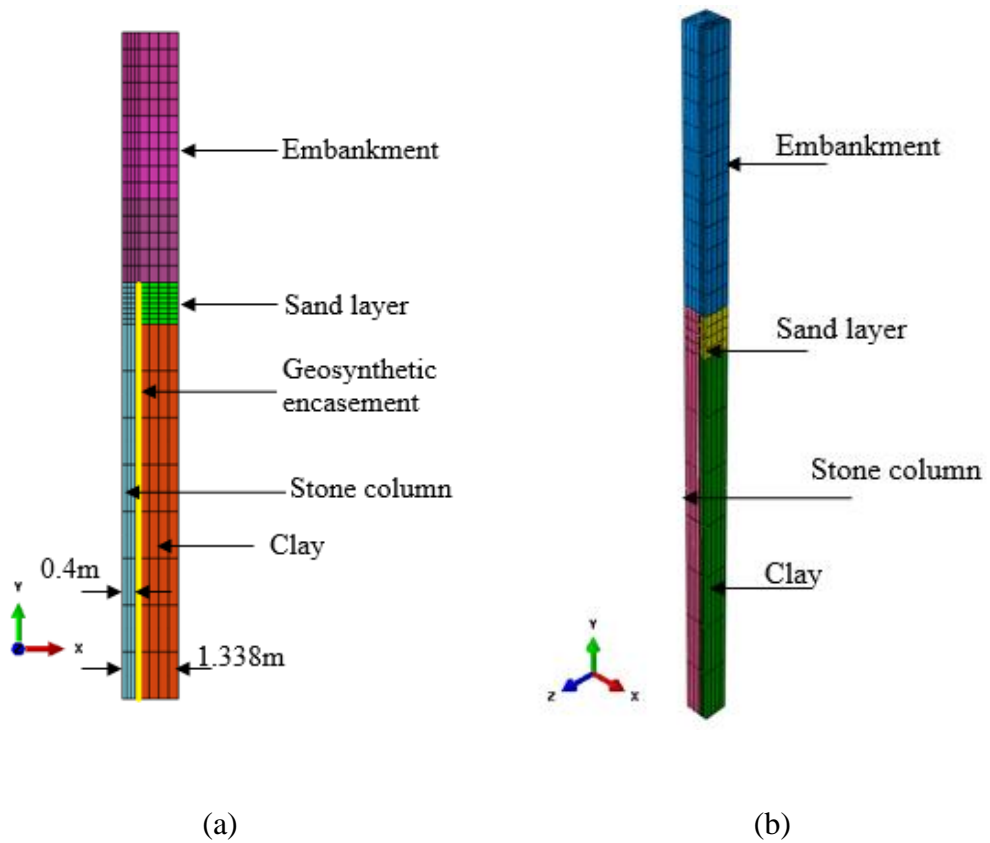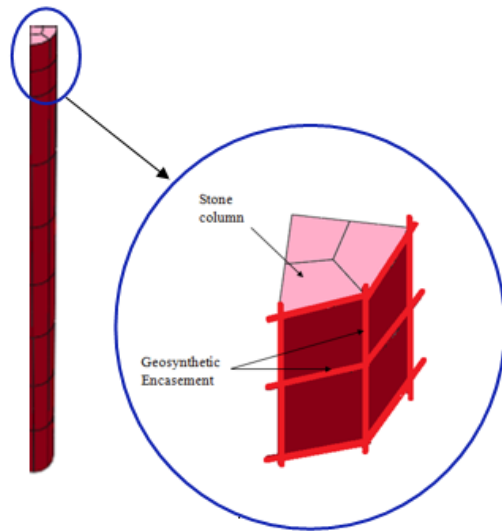
(c)
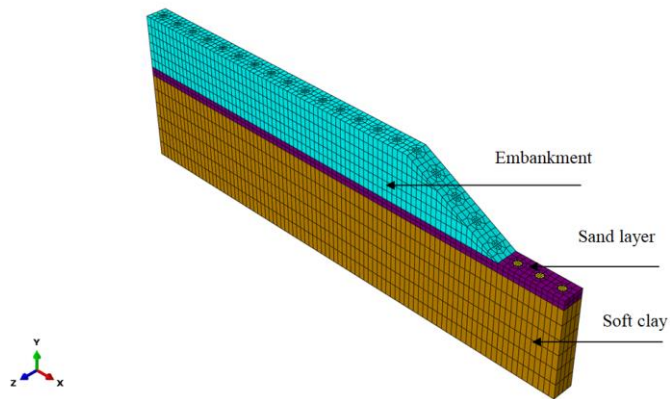


(d)
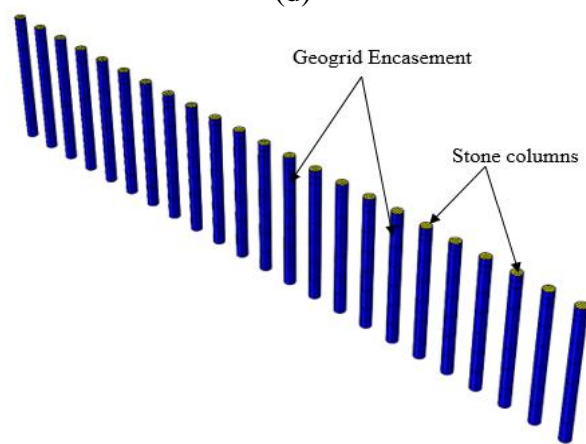


(e)

Fig. 3.8 Finite element models developed (a) axisymmetric model (b) 3D column model (c) geosynthetic encasement (3D) (d) full 3D model and (e) geogrid encased stone columns in full 3D

### 3.11.2 Constitutive models

The soft clay soil was modeled using the Modified Cam Clay model. A linear-elastic perfectly plastic Mohr-Coulomb model was used to simulate the embankment fill, sand layer, and stone columns. The geogrid was modeled as an isotropic linear elastic material. Table 3.2 summarizes the material properties used in the analyses.

Table 3.2 Material properties used in the analyses (Yoo and Kim 2009)

| Property | Clay | Stone column | Sand/Fill |
|---|---|---|---|
| Model used | Modified cam clay | Mohr–Coulomb | Mohr–Coulomb |
| Unit weight ($kN/m^3$) | 18 | 19 | 19 |
| Young's modulus (kPa) | - | 40000 | 15000 |
| Poisson's ratio, $\nu$ | 0.3 | 0.3 | 0.3 |
| Cohesion, c (kPa) | - | 5 | 3 |
| Friction angle, $\Phi$(degree) | - | 40 | 28 |
| Dilation angle, $\varphi$ | - | 20 | 10 |
| Critical state stress ratio, M | 1.0 | - | - |
| Logarithmic hardening constant for plasticity, $\lambda$ | 0.2 | - | - |
| Logarithmic bulk modulus for elastic material behavior, K | 0.02 | - | - |
| Initial yield surface size, $a_o$ (kPa) | 50 | - | - |
| Initial void ratio, $e_o$ | 1 | - | - |
| Permeability, k (m/s) | $1.2 \times 10^{-6}$ | $1.2 \times 10^{-2}$ | $1.2 \times 10^{-2}$ |

### 3.11.3 Boundary conditions

The model was fixed in horizontal directions on the vertical sides, and full fixity on the base was assumed. The vertical boundaries and the bottom surface were treated as impermeable boundaries. About the drainage boundary conditions, the water table was assumed to be at a depth of 1.0 m below ground level, and the initial pore pressures before the embankment construction are taken to be hydrostatic. A zero pore pressure boundary condition was applied at the top boundary of the clay layer to model the free drainage.

### 3.11.4 Elements used for meshing

The size of the mesh was decided based on several trial analyses with different numbers of elements. In axisymmetric and 3D column models, the meshes were arranged to have the same element size vertically to eliminate any possible errors arising from the mesh arrangement.

In the axisymmetric model, eight noded stress–pore pressure coupled axisymmetric elements CAX8RP (biquadratic displacement and bilinear pore pressure) were used to represent the clay layer and the stone column. Eight noded biquadratic axisymmetric quadrilateral elements (CAX8R) were used for the embankment fill. In the 3D column model and full 3D model, 20-nodedcoupled elements with reduced integration (C3D20RP) were used to represent the clay layer and stone columns, and 20- node stress only elements (C3D20R) were used for the embankment fill.

The geosynthetic reinforcement was modeled using the membrane elements MAX2 (A 3-node quadratic axisymmetric membrane) and M3D8R, respectively, in both the axisymmetric and the 3D modeling. The membrane elements are surface elements that offer strength in the plane of the element but have no bending stiffness. Membrane elements are particularly useful in modeling the geosynthetic encasement as they offer resistance against out-of-plane bulging. Membrane elements were used to wrap around the stone columns, as shown in Fig. 3.8(c). For axisymmetric membrane elements, the positive normal is defined by a 90° counterclockwise rotation from the direction going from node 1 to node 2 as shown in Fig 3.9. The top surface of a membrane element in the positive direction of the normal is called the SPOS face for

contact definition. The bottom surface in the negative direction along the normal is called the SNEG face for contact definition.
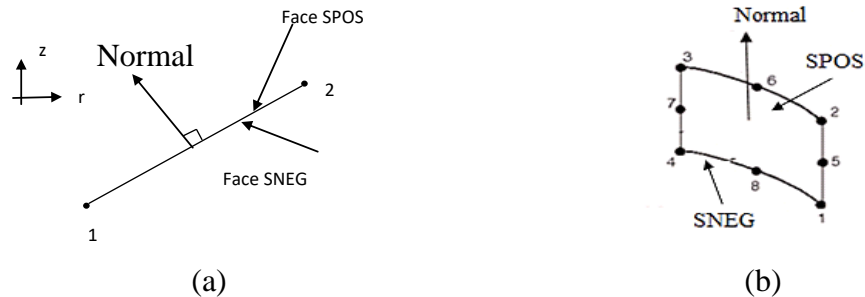


Fig. 3.9 Membrane elements for reinforcement modeling (a) axisymmetric and (b) 3D column

## 3.11.5 Contact

In the present study, the tied contact is used to model the interaction between the stone column and reinforcement. Tied contact constrains each of the nodes on the slave surface to have the same value of displacement and pore pressure as the point on the master surface that it contacts. The stiffer material acts as the master surface, and the flexible material acts as the slave surface.

## 3.11.6 Methodology

After establishing the initial geostatic stress and pore pressure distribution with appropriate boundary conditions, the stone columns and the geosynthetic reinforcement were installed by activating the corresponding elements. The effect of stone column installation was not considered in this thesis. The embankment construction was then simulated in three lifts, including the geosynthetic-reinforced layer, by adding layers of elements representing the embankment. Each embankment layer was constructed in 15 days, followed by a consolidation time of 10 days. When an embankment layer is added, it is situated on the deformed layer that was added earlier. As consolidation analysis was carried out in each step, settlements started immediately when the first embankment layer was constructed. After full placement of the embankment (6 m), the analysis was carried out until the excess pore water pressure fell below a specified near-zero value.

## 3.12 VALIDATION OF THE DEVELOPED MODELS

Numerical results from the analyses were compared with the published results of Yoo and Kim (2009) for an encased stone column supported embankment without a geogrid layer at the embankment base. The embankment height considered was 6 m. The lateral deformation of geogrid along the stone column depth obtained from the 2D axisymmetric analysis, 3D column, and full 3D analysis is presented in Figs. 3.10 -3.12.
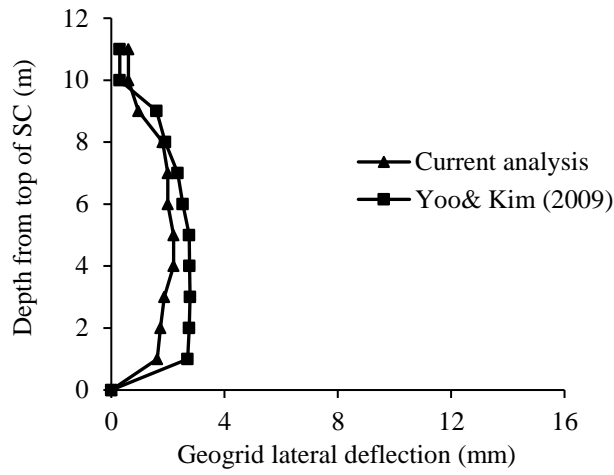


Fig. 3.10 Lateral deflection of GESC from the axisymmetric analysis
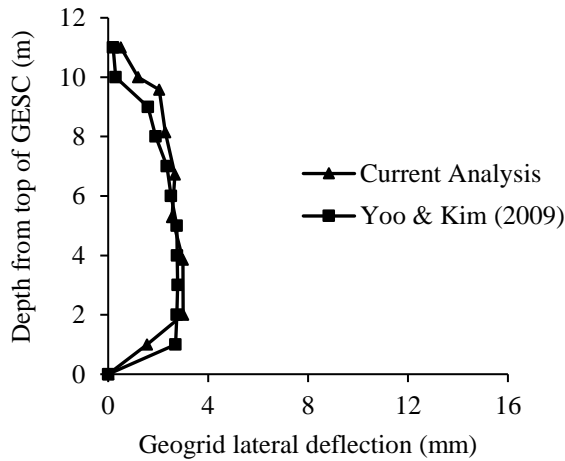


Fig. 3.11 Lateral deflection of GESC from the 3D column analysis

68
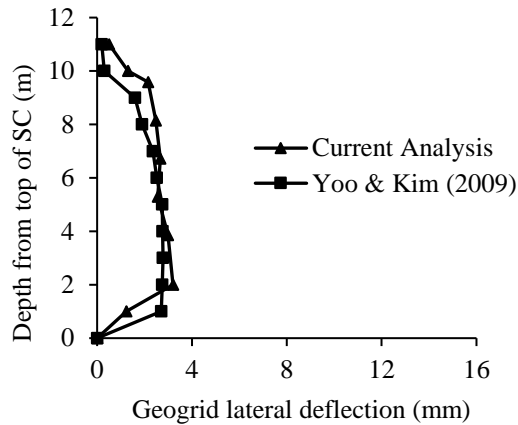
Fig. 3.12 Lateral deflection of GESC from the full 3D analysis

The bulging behavior of encased stone column obtained from the axisymmetric, 3D column and full 3D analysis results shows good agreement with the results of Yoo and Kim (2009).

The geosynthetic hoop strain profiles are shown in Figs. 3.13-3.15. Hoop strain is defined as the ratio of lateral deformation to the initial radius of the geosynthetic encasement. The geosynthetic hoop strains need to be accurately evaluated for a given loading condition to check the adequacy of the geosynthetic reinforcement in terms of rupture. Any numerical model evaluating the performance of GESC-reinforced ground needs to have the ability to predict the strains in the geosynthetic encasement correctly. Numerical results from the axisymmetric, 3D column and full 3-dimensional analyses follow the general trend of the deformation pattern and the strain profiles of the stone column given in Yoo and Kim (2009).
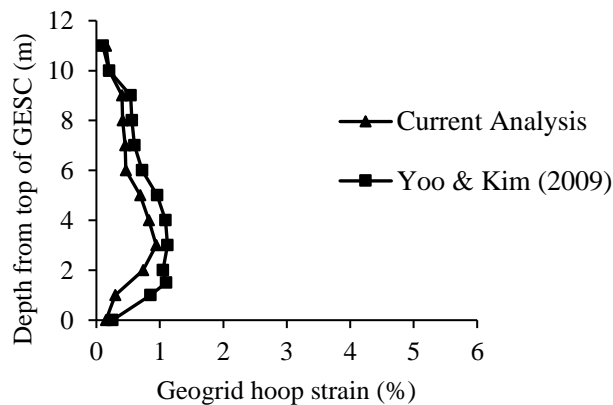


Fig. 3.13 Hoop strain in encasement from the axisymmetric analysis
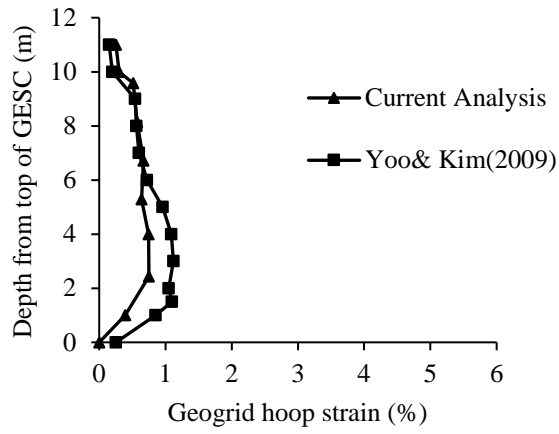
Fig. 3.14 Hoop strain in encasement from the 3D column analysis
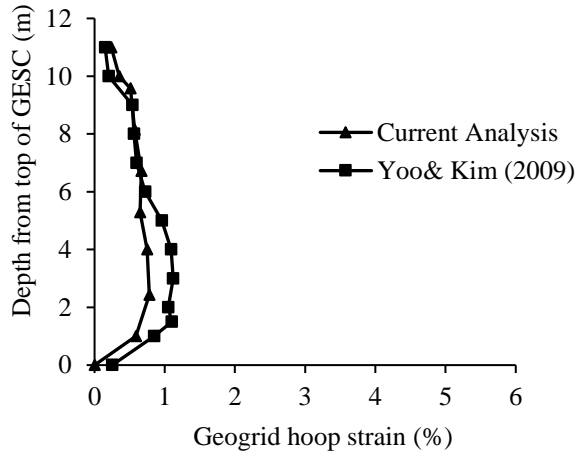


Fig. 3.15 Hoop strain in encasement from the full 3D analysis

# CHAPTER 4

# MATERIALS AND METHODS

## 4.1   GENERAL

Typical laboratory tests were conducted on model stone columns installed in lithomargic clay prepared in the laboratory under controlled conditions. The stone columns were subjected to vertical loading. The behavior of the ordinary stone columns (OSC), geogrid encased stone columns (GESC), encased stone columns with a horizontal layer of geogrid on the top, and a group of stone columns was studied mainly based on the pressure-settlement responses observed from the loading tests. Also, the bulging of the stone column was studied by examining the deformed shape after each test. All experiments were performed on a unit cell tank, modeled as per the unit cell concept. This chapter presents various details of the materials used, procedures adopted for the laboratory tests, and the analysis of the test results. The validation of the developed model with respect to experimental data and case studies reported in the literature are also given in this chapter.

## 4.2   MATERIAL PROPERTIES

In this section, the properties of various materials used for experimental investigations are described.  Four basic materials used were lithomargic clay (locally known as Shedi soil), stone aggregates, sand, and geogrid.

### 4.2.1   Lithomargic Clay

Lithomargic clay is extensively found along the western coast of Southern India, extending from Cochin to Goa. They are usually located below lateritic soil, varying in large depths. Lithomargic clays are locally called Shedi soils. These soils behave as dispersive soils and are also highly erosive. Since there is a drastic reduction in strength under saturated conditions, construction activities in such soils are challenging.  Hence some in situ ground modification techniques are required for these types of soils.

71

The lithomargic clay used for the experiments was procured from Kolnad near Mulki, Mangalore, Karnataka (Fig.4.1).



Fig. 4.1 Sample procurement site

The soil is of MI classification, and other properties of soil are listed in Table 4.1. All the tests were conducted according to SP 36 (Part 1) – 1987 of the Indian Standard (IS) specifications. The gradation curve and compaction curve for the soil are shown in Fig. 4.2 and Fig. 4.3, respectively.

Table 4.1 Properties of lithomargic clay

| Sl.No. | Properties | | Value |
|---|---|---|---|
| 1 | Particle size distribution | Sand size (%) | 34 |
| | | Silt size (%) | 53.5 |
| | | Clay size (%) | 12.5 |
| 2 | Specific gravity | | 2.56 |
| 3 | Atterberg limits | Liquid limit (%) | 49 |
| | | Plastic limit (%) | 31 |
| | | Shrinkage limit (%) | 29 |
| | | Plasticity Index (%) | 18 |
| 4 | Compaction characteristics (Light compaction Test) | Maximum Dry unit weight (kN/m$^3$) | 15.3 |
| | | Optimum moisture content (%) | 19 |
| 5 | IS Soil Classification Symbol | | MI |

Fig. 4.2 Gradation curve for lithomargic clay, sand, and stone aggregate



Fig. 4.3 Compaction curve for lithomargic clay

Unconfined compressive strength (UCS) tests were carried out on soil samples at different water contents, and the variation of UCS with water content is shown in Fig. 4.4.
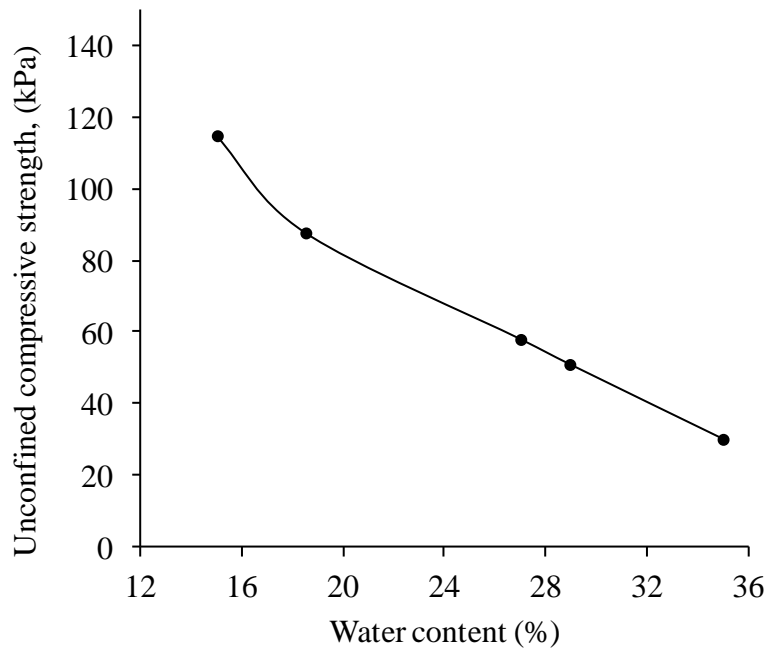
Fig. 4.4 Variation of UCS with water content

Based on the unconfined compressive tests, the water content of 35% and dry unit weight of 13.37 kN/m$^3$ was selected for the soil bed preparation, and the corresponding UCS strength of the bed was found to be 30 kPa.

### 4.2.2 Stone aggregates

The stone aggregates used to form the stone columns were of size 2 to 10 mm and having uniform gradation. The gradation curve for the stone aggregate is included in Fig.4.2. The maximum and minimum dry unit weights aggregates are 17.7 kN/m$^3$ and 15.7 kN/m$^3$, respectively. The stone aggregate in all the tests was compacted to a dry unit weight of 16 kN/m$^3$, corresponding to a relative density of 85%.

### 4.2.3 Sand

The sand used as the granular blanket is of clean river sand of size less than 4.75 mm. The gradation curve of sand is also included in Fig. 4.2.

### 4.2.4 Geogrid

For encasing the stone columns, geogrid material is used. The same geogrid material is placed on the top as the basal reinforcement layer. The tensile strength properties of

74

geosynthetic are determined from standard Wide-width tension tests (ASTM-D4595, 2011) and given in Table 4.2. The aperture size of the geogrid was found to be 9mm x 6 mm.

Table 4.2 Properties of geogrid used for the encasement and basal reinforcement

| Strength Properties | Geogrid |
| --- | --- |
| Shape | Sheet |
| Thickness (mm) | 2 |
| Aperture size (mm) | 9 x 6 |
| Specific gravity | 0.91 |
| Ultimate tensile strength (kN/m) | 0.62 |
| Elongation (%) | 32 |
| Stiffness (kN/m) | 1.94 |

## 4.3  LOAD TESTS ON STONE COLUMNS

### 4.3.1  Unit cell Concept

The stone columns are usually arranged in a triangular pattern or a square pattern. The equilateral triangular pattern is more commonly used as the coverage by a single column in its influence area is better than that in the square pattern. It is convenient to consider a typical stone column and the associated tributary area of soil surrounding the column for analysis purposes. Although the tributary area forms a square or regular hexagon around the stone column, it can be closely approximated as an equivalent circle having the same plan area. For an equilateral triangular pattern of stone columns, the equivalent circle has an effective diameter of 1.05S. For a square grid, it is 1.13S, where S is the center to center spacing between the stone columns. A typical set of experiments on stone columns were performed considering the stone column in a unit cell tank, modeled as per the unit cell concept. The unit cell can be physically modeled as a cylindrical-shaped container having a frictionless, rigid exterior wall symmetrically located around the stone column.

### 4.3.2 Experimental Programme

Three sets of experiments were planned to study the behavior of stone columns. Initially, for the first set, a load test on the untreated ground was carried out. In the second set, single column tests were carried out for ordinary stone columns, geogrid encased stone columns, and geogrid encased stone columns with a horizontal geogrid on the top. The third set consists of a load test on a group of columns for all the three cases mentioned above with the same area ratio.

### 4.3.3 Test Bed Preparation

In the present work, water content of 35% was selected, corresponding to the undrained shear strength of 30 kPa from Fig. 4.4. The unit weight of lithomargic clay at this water content was determined to be 13.37 kN/m$^3$. To minimize the friction between the tank wall and the test soil, the inner surface of the tank was initially lubricated with grease. Layered construction was followed with a measured quantity of lithomargic clay for each layer to maintain the unit weight of soil. Each layer was uniformly compacted with a tamping rod to achieve a compacted height of 60 mm. After placing each layer of lithomargic clay, a known volume of representative sample was taken out without disturbance to determine undrained shear strength, moisture content, and unit weight. Similar values of these parameters at different locations of the testbed confirmed the uniformity of the prepared testbed.

### 4.3.4 Stone Column and Geogrid Installation

After placing a 60 mm (equal to the diameter of stone column) thick basal lithomargic clay layer, a 2 mm thick open-ended seamless steel pipe of outer diameter equal to that of stone column diameter was placed at the center for stone column installation. The outer surface of the casing pipe was coated with a thin layer of grease for easy withdrawal. Coating with grease also helps in maintaining minimum disturbance to surrounding soil during stone column installation. By keeping a casing pipe in the middle, its surrounding portion was filled with lithomargic clay. Simultaneously, the casing pipe was charged by a premeasured amount of stone aggregates to the required layer depth of 60 mm. A 5 mm overlap was always provided between successive layers of stones and the foot of the casing pipe to maintain continuity while lifting the casing

pipe. This also helps prevent the entry of surrounding soil into casing pipe in case of Ordinary Stone Column (OSC) and the neck formation (horizontal push by the surrounding lithomargic clay) of encasement in case of Geosynthetic Encased Stone Column (GESC). For ensuring 85% relative density, each aggregate stone layer was compacted with 25 blows by a 2 kg circular tamper dropping from 250 mm height. The entire procedure was repeated until the required height of the stone column was attained.

Fig.4.5 (a) and (b) show a single encased stone column, Fig. 4.5 (c) shows the placement of basal geogrid layer at the top of an encased stone column, and Fig. 4.5 (d) shows a group of three encased stone columns after installation in lithomargic clay. After leveling the top surface, river sand of thickness 30 mm was positioned over it as a granular blanket. A granular blanket facilitates easy drainage and uniform load distribution. In the case of GESC, the casing pipe was wrapped with geogrid material before placing it on the soil bed, as in Fig. 4.6. The same geogrid material was used as basal reinforcement at the top of columns in the middle of the sand layer of 30 mm thickness, as shown in Fig. 4.5 (d) for providing vertical confinement.

### 4.3.5 Experimental Set-Up and Test Procedure

All laboratory tests were performed in a model circular tank with the stone column at the center and the tributary soft soil surrounding it. The diameter of the circular tank used for the model tests is equal to the corresponding unit cell diameter, i.e., 157.5 mm, which depends upon the spacing and arrangement of columns.

Based on the work of previous reserachers (Cheng et al. 2005; Fattah et al. 2016), an equilateral triangular pattern of installation with a center to center spacing of 2.5D where D is the stone column diameter and an area replacement ratio (ratio of stone column area to the unit cell area) of 15 was chosen for the single column and group columns tests. Fig. 4.7 shows the typical experiment setup. All experiments were conducted on stone columns with and without geogrid encasement in lithomargic clay with L/D ratio 5, which is required to develop the full limiting axial stress on the column (Mc Kelvey et al. 2004).

77

(a)
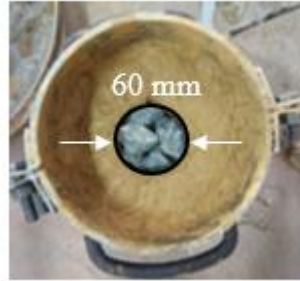


(b)



(c)
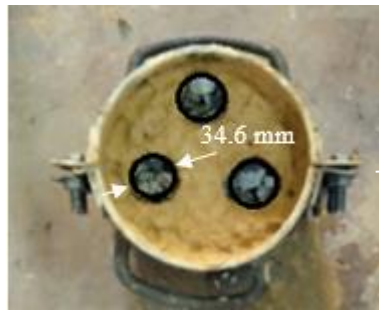


(d)

Fig. 4.5 Installation of the stone column in the unit cell (a) single column during construction (b) encased stone column after construction with area ratio =15% (GESC) (c) placement of basal geogrid layer at the top of encased stone column (GESC+ BASAL GEOGRID) and (d) group of three encased stone columns with area ratio =15%



Fig. 4.6 Encasing the casing pipe with geogrid material

The vertical load was applied to the entire area at a constant displacement rate of 0.06 mm/min. The loads corresponding to different displacements (in the stone column) were measured through a pre-calibrated proving ring. 12 mm thick mild steel plate with a diameter slightly less than the unit cell tank was used for uniform load distribution. A 30 mm thick sand layer was placed at the top as a drainage blanket. Two settlement gauges were used to record the settlements. The stone column loading was continued until a vertical displacement of 10 mm (IS: 15284-2003). Fig. 4.8 shows the setup for the load test in the laboratory.

After completing each test, the deformed shape of the stone column was obtained by pouring a concentrated slurry of cement into the stone column and allowing it to set for a day. After the slurry got hardened, the surrounding soil was removed, and the diameter of the stone column at various depths was measured with a vernier caliper.
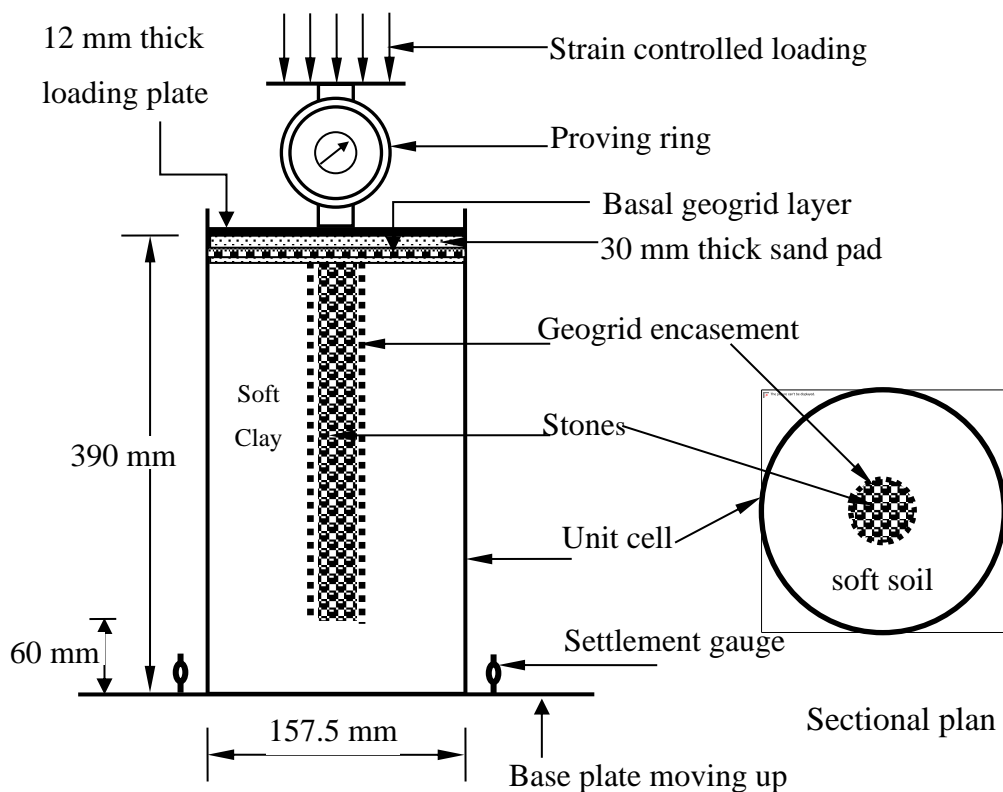


Fig. 4.7 Schematic diagram of the experiment set up

Fig. 4.8 Load tests on stone columns in a unit cell

## 4.4 NUMERICAL ANALYSES

To simulate the actual conditions, it is necessary to carry out a coupled analysis that essentially couples pore fluid flow and stress-strain behavior together. This helps in better convergence to the practical soil behavior as both pore fluid pressure and displacement degrees of freedom at nodal points were considered. The problem was investigated numerically using the finite element package ABAQUS (2016).

### 4.4.1 Models Developed

Full three-dimensional models of single and group columns considered in the experimental studies were developed and analyzed using the FEA software, ABAQUS. Three different cases were considered for both single column and column group tests; OSC, GESCs, GESCs with a single layer of geogrid at the middle of the sand layer. The developed 3-dimensional finite element models are shown in Fig. 4.9.

A linear elastic perfectly plastic model with Mohr-Coulomb failure criteria was adopted for modeling stones and sand in the numerical analyses. Lithomargic clay was

modelled using the Modified Cam Clay model. The material parameters used in the analyses are summarized in Table 4.3.

*Stones*: The angle of internal friction was determined using a 450 mm x 450 mm x 200 mm large-scale direct shear box. The crushed stones were compacted to a unit weight of 19 kN/m$^3$ and sheared at a constant rate of 1.25 mm/min under normal pressures of 50, 75, and 125 kPa to determine the angle of internal friction. Young's modulus of the stones is the constrained modulus obtained by loading the stones at an initial unit weight of 19 kN/m$^3$ in a cylindrical mould of 150 mm diameter and 180 mm height (Ambily and Gandhi 2007). The Poisson's ratio is as per Bowles (1988), and the dilation angle is determined as friction angle, $\phi°$ - 30°.
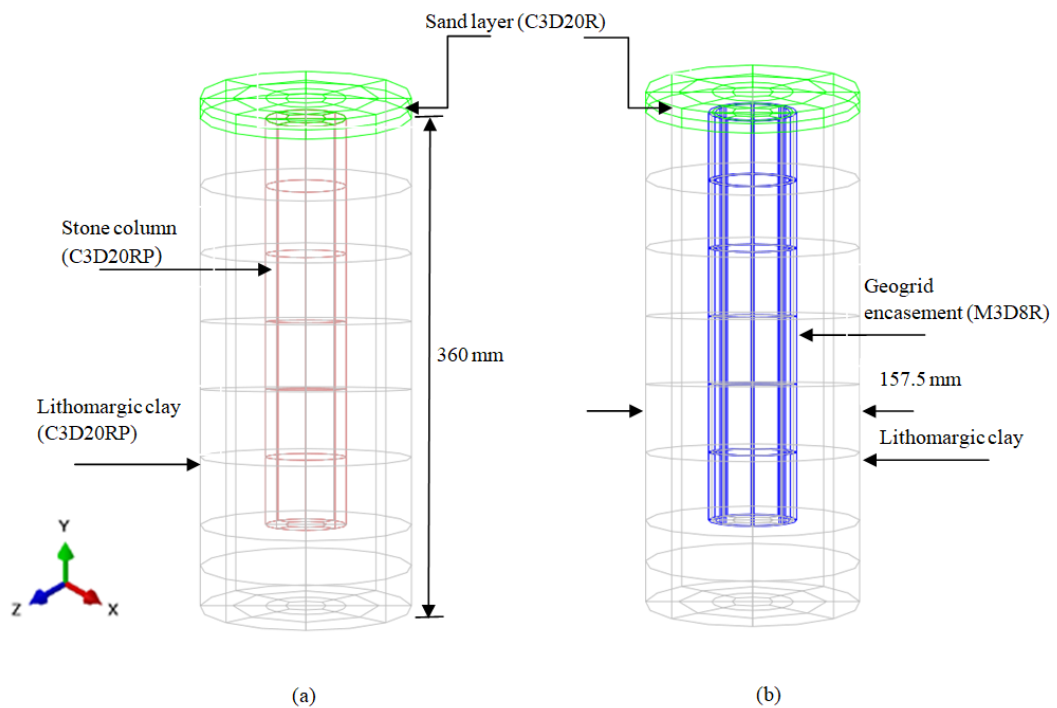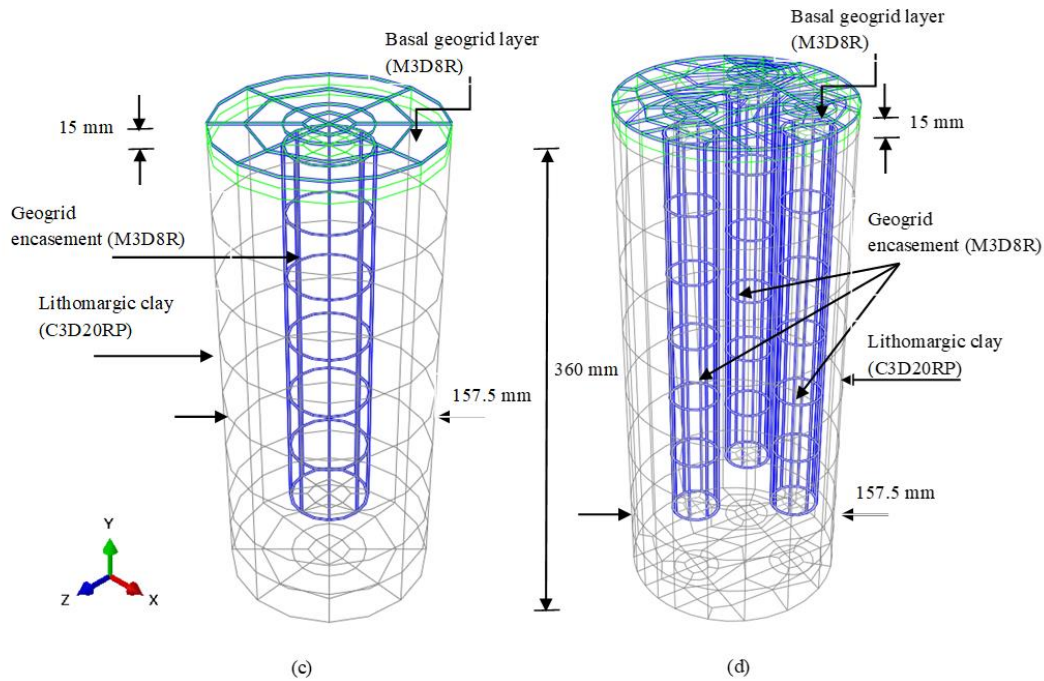
Fig. 4.9 Finite element models developed (a) OSC (b) GESC (c) GESC with basal geogrid layer and (d) GESC group with a basal geogrid layer

Table 4.3 Material properties used in the numerical analyses

| Property | Lithomargic Clay | Stones | Sand |
|---|---|---|---|
| Young's modulus (kPa) | - | 42000 | 12000 |
| Unit weight (kN/m$^3$) | 18.6 | 19 | 19 |
| Permeability, k (m/day) | 0.00349 | 1036.8 | 950.4 |
| Logarithmic hardening constant for plasticity, $\lambda$ | 0.05 | - | - |
| Logarithmic bulk modulus for elastic material behavior, $\kappa$ | 0.008 | - | - |
| Critical state stress ratio, M | 0.48 | - | - |
| Initial void ratio, $e_0$ | 0.78 | - | - |
| Poisson's ratio, $\nu$ | 0.3 | 0.3 | 0.3 |
| Friction angle, $\phi$ (degree) | - | 42 | 28 |
| Dilation angle, $\varphi$ (degree) | - | 12 | 4 |
| Cohesion, c (kPa) | - | 0 | 0 |

*Sand*: Values of the angle of internal friction, angle of dilation, and Young's modulus of the sand reported in Table 4.3 are based on a series of direct shear tests. The Poisson's ratio of sand used is as per Bowles (1988).

*Lithomargic clay*: For the Modified Cam-Clay model, five material parameters are required: Slope of the virgin consolidation line $\lambda$, the slope of the swelling line $\kappa$, initial void ratio $e_0$, the slope of the critical state line $M$, and Poisson's ratio $\mu$. Values of these parameters are shown in Table 4.3. Values for $\lambda$, $\kappa$, and $e_0$ were obtained from one-dimensional compression tests in an oedometer. The values of *M and* $\mu$ were obtained from a series of undrained triaxial tests.

### 4.4.2 Boundary conditions

Boundary conditions were applied in the vertical faces, bottom, and top of the unit cell model. All nodes were restrained from moving in the radial directions on the vertical faces, and all nodes on the base of the model were restrained from moving in vertical and radial directions. The vertical boundaries and the bottom surface were treated as impermeable boundaries. The nodes on the top surface were free to move in any direction.

### 4.4.3 Elements Used

In all the models, the meshes were arranged in order to have the same element size vertically to eliminate any possible errors arising from the mesh arrangement. Several trial analyses were carried out with a different number of elements, and based on the results, the mesh size was fixed. In the 3D model, for lithomargic clay and the stone column, 20-node stress–pore pressure elements with reduced integration (C3D20RP) were used, and 20- node stress-only elements (C3D20R) were used for the sand layer. The geogrid reinforcement was modeled using the membrane elements M3D8R. Membrane elements offer strength in the plane of elements without bending stiffness and resistance against the out-of-plane bulging. Membrane elements (M3D8R) were also used to model the geogrid encasement around the stone columns (Fig.4.10). The top surface of a membrane element in the positive direction of the normal is defined as the SPOS face, and the bottom surface in the negative direction along the normal is defined as the SNEG face for contact definition.
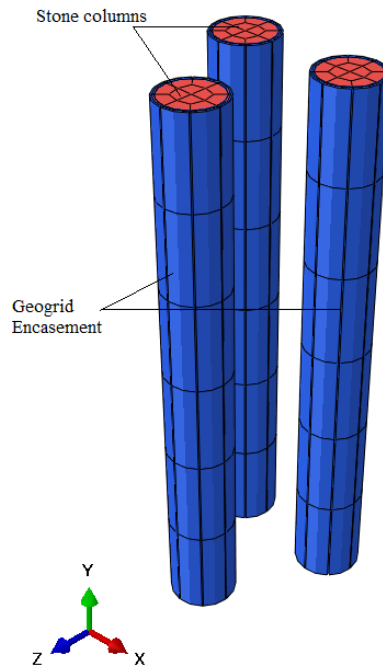
Fig. 4.10 Geogrid encasement around stone columns modeled using membrane elements (M3D8R)

### 4.4.4 Contact

In the present study, tied contact was used to model the interaction between the lithomargic clay, stone column, and confining reinforcement and between the basal reinforcement and sand layers. It constrains each of the nodes on the slave surface to have the same value of displacement and pore pressure as the point on the master surface that it contacts. Master surfaces and slave surfaces were chosen based on the stiffness values of the materials. The surface with higher stiffness acts as the master surface, and the surface with relatively lower stiffness will be the slave surface.

### 4.4.5 Methodology

To model stone column installation, the soil elements were removed and replaced by the column elements as if wished in place. The effect of stone column installation was not considered in this thesis. Suitable boundary conditions and pore pressure distribution were given. After that, the initial stress condition of the soft soil bed was established by using the geostatic option. Once the geostatic equilibrium was achieved,

incremental loading was applied at the top. The loading was continued till the vertical settlement reached a value of 10 mm, as done in the experimental study.

## 4.5 LOAD SETTLEMENT RESPONSE OF STONE COLUMNS

The behavior of the stone columns was studied mainly based on the pressure-settlement responses observed from the loading tests.

### 4.5.1 Load Tests on Single Stone Columns

The pressure–settlement responses observed from the laboratory model tests on unreinforced lithomargic clay bed, ordinary stone column (OSC) supported lithomargic clay bed, geogrid encased stone column (GESC) supported bed and geogrid encased stone column with a horizontal layer of geogrid at the top (GESC + BASAL GEOGRID), are shown in Fig. 4.11. The results were compared with those obtained from the numerical analyses, as shown in Fig. 4.11. The comparison was found to show good agreement between the predicted and experimental observations, with less than 5% variation in the results between the different tests. Some of the tests were repeated to verify the consistency of the data.

The study aims to evaluate the effect of reinforcing lithomargic clay soil with stone columns and the contribution of encasement and a horizontal layer of planar reinforcement on the load carrying capacity. Based on the pressure-settlement responses, it is clear that the OSC improves the bearing pressure of unreinforced ground by around 39 %. Compared to OSC, GESC did not show any signs of failure even at large settlement levels. The pressure was observed to increase in proportion to the settlement without any indication of failure. The pressure on the GESC corresponding to a 10 mm settlement is about two times larger than that of the OSC. Also, nearly three times improvement in load-bearing capacity was observed for GESC along with the basal geogrid compared to untreated soil. It can be concluded that the provision of a horizontal layer of reinforcement further enhances the load-bearing capacity of geogrid encased stone columns.
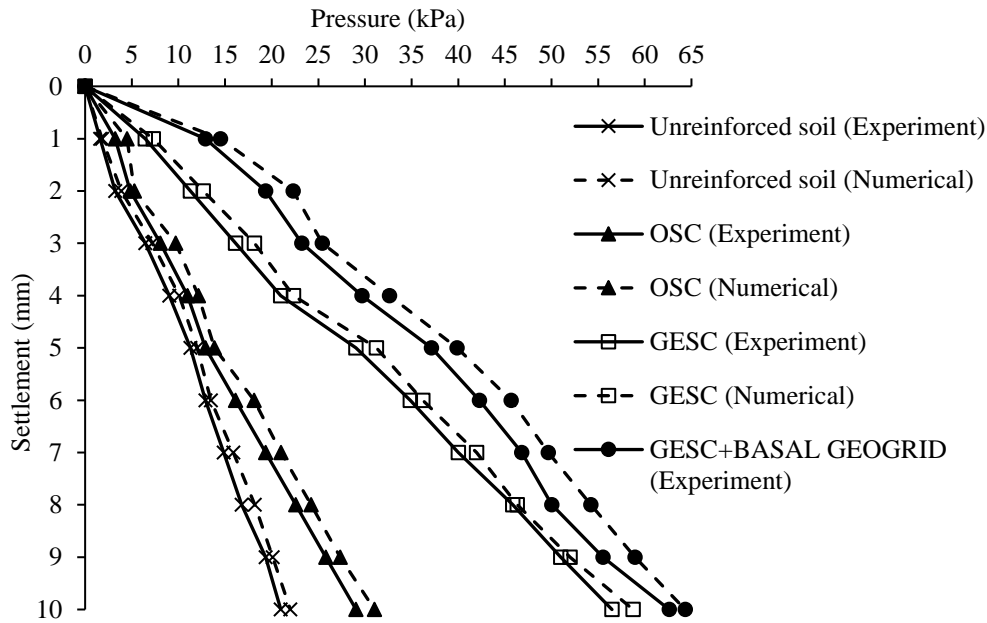
Fig. 4.11 Responses of single stone columns in unit cell tank

Table 4.4 summarises the load carrying capacity of a single stone column (at 10 mm settlement) under different cases and the percentage increase in load carrying capacity due to encasement and provision of basal reinforcement. The results obtained from numerical analysis were in good agreement with experimental results. The percentage difference in load carrying capacity from experiment and numerical analyses for single OSC, GESC, and GESC+ BASAL GEOGRID is varied between 2.8% to 4.9%.

Table 4.4 Summary of load carrying capacity at different cases

| Different cases | Load carrying capacity (experiment) (kPa) | Load carrying capacity (Numerical)(kPa) | % increase in load carrying capacity (experiment) | % increase in load carrying capacity (Numerical) |
|---|---|---|---|---|
| Unreinforced soil | 20.98 | 22.0 | - | - |
| OSC | 29.05 | 31.02 | 39 | 41 |
| GESC | 56.48 | 58.75 | 169 | 167 |
| GESC+ BASAL GEOGRID | 62.61 | 64.33 | 198 | 192 |

### 4.5.2 Improvement Factor (IF) from Single Column Tests

The increase in load-carrying capacity in terms of stiffness of the unreinforced soil was quantified by a dimensionless parameter known as Improvement Factor (IF). It is defined as the ratio of load carrying capacity of the reinforced soil to that of unreinforced soil at equal settlement values. The variation of IF against normalized settlement values (ratio of settlement values, s in terms of diameter of the column, D) for all the settlement values from 1 mm to 10 mm were plotted for the three cases in Fig. 4.12. From Fig. 4.12, it is clear that for all the cases considered, the improvement factor is high at the beginning of settlement and then decreases temporarily.

According to Debnath and Dey (2017), axial compression of the granular column at the beginning of loading increases the load capacity which in turn increases the improvement factor. With an increase in the s/D ratio, the bulging of the stone column causes a reduction in IF for all the three cases considered. Due to the gradual transfer of load from the column to the surrounding soil, a small improvement in load capacity can be observed (Fig. 4.12). Improvement factor becomes constant at a settlement of 10% as the passive resistance with time attains a constant value and there is no increase in load carrying capacity. The numerical value of IF for OSC, GESC and GESC with basal geogrid was 1.38, 2.69 and 2.98 respectively. Hence, it can be concluded that geosynthetic encased stone columns with basal geogrid improves the load carrying capacity in comparison to ordinary stone columns and geogrid encased stone columns.
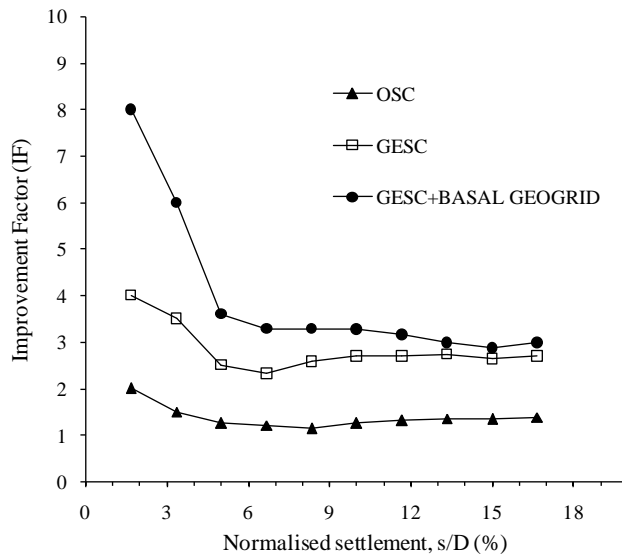
Fig. 4.12 Variation of Improvement Factor for single column tests

### 4.5.3 Load Bearing Mechanism of Single Stone Column

The provision of a horizontal layer of reinforcement and GESC transfers more load to the column, which can be explained as follows: The vertical load applied normal to the surface of the reinforcement generates tension in the membrane, creating the membrane effect. The vertical component of the mobilized tensile force is transferred to the stone columns made stiffer by the geogrid encasement. The effect is to reduce the stress acting on the lithomargic clay foundation soil, resulting in decreased vertical settlement. The contribution of membrane effect on bearing capacity, Δp is given by,

$$\Delta p = \left( \frac{2T \sin \alpha}{b_n} \right) \tag{4.1}$$

Here,   T = tensile strength of geogrid material.

   α = horizontal angle of tensile force, T

   $b_n$= width of the uniform load

The geogrid encasement increases the stone column's stiffness and acts as a filter aiding in drainage. The hoop tension developed in the geogrid encasement due to the dilation of stones during vertical loading imparts additional radial confinement to the stone column enabling a stiffer and stronger response. The hoop tension can mobilize the required lateral pressure from the surrounding soft soil. As a result, the stress concentration on the stone column is more, and lesser vertical stress was observed

88

in the surrounding soil. This, in turn, resulted in significant settlement reduction and improved load carrying capacity

### 4.5.4 Load Tests on Group of Stone Columns

Experimental investigations were carried out to determine the influence of column configuration, i.e., increasing the number of columns of smaller diameter for the same depth keeping the area ratio the same as before. An area replacement ratio of 15% was chosen for all single column tests, and this area replacement ratio was attained with a group of smaller diameter columns, as shown in Fig. 4.13. All the tests were conducted in the same unit cell tank with a diameter of 157.5 mm.



60mm diameter stone column

Unit cell tank of 157mm diameter

34.6 mm diameter stone columns

(a)          (b)
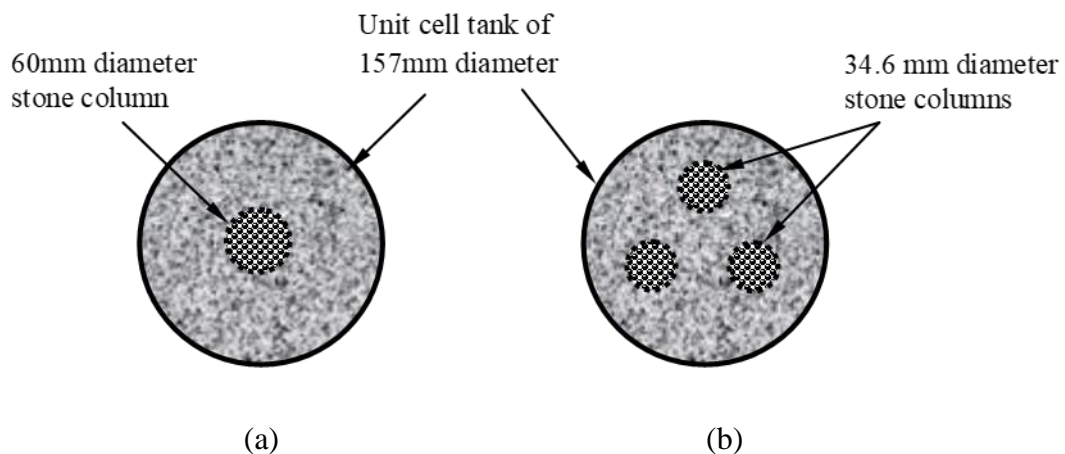
Fig. 4.13 Column configurations for same area ratio (a) single column and (b) three columns

Load tests were carried out for a group of three columns, each of diameter 34.6 mm. Loading was done on the entire unit cell area, and the pressure-settlement curves are plotted in Fig. 4.14. Table 4.5 gives the bearing pressure values at 10mm settlement for the different cases considered in the study.
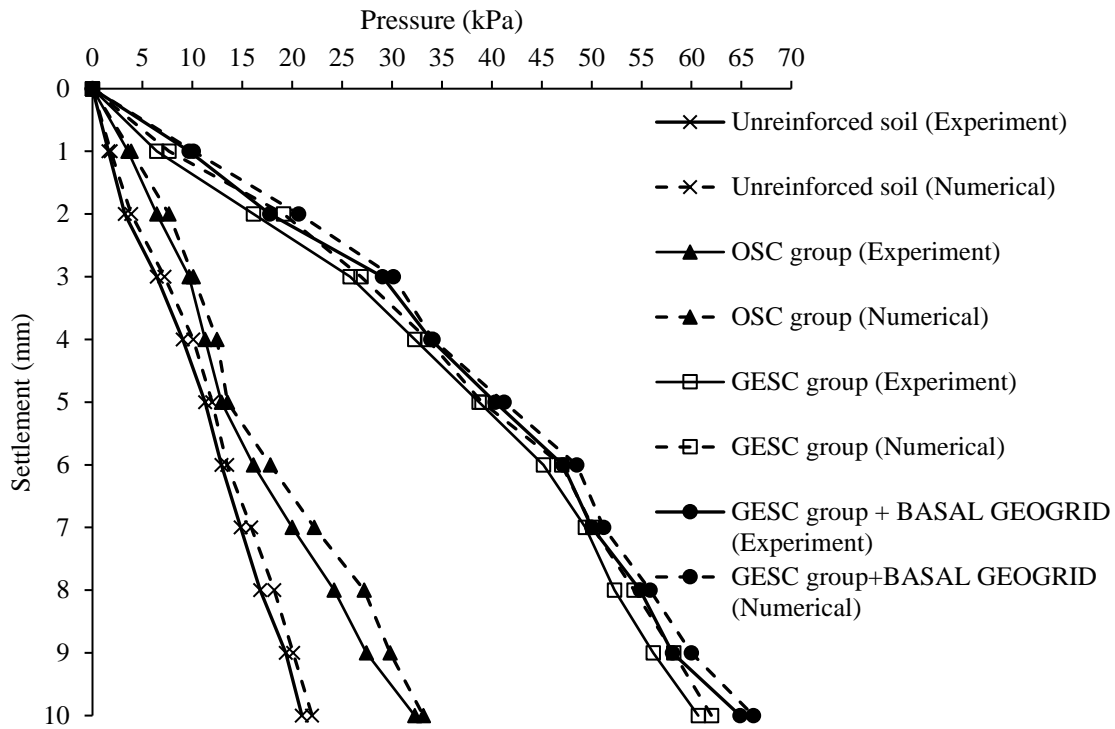
Fig. 4.14 Pressure – settlement responses for a group of three columns

Table 4.5 Summary of the load carrying capacity of a group of stone columns

| Different cases | Load carrying capacity (experiment)(kPa) | Load carrying capacity (Numerical)(kPa) | % Increase in load carrying capacity (experiment) | % Increase in load carrying capacity (Numerical) |
|---|---|---|---|---|
| Untreated soil | 20.98 | 22.0 | - | - |
| OSC group | 32.27 | 33.14 | 54 | 51 |
| GESC group | 60.68 | 62 | 189 | 182 |
| GESC group+ BASAL GEOGRID | 64.87 | 66.21 | 210 | 201 |

Table 4.5 shows that compared to untreated soil, the OSC group displayed a 54% increment in load carrying capacity. In contrast, for GESC and GESC with basal geogrid, the improvement was 189 % and 210 %, respectively, from the experimental results. The results obtained from numerical analysis were in good agreement with experimental results. The percentage difference in load carrying capacity from

experiment and numerical analyses for a group of OSC, GESC, and GESC+ BASAL GEOGRID was varied between 2.1 to 2.8%.

### 4.5.5    Effect of Column Configuration on Load Carrying Capacity

The pressure-settlement behavior of a single column and a group of three columns with the same area replacement ratiofor the different cases considered is shown in Figs 4.15, 4.16, and 4.17.
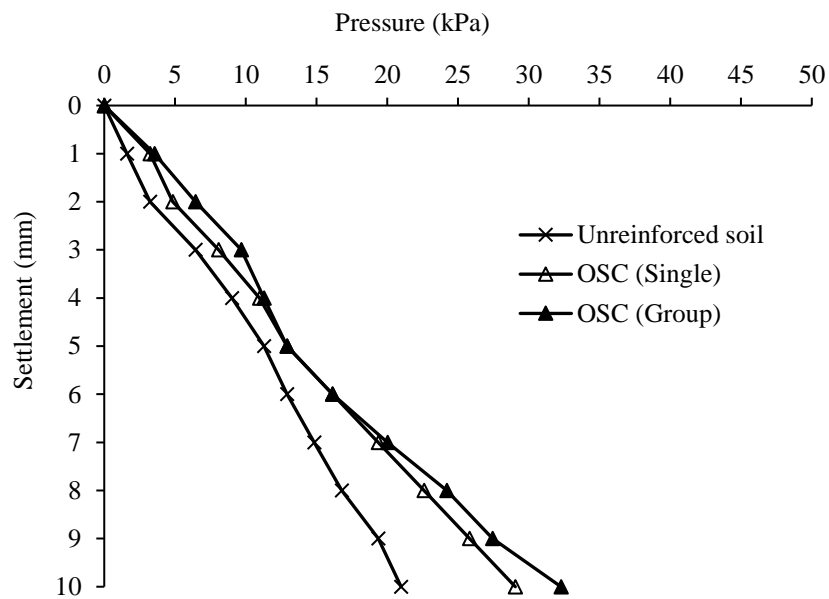


Fig. 4.15 Pressure- settlement responses of single and group of three OSCs
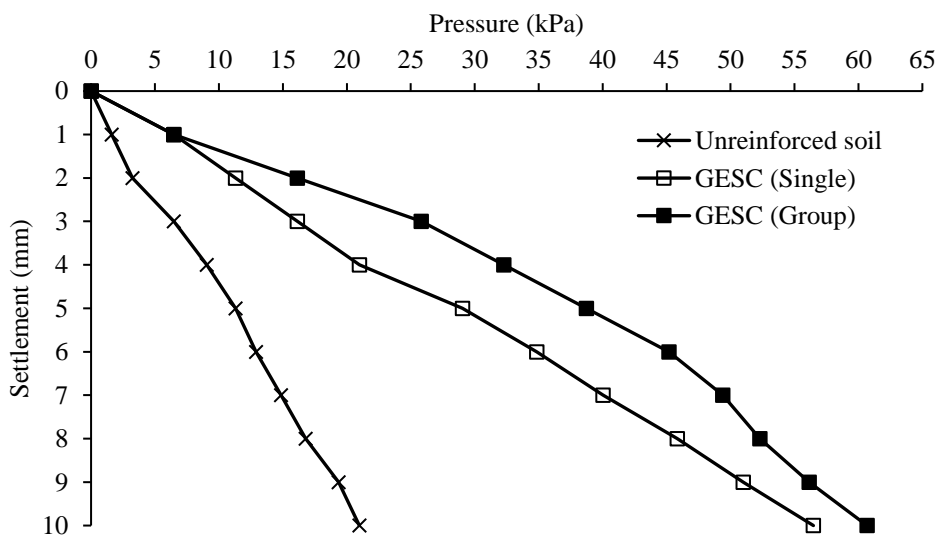


Fig. 4.16 Pressure- settlement responses of single and group of three GESCs
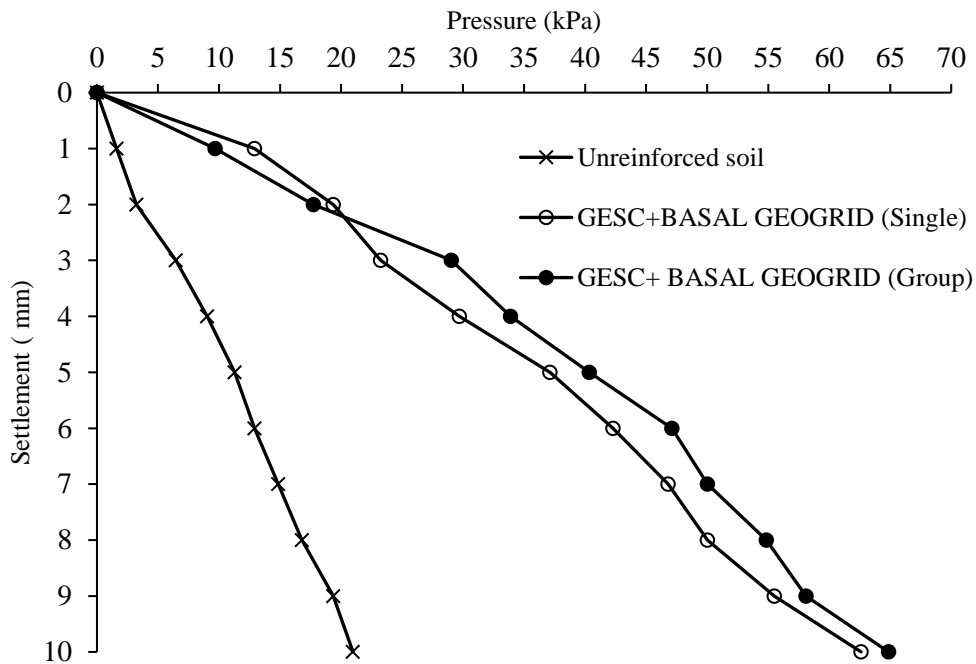
Fig. 4.17 Pressure-settlement responses of single and group of three GESCs with a layer of geogrid at top

For a group of columns with the area ratio same as that of a single column, the load-bearing capacity is slightly more than that of a single column for all the three cases considered in this study. Table 4.6 reports the percentage increment in load-bearing capacity from experimental studies.

Table 4.6 Summary of the load carrying capacity of a group of stone columns

| Different cases | Load carrying capacity (kPa) | | % Increase in load carrying capacity |
|---|---|---|---|
| | Single column- 60 mm dia | Group of columns- 3 nos of 36.4 mm dia | |
| OSC | 29.05 | 32.27 | 11 |
| GESC | 56.48 | 60.68 | 8 |
| GESC + BASAL GEOGRID | 62.61 | 64.87 | 4 |

Figs 4.15- 4.17 show that the load carrying capacity for a group of OSCs was 11% more than that of a single stone column having the same area ratio. The percentage increment in the load carrying capacity of a group of GESC compared to a single GESC

was 8%, and for the GESC group with basal geogrid, the increment was 4%. Thus, from the load carrying capacity point of view, the group of columns will be slightly advantageous for the same area ratio.

### 4.5.6 Load Bearing Mechanism of a Group of Three Columns

From Fig. 4.18, when a single column was replaced by three columns of smaller diameter having the same area replacement ratio, the stiffness improvement factor was found to increase. The diameter and spacing of stone columns have a major role in the performance of the overall system (Castro and Karstunen 2010). For smaller diameter columns, the absolute spacing between the columns reduced compared to a single column, which densified the surrounding soil. This increased the confining effect, which in turn led to increased load carrying capacity. i.e., for the same area ratio, a group of smaller diameter stone columns will be more advantageous than a single column.
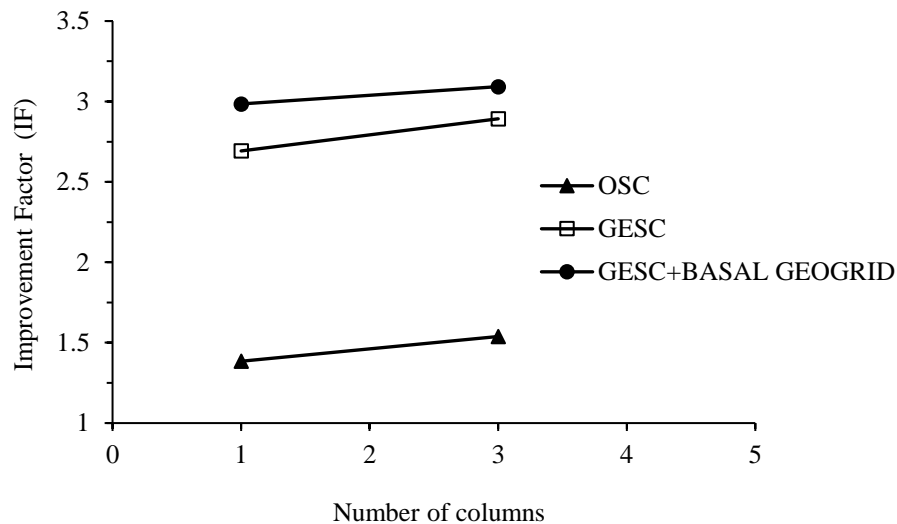


Fig. 4.18 Variation of improvement factor with column configuration

The membrane effect for a basal geogrid layer placed at the middle of the sand layer in a three-column group was evident in the stress contours obtained from the numerical analyses carried out (Fig. 4.19). The maximum tensile stresses were accumulated at the edge of the geogrid layer, and minimum stresses were observed around the column region. Due to the membrane action, more load was transferred to

93

stone columns leaving behind a lesser mobilized tensile strength region in the basal geogrid.
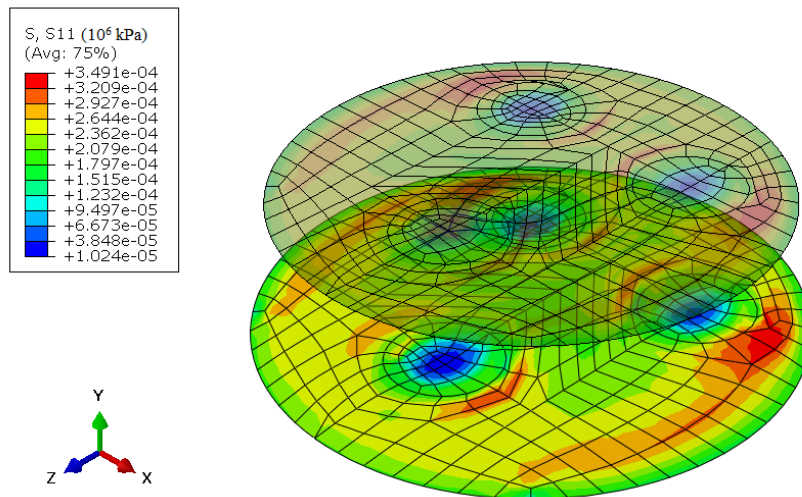


Fig. 4.19 Membrane effect-Tensile stress contours in the basal geogrid layer for a three-column group

### 4.5.7 Stress Concentration Ratio

The symmetry of load and geometry allows only vertical settlement and drainage at the radial boundary of the unit cell. So, the external load applied on the top of the unit cell will remain within it. The quantification of the stress distribution between stone columns and soil can be explained by the term stress concentration ratio (SCR), which is the ratio of stress in the stone column to that of the surrounding soil (Ng and Tan 2015). Being stiffer, the stone column takes more load than the foundation soil, resulting in a concentration of stress around the column region. The contribution of geogrid encasement and basal geogrid layer (middle of the sand layer) on stress concentration ratio was analyzed using the vertical stress contours obtained from finite element analyses (Fig. 4.20). Fig.4.21 shows the variation of stress concentration ratio at the top of the stone column against normalized settlements. The comparison between the performance of single and group of columns is shown in these figures. In this study, average stresses at the top of stone columns were considered to calculate the stress concentration ratio.

(a)                          (b)
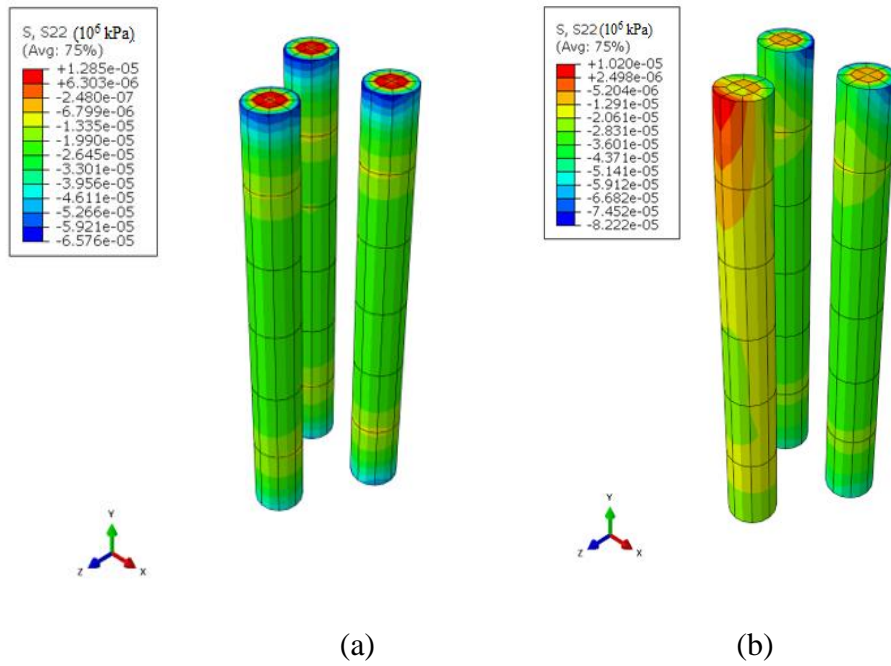
Fig. 4.20 Vertical stress contours in stone columns (a) GESC group and (b) GESCs + BASAL GEOGRID group
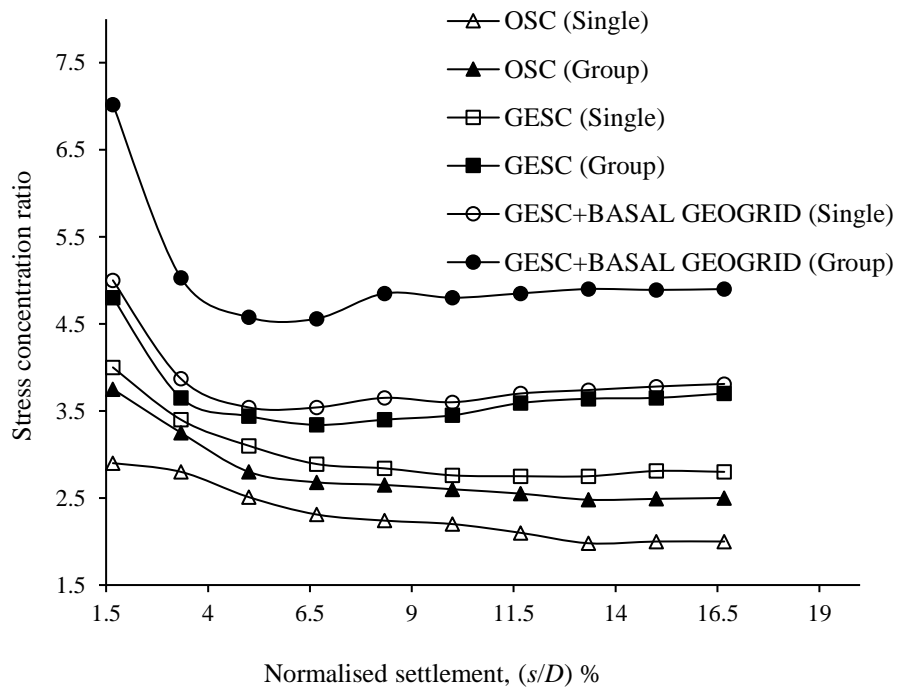


Fig. 4.21 Variation of stress concentration ratio for single and group of three columns

From Fig. 4.21, it is evident that the stress concentration ratio decreases after an initial increase in all six cases. The decrease is due to the change in the stiffness of the stone column with loading. The maximum stress concentration ratio was observed for the geogrid encased stone column group with basal geogrid layer, and the minimum was for the single ordinary stone column. The range of stress concentration ratio for single columns is 2 to 2.9 for OSC, 2.75 to 4 for GESC, and 3.54 to 5 for GESC with a basal geogrid layer. For a group of three columns, SCR varies between 2.5 to 3.75 for OSCs, 3.2 to 4.8 for GESCs, and 4.56 to 7.02 for GESCs with a basal geogrid layer. By encasing the OSC with geogrid, the stiffness of the stone column increases, and more load is transferred to columns, thereby increasing the value of the stress concentration ratio.

Further increase in SCR value was observed when a layer of geogrid sandwiched between sand layers was provided with GECs. Due to membrane action, the basal geogrid layer transferred more load to encased stone columns, which increased the SCR. Also, an increasing SCR trend was noted in GESCs with a basal geogrid layer at higher settlement. An increase in stress concentration ratio maybe because of the improvement in the effectiveness of geogrid with strain rate. Group of ordinary stone columns displayed slightly different trends as the SCR was invariably the same at the higher settlement levels (Murugesan and Rajagopal 2007).

Fig. 4.22 shows the stress concentration profile along with the depth of the column. For all the cases considered, the maximum SCR was observed at the surface and showed a decreasing trend up to a certain depth. SCR then increased slightly and became almost constant at deeper depths of the column. The depth of minimum SCR was nearly the same as the depth of maximum lateral bulging for columns. The depth of bulging is determined by the confinement offered by the surrounding soil, and maximum bulging occurred at the depth where the least confining stress is mobilized (Murugesan and Rajagopal 2007). The total load supported by the granular column is reduced due to bulging, which resulted in reduced SCR (Debnath and Dey 2017). SCR value is more for encased stone columns with a basal geogrid layer, which shows that the provision of the basal layer gives better performance than the ordinary stone column and the encased stone column.
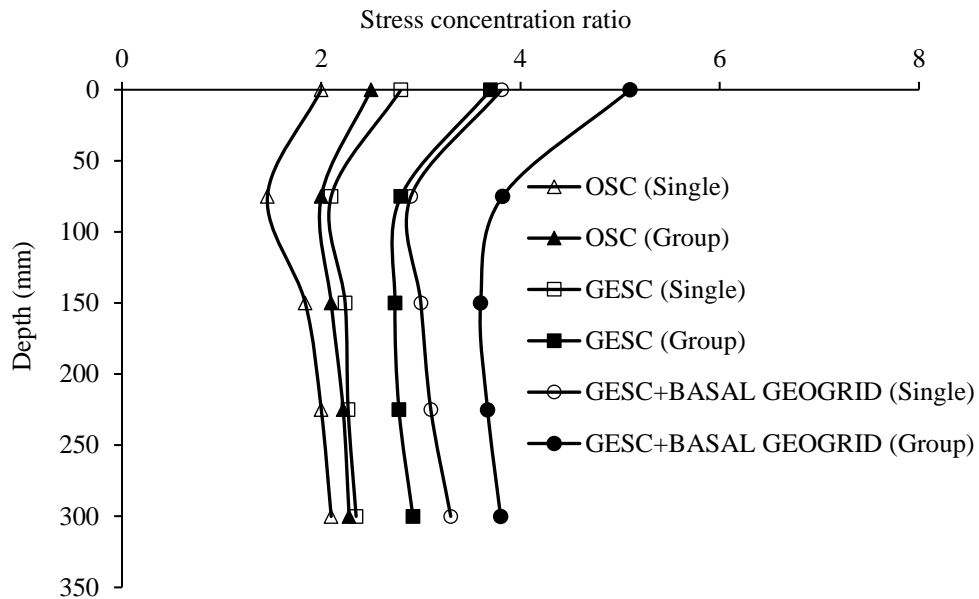
Fig. 4.22 Variation of stress concentration ratio along with the depth of the column

### 4.5.8 Bulging Characteristics of Stone Columns

The bulging profile of stone columns was obtained by pouring cement slurry through the column after each test. After the slurry was set, the soil around the stone column was removed to get the deformed shape. The stone column diameter was measured in four different directions using a vernier caliper, and the mean value was taken for better accuracy. Figs. 4.23 (a), (b) & (c) show the pictures of the exhumed stone column (single) for the three different cases considered in the study. The bulging profile for a group of encased stone columns is shown in Fig.4.23 (d).

From Fig. 4.23 (a), it is clear that OSCs underwent large bulging near the top end of the column. In OSC, the maximum stress concentration was seen just near the loading plate, which causes large lateral deformation at the top. The encased stone columns did not undergo much bulging as illustrated in Fig. 4.23(b). The major advantage of encasing the stone columns is the reduction in bulging by the geogrid encasement. The geogrid encasement reduced the bulging tendency of the stone columns by confining them and thereby reducing the surface settlements. In the case of GESCs, the bulging has been controlled by the encasement, and the settlement of the stone column was mainly due to the elongation of the geosynthetic encasement. By placing a basal geogrid layer on the top of a stone column, the stiffness of the base soil

was improved, and the passive resistance offered by the surrounding soil against the stone column bulging also increased (Fig. 4.23 (c)). Thus, the load is effectively transferred to deeper depths of foundation soil. The percentage bulging for different cases is presented in Table 4.7.



(a)  (b)  (c)



(d)
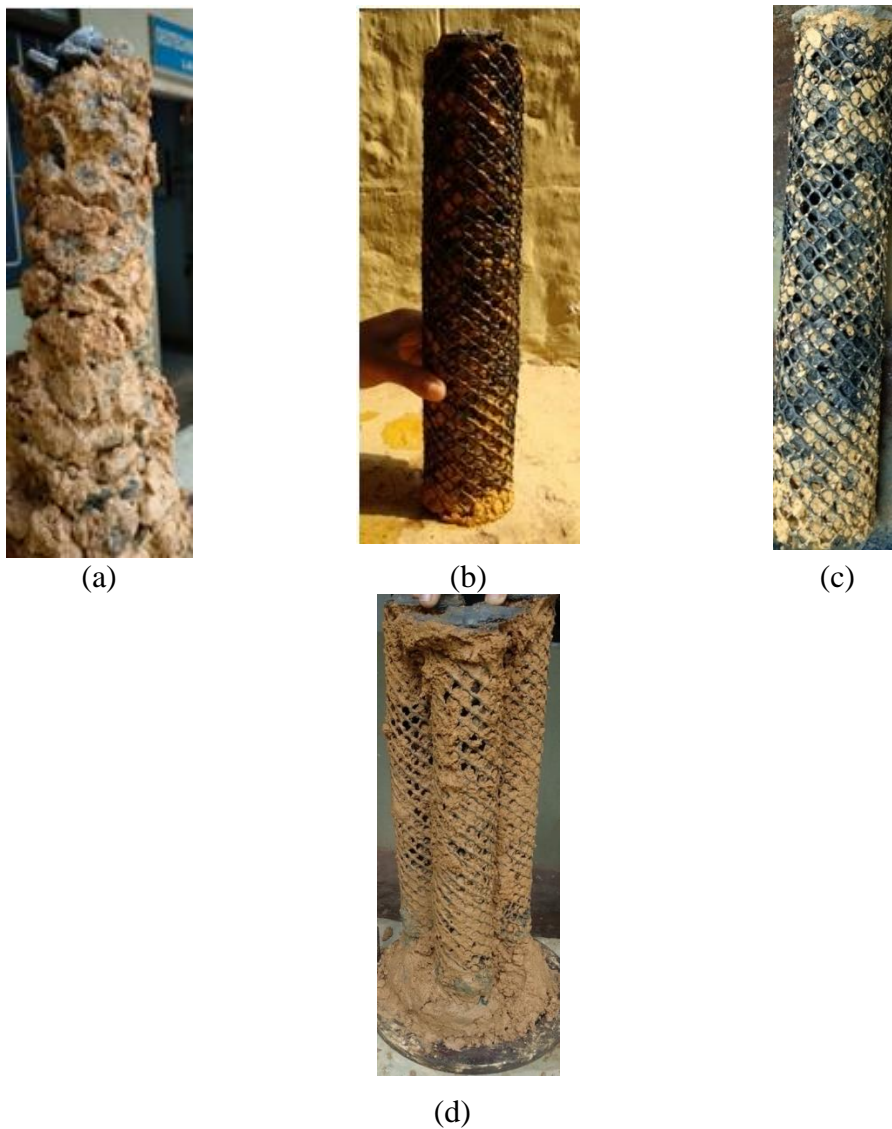
Fig. 4.23 Bulging in stone columns after the load test (a) OSC (b) GESC (c) GESC+ BASAL GEOGRID and (d) GESC group

The lateral bulging for single columns and a group of columns are plotted in Fig. 4.24 and Fig. 4.25. The lateral bulging at various depths is presented in terms of the increase in diameter at different depths normalized with the original diameter of the stone column (D). Earlier studies showed that the predominant bulging of the stone

columns occurs only in the top portion over a height equal to about 4 times the diameter (Greenwood 1970; Hughes and Withers 1975).

Table 4.7 Maximum Percentage of lateral bulging for different cases

| Different cases | Maximum Lateral Bulging (%) |
|---|---|
| OSC$_{Single}$ | 5.50 |
| GESC $_{Single}$ | 3.40 |
| GESC + BASAL GEOGRID$_{Single}$ | 3.03 |
| OSC$_{Group}$ | 3.47 |
| GESC $_{Group}$ | 2.70 |
| GESC + BASAL GEOGRID$_{Group}$ | 2.33 |
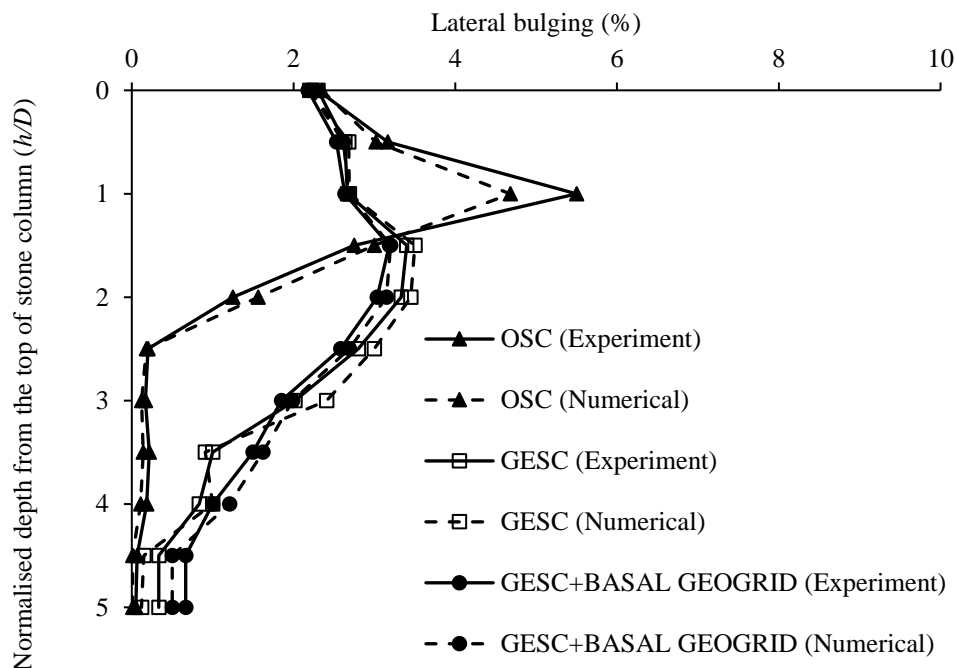


Fig. 4.24 Lateral bulging for a single stone column

For a single ordinary stone column, maximum bulging occurs at a depth of 0.5 to 1D, and it exists till 4D. It was observed that in the OSC, there was severe bulging near the ground surface up to a depth equal to the diameter of the stone column. On the

other hand, the GESCs have undergone much lesser lateral expansion near the ground surface. The encased columns have undergone slightly higher lateral expansions at deeper depths than the ordinary stone columns. This is because the applied surface load is transmitted deeper into the column due to encasement effects. For GESC, maximum bulging was visible at a depth of 1.5D. The lateral bulging was further reduced by placing a horizontal layer of geogrid on the top of stone columns, and the load was transferred to a deeper depth. A group of stone columns with the same area ratio exhibited lesser lateral bulging than a single column. The depth corresponding to the maximum bulging remained unchanged in all the cases.
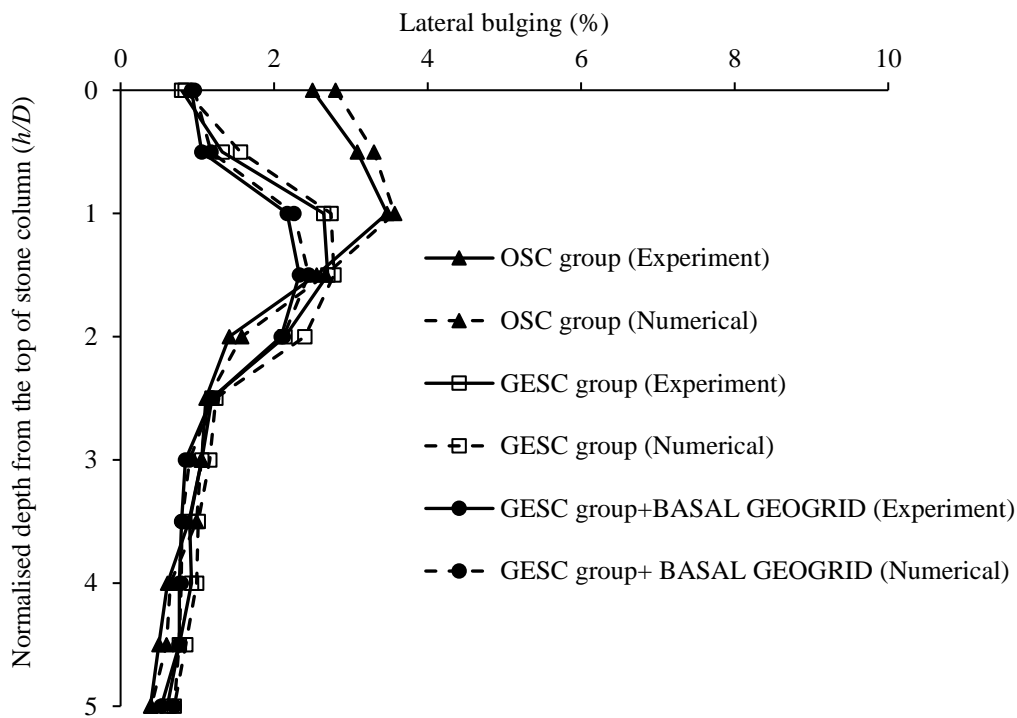


Fig. 4.25 Lateral bulging for a group of stone columns

# CHAPTER 5

# NUMERICAL ANALYSES USING UNIT CELL MODELS

## 5.1 GENERAL

Numerical methods are commonly used to study stone column-supported embankments due to improved computing power and the availability of complex models to simulate soil behavior better. As an initial part of the research work, the accuracy of the numerical models developed for the study of encased stone columns was evaluated using the data from the case reported by Yoo and Kim (2009). The details are given in chapter 3. From the literature review carried out, it was observed that there is a paucity of related numerical studies carried out to investigate the behavior of embankments supported on encased stone columns and with geocell as basal reinforcement.

In this chapter, the effectiveness of basal reinforcements as a load transfer platform in encased stone column supported embankment was investigated by carrying out time-dependent 3D coupled analyses. The behavior of the ordinary stone columns (OSC), geogrid encased stone columns (GESC), encased stone columns with single (GESC+ One basal layer) and multiple layers (GESC+ Two basal layers) of horizontal geogrid on the top and encased stone columns with geocell sand mattress (GESC+ GEOCELL) on the top was evaluated through comprehensive parametric studies. Parameters studied mainly include maximum and differential settlements, arching, stress concentration, tensile force distribution, and excess pore pressure distribution. The developed models also studied the bulging profile of the stone columns. The various input parameters used, material modeling details, parametric studies, and the overall system's time-dependent behavior are discussed in this chapter. Comparing the proposed system with the performance of Geosynthetic Reinforced Piled Embankment Systems (GRPES) is also included.

## 5.2 FINITE ELEMENT ANALYSES

All the finite element analyses were performed using the finite element program ABAQUS (SIMULIA 2016), which uses Biot's generalized consolidation theory (1941) for carrying out time-dependent 3D coupled analysis. In this section, the properties of various materials used for numerical investigations are described. Different materials used were lithomargic clay (shedi soil), stone aggregates, sand/embankment soil/infill soil, geogrid, and geocell.

### 5.2.1 Description of the case study considered for analyses

Numerical models (2D and 3D column) based on the unit cell approach were developed to investigate the influence of basal geogrid on the time-dependent behavior of geogrid reinforced encased stone column supportedembankment. The models used in the present study were based on the models proposed by Yoo and Kim (2009) for a geosynthetic encased stone column supported embankment resting in a soft clay bed. Due to the symmetry of the embankment, only the right half of the embankment is shown in Fig. 5.1.

The embankment was 45 m wide and 6 m high with a 1V:2H side slope comprising sandy soil and rested on a 10 m deep lithomargic clay layer overlying a firm stratum. The foundation soil was reinforced with 0.8 m diameter encased stone columns arranged in a square grid pattern with 2.4 m center to center spacing. The groundwater table was set at the top of the lithomargic clay surface. A drainage blanket was placed over the columns, and the geogrid layer was placed at the base of the embankment. In the case of a multi-layer system, two geogrids are placed at 0.15 m intervals. Analyses were carried out by replacing the multilayers with a 0.15 m high geocell-sand mattress at the embankment base.

### 5.2.2 Constitutive models

The stone column, embankment soil, infill soil, and the sand blanket were modeled as isotropic linear elastic perfectly plastic material with Mohr-Coulomb failure criteria. The lithomargic clay was modeled using the Modified Cam Clay (MCC) model. A summary of the constitutive model parameters for lithomargic clay, stone column, and sand/fill is given in Table 5.1. Values for $\lambda$, $\kappa$ and $e_0$ were obtained from one-

dimensional compression tests in oedometer. The values of $M$ and $\mu$ were obtained from a series of undrained triaxial tests. The Poisson's ratio ($\mu$) used for stones and sand is as per the typical values suggested by Bowles (1988). The geogrid and geocells were modeled as a linear elastic material. Based on Biabani et al. (2016a), the hexagonal shape was considered for modeling the geocell pockets. Table 5.2 summarises the properties of geogrid and geocell used in the analyses. The properties of geogrid and geocell were selected based on the work carried out by various researchers (Yoo and Kim 2009; Hegde and Sitharam 2015a; Biabani et al. 2016a).
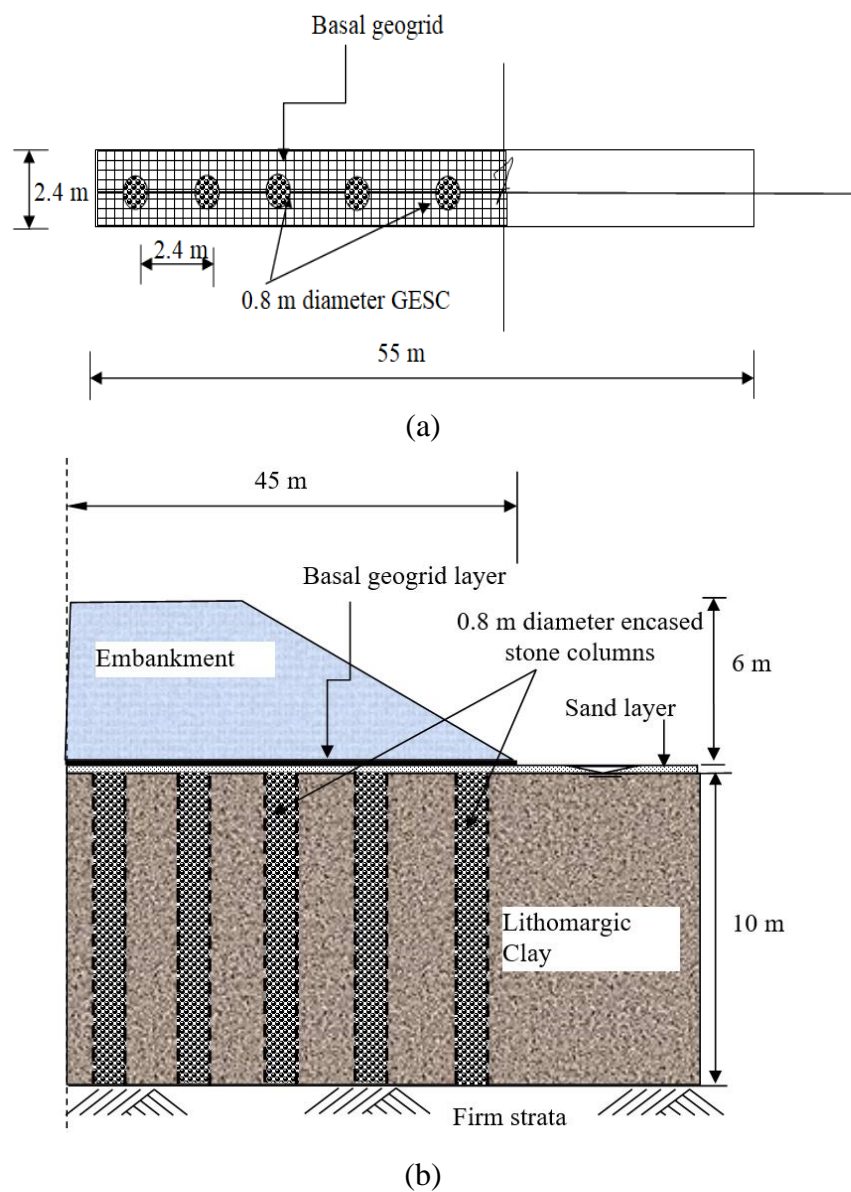


Fig. 5.1 Geosynthetic reinforced encased stone column supported embankment
(a) plan and (b) cross-section

Table 5.1 Constitutive model parameters for lithomargic clay, stone column, and sand/fill

| Property | Lithomargic Clay | Stone Column | Sand/Embankment soil/Infill |
|---|---|---|---|
| Young's modulus (kPa) | - | 40000 | 15000 |
| Unit weight (kN/m$^3$) | 18.6 | 19 | 19 |
| Permeability, k (m/day) | 0.00349 | 1036.8 | 950.4 |
| Logarithmic hardening constant for plasticity, λ | 0.05 | - | - |
| Logarithmic bulk modulus for elastic material behavior, κ | 0.008 | - | - |
| Critical state stress ratio, M | 0.48 | - | - |
| Initial void ratio, $e_0$ | 0.78 | - | - |
| Poisson's ratio | 0.3 | 0.3 | 0.3 |
| Friction angle (°) | - | 40 | 28 |
| Dilation angle (°) | - | 20 | 10 |
| Cohesion (kPa) | - | 0 | 0 |

All numerical models were run on a high-performance workstation of Intel Xenon E5-1620, 3.5 GHz, 3501 MHz processor with 8GB RAM. The running time for an axisymmetric model and single 3D column analysis was approximately 30 minutes and 420 minutes of CPU time, respectively. Table 5.3 shows the total number of elements used for the modeling of each material.

### 5.2.3 Numerical models

Three numerical models were developed for the analyses; (a) Axisymmetric unit cell (ii) 3D column model as shown in Fig. 5.2 (a) and (b). Axisymmetric and 3D column analyses being computationally less intensive and the results comparable to full three-dimensional analyses, are widely used to model actual field problems (Yoo and Kim 2009; Khabbazian et al. 2010; Bhasi and Rajagopal 2015).

Table 5.2 Properties of geogrid and geocell

| Strength Properties | Values |
| --- | --- |
| **Geogrid** | |
| Shape | Sheet |
| Thickness (mm) | 15 |
| Stiffness (kN/m) | 2500 |
| Poisson's ratio | 0.3 |
| **Geocell** | |
| Shape | Hexagonal |
| Poisson's ratio | 0.45 |
| Thickness (mm) | 1.53 |
| Cell seam strength (kN) | 2.15 |
| Yield strength (kN/m) | 20 |
| Modulus (MPa) | 275 |

The 3D column model considers a single column and the associated tributary area of the soil surrounding the column for analysis. As shown in Fig. 5.2b, only one-quarter of the column and its tributary area were modeled due to the symmetry.

The mesh size was selected after several trial analyses with a different number of elements. The element size was kept the same in the vertical direction to avoid errors in mesh arrangement. An initial time step of 0.003 days was considered for consolidation analyses to satisfy the stability criterion given by Vermeer and Verruijt (1981). In the 2-dimensional analyses, the lithomargic clay and stone columns were represented by eight-node stress pore pressure coupled axisymmetric elements (CAX8RP). The embankment soil, drainage layer, and infill soil were modeled using CAX8R elements. In 3D analyses, the lithomargic clay layer and the stone column were discretized using twenty node stress-pore pressure coupled brick elements with reduced integration (C3D20RP). The embankment fill, infill soil in the geocell-sand mattress, and drainage blanket were modeled using twenty node stress only elements (C3D20R). The geogrid encasement, basal geogrids, and geocell were represented using MAX2 elements in the axisymmetric model and eight-node membrane elements with reduced

integration (M3D8R) in 3-dimensional analyses. Membrane elements are suitable for modeling the membrane effect of geogrids and geocells.

Table 5.3 Total number of elements used in the numerical model

| Material | Total number of elements |
|---|---|
| **3D Column model** | |
| Lithomargic clay | 192 |
| Stone column | 72 |
| Sand | 176 |
| Embankment | 528 |
| Infill soil | 1024 |
| Geogrid encasement | 24 |
| Basal geogrid | 120 |
| Geocell | 400 |
| **Axisymmetric model** | |
| Lithomargic clay | 64 |
| Stone column | 64 |
| Sand | 32 |
| Embankment | 120 |
| Geogrid encasement | 16 |
| Basal geogrid | 4 |
| Geocell | 32 |

### 5.2.4 Boundary conditions

Full fixity was assumed at the bottom of the finite element to restrict displacement in the three coordinate directions. In the two vertical planes of symmetry, the model was fixed in the horizontal directions. The water table was set at the top of the lithomargic clay layer, and the initial pore pressures before the embankment construction were taken to be hydrostatic. Free drainage was allowed at the bottom of the sand blanket by giving zero pore pressure boundary conditions.

| (a) | (b) |
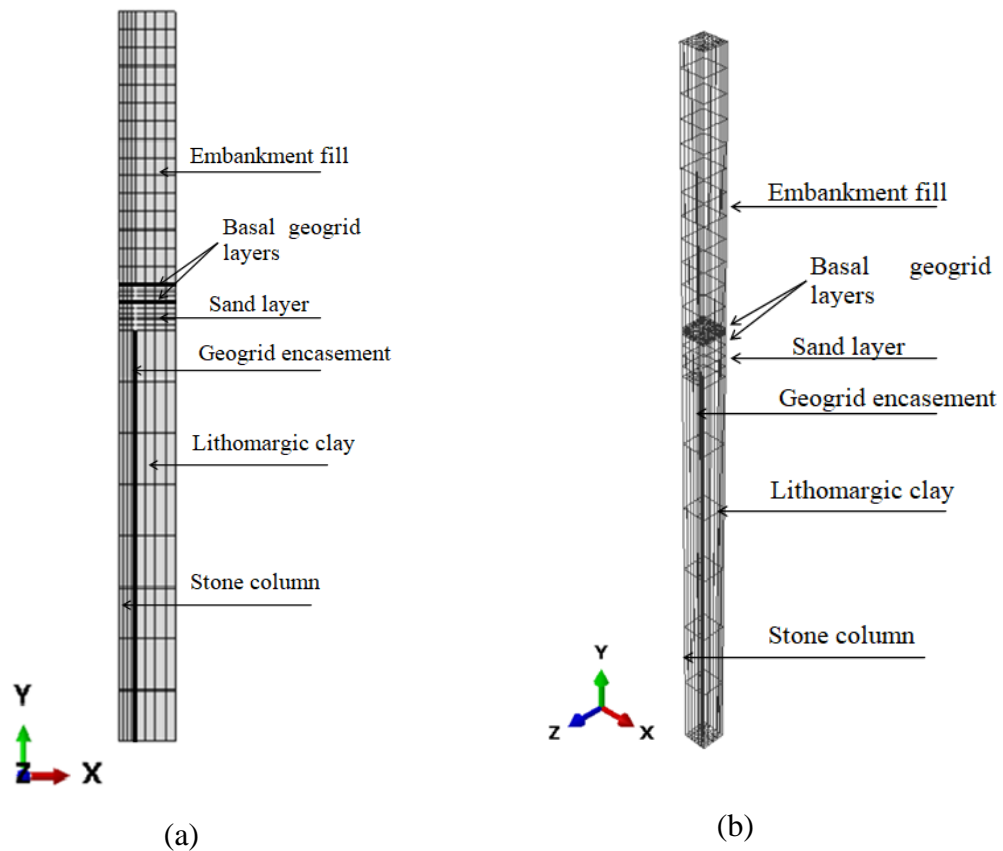
Fig. 5.2 Developed models for geogrid reinforced encased stone column supported embankment (a) axisymmetric and (b) 3D column model

## 5.2.5  Interaction

The load transfer mechanism in geosynthetic reinforced encased stone supported embankments depends on the interaction between various elements: geogrid-surrounding soil; encased stone column-lithomargic clay bed. The membrane action of the reinforcement layer can be simulated by giving proper interaction between the reinforcement and embankment fill. When a single layer of geocell replaces reinforcement layers (planar), the interaction between geocell walls and the infill soil plays an essential role in transferring embankment load to the stiffer columns below. Contact in ABAQUS requires defining interacting surfaces known as contact pairs. The more rigid material acts as a master surface and the flexible material as the slave surface among the two contacting surfaces. Hard contact was assumed at the geocell–infill soil interface, and no separation was allowed in the normal direction (Leshchinsky and Ling 2012). The Coulomb friction model was used in the tangential direction to define the

critical shear stress ($\tau_{crit}$). The shear behavior was specified by the friction coefficient μ ($\tau_{crit=}$ μσ´= [tanδ] σ´ where σ´ is the normal stress between the surfaces). The interface friction angle (δ) was taken as 2/3 of the infill soil friction angle (Biabani et al. 2016a). An elastic slip of 1 mm was considered in the analyses, limiting relative shear displacement before the allowable interface shear stress is reached.

Tie constraints were used to define the interaction between geogrid encasement, stone columns, and lithomargic clay. Tight interlocking was assumed between the stone column and the surrounding soil (Castro 2017). The soil being stiffer is taken as the master surface and the flexible geogrid used for encasement as the slave surface. The slave surface has the same degree of freedom as the master surface in transitional and rotational movement.

### 5.2.6 Methodology

All the nodal displacements were set to zero once the geostatic initial stresses were established in the foundation soil (Lithomargic clay). In the second step, the stone column and the encasement were added as "wished-in-place". The effect of stone column installation was not considered in this work. Later, basal reinforcements were placed over the drainage blanket. In the geocell layer case, infill soil was filled in the cell pockets. Once the reinforcement was placed, the interaction was activated along with the reinforcement- soil interfaces. The embankment construction was then simulated in three equal lifts of 2 m each. A construction period of 15 days and a consolidation time of 10 days were given for each embankment layer. After the full placement of embankment layers, consolidation analysis was carried out until the excess pore water pressure fell below a specified near-zero value.

### 5.3   LOAD TRANSFER FROM THE SOIL TO THE STONE COLUMN

The load transfer in the geosynthetic reinforced encased stone column supported embankment was explained by various mechanisms such as (i) soil arching, (ii) membrane effect, etc. Different terms used to describe the mechanisms were (a) maximum surface settlement, (b) Differential settlement, (c) Arching ratio, (d) Stress concentration ratio, and (e) Pore water pressure distribution. The amount of embankment load transferred to the columnar structures can be evaluated by analyzing

108

these parameters. The variation of these parameters with different reinforcement conditions is explained in subsequent sections. The results obtained from the developed 2-dimensional axisymmetric and 3D column models are given in this chapter.

The results from a comparative study of three cases (a) ordinary stone column (OSC), (b) geogrid encased stone column (GESC), and (c) geogrid encased stone column with a horizontal layer of geogrid at the embankment base (GESC + One basal layer) is presented.

### 5.3.1 Settlement-Time Response

The surface settlement ($\Delta s$) is measured at the top surface of the lithomargic clay layer. Fig. 5.3 shows the variation of foundation surface settlement with time obtained from 3D column analyses for the different embankment support considered. The foundation soil surface settlement reduced considerably compared to an unreinforced foundation soil with the introduction of basal geogrid and encased stone columns. The geogrid encasement increased the stiffness of the stone column. It decreased the excess pore water pressure generation (Yoo and Kim 2009). Due to the membrane action of the basal geogrid layer, more embankment load is transferred to the stiffer stone columns, resulting in lesser settlement of the foundation soil (lithomargic clay).

Table 5.4 compares the foundation surface settlement at various times for the different cases considered in the study. For 3D column analyses, a reduction of 72% in the surface settlement was obtained with GESC than an unreinforced foundation soil at the end of the consolidation stage. In the case of GESC with one basal geogrid layer, the reduction in the settlement was 78%. The axisymmetric model gives slightly higher values of settlement in all the cases.

### 5.3.2 Stress Concentration Ratio (SCR)

The stress transfer in geosynthetic encased stone column (GESC) supported embankments with basal geogrid is quantified by the term stress concentration ratio (SCR), which is the ratio of stress acting on the stone column to that of the surrounding soil. Being stiffer, encased stone columns take more load than the surrounding lithomargic clay.
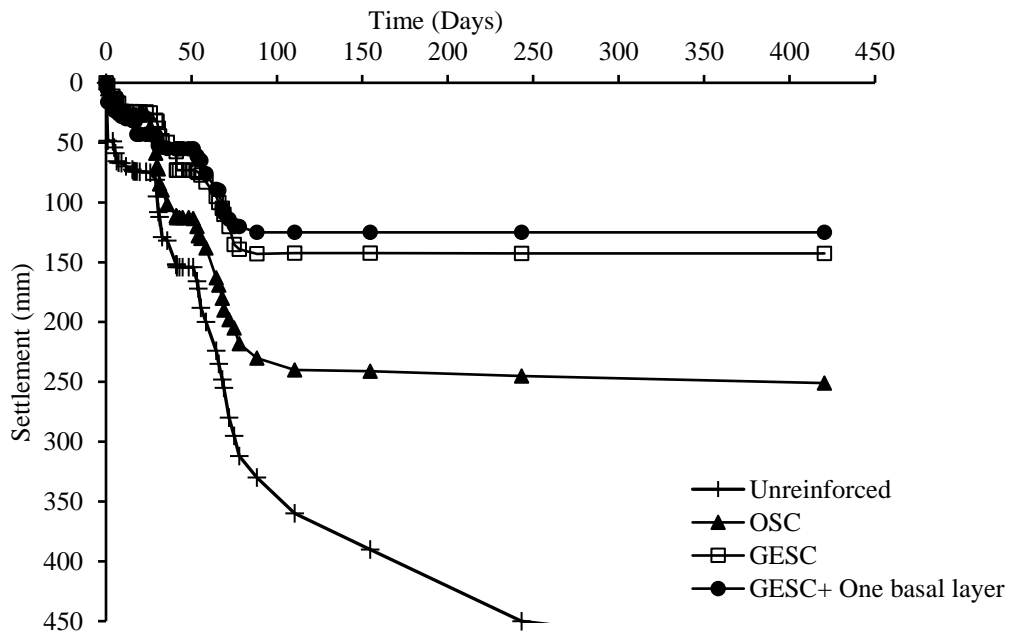
(a)
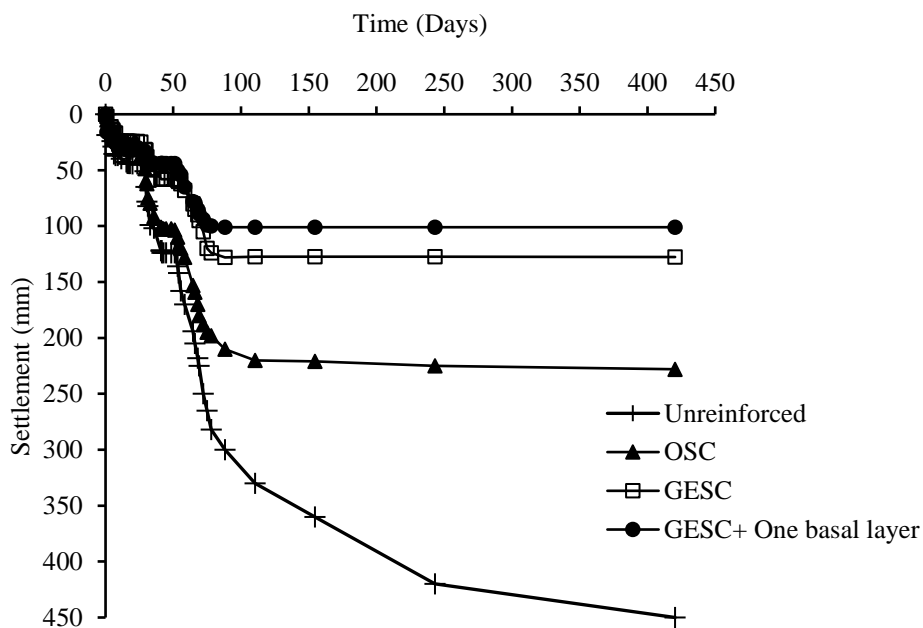


(b)

Fig. 5.3 Time-settlement graph (a) axisymmetric analysis and (b) 3D column analyses

The variation of stress concentration ratio with time and with embankment height at the mid-depth of the lithomargic clay layer is given in Fig. 5.4 and Fig. 5.5, respectively. Fig. 5.4 shows that the stress concentration ratio is not constant and increased with time for all three cases considered. By providing a geogrid layer on the

top of GESC, the stress concentration ratio improved by 52% at the end of consolidation than OSC alone. The membrane action in geogrid due to the mobilized tensile strength and the loading platform's stiffness improvement led to increased SCR.

Table 5.4 Variation of foundation surface settlement with time

| Cases | Foundation Settlement(mm) | | | | Percentage reduction with respect to unreinforced soil (%) | | | |
|---|---|---|---|---|---|---|---|---|
| | End of embankment construction | | End of foundation soil consolidation | | End of embankment construction | | End of foundation soil consolidation | |
| | 3D column | Axi symmetry | 3D column | Axi symmetry | 3D column | Axi symmetry | 3D column | Axi symmetry |
| Unreinforced | 205 | 230 | 450 | 480 | - | - | - | - |
| OSC | 159 | 170 | 228 | 251 | 23 | 26 | 49 | 48 |
| GESC | 85 | 100 | 128 | 144 | 58 | 56 | 72 | 70 |
| GESC+ One basal layer | 79 | 90 | 101 | 125 | 62 | 61 | 78 | 74 |

Table 5.5 summarizes the stress concentration ratio at the end of consolidation (long-term stability) for all three cases considered in the study. The axisymmetric model gave higher stress concentration ratio values compared to the 3D column model. For GESC+ One basal layer, only 3% variation was observed between the 3D column and axisymmetric model.

Table 5.5 Variation of SCR for different cases

| Cases | SCR (At the end of consolidation) | | Percentage increase with respect to OSC (%) (%) | |
|---|---|---|---|---|
| | Axisymmetric | 3D column | Axisymmetric | 3D column |
| OSC | 5.1 | 4.6 | - | - |
| GESC | 6 | 5.8 | 18 | 26 |
| GESC+ One basal layer | 7.2 | 7 | 41 | 52 |
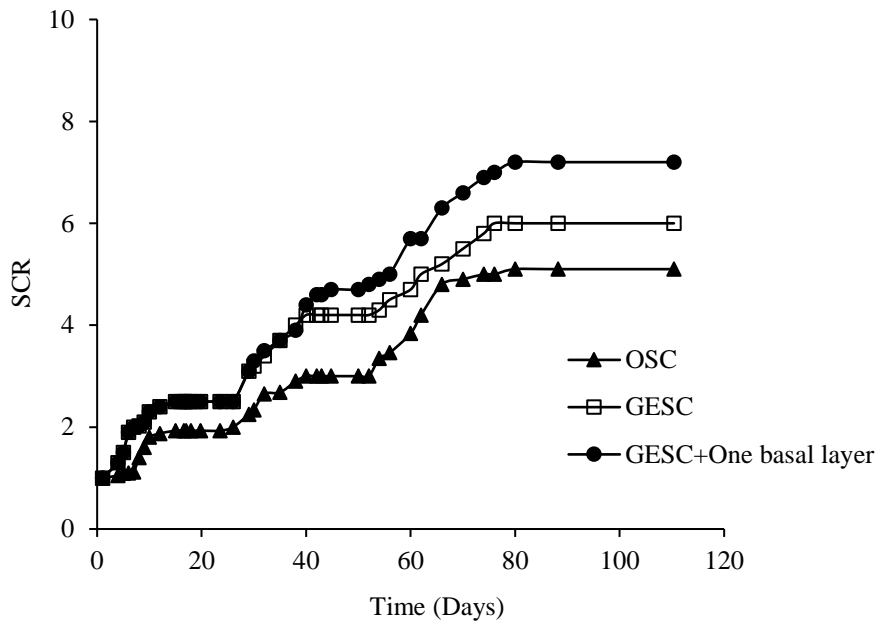
(a)
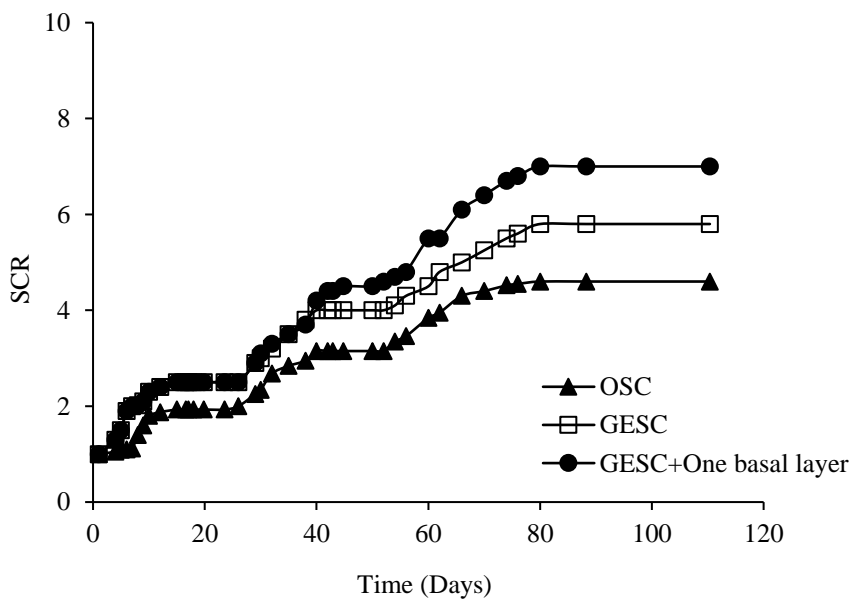


(b)

Fig. 5.4 Variation of SCR with time(a) axisymmetric analysis and (b) 3D column analyses

The effect of embankment height on the stress concentration ratio was evaluated by plotting the stress concentration ratio against a non-dimensional embankment height H/(S-D) in Fig. 5.5. Here, 'H' is the embankment height, 'S' is the center to center spacing of encased stone columns, and 'D' is the diameter of the stone column. Fig. 5.5 shows that the stress concentration ratio increased with embankment height due to the increase in the load transferred to the stone column with height. For low height embankments, encased stone columns with and without basal geogrid showed almost the same stress concentration ratio values. With an increase in embankment height (H> 2(S-D)), the basal reinforced system showed a significant improvement in stress concentration ratio than the ordinary GESC supported embankment. Higher embankment height generated more stress at the embankment base. The geogrid reinforced system could transfer more load to the encased stone column, which reduced the stress coming to the lithomargic clay bed.
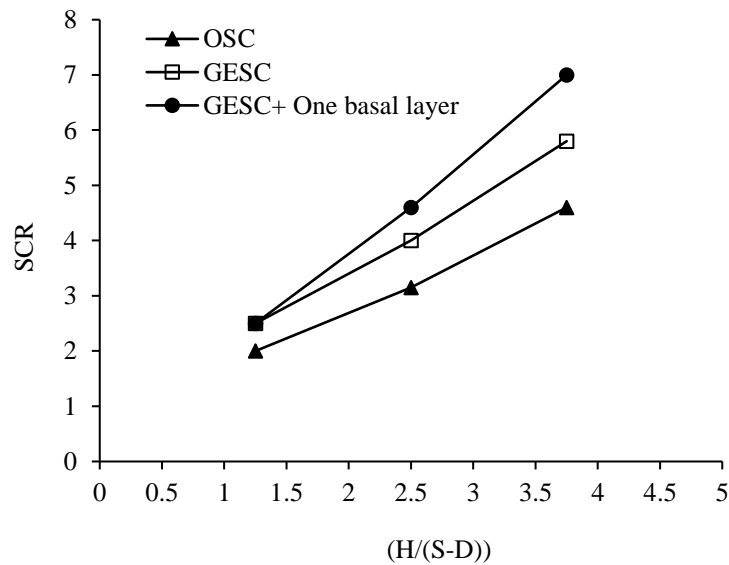


Fig. 5.5 Variation of SCR with the height of the embankment (3D column analyses)

### 5.3.3   Soil Arching

Due to the stiffness difference between an encased stone column and the surrounding soil, the settlement above the stone column and soft soil are not the same. The term differential settlement quantifies the difference in the settlement. The embankment fill mass between the columns has a tendency to move downwards under the influence of fill weight. Differential settlement tends to occur between the relatively rigid columns

and the soft foundation material. This causes the soil material between the columns to settle more than the material above the columns. The downward movement is partially restrained by the shear resistance from the embankment fill. Shear resistance developed along the interface increases the load transferred to the columns and reduced the load acting on the soil. This load transfer mechanism is termed as soil arching (Fattah et al. 2015). Even though not very prominent, the load transfer by soil arching is present in the stone column supported embankments. The arching effect depends on the properties of foundation and embankment soils, the presence of basal geosynthetic layer and its stiffness, stone column spacing and stiffness, the degree of consolidation of the foundation soil, and the height of embankment (Deb 2010).

From Fig. 5.6, it is clear that the inclusion of a geogrid layer on the top of the drainage blanket effectively reduces the differential settlement since it restricts the embankment fill movement between the stone columns. As the embankment height increases, the differential settlement at the level of the stone column top also increases. In GESC, geogrid encasement makes the stone columns stiffer, and the stiffness difference between soft soil and stone columns resulted in higher differential settlement than OSC alone. Compared to the unreinforced GESC supported embankment, a reduction of 60 % in the differential settlement was observed for a 6 m high embankment with geogrid reinforcement (Fig. 5.6).
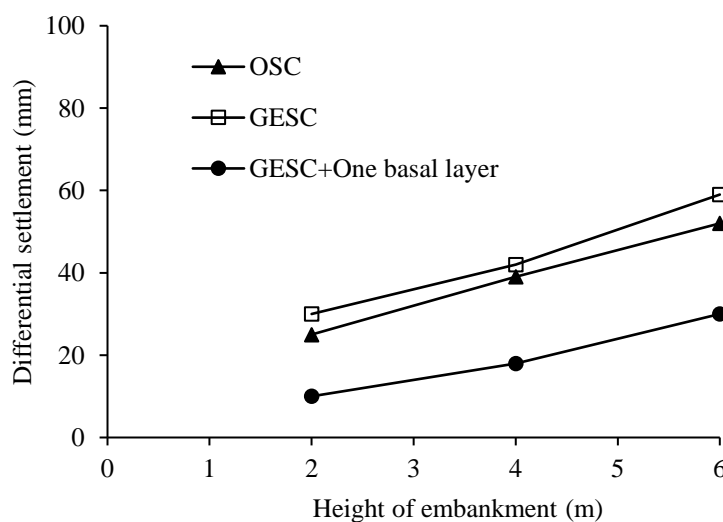


Fig. 5.6 Influence of embankment height on differential settlement (3D column analyses)

114

The degree of soil arching is quantified using the term arching ratio or stress reduction ratio (SRR). Arching ratio (AR) is defined as, AR= $\sigma_s/(\gamma_e H + q_s)$, where $\sigma_s$ is the stress in the soil, $\gamma_e$ is the unit weight of embankment fill, H is the height of the embankment, and $q_s$ is the surcharge applied on the surface of the embankment (McNulty 1965). An arching ratio of '0' corresponds to full arching, and '1' corresponds to no arching (Liu et al. 2007; Das and Deb 2018). Fig. 5.7 shows that the arching ratio of the geogrid reinforced encased stone column supported embankment is more than that of the encased stone column supported embankment. The basal geogrid layer increases the stiffness of the drainage layer, which hinders the arching action.
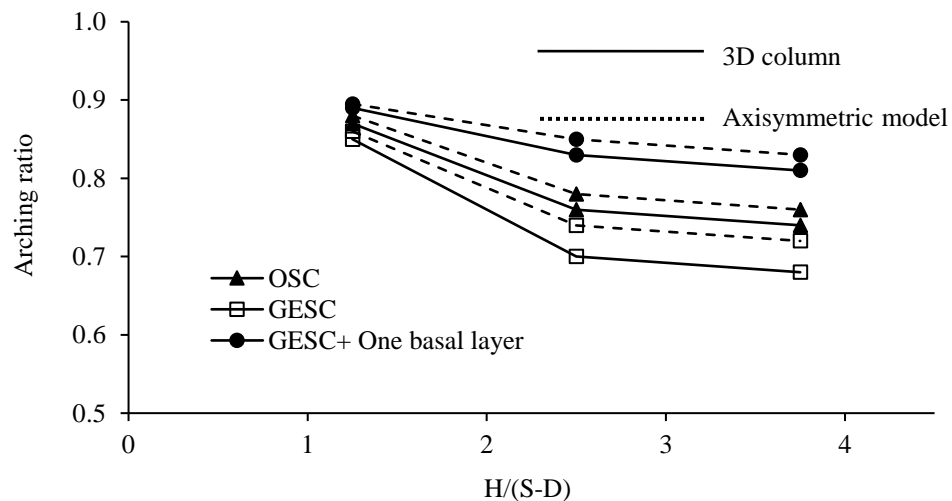
Fig. 5.7 Variation of arching ratio with embankment height for GESC and GESC+ One basal layer

The arching ratio inversely varies with the embankment height for OSC, GESC, and GESC+ One basal layer supported embankments. Also, from Fig. 5.7, it can be observed that after a particular height (H > 2.5 (S-D)), the arching ratio is approaching a constant value. In ordinary and encased stone column supported embankments, with an increase in the embankment height, the shear resistance accumulated is more, promoting soil arching. The stiffening effect due to the basal geogrid layer effectively reduces the differential settlement in the embankment soil and hinders the arching development. The reduction in the differential settlement due to basal reinforcement can be considered the cause of the increased arching ratio. The axisymmetric unit cell

model yields higher stress values in the soil, resulting in a higher arching ratio than 3D column models.

The orientation of principal stresses in the numerical analyses shows the formation of the arches in the embankment (Fig 5.8). The stresses are concentrated towards the stone columns due to arching. Thus, the bottom-most reinforcement layer will undergo maximum deformations.
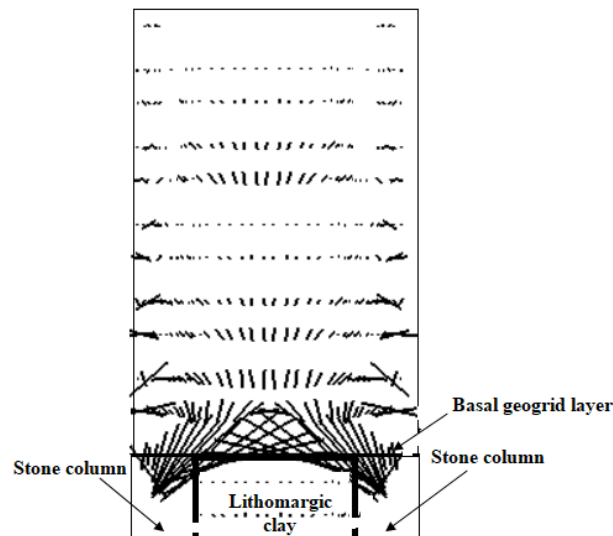


Fig. 5.8 Orientation of principal stresses in the case of GESC+ One basal layer

### 5.3.4 Bulging Characteristics of Stone Columns

Due to the embankment loading, the stone column bulges and gets lateral support from the encasement and the surrounding soil (Murugesan and Rajagopal 2007). Fig. 5.9 shows the change in stone column diameter (%) versus normalized depth (h/D), where 'h' is the stone column depth, and 'D' is the stone column's initial diameter. The vertical confinement of the basal geogrid layer effectively redistributes the embankment load to deeper depths. This decreases the horizontal extent of the stone column bulging. Almost 69% reduction in the lateral bulging occurred for GESC with a single basal layer than OSC alone. In geogrid reinforced encased stone column supported embankment, the maximum bulging happened in the upper 3.5D zone of stone columns. For GESC supported embankments, the corresponding zone is 3D, and for OSC, it is 2.5D. The maximum value for lateral bulging obtained from the axisymmetric model is larger than the 3D column results. The depth of maximum bulging remains the same in

both models. For GESC+ One basal layer, a 12% increase in lateral bulging was obtained with axisymmetric models.
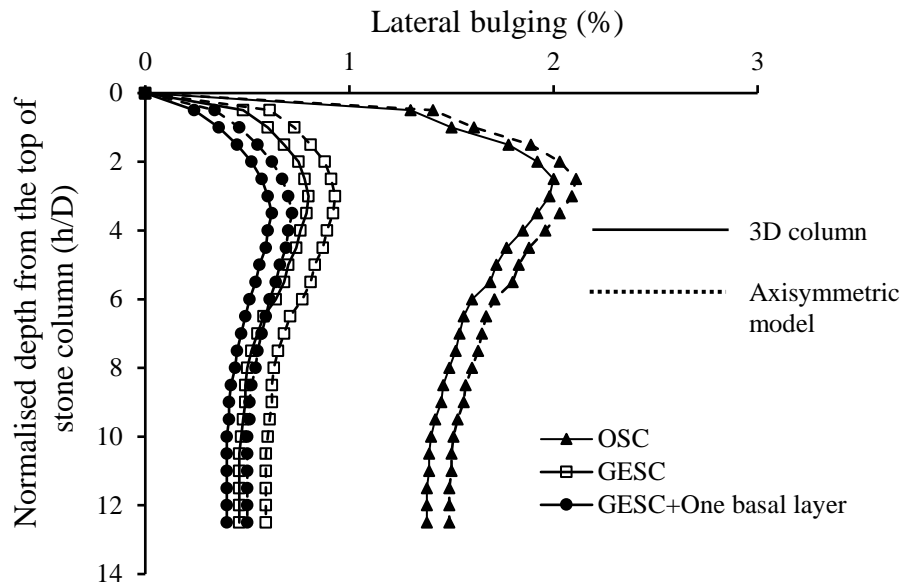


Fig. 5.9 Lateral bulging profile of stone column for OSC, GESC and GESC+ One basal layer

## 5.4   PARAMETRIC STUDIES

Different reinforcement conditions such as OSC, GESC, and GESC+ One basal layer was compared and quantified the improvement. In this section, various parameters that influence geogrid reinforced encased stone column supported embankment were analyzed using the developed 3D column models. Compared to axisymmetric models, 3D column models gave more accurate results than full three-dimensional analyses (Bhasi and Rajagopal 2015). Hence, the parametric analyses were carried out with the help of a 3D column model as the computational time required for the full three-dimensional analyses is typically an order of magnitude more. The parameters considered are given below,

(i)   Stiffness of the basal geogrid: The stiffness of the basal geogrid was varied between 1000 kN/m to 6000 kN/m

(ii)   Modular ratio: The modular ratio (ratio of elastic modulus of stone column material ($E_c$) to surrounding soil ($E_s$)) was varied from 10 to 40.

(iii)    Drainage layer thickness: The influence of drainage layer thickness on the performance of encased stone column supported geogrid reinforced embankment was studied by varying the thickness from 0.5 m to 1 m.

### 5.4.1    Effect of Stiffness of Basal Geogrid

In the present study, the basal reinforcement's stiffness varied between 1000 kN/m to 6000 kN/m, and the effect on foundation settlement, SCR, and arching ratio was found. The results were depicted in Figs. 5.10 to 5.12.

From Fig. 5.10, it is clear that foundation settlement decreases with an increase in the stiffness of basal geogrid. After a value of 4000 kN/m, the reduction is not that significant. The stress concentration ratio directly varies with the increase in basal geogrid stiffness (Fig. 5.11). The additional tensile component of the basal reinforcement and stiffening effect imparts the improvement. The arching ratio (AR) also shows the same trend as SCR (Fig. 5.12). When the basal reinforcement gets stiffer, the differential settlement decreases, and thus soil arching is minimized. Deb and Mohapatra (2013) also observed similar trend in basal reinforced stone column supported embankment.
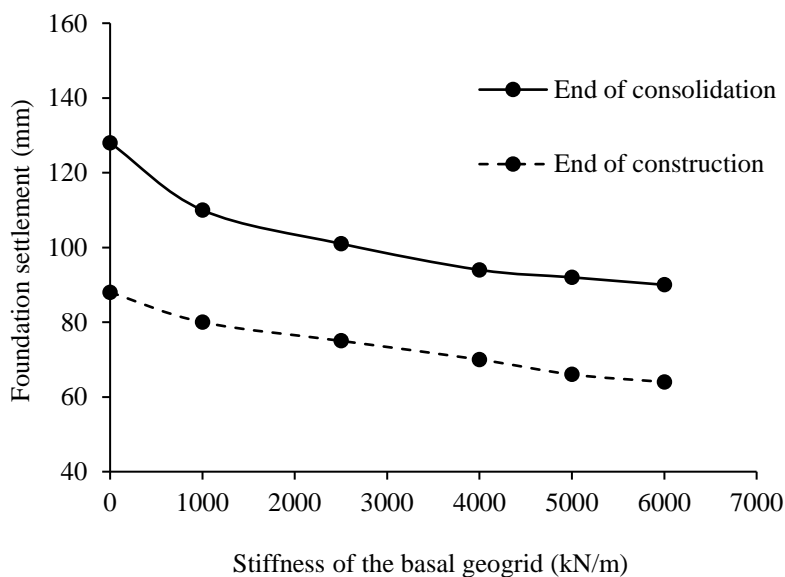


Fig. 5.10 Effect of basal geogrid stiffness on foundation settlement
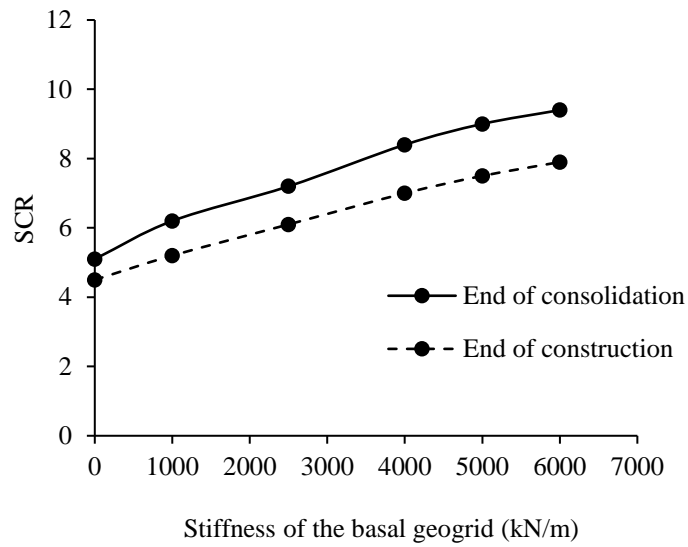
Fig. 5.11 Effect of basal geogrid stiffness on the stress concentration ratio
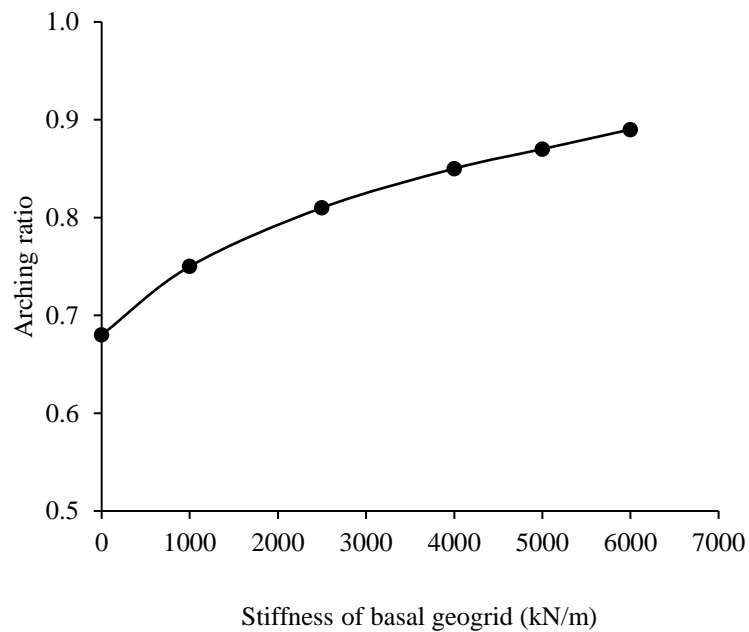


Fig. 5.12 Effect of basal geogrid stiffness on the arching ratio

### 5.4.2 Effect of Modular Ratio

The foundation settlement is found to be decreasing with the increase in modular ratio (Fig. 5.13). This can be explained by the increased load transfer from the foundation soil to the stone column when the stiffness difference between the stone column and the foundation soil is more. Fig. 5.14 supports these observations where the stress

concentration ratio increases with an increase in columns' modular ratio/ stiffness. In Fig. 5.15 arching ratio was plotted against different modular ratios (ratio of elastic modulus of stone column material ($E_c$) to surrounding soil ($E_s$)). The arching ratio was found to decrease with the increase in modular ratio. When the modular ratio or the stone column's stiffness is increased, the soil arching effect also increased, which resulted in a lesser arching ratio. Fig. 5.15 shows that the consolidation of foundation soil resulted in an increased load transfer from foundation soil to columns, which decreased the arching ratio.
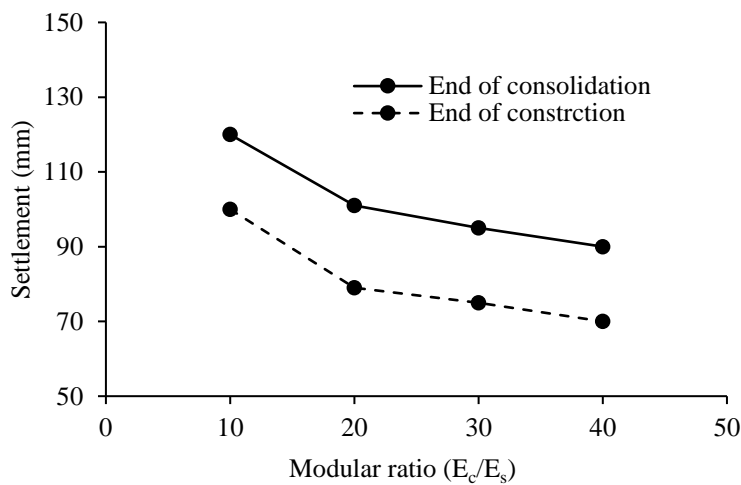


Fig. 5.13 Effect of modular ratio on foundation settlement
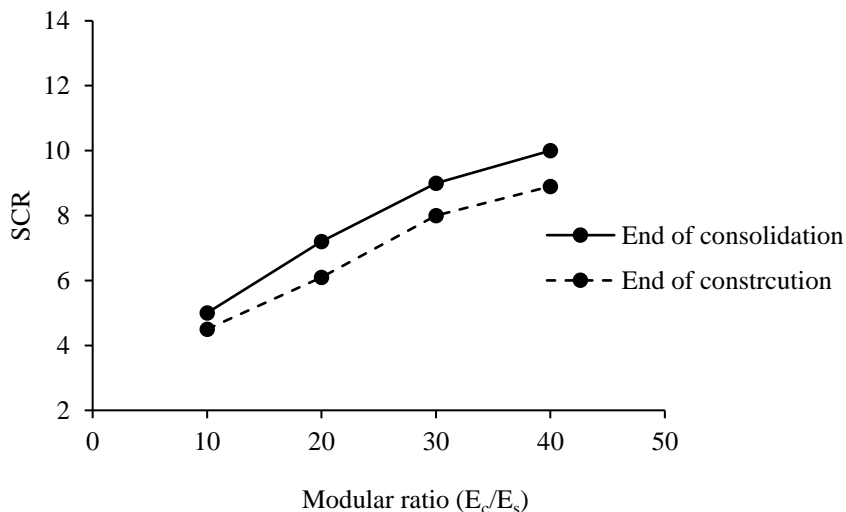


Fig. 5.14 Effect of modular ratio on the stress concentration ratio
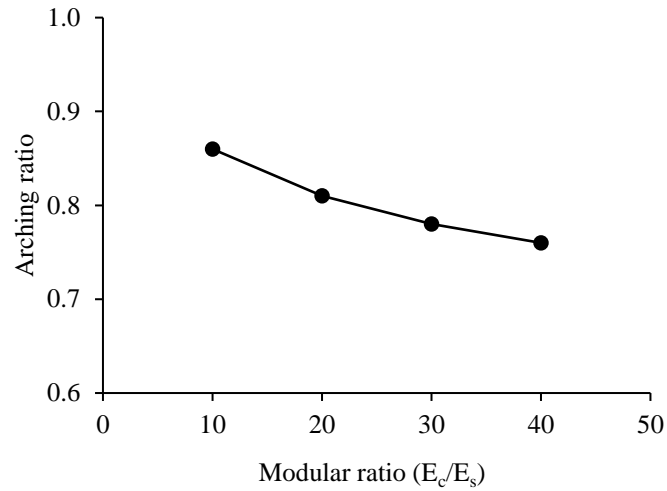
Fig. 5.15 Effect of modular ratio on the arching ratio

### 5.4.3 Effect of Drainage Layer Thickness

The sand layer placed above the stone columns helps in drainage as well as distributing the embankment load. A drainage blanket of thickness 30 cm or more is provided for stone column reinforced ground (Mitchell 1981). The influence of drainage layer thickness on the performance of stone column supported geocell reinforced embankment is studied by varying the thickness from 0.5 m to 1 m. The performance was evaluated based on foundation settlement, stress concentration ratio (SCR), and the stone column's bulging characteristics.

From Figs. 5.16 and 5.17, it was clear that the drainage layer thickness inversely affected the foundation soil settlement and directly influenced the stress concentration ratio. The higher shear modulus of the drainage blanket transfers more embankment load to the stone column, resulting in a higher SCR and reduced foundation soil settlement (Deb 2008). Debnath and Dey (2017) also observed that load-carrying capacity of the stone columns with unreinforced sand bed and geogrid reinforced sand bed increases as the thickness of the sand bed increases. The stone column's bulging profile was plotted against the normalized depth 'h/D,' where h is the stone column length, and D is the stone column diameter. It can be observed from Fig. 5.18 that with an increase in drainage layer thickness, lateral bulging of the stone column was reduced. The drainage layer acted as a stress distributor, and when the thickness is more, the

effective transfer of load occurs to a deeper depth, which reduces the bulging diameter (Nassaji and Asakereh 2013). A 26 % reduction in maximum bulging diameter, a 27% decrease in the settlement, and a 10 % increase in SCR were observed when the drainage layer thickness increased from 0.5 m to 1 m. For all the cases, the maximum bulging depth remained the same as 3.5 D, where D is the stone column diameter.
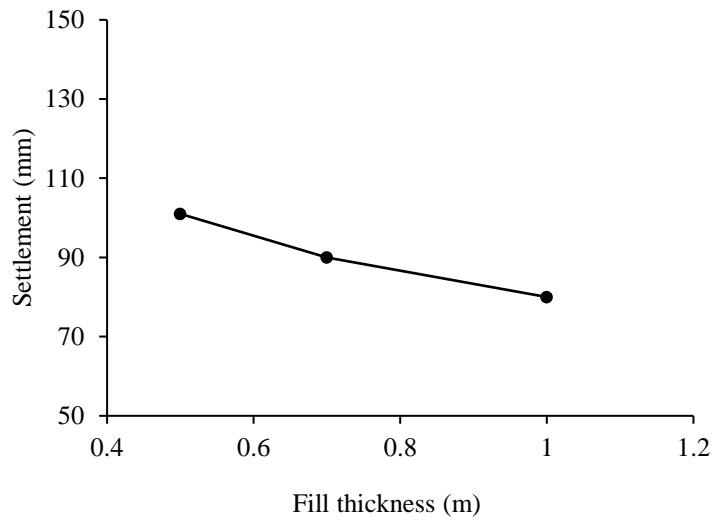


Fig. 5.16 Effect of drainage layer thickness on foundation soil settlement
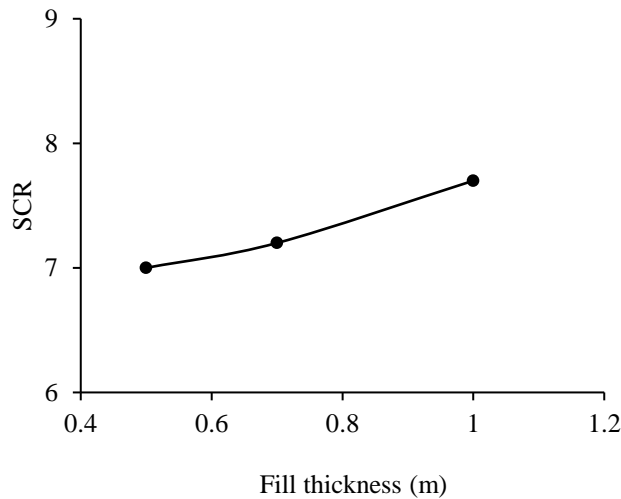


Fig. 5.17 Effect of drainage layer thickness on the stress concentration ratio
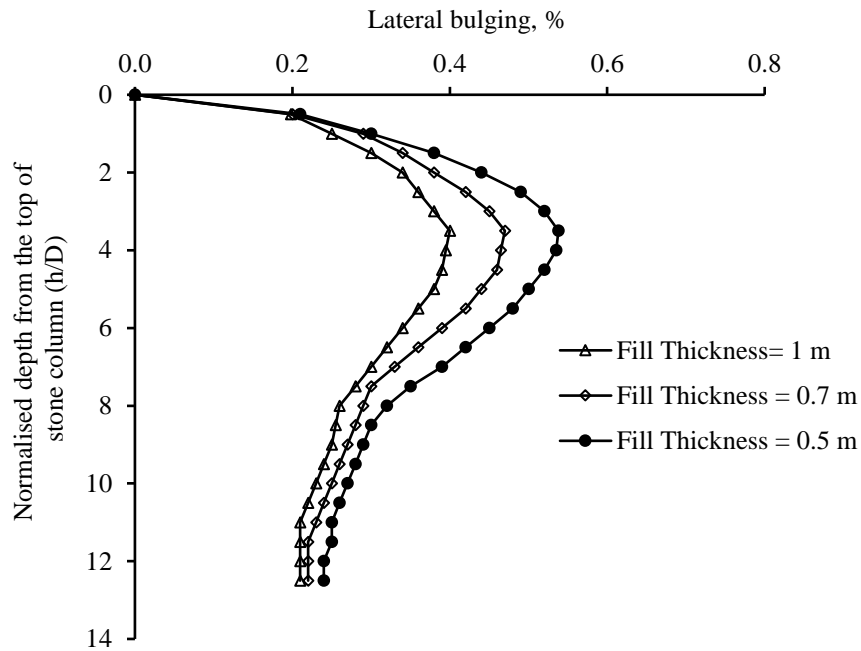
Fig. 5.18 Effect of drainage layer thickness on lateral bulging of stone column

## 5.5 EFFECT OF MULTIPLE REINFORCEMENT LAYERS ON LOAD TRANSFER

The influence of a multilayer reinforcement system on embankment load transfer to stone columns was analyzed in this section. Instead of a single basal geogrid layer of 2500 kN/m, two layers of geogrids, each having a stiffness value of 1250 kN/m, are provided at the embankment base (Fig. 5.19), and their effect on various parameters is evaluated with the developed 3D column models.

### 5.5.1 Comparison with the single-layer system

The variation of foundation settlement with time was plotted in Fig. 5.20. A reduction of 10% in the settlement was observed at the end of consolidation when the number of basal geogrids increased from 1 to 2. The SCR value also increased with the number of basal layers, and the improvement is 9% (Fig. 5.21). A 16% reduction in the differential settlement was observed for a 6 m high embankment (Fig. 5.22), and the increased arching ratio indicated less arching in a multi-layered system (Fig. 5.23).

(a)



(b)
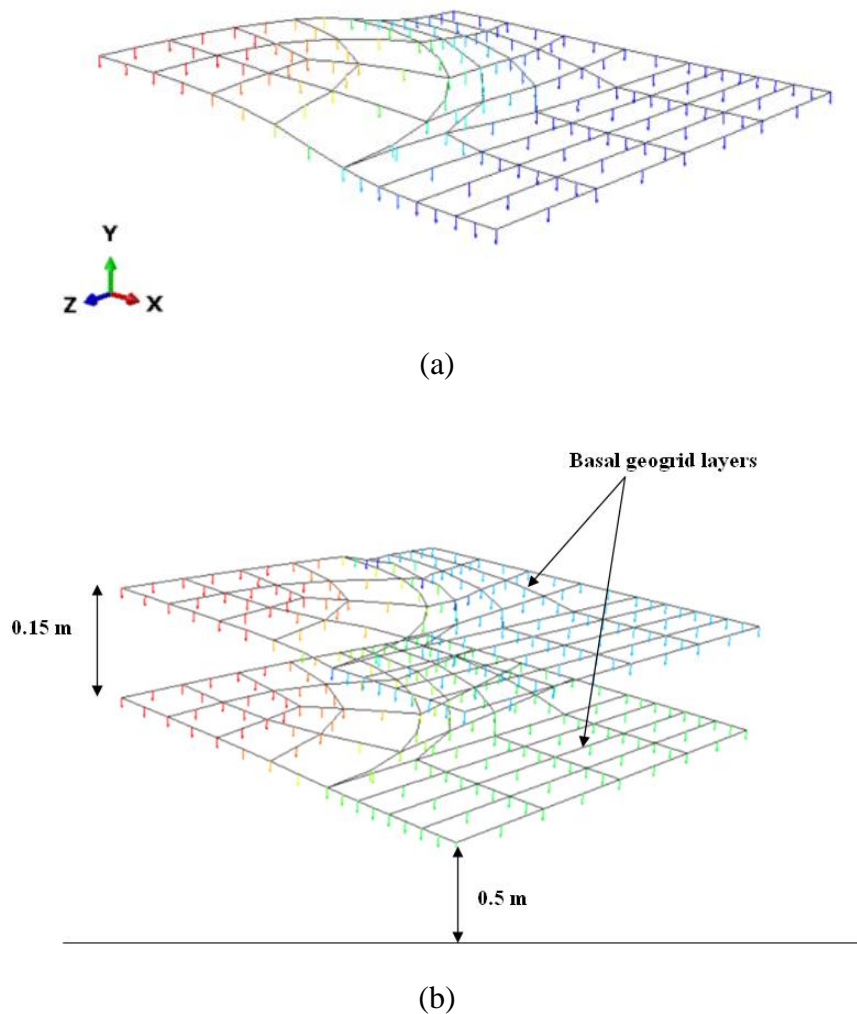
Fig. 5.19 Different arrangement of reinforcement layers used in analyses (a) single reinforcement layer and (b) two reinforcement layers

## 5.6   USE OF GEOCELL SAND MATTRESS AS LOAD TRANSFER PLATFORM

The results from the previous sections showed that multiple layers of reinforcement provided at the base of the embankment act as a load transfer platform [LTP] to transfer the load from the embankment above LTP to the columns beneath. The combined use of columnar systems and multiple layers of reinforcement is effective in load transfer, which reduced the total and differential settlement. The above observations motivated to study the system's performance when multiple layers of geogrids are replaced by a

single layer of geocell, considered a superior form of reinforcement because of the three-dimensional confinement offered to the infill material.
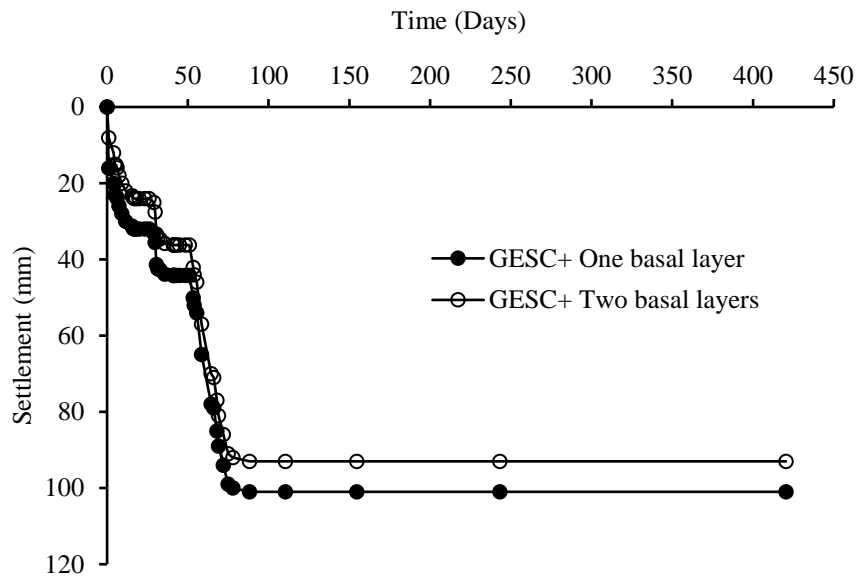


Fig. 5.20 Variation of foundation settlement with time for different basal layers
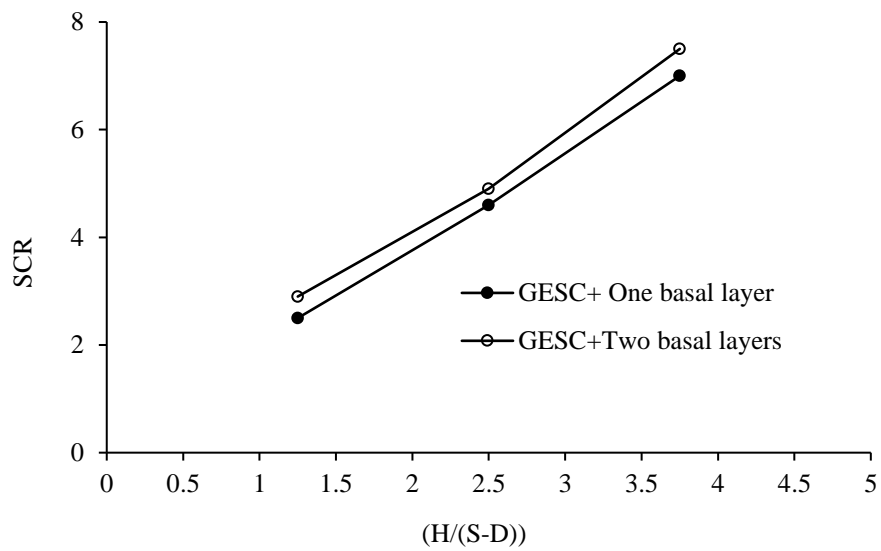


Fig. 5.21 Variation of SCR with embankment height for different basal layers
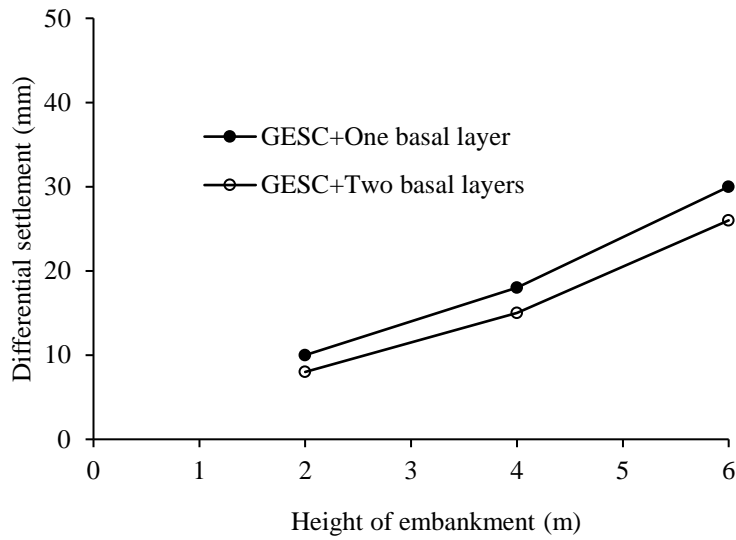
Fig. 5.22 Variation of differential settlement with embankment height for different basal layers
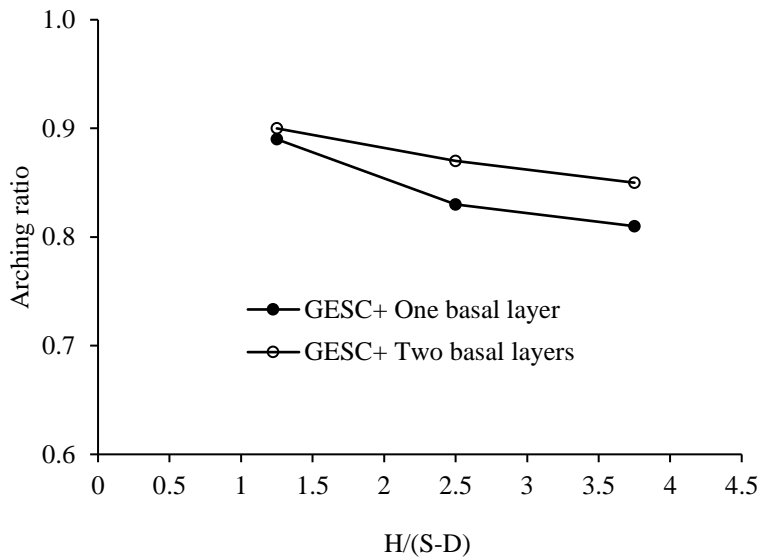


Fig. 5.23 Variation of arching ratio with embankment height for different basal layers

The numerical modeling of geocell is intricate due to its complex three-dimensional honeycomb structure. Earlier researchers adopted an equivalent composite approach (ECA) for the geocell reinforced soil's numerical simulations. The shortcomings of the equivalent composite approach led to advancements in geocells' three-dimensional modeling considering the geocell curvature and the geocell-infill soil interaction. The circumferential strain developed due to the 3D honeycomb structure of

geocells provides additional confinement, which is not considered in the ECA approach. Thus, there is a necessity for a three-dimensional framework for numerical modeling of geocells. The proposed 3D model considers geocell's actual shape and uses two different constitutive models for infill soil and geocells. The model developed also considers the interaction between the geocell and infill soil, which plays an essential role in distributing the embankment load to the stiffer stone columns. The concept of encased stone columns and the geocell-sand mattress can be considered equivalent to a flexible pile raft system. In this study, the geocell-sand mattress's effectiveness as a load transfer platform in encased stone column supported embankment was investigated by carrying out time-dependent 3D coupled analyses.

### 5.6.1 Description of the Finite Element Analyses

The 3D column model used in the present study was based on the simplified models proposed by Yoo and Kim (2009) for a geosynthetic encased stone column supported embankment resting in a soft clay bed. A detailed description of the case study was given in Section 5.2. The multiple reinforcement layers at the embankment base were replaced by a 0.15 m depth geocell sand mattress. The developed 3D column model is shown in Fig. 5.24.

### 5.6.2 Stress Transfer Mechanism

The results from a comparative study of three cases (a) ordinary stone column (OSC), (b) geogrid encased stone column (GESC), and (c) geogrid encased stone column with a horizontal layer of the geocell-sand mattress at the embankment base (GESC + GEOCELL) is presented. Fig. 5.25 shows the variation of stress concentration ratio (SCR) with time and embankment height at the mid-depth of the lithomargic clay layer. Fig. 5.25a shows that the stress concentration ratio increased with time for all three cases considered. By providing a geocell layer on the top of GESC, the stress concentration ratio improved by 47% at the end of consolidation compared to GESC alone. Compared to multi reinforcement layers, the geocell sand mattress showed improved SCR (increment of 13% compared to GESC+ Two basal layers). The membrane effect in geocells due to the mobilized tensile strength (Zhang et al. 2010) and the stiffness improvement of the loading platform due to the geocell-sand mattress

(Emersleben and Meyer 2011) led to the increase in SCR. Table 5.6 summarizes the stress concentration ratio immediately after the embankment construction (short-term stability) and at the end of consolidation (long-term stability) for all three cases. In layered construction, each embankment layer construction is followed by a waiting period for consolidation, which results in less variation in SCR value in the time between embankment construction and the end of lithomargic clay consolidation.
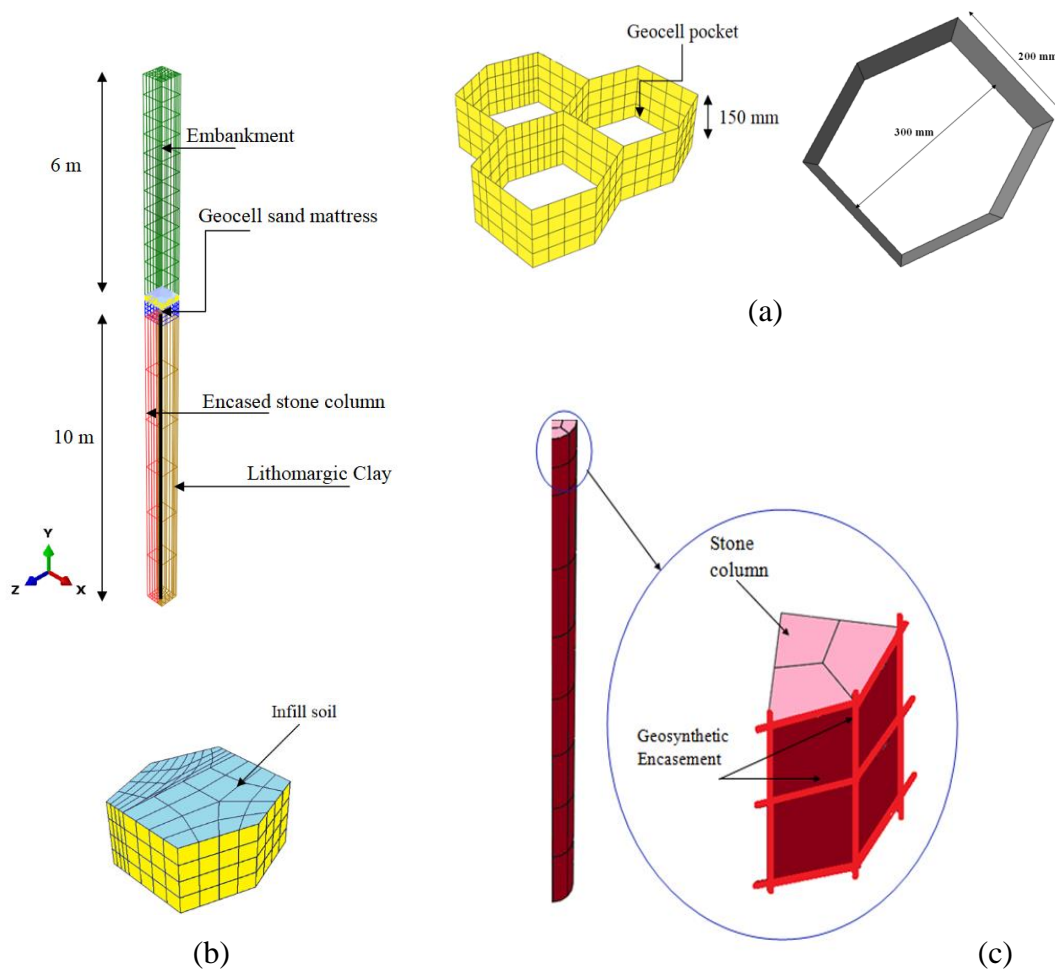


Fig. 5.24 3D column model developed (a) geocell pockets (b) single geocell pocket with infill material and (c) geogrid encased stone column
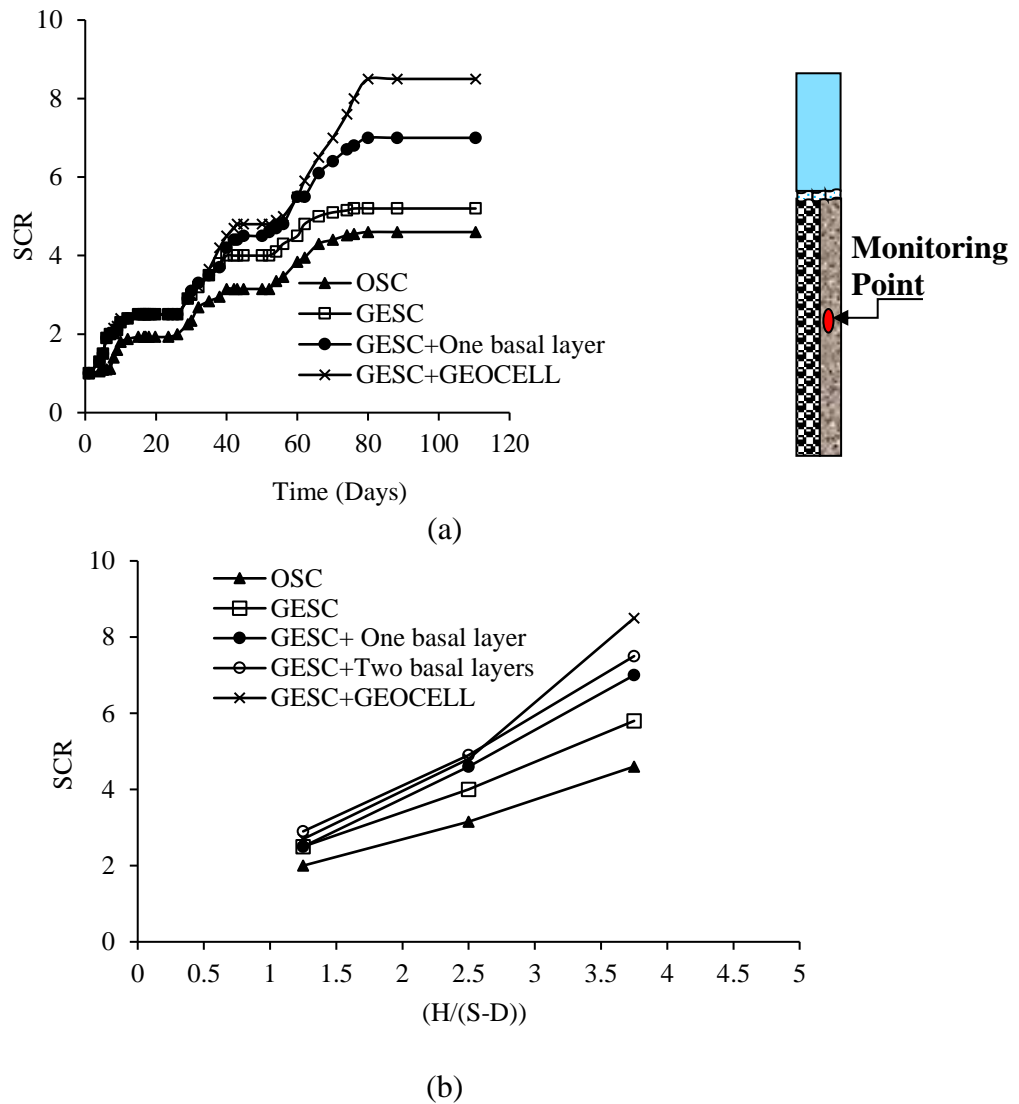
Fig. 5.25 Variation of SCR (a) with time and (b) with the height of the embankment

For low-height embankments, encased stone columns with basal geogrids and geocells showed almost the same stress concentration ratio values (Fig. 5.25b). With an increase in embankment height ($H > 2.5(S-D)$), the geocell reinforced system showed a significant improvement in stress concentration ratio than other cases. The geocell – sand infill system could transfer more load to the encased stone column, which reduced the stress coming to the lithomargic clay bed.

Table 5.6 Variation of SCR with time (3D column analyses)

| Cases | SCR | | Percentage increase with respect to OSC (%) | |
|---|---|---|---|---|
| | End of embankment construction | End of foundation soil consolidation | End of embankment construction | End of foundation soil consolidation |
| OSC | 4.3 | 4.6 | - | - |
| GESC | 5.0 | 5.8 | 14 | 26 |
| GESC+ One basal | 6.1 | 7.0 | 42 | 52 |
| GESC+ Two basal layers | 6.4 | 7.5 | 49 | 63 |
| GESC+GEOCELL | 6.8 | 8.5 | 58 | 85 |

The three-dimensional honeycomb structure of geocells confines the soil present in the cells (Fig. 5.26), and the applied load induces stress inside each section of the geocell. The induced stress causes lateral movement of the confined soil, which exerts pressure on the geocell walls, and deformation of the geocell membrane occurs. Due to the circumferential deformation, the geocell membrane's stress gets mobilized, and thus confinement pressure of soil increases (Bathurst and Karpurapu 1993). The three-dimensional confinement restricts the infill soil's lateral movement, resulting in a more stable and stiffer composite structure.

Fig. 5.27 shows the load transfer mechanism in geocell reinforced soil. Load transfer due to geocells is attributed to three mechanisms: (a) Lateral resistance effect: the shear force between the geocell wall and the infill soil imparts the lateral resistance component; (b) Vertical stress dispersion effect: the interconnected cells form a panel which acts as a slab and redistribute the applied load; (c) Membrane effect: due to the vertical loading, geocell deflects and generates additional tensile force transferring more load to the columnar inclusions beneath the geocell. All the above three mechanisms together contribute towards improving the bearing capacity of soft foundation soils.

Fig. 5.26 Confining effect of geocell reinforced sand
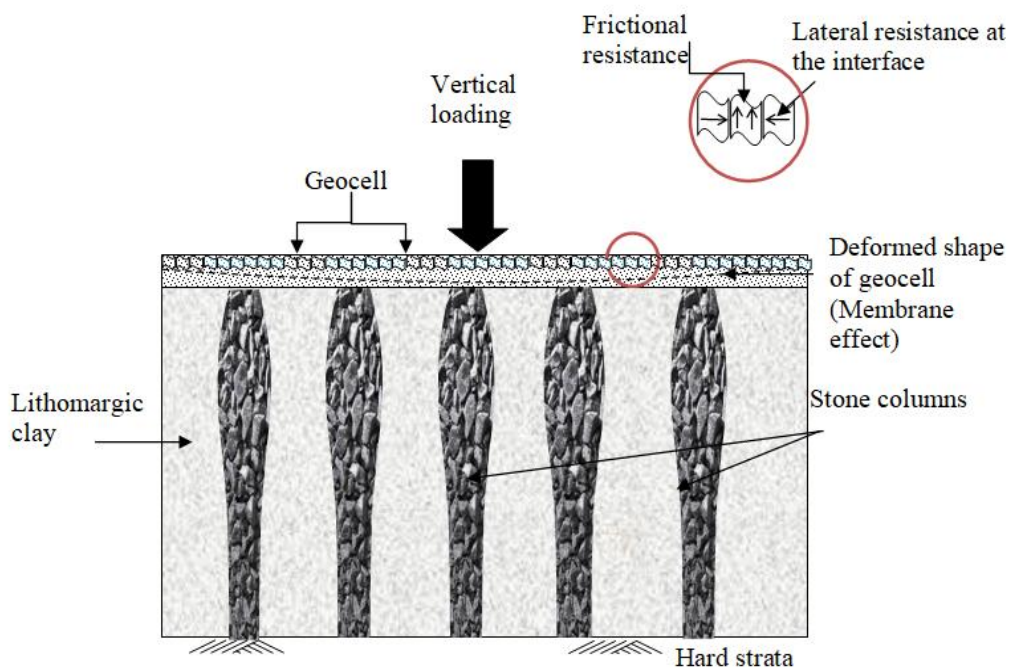


Fig. 5.27 Load transfer mechanism in geocell-sand mattress

### 5.6.3 Settlement-Time Response

Fig. 5.28 shows the settlement profile with time for the different embankment support considered in the analyses. With the introduction of geocells and geogrid encased stone columns, the foundation soil surface settlement reduced considerably compared to an unreinforced foundation soil. The geocell-sand mattress's interconnected pockets acted as a rigid mat with high bending and shear stiffness (Dash et al. 2003). The three-

dimensional confinement effect of infill material inside the geocell pockets further improved the overall system's efficiency. The results demonstrate the geocell-sand mattress's effectiveness in transferring the embankment load to encased stone columns, resulting in lesser settlement of the foundation soil.
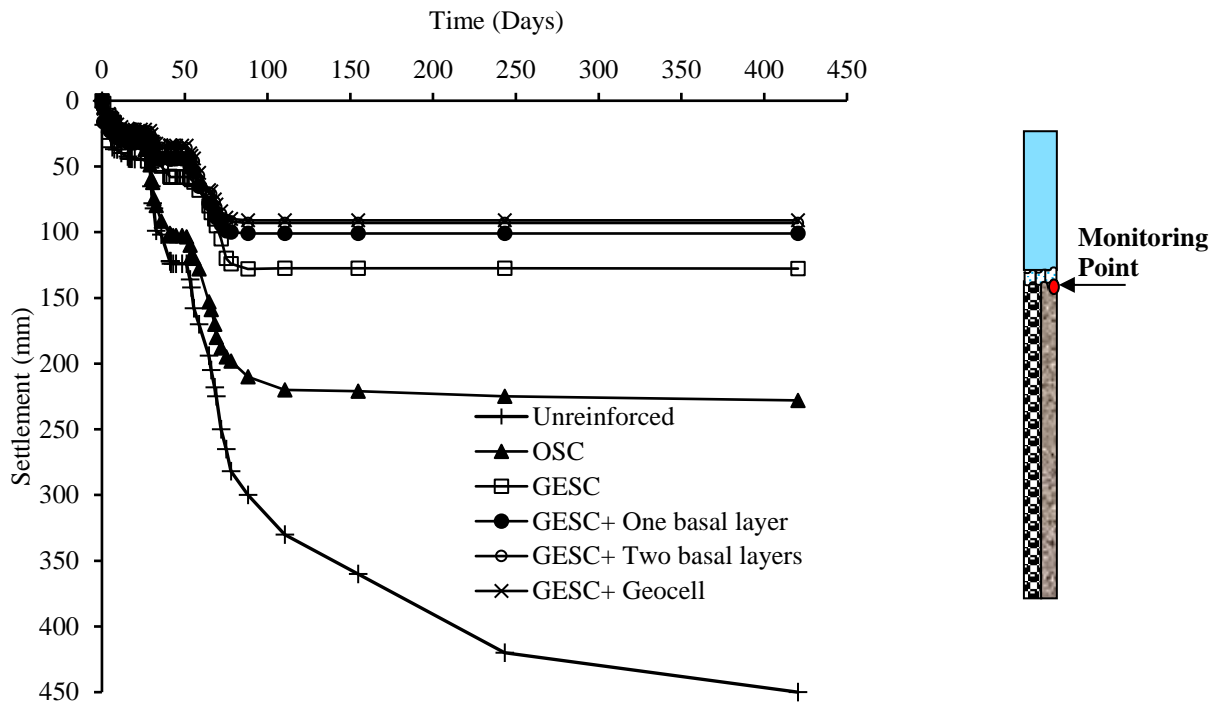


Fig. 5.28 Time-settlement graph (3D column analyses)

Table 5.7 compares the foundation surface settlement at various times for the different cases considered in the study. In the case of GESC with a geocell-sand mattress, the reduction in the settlement was 80%. The stiffer geocell-sand mattress transferred more embankment load to columns, which reduced the load coming to the lithomargic clay. To verify the geocell-sand mattress's effectiveness, excess pore water pressure was measured at the lithomargic clay layer's mid-depth and plotted in Fig. 5.29. From the Figure, it is clear that the excess pore water pressure generated in lithomargic clay is less in the case of GESC+ GEOCELL compared to GESC, which shows the increased load transfer by geocell-sand mattress system. Fig. 5.30 shows the variation of the degree of consolidation with time. It can be observed that for unreinforced ground, the degree of consolidation is 58% at the end of embankment construction. With GESC, 93% of the degree of consolidation was achieved during the construction period itself, and for GESC+GEOCELL, the degree of consolidation

132

achieved is 98%. This could be due to less excess pore pressure in the lithomargic clay due to stiffer geocell-sand mattresses at the embankment base. A considerable amount of consolidation takes place during the staged construction period itself.

Table 5.7 Variation of foundation surface settlement with time

| Cases | Foundation Settlement (mm) | | Percentage reduction with respect to unreinforced soil (%) | |
|---|---|---|---|---|
| | End of embankment construction | End of foundation soil consolidation | End of embankment construction | End of foundation soil consolidation |
| Unreinforced | 205 | 450 | - | - |
| OSC | 159 | 228 | 23 | 49 |
| GESC | 85 | 128 | 58 | 72 |
| GESC+ One basal | 79 | 101 | 62 | 78 |
| GESC+ Two basal layers | 71 | 93 | 65 | 79 |
| GESC+GEOCELL | 89 | 91 | 66 | 80 |
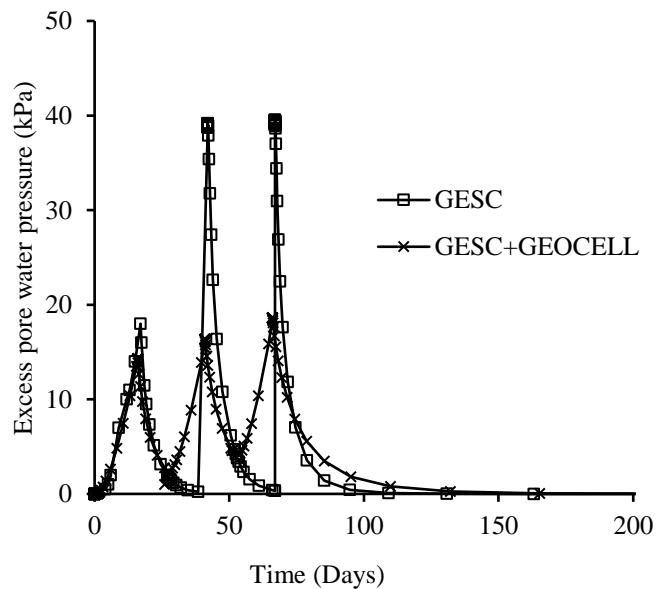


Fig. 5.29 Variation of excess pore water pressure with time
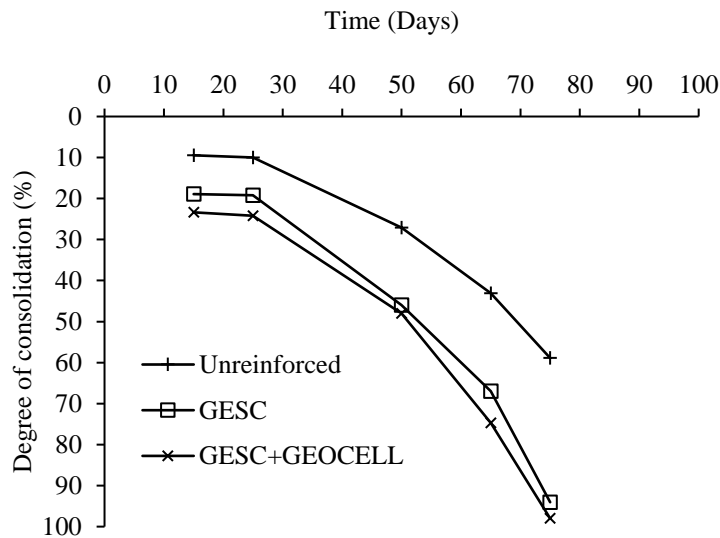
Fig. 5.30 Variation of degree of consolidation with time

### 5.6.4 Bulging Characteristics of Stone Columns

Due to the embankment loading, the stone column bulges and gets lateral support from the encasement and the surrounding soil (Murugesan and Rajagopal 2007). Fig. 5.31 shows the change in stone column diameter (%) versus normalized depth (h/D), where 'h' is the stone column depth, and 'D' is the stone column's initial diameter. It can be seen that the column bulging increased with time for GESC as well as GESC+GEOCELL. Column bulging at the end of consolidation is more than that at the end of construction as more load is transferred to the column during consolidation.

The geocell-sand mattress behaves like a structural beam ('Multilayer theory'- Collin et al. 2005). The vertical confinement of the geocell-sand mattress effectively redistributes the embankment load to deeper depths. This decreases the horizontal extent of the stone column bulging. Almost 83% of the bulging occurred by the end of embankment construction in GESC with geocell-sand mattresses. In geocell reinforced encased stone column supported embankment, the maximum bulging happened in the upper 3.5D zone of stone columns. For GESC supported embankments, the corresponding zone is 3D.
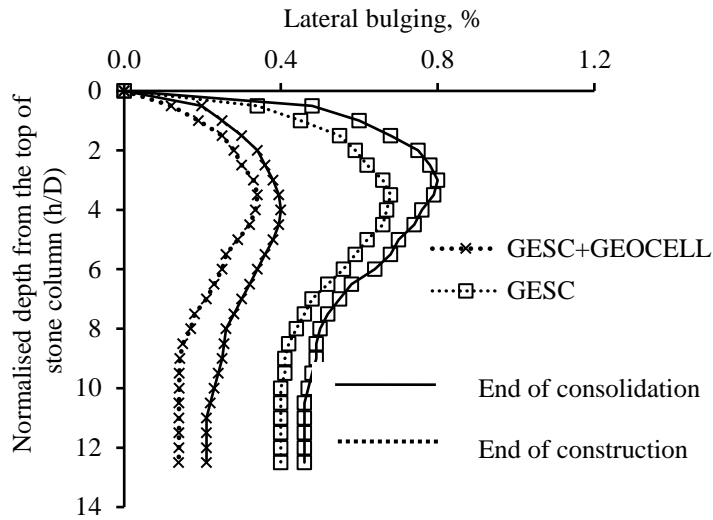
Fig. 5.31 Lateral bulging profile of stone column for GESC and GESC+GEOCELL

The vertical stress contours in the encased stone column for different cases are shown in Fig. 5.32. The vertical stress acting on the upper part of the stone column (3D region) is less for geocell reinforced GESC than GESC alone. On the contrary, higher stress values were observed at deeper levels for geocell reinforced GESC. This indicates that the geocell-sand mattress act as a stress distributor that distributes vertical stress to a greater depth of the stone column.



(a)          (b)
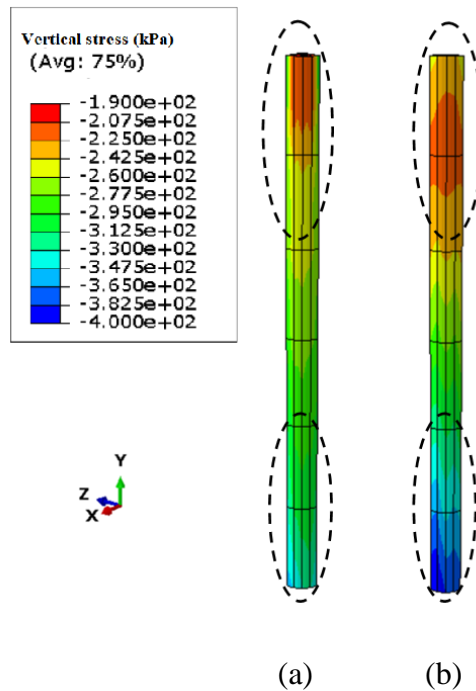
Fig. 5.32 Vertical stress distribution for (a) GESC and (b) GESC+GEOCELL

### 5.6.5 Stress-Strain Behaviour of Geocell

The performance of geocell reinforced stone column supported embankments dependent upon the tensile stress distribution in the geocell pockets. Fig. 5.33 shows the stress contours along the walls of the geocell pockets. Tensile stress distribution along the geocell-sand mattress is non-uniform, and the maximum stress was observed at the mid-height of the geocell pockets. The stress gradually decreased towards the edges. Though the mobilized tensile stress in the geocell pockets varied for an embankment loading, the tensile strength was assumed to be constant in designs. Elongation of the geocell material due to the membrane action produces a higher stress concentration in the middle of the geocell pockets than the edges.

In the present study, the maximum tensile stress mobilized in the geocell was 42.4 kPa for an embankment height of 6 m. The maximum tensile stress mobilized was only 15% of the geocell constituent material tensile strength. At lower strain levels, geocell reinforced samples' behavior depended upon the geocell's tensile stiffness rather than the ultimate tensile strength (Song et al. 2019). The mobilized tensile stress due to geocell's circumferential deformation offers lateral confinement to the infill material, preventing the infill soil's horizontal movement (Fig. 5.34).
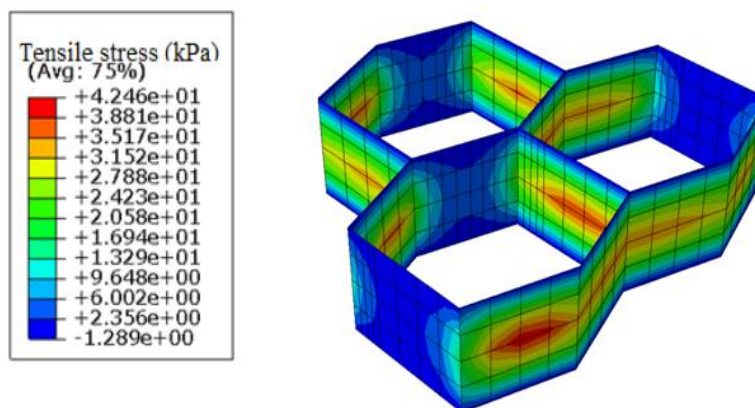


Fig. 5.33 Tensile stress distribution in the geocell pockets

The maximum lateral strain was observed at the mid-height of geocell pockets. Fig. 5.35 shows the variation of lateral strain in a cell pocket exactly above the stone column for different embankment heights along the symmetry *y*-axis. The maximum geocell width is denoted as "$b_1$," and "w" denotes different distances along the width.

The strain in the geocell increased with embankment height. With an increase in embankment loading, the horizontal stresses distributed to neighboring pockets mobilized tensile strain in the geocell. The maximum tensile strain at the middle geocell pocket for 6 m high embankment was twice that of 2 m high embankment after achieving full consolidation in the present study.
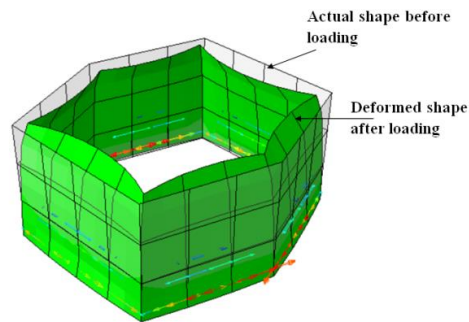


Fig. 5.34 Circumferential deformation of middle geocell pocket after loading
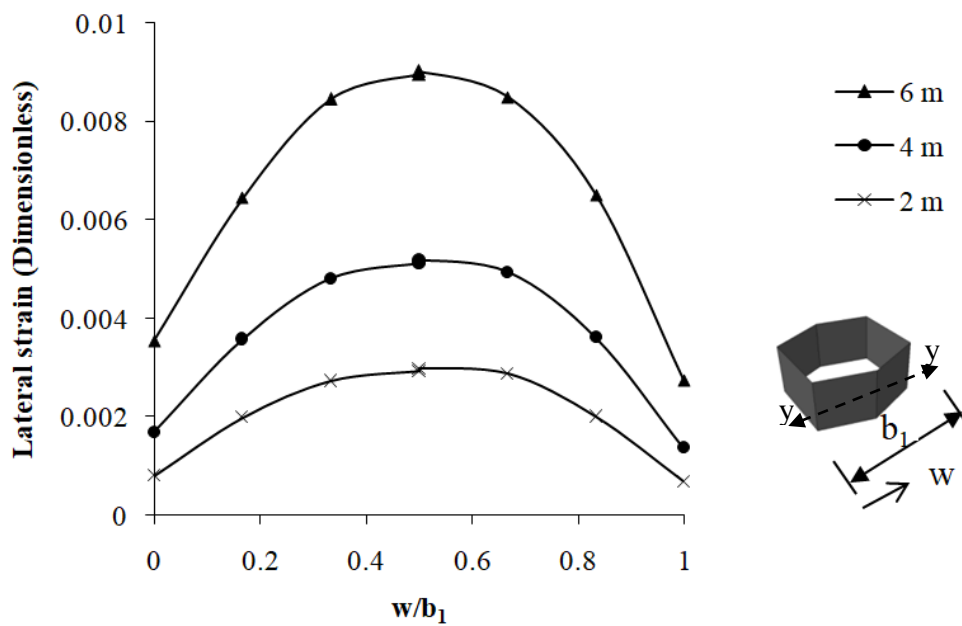


Fig. 5.35 Lateral strain distribution at the mid-height of geocell pocket at different embankment height

137

### 5.6.6 Effect of Stiffness of Geocell

Geocells are manufactured from high-density polyethylene (HDPE) sheets or novel polymeric alloy (NPA), with the height generally varying from 100 mm to 200 mm. If the height of the geocell required in the site is high, the geocells are fabricated from geogrids of suitable stiffness connected at the joints. In the present study, the stiffness of geocell was varied from 50 MPa to 1500 MPa, representing a wide variety of polymeric materials used for the manufacturing of geocell. The influence of geocell's stiffness on stress concentration ratio and the settlement at the foundation soil surface was studied for short-term and long-term stability conditions.

From Fig. 5.36, it is evident that an increase of the geocell stiffness makes the drainage blanket stiffer and promotes a significant transfer of embankment weight to stone columns. Also, higher geocell stiffness causes an increase in the confining pressure on the infill material. Fig. 5.37 shows the variation of ground surface settlement with geocell stiffness. A reduced settlement with an increase in geocell stiffness can be explained by the 3D honeycomb structure of geocells increasing the stress concentration from weak foundation soil to encased stone column.
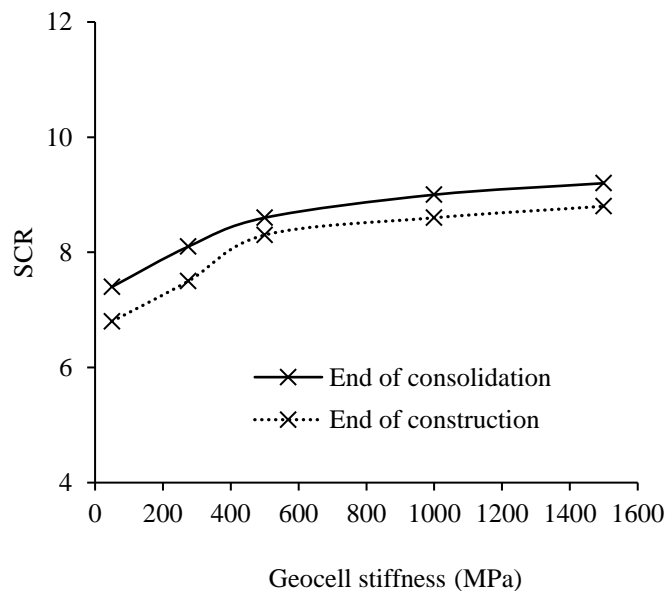


Fig. 5.36 Effect of geocell stiffness on SCR
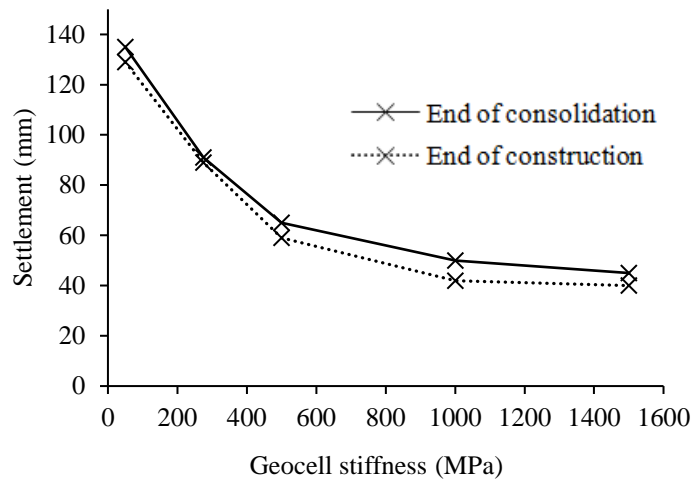
Fig. 5.37 Effect of geocell stiffness on ground surface settlement

## 5.6.7    Effect of Geocell Infill Material Properties

The suitability of poorly graded sand, aggregate, and quarry dust as geocell infill material was studied in the present work. A linear elastic, perfectly plastic model with Mohr-Coulomb failure criteria was used to model the infill materials. The summary of the constitutive model parameters used in the analysis is given in Table 5.8.  Fig.5.38 shows the stress concentration ratio variation with a non-dimensional embankment height, H/(S-D), for different infill materials.

As shown in Fig. 5.38, the stress concentration ratio varied with the type of infill material, and the range of SCR was found to be between 3.4-9.2 for aggregates, 2.5-8.5 for poorly graded sand 1.9-7 for quarry dust. Aggregates possess the highest friction angle and interlocking properties among the three different infill materials, contributing to high SCR values. It is seen that the frictional force developed between the infill material and the geocell walls contributes to the performance of the overall system (Hegde and Sitharam 2015b). The interlocked aggregates, along with geocell, act as a rigid slab, which effectively transfers a larger portion of the embankment load to encased stone columns. Among the three different infill materials, the ground surface settlement was the minimum for aggregates, and the maximum was for quarry dust (Fig. 5.39).
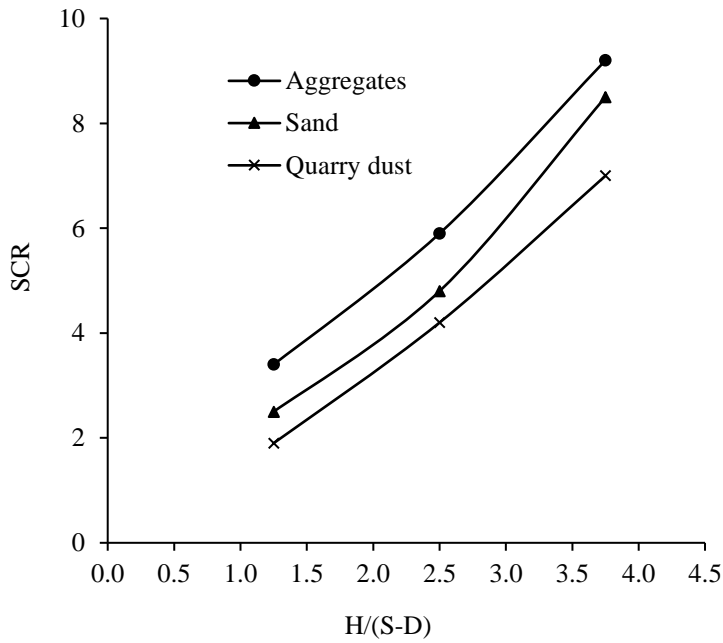
Fig. 5.38 Effect of infill material on SCR
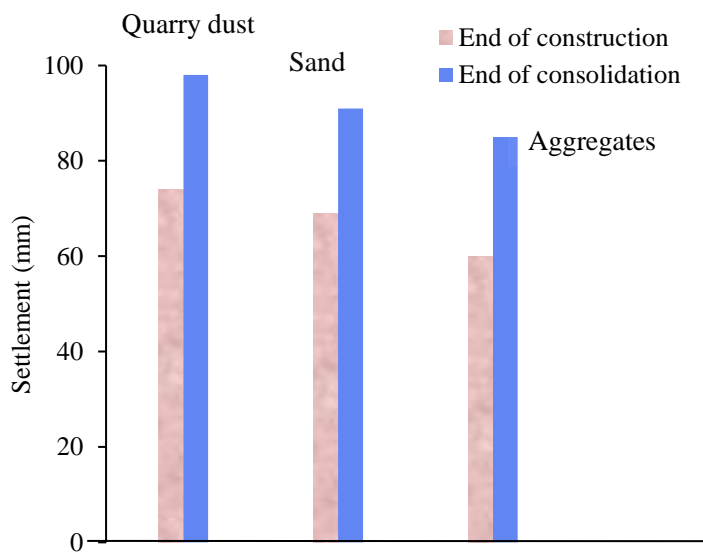


Fig. 5.39 Effect of infill material on ground surface settlement

Fig. 5.40 shows the variation of lateral strain in the middle of the geocell pocket with different infill materials. With aggregates, lateral spreading was prevented by the large hoop strain in the geocells, which generated high tensile stresses. The hoop tension developed in quarry dust is less, and thus, lower strains were reported. The

above observations demonstrate that aggregates are the best-suited infill material out of the different infill materials considered.

Table 5.8 Properties of various infill materials (Sand and aggregate properties based on Hegde and Sithram 2015c; quarry dust properties based on Han et al. 2008)

| Type of infill soil | Unit weight (kN/m$^3$) | Cohesion, c (kPa) | Friction angle, $\phi$ (degree) | Modulus of elasticity (kPa) | Poisson's ratio |
|---|---|---|---|---|---|
| Sand | 19 | 3 | 28 | 12000 | 0.3 |
| Aggregate | 19 | 5 | 40 | 42000 | 0.3 |
| Quarry dust | 18.5 | 23 | 19 | 4200 | 0.3 |
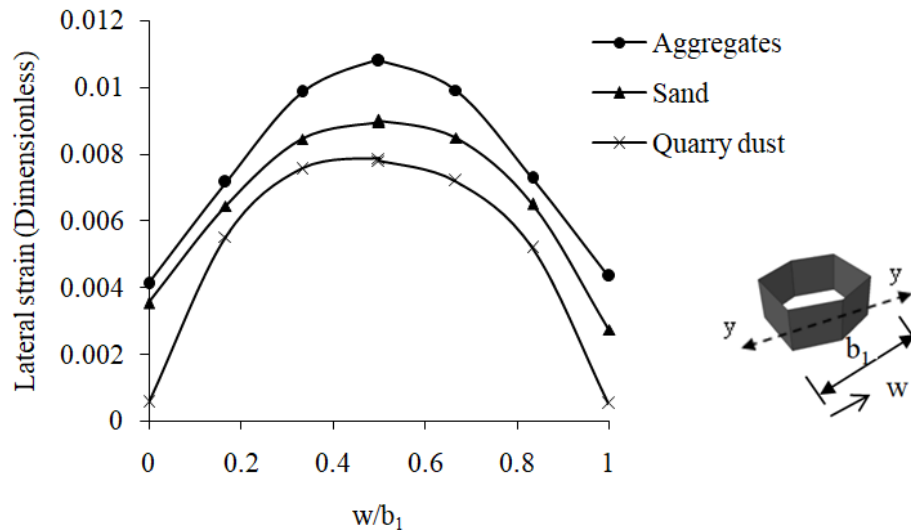


Fig. 5.40 Lateral strain distribution at the mid-height of geocell pocket with different infill material

### 5.6.8 Comparison with Equivalent Composite Approach (ECA)

In the equivalent composite approach, the geocell-sand mattress is modeled in a 2-dimensional framework as a soil layer with improved shear strength and stiffness properties (Rajagopal et al.1999; Latha and Rajagopal 2007). It was observed that geocell confinement induces apparent cohesion in the soil, and the soil's friction angle remains constant. The membrane stresses developed in the geocell walls due to the vertical loading confines the soil particles, creating apparent soil cohesion. Apparent cohesion is added with the original cohesion of the infill soil to get the cohesive strength of the geocell-sand mattress.

Table 5.9 Comparison between ECA and proposed 3-dimensional model of geocell

| At the end of consolidation | 3-dimensional model | Equivalent composite approach (ECA) | Percentage difference |
|---|---|---|---|
| SCR | 8.5 | 9 | 6 |
| Ground surface settlement | 91 | 81 | 11 |

The equivalent stiffness parameters of the geocell-sand mattress depend on the tensile modulus of geocell material, stiffness of the infill material, and the interaction parameter due to the interaction between cell pockets. The values of the properties of equivalent composite system are calculated using the equations given in Section 2.2.4: apparent cohesion-18.3 kPa, friction angle-30°, and Young's Modulus-20.33 MPa. The numerical model was modified for the ECA method, where the geocell-sand mattress was modeled as a soil layer with improved strength and stiffness values. The results were compared with the developed 3-dimensional model where geocells and infill soil were modeled separately, giving interaction between the geocell and infill surfaces. Fig. 5.41 and Fig. 5.42 show that the variation of ECA results to the proposed 3-dimensional numerical model with consolidation.
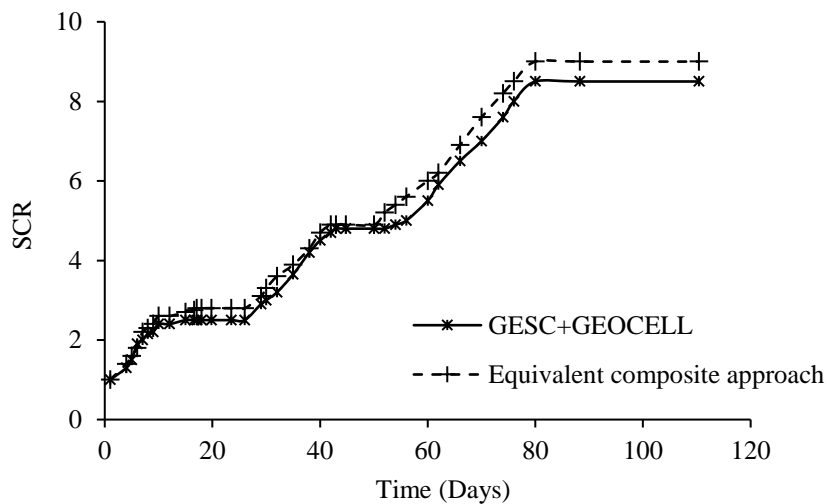


Fig. 5.41 Variation of SCR with time from ECA approach and 3-dimensional analyses
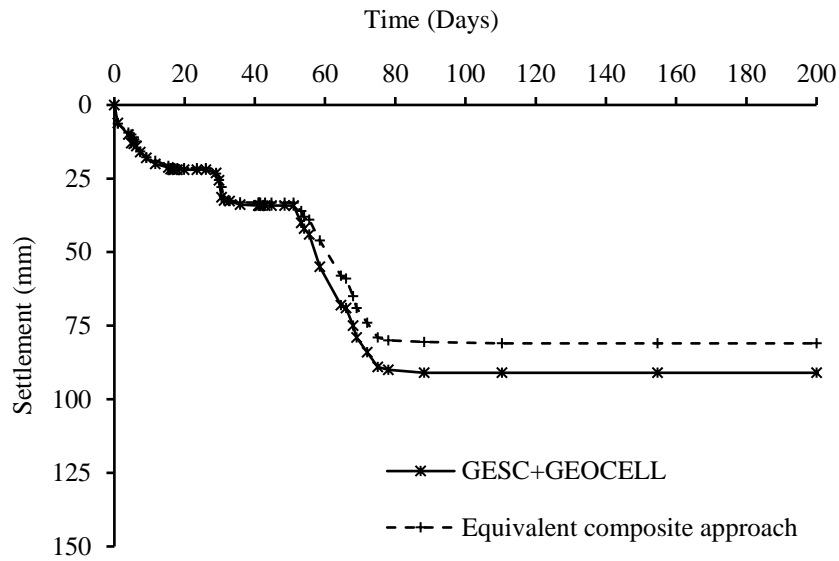
Fig. 5.42 Variation of ground surface settlement with time from ECA approach and 3-dimensional analyses

At the end of consolidation, the stress concentration ratio predicted by the equivalent composite approach was found to be 6% higher than the value obtained from 3-dimensional numerical analyses. ECA model over-predicted the stresses, which resulted in a higher value for stress concentration ratio, and this is in agreement with the observations of Hegde and Sitharam (2015a). However, the computed ground surface settlement at the end of foundation soil consolidation using the ECA method underpredicted the 3-dimensional numerical value by 11% (Table 5.9). Limitations in the 2-dimensional framework's assumption in developing the equivalent composite approach caused the variation in SCR and settlement values.

In the ECA method, rather than the size and actual shape of the geocell, the material properties were given importance. But in a practical situation, the geocells' size and shape play a significant role in the stress distribution pattern. The ECA method models a geocell-sand mattress as a square box, where the accumulation of stresses occurs in the corner edges, as shown in Fig. 5.43. This accumulation of stresses leads to the misinterpretation of the results in the ECA method. The actual distribution of compressive stresses in geocell pockets from the 3-dimensional numerical model is illustrated in Fig. 5.44. In the ECA method, the interaction between geocell and the infill soil cannot be simulated, leading to an overestimation of SCR and bearing

capacity. The apparent cohesion is estimated as a function of the axial strain of geocell reinforced soil at failure. But in the actual practice, the strain varies from geocell pocket to pocket depending on the loading pattern (Hegde and Sitharam 2015a; Sanjei and Silva 2016). The ECA method applies only to geocells with an aspect ratio between 0.5 to 2.1 (Latha and Somwanshi 2009). Also, the ECA method is not suitable for field situations where a combination of reinforcements is used. The proposed 3-dimensional numerical model of geocell infill mattress overcomes all the limitations mentioned above and is a more realistic and appropriate approach for actual field conditions.
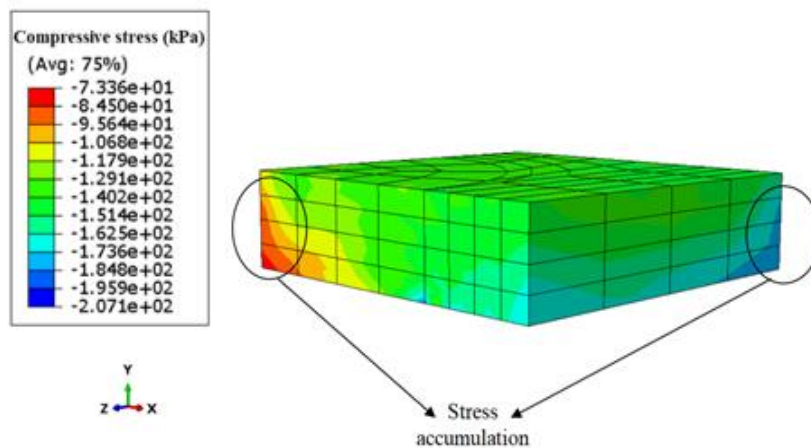


Fig. 5.43 Compressive stresses distribution in the geocell soil composite layer from the ECA approach
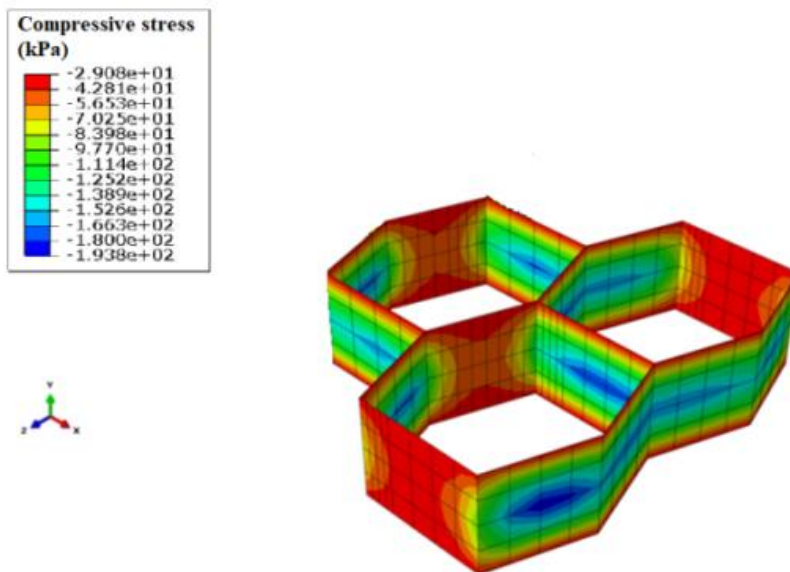


Fig. 5.44 Compressive stresses distribution in the geocell from the 3-dimensional model

144

## 5.7 GEOSYNTHETIC REINFORCED PILED EMBANKMENT SYSTEMS (GRPES)

Columnar structures provide an effective solution to the problem of constructing embankments over soft soils. One of the techniques to overcome surface settlement is using vertical plain concrete piles with single or multiple layers of reinforcement placed above the piles close to the embankment base known as geosynthetic reinforced piled embankment systems (GRPES) (Han and Gabr 2002; Bhasi and Rajagopal 2015). A single layer of reinforcement is assumed to act as a tensioned membrane (catenary) under the vertical load enabling the deflected basal reinforcement to be analyzed as a parabola. Pile supported earth platforms has many advantages, such as,

- The waiting period for the construction of the superstructure can be reduced.
- The surface settlement and differential settlement can be effectively reduced
- The excavation and replacement of soil can be avoided.

GRPES is a popular ground improvement technique for constructing structures with strict settlement criteria, and there is a need for faster construction. Conceptually Geosynthetic Reinforced Piled Embankment Systems (GRPES) are equivalent to a piled-raft system (Fig. 5.45). Although it is hugely popular in European and Scandinavian countries, due to the high initial cost of GRPES compared to the traditional construction methods, the system is not popular in India.
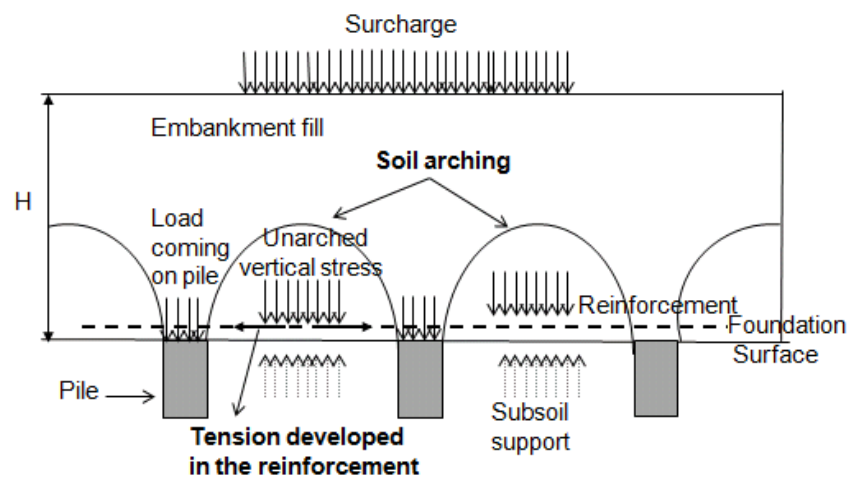


Fig. 5.45 Load transfer mechanism in Geosynthetic Reinforced Piled Embankment Systems (GRPES) (After Lawson 2012)

### 5.7.1  Load Bearing Mechanism

In GRPES, the central phenomenon responsible for load transfer is the arching mechanism. The embankment fill mass between the piles tends to move downwards under the influence of fill weight. Differential settlement occurs between the relatively rigid piles and the soft foundation material due to the difference in stiffness. Differential settlement causes the soil material between the piles to settle more than the material above the piles. The shear resistance partially restrains the downward movement from the embankment fill. Shear resistance developed along the interface increases the load transferred to the piles and reduced the load acting on the geosynthetic. This load transfer mechanism is termed soil arching by Terzaghi (1943). The arches span the soft soil, and the applied load is transferred onto the piles and from piles to the firm bearing stratum.

The membrane effect of the geosynthetic layers and stress concentration are the other two mechanisms responsible for load transfer in GRPES. The unarched vertical stress between the columns is considered to be carried by the geosynthetic reinforcement. A portion of the embankment load applied normal to the surface of the reinforcement creates tensile forces in the membrane. The load is transferred to the piles through the vertical component of the tensile forces in the membrane (Han and Gabr 2002), known as the membrane effect. When the geosynthetic reinforced platform is perfectly rigid, there will not be any differential settlement causing soil arching or membrane effect. In such cases, load transfer occurs due to stress concentration from the soil to the piles due to the difference in material stiffness.

### 5.7.2  Numerical Modelling

The performance of GESC+GEOCELL supported embankment is compared with the performance of GRPES by the developed 3D column models. The case study used in section 5.6.1 was taken for analysis by replacing the 0.8 m diameter encased stone columns with rigid concrete piles. The pile was modeled as a linear isotropic elastic material with Young's modulus of 10 GPa and a Poisson's ratio of 0.2. Twenty noded brick elements with reduced integration (C3D20R) were used to represent the pile. The

basal geogrid used at the base of pile-supported embankment has the same stiffness as that of geocell used in GESC supported embankment.

### 5.7.3    Comparison Based on Embankment Load Transfer

The settlement-time response was plotted in Fig. 5.46 for GRPES and GESC+GEOCELL. It was observed that the foundation settlement for GESC+GEOCELL at the end of consolidation is 14% higher than that of GRPES. Due to the stiffness difference between pile and GESC, more stress transfer occurs in GRPES, resulting in lesser foundation settlement.

From Fig. 5.47, it is clear that GESC+GEOCELL achieve 80% consolidation at the construction stage itself. Whereas for GRPES, the degree of consolidation achieved was 78%. The percentage of embankment load transferred to the pile was found out by using the term pile efficacy ($E_f$) introduced by Hewlett and Randolph (1988).

$$E_f = \frac{P}{S^2 \gamma_e H} \tag{5.23}$$

here, P is the load carried by the pile, S is the center to center spacing of columns, $\gamma_e$ is the unit weight of the embankment soil, and H is the embankment height.

The efficacy at the end of the construction stage for different embankment heights was calculated using the developed 3D column model. The percentage of load carried by the columns in different reinforcement conditions is plotted in Fig. 5.48.

In both the reinforcement cases, the efficacy showed the same trend. The embankment load transferred to the columns increases with the embankment height, and the column load remained constant after a height of 4 m. Compared to geogrid reinforced pile embankments, a reduction of 13% in load transfer to the columns was observed for GESC+GEOCELL for an embankment height of 6 m.

The stress concentration ratio (SCR) was plotted against the non-dimensional height (H/(S-D)) and is shown in Fig. 5.49. The stress transfer from the foundation soil to the columnar structure was quantified by the term SCR, and it is observed that for an embankment height of 6 m, the GRPES exhibited a higher SCR value than the GESC+GEOCELL. The difference in SCR value between GRPES and GESC+GEOCELL is 17%. But when the modular ratio increases, the SCR value for

GESC+GEOCELL also increases. When the modular ratio is more than 40, the stress transfer is almost similar to GRPES (Fig. 5.50).
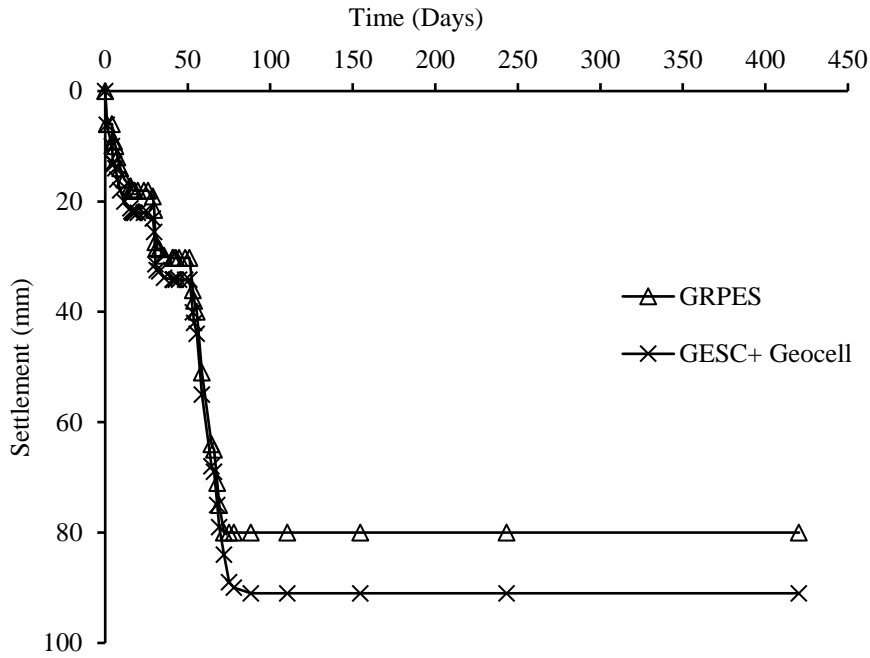
Fig. 5.46 Settlement-time response
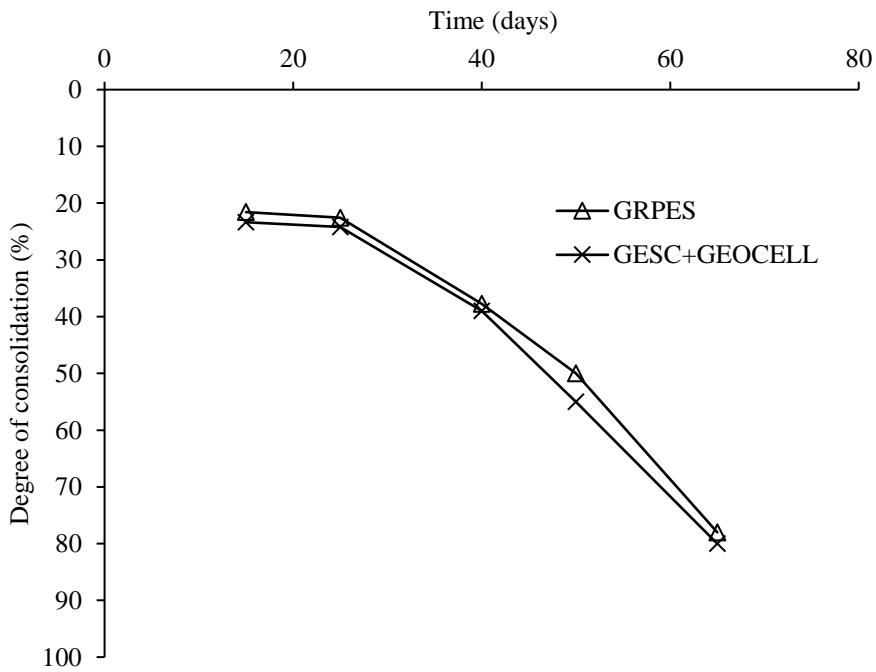
Fig. 5.47 Variation of degree of consolidation
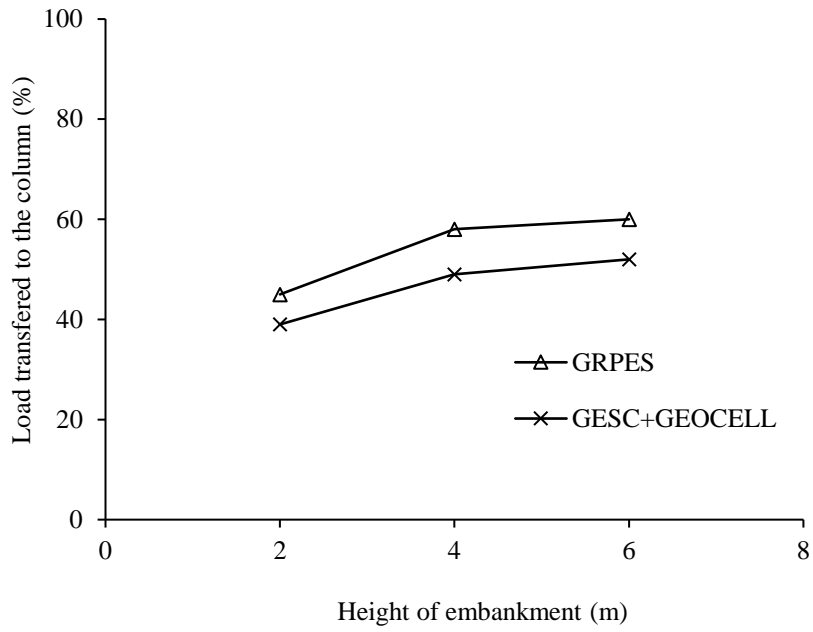
Fig. 5.48 Column efficacy for different embankment heights
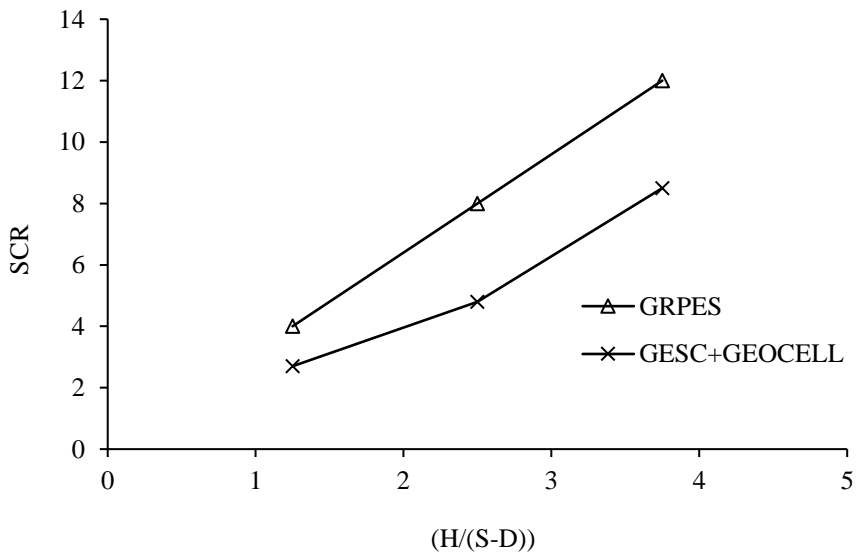


Fig. 5.49 Variation of SCR with embankment height
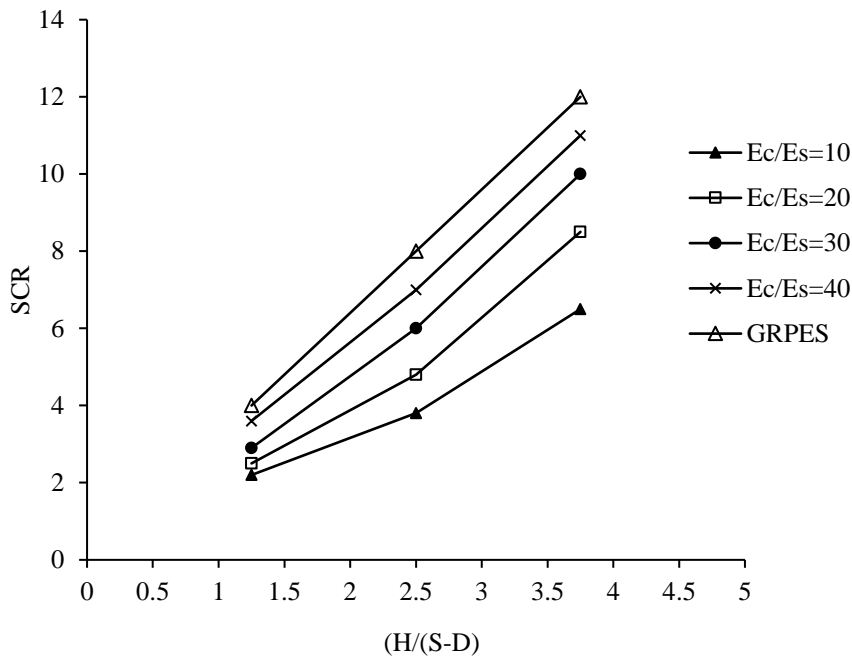
Fig. 5.50 Variation of SCR with embankment height for different modular ratio for GESC+GEOCELL

Fig. 5.51 shows that the arching ratio of stone column supported geocell reinforced embankment is more than the geogrid reinforced pile-supported embankment. Geocell-sand mattress acts like a rigid slab hindering the arching action. The arching ratio inversely varies with the embankment height for pile and GESC+ GEOCELL supported embankments. In the case of unreinforced column supported embankments, with an increase in the embankment height, the shear resistance accumulated is more, promoting soil arching. The stiffening effect due to the basal geocell-sand mattress effectively reduces the differential settlement in the embankment soil and hinders the arching development.

Fig. 5.52 shows the arch-shaped stress contours formed by a 6 m high embankment for GESC+GEOCELL and GRPES with dotted lines. As per BS 8006 and Hewlett and Randolph (1988), the orientation of arches forms a semi-circle between columns. From Fig. 5.51, it is evident that arches are formed just above the column and embankment interface. Also, arches are not visualized at the top portion of the embankment fill because there is no differential settlement at greater heights. The

maximum height of the arch for GESC+GEOCELL was only half of that of GRPES. This supports the observation that the stress transferred by soil arching is less when a geocell-sand mattress is provided at the base of the embankment above the columns.
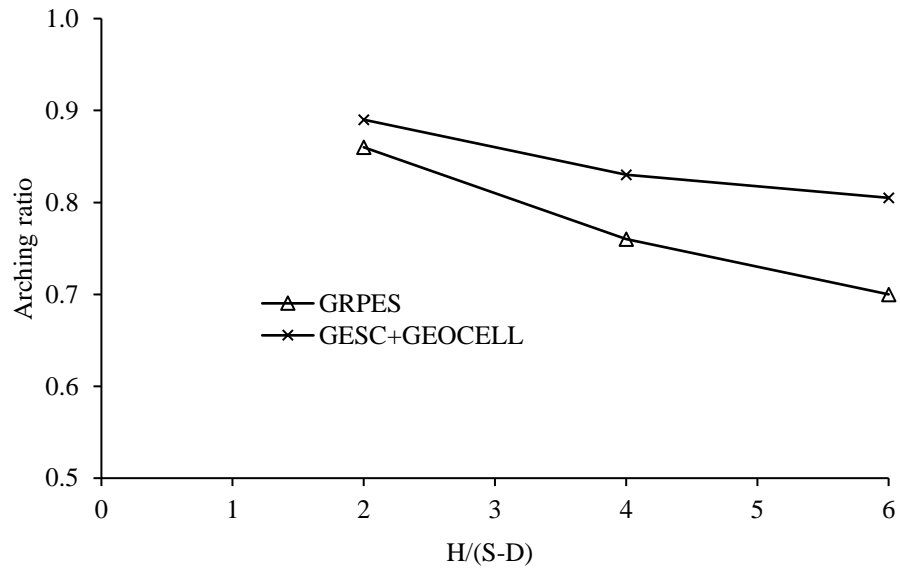


Fig. 5.51 Variation of arching ratio with embankment height for GRPES and GESC+GEOCELL



(a)

(b)
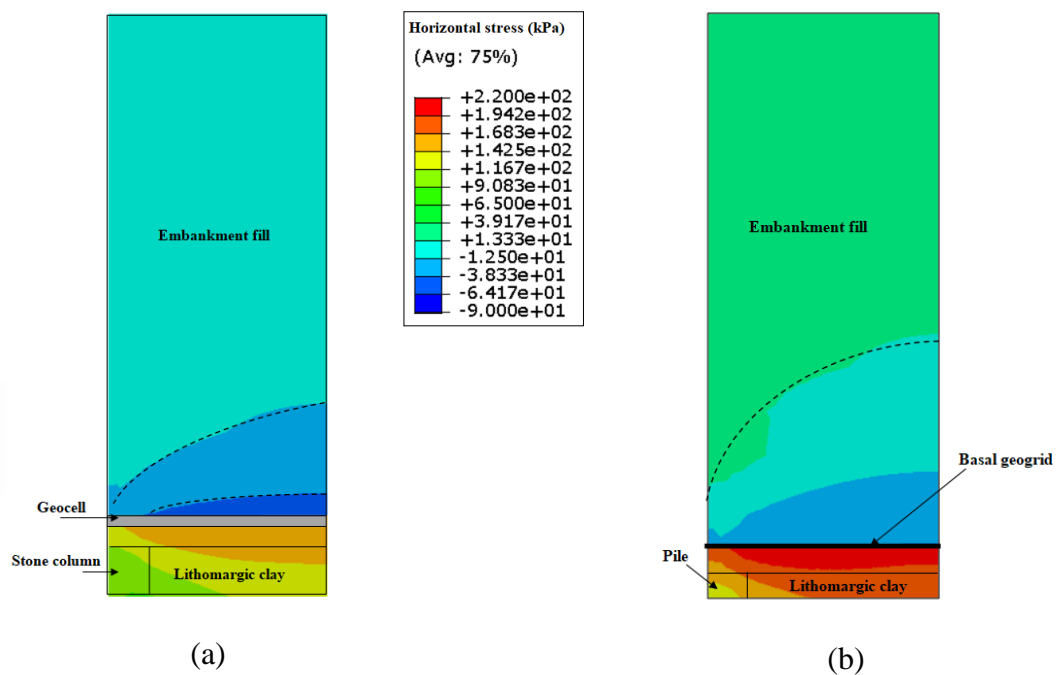
Fig. 5.52 Horizontal stress contours for (a) GESC+GEOCELL and (b) GRPES

### 5.7.4 Summary

Though the load transfer mechanism is different for GRPES and geocell reinforced GESC supported embankments, the various parameters used to describe the load transfer showed similar trends and comparable values. When the modular ratio of GESC+GEOCELL is more than 40, the performance is quite similar to GRPES. Thus GESC+GEOCELL can be an economically practical solution to replace GRPES.

# CHAPTER 6

# NUMERICAL ANALYSES USING FULL THREE DIMENSIONAL MODELS

## 6.1 GENERAL

This chapter evaluated the time-dependent behavior of encased stone column supported embankment with geosynthetic basal reinforcement by carrying out full three-dimensional analyses. The behavior of the embankment reinforced with encased stone columns (GESC), encased stone columns with a single basal geogrid layer (referred to as GESC+ One basal layer), and encased stone columns with double basal geogrid layers (referred as GESC+ Two basal layers) was analyzed. The numerical results were compared with the results obtained from available design methods.

## 6.2 NUMERICAL MODELING

A single basal geogrid layer of stiffness 2500 kN/m and two basal layers, each of stiffness 1250 kN/m, were considered for the analyses. The details of the case study are given in section 5.2.1. Full 3-dimensional (3D) models require high computational time and memory but give more accurate results by simulating more realistic conditions. The running time for a full 3D analysis was approximately 1440 minutes of CPU time (high-performance work station of Intel Xenon E5-1620, 3.5 GHz, 3501 MHz processor with 8GB RAM). Table 6.1 shows the total number of elements used for the modeling of each material.

The lithomargic clay layer and the stone column were discretized using twenty node stress-pore pressure coupled brick elements with reduced integration (C3D20RP). The embankment fill and drainage blanket were modeled using twenty node stress-only elements (C3D20R). The geogrid encasement and basal geogrids were represented using eight-node membrane elements with reduced integration (M3D8R).

The constitutive models, boundary conditions, interaction, and methodology used were the same as that of the 3D column model (Section 5.2). The developed full

3-dimensional model for geogrid reinforced encased stone column supported embankment is shown in Fig. 6.1.

Table 6.1 Total number of elements used in the full 3-dimensional model

| Full 3D model | |
| --- | --- |
| Material | Total number of elements |
| Lithomargic clay | 1920 |
| Stone column | 552 |
| Sand | 1472 |
| Embankment | 2392 |
| Geogrid encasement | 368 |
| Basal geogrid | 640 |
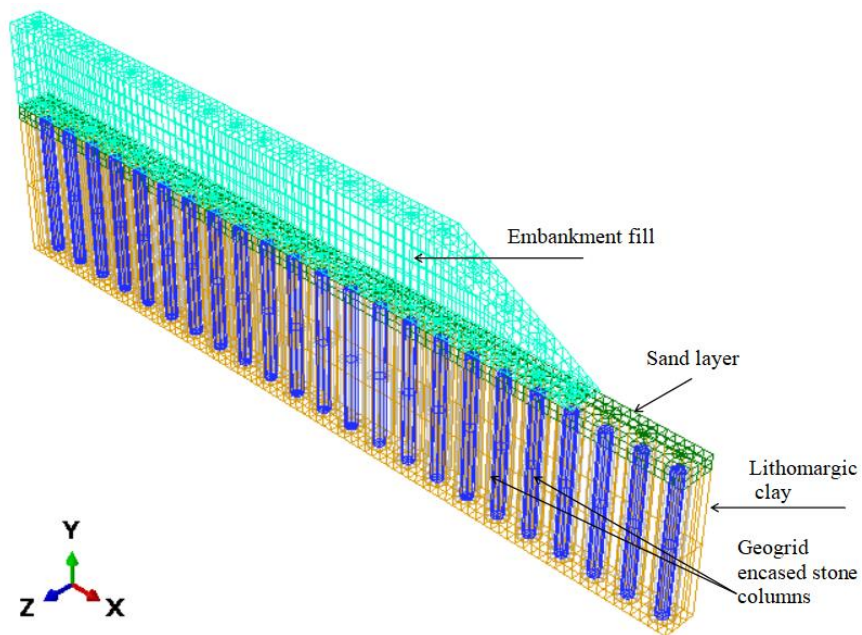


(a)
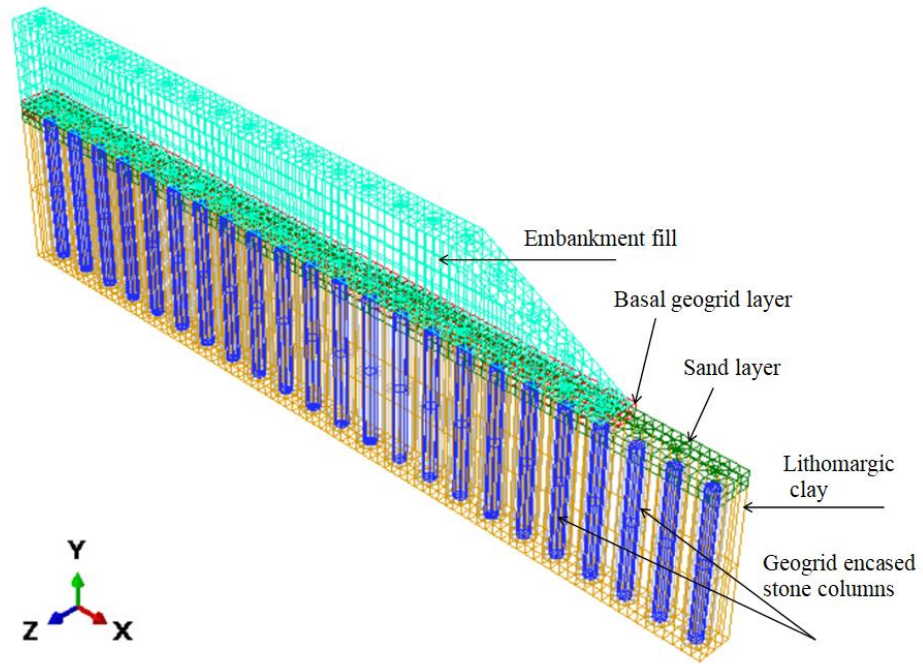
(b)
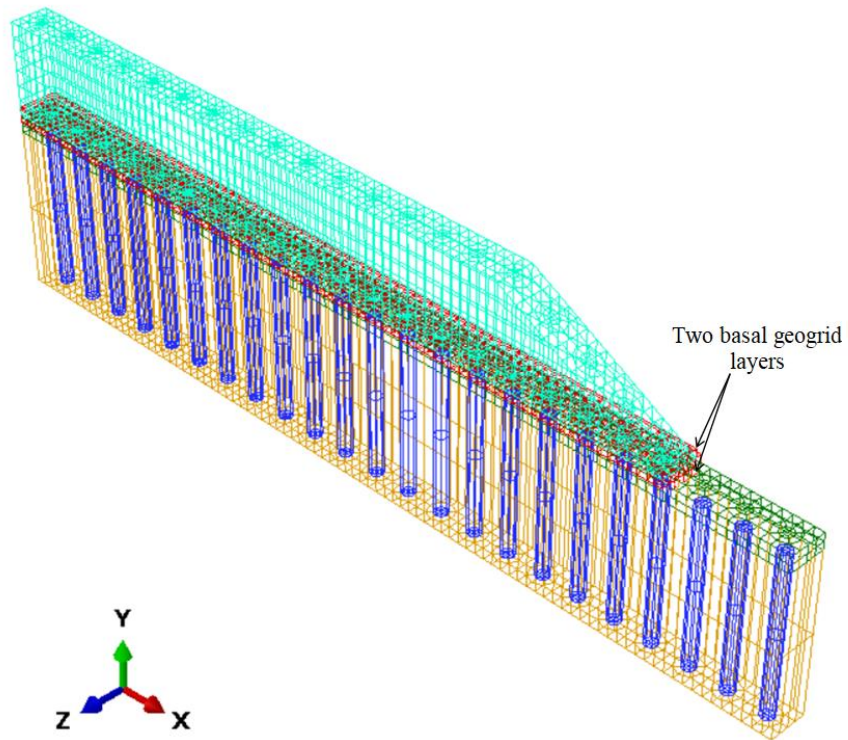


(c)

Fig. 6.1 Full 3-dimensional models developed (a) GESC (b) GESC + One basal layer and (c) GESC+ Two basal layers

## 6.3    VARIATION OF FOUNDATION SURFACE SETTLEMENT

Fig. 6.2 (a) and (b) show the settlement profile of the lithomargic clay layer at the end of consolidation for unreinforced and GESC supported embankment, respectively. The settlement profile of the lithomargic clay layer for GESC with single and two basal layers is shown in Fig. 6.3. The maximum settlement was observable at the top surface and near the embankment center in all the cases. The foundation surface settlement at the end of consolidation for the different cases considered in the analyses is given in Table 6.2. The foundation settlement was being reduced with the introduction of basal reinforcements. The 3D column models also gave almost the same settlement values as full 3-dimensional models; the percentage difference is negligible. The axisymmetric models gave 20-24% larger values than the full 3-dimensional models for all the different cases considered in this study.

Table 6.2 Foundation surface settlement at the end of consolidation

| Different cases | Foundation surface settlement (mm) | | |
|---|---|---|---|
| | Full 3D | 3D column | Axisymmetry |
| GESC | 128 | 128 | 144 |
| GESC+ One basal layer | 101 | 101 | 125 |
| GESC+ Two basal layers | 98 | 93 | 118 |

A reduction of 21% and 25% in foundation surface settlement was obtained for GESC+ One basal layer and GESC+ Two basal layers, respectively, compared to GESC alone. On increasing the number of reinforcement layers, the foundation surface settlements have noticeably reduced.
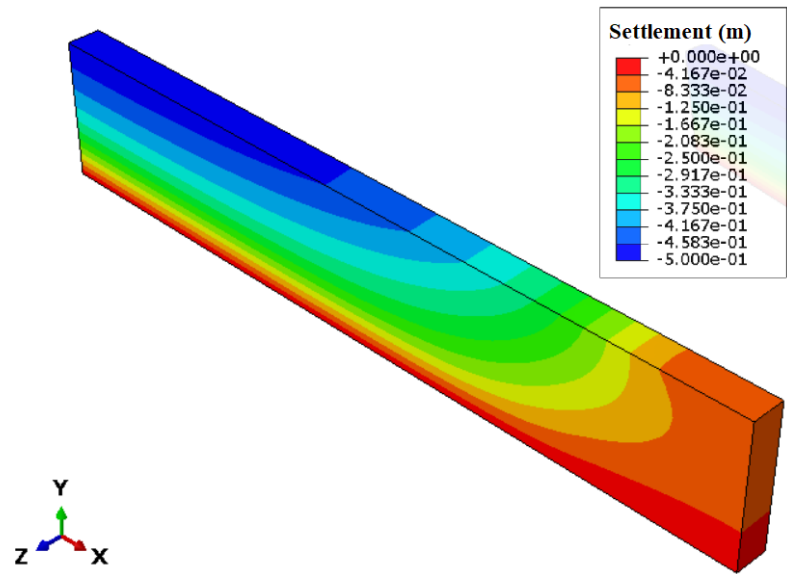
(a)
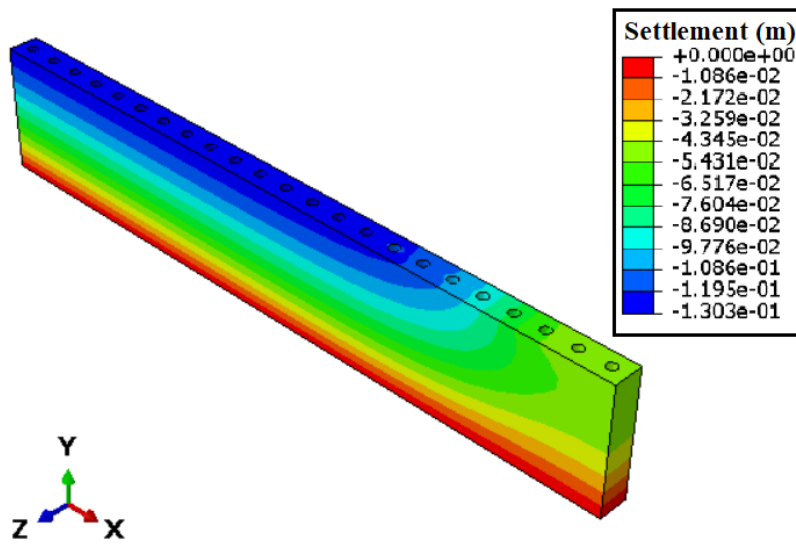


(b)

Fig. 6.2 Foundation settlement contours at the end of consolidation for (a) unreinforced lithomargic clay and (b) GESC

Settlement (m)

-8.462e-03
-1.692e-02
-2.538e-02
-3.385e-02
-4.231e-02
-5.077e-02
-5.923e-02
-6.769e-02
-7.615e-02
-8.462e-02
-9.308e-02
-1.015e-01
-1.100e-01

(a)

Settlement (m)

+0.000e+00
-8.263e-03
-1.653e-02
-2.479e-02
-3.305e-02
-4.131e-02
-4.958e-02
-5.784e-02
-6.610e-02
-7.436e-02
-8.263e-02
-9.089e-02
-9.915e-02
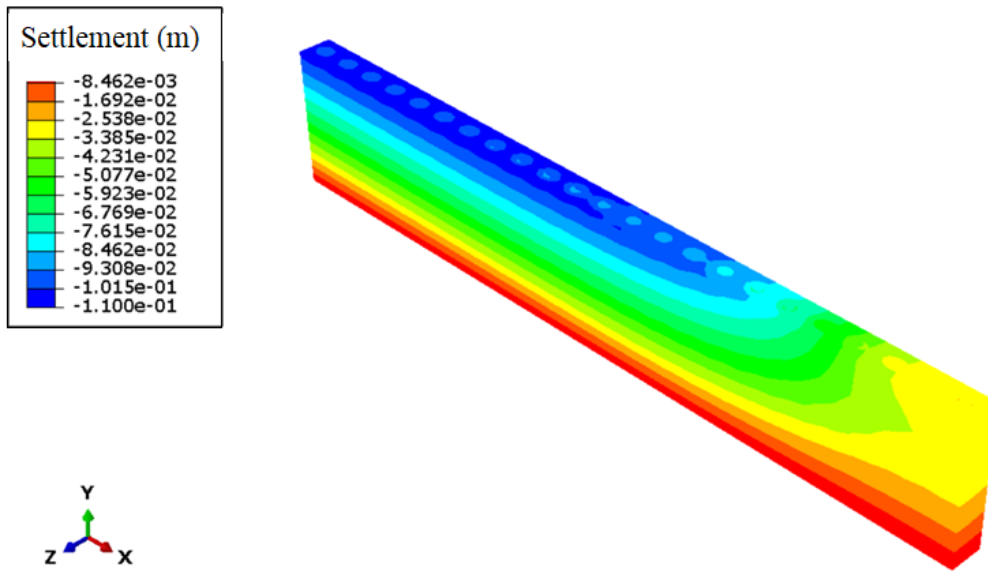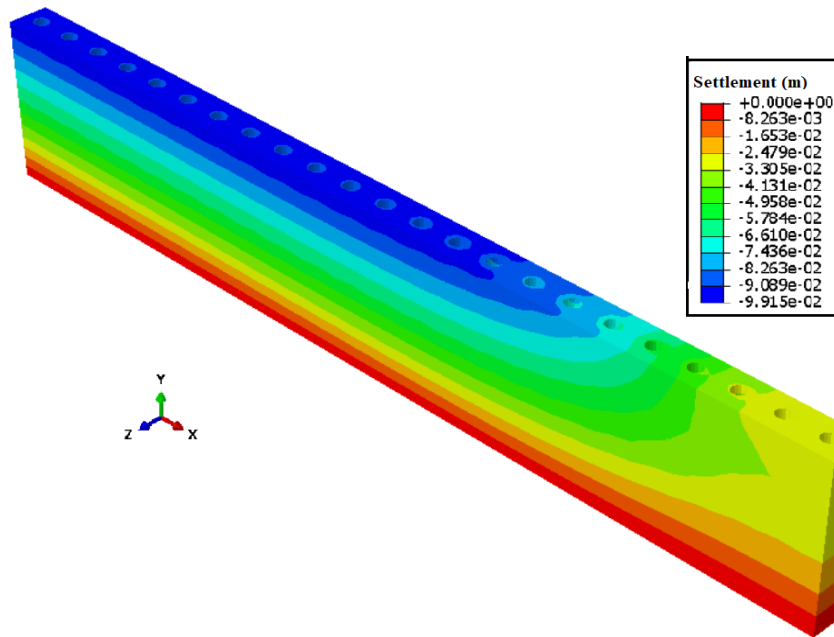
(b)

Fig. 6.3 Foundation settlement contours at the end of consolidation for (a) GESC+ One basal layer and (b) GESC+ Two basal layers

158

## 6.4 EXCESS PORE PRESSURE DISTRIBUTION

Excess pore-water pressures generated at the mid-depth of the lithomargic clay layer by the end of embankment construction (short-term stability) were studied. The reference point was selected at the center line of the embankment at the mid-depth of lithomargic clay.
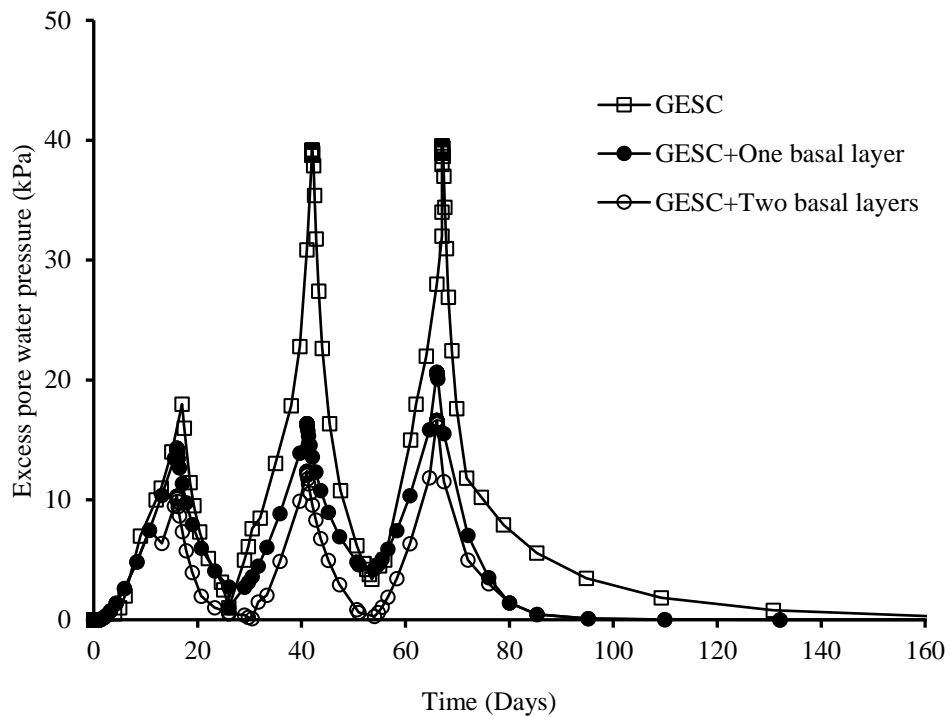


Fig. 6.4 Variation of excess pore pressure with time at the mid-depth of lithomargic clay

Under the 6 m embankment loading, the maximum excess pore water pressure developed during consolidation for GESC was 40 kPa, whereas GESC+ One basal layer and GESC+ Two basal layers showed only a maximum value of 21 kPa and 17 kPa, respectively (Fig 6.4). The embankment load transferred to the foundation soil is less with an increase in geogrid layers. Due to membrane action, reinforcement transfers a portion of the embankment load to the columns, reducing the load directly acting on foundation soil, which reduces the pore pressure. The contours of excess pore pressure at the end of embankment construction for the different reinforcement cases are shown in Fig. 6.5.
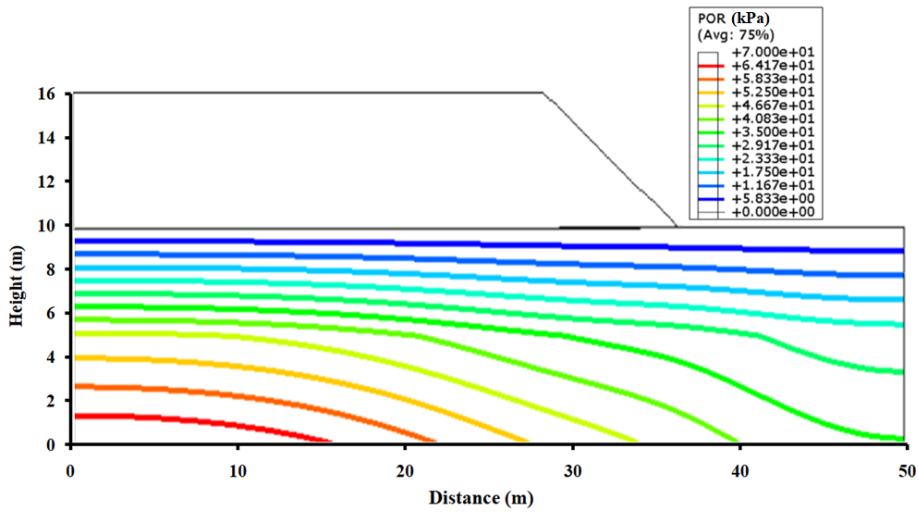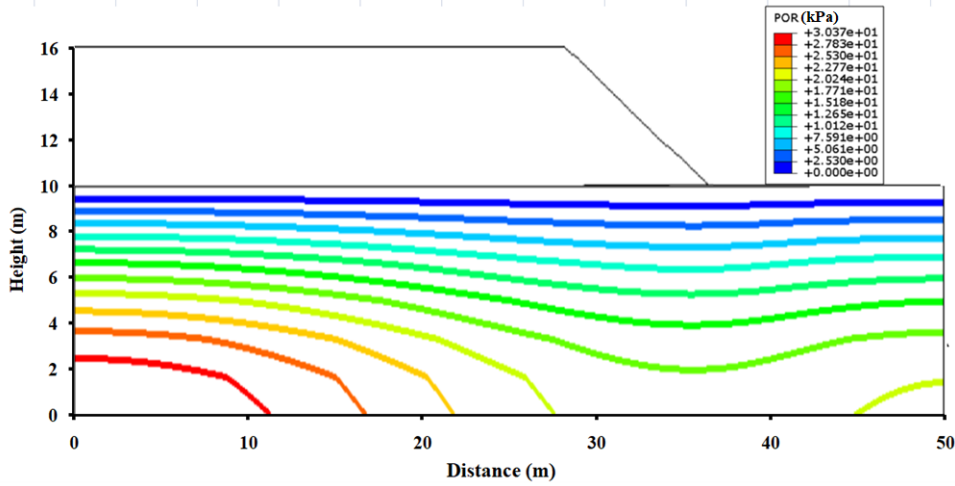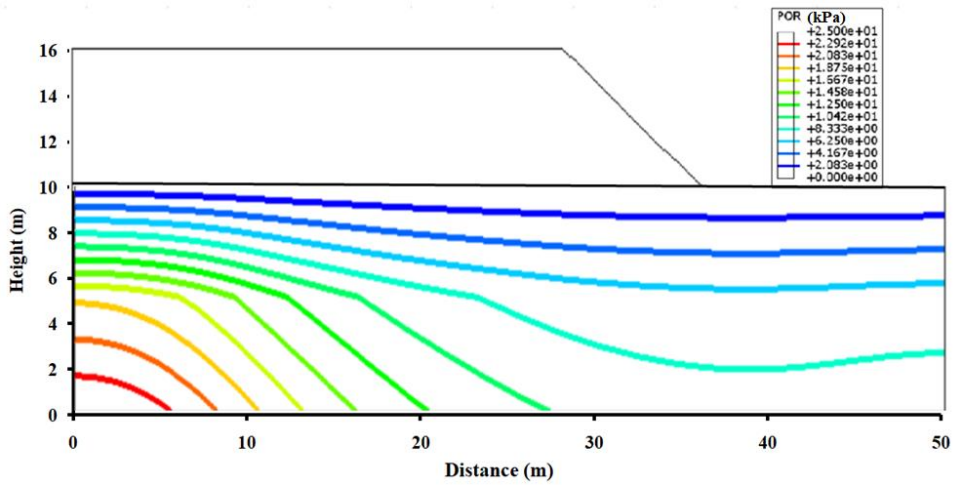
Fig. 6.5 Pore water pressure distribution at the end of construction for (a) GESC (b) GESC+ One basal layer and (c) GESC+ Two basal layers

160

From the Figures, it is clear that maximum pore water pressure at the end of construction was observed in GESC without basal layer. The excess pore water pressure generated in lithomargic clay is less in GESC+ Two basal layers than GESC+ One basal layer, which shows the increased load transfer to columns by two basal geogrid layers. The results indicate that the effectiveness of using multiple layers of reinforcement at the base of embankment supported on columns. According to Skempton and Bjerrum (1957), the excess pore pressure induced in the soil could be less than the vertical stress increment in a three-dimensional consolidation situation. This reduction happened due to the lateral deformation of the consolidating soil, in addition to vertical settlement. Development of lesser pore pressures in all the cases can also be due to the consolidation of foundation soil during the embankment construction.

According to Rowe & Soderman (1985) and Liu *et al.* (2007), if the embankment is constructed at a rate $\overline{B}_{max}$ [ $\overline{B}_{max} = \dfrac{\text{Maximum excess pore pressure}}{\text{Total applied vertical stress}}$ ] which is substantially greater than 0.34, bearing capacity failure of the embankment can occur during construction. The vertical stress on the foundation surface at the end of construction was about 53 % of the embankment load. For the present case of one basal layer and two basal layers, the estimated $\overline{B}_{max}$ was 0.33 and 0.31 respectively. Thus, there was no bearing capacity failure of the embankment during construction.

## 6.5    LATERAL DEFORMATION OF THE FOUNDATION SOIL

Stone columns are usually designed for vertical compressive loads. However, in field conditions where stone columns are installed under widely loaded areas such as an embankment base, it undergoes shear deformation. The geogrid encasement improves the shear resistance of the stone columns and makes them behave like semi-rigid piles (Murugesan and Rajagopal 2009). The shape of the lateral displacement along the foundation depth under the toe of the embankment is captured by carrying out full three-dimensional analyses for the different cases (Fig 6.6). Table 6.3 shows the maximum value of lateral displacement obtained for different cases. The lateral displacement tends to increase with the foundation soil consolidation. Fig. 6.7 shows the lateral displacement contours for unreinforced, GESC, GESC+ One basal layer, and GESC+ Two layers.

161
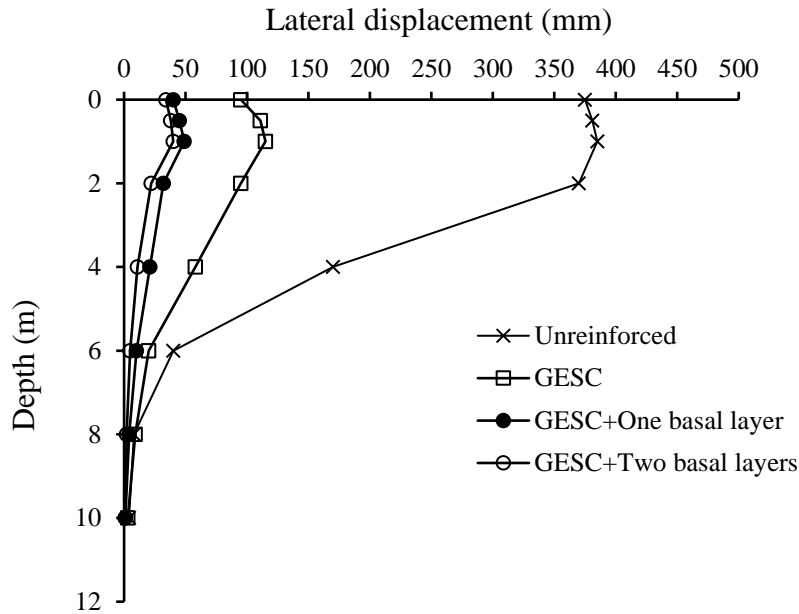
Fig. 6.6 Lateral displacement of foundation soil under the embankment toe at the end of consolidation

Table 6.3 Maximum lateral displacement under the embankment toe

| Different cases | Lateral displacement (mm) | |
| --- | --- | --- |
| | End of construction (*short-term stability*) | End of consolidation (*long-term stability*) |
| Unreinforced | 310 | 385 |
| GESC | 101 | 115 |
| GESC+ One basal layer | 41 | 49 |
| GESC+ Two basal layers | 34 | 40 |

The stability of the slope is greatly influenced by the lateral deformation of the foundation soil near the embankment toe. Maximum lateral deformation was observed for GESC supported embankment without any basal reinforcement. With the increase in the number of basal layers, the lateral deformation got decreased. Compared to an unreinforced embankment, 87% reduction in lateral deformation near the toe was observed for GESC+ One basal layer at the end of consolidation, and 90% reduction in the lateral deformation was obtained when two layers of geogrids (stiffness equivalent to that of a single layer) was provided at the base. The decrease is attributed to the

162

reinforcement layers resisting the shear failure in the foundation soil. It prevents the embankment fill from sliding, which adds to the stability of the embankment constructed on lithomargic clay.



(a)

(b)

(c)

(d)
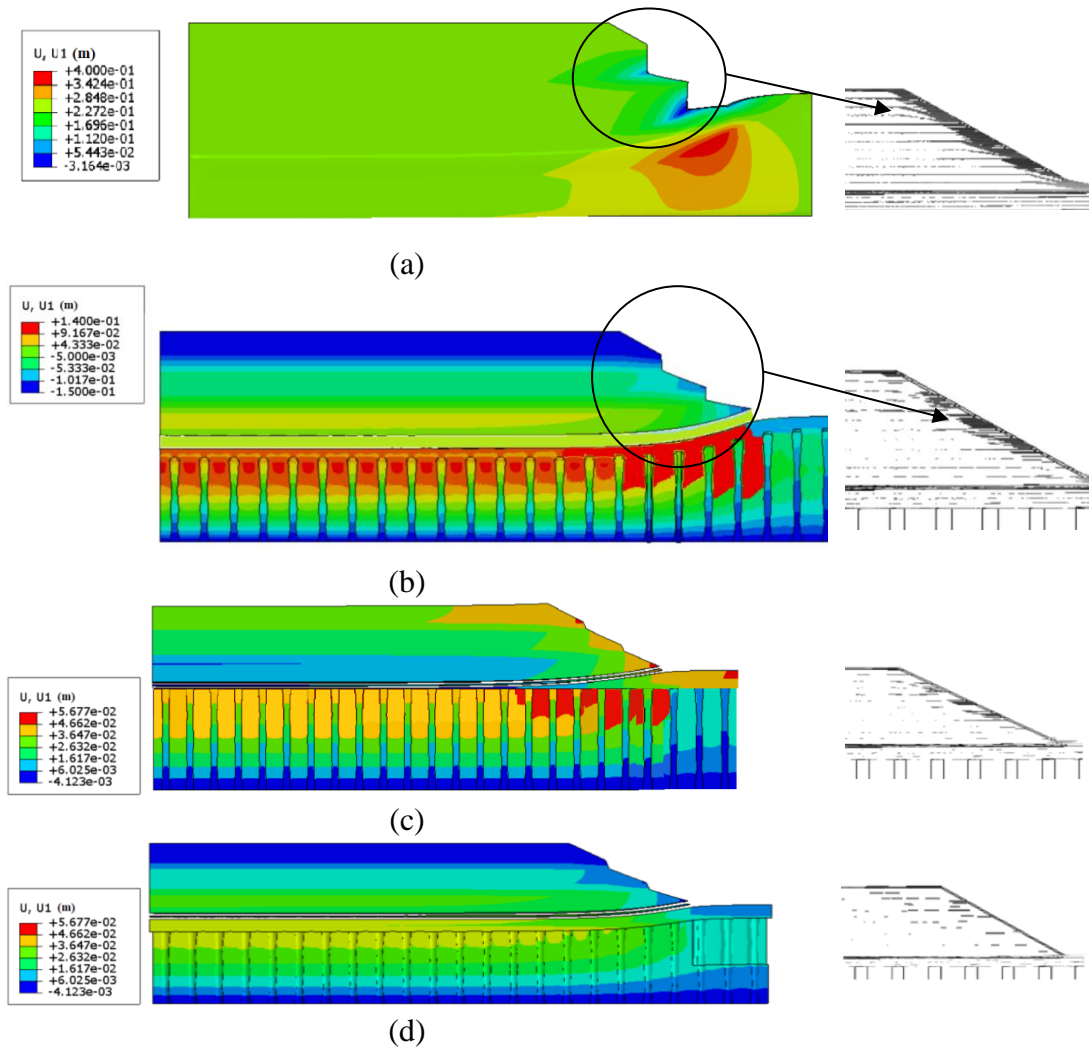
Fig. 6.7 Lateral displacement contours for (a) unreinforced (b) GESC (c) GESC+ One basal layer and (d) GESC+ Two basal layers

According to Indraratna et al. (1992), the ratio of the maximum lateral displacement at the toe to the maximum settlement at the center line of an embankment gives a good indicator of embankment stability. A small value of the ratio is necessary to maintain the stability of the embankment over foundation soil. At the failure point, the value is larger than 0.5. In the present case of GESC+ Two basal layers, the ratio is 0.4, and for GESC+ One basal layer, the ratio is 0.47. The results indicate that the basal geogrids improve the stability of the slope significantly.

## 6.6 TENSILE STRESSES IN THE REINFORCEMENT LAYERS

In the present study, the maximum tension developed in the bottom geogrid layer at the end of the construction period was analyzed for single and two-layer cases. The upper layer of the geogrid carries relatively little tension compared to the bottom layer in a two-layer system. Fig. 6.8 (a) and (b) shows the deflected shape of the bottom reinforcement due to embankment loading for single and two layers. The tensile stress variation in the bottom geogrid layer along the embankment width for different reinforcement cases was shown in Fig. 6.9 (a) and (b).



(a)



(b)
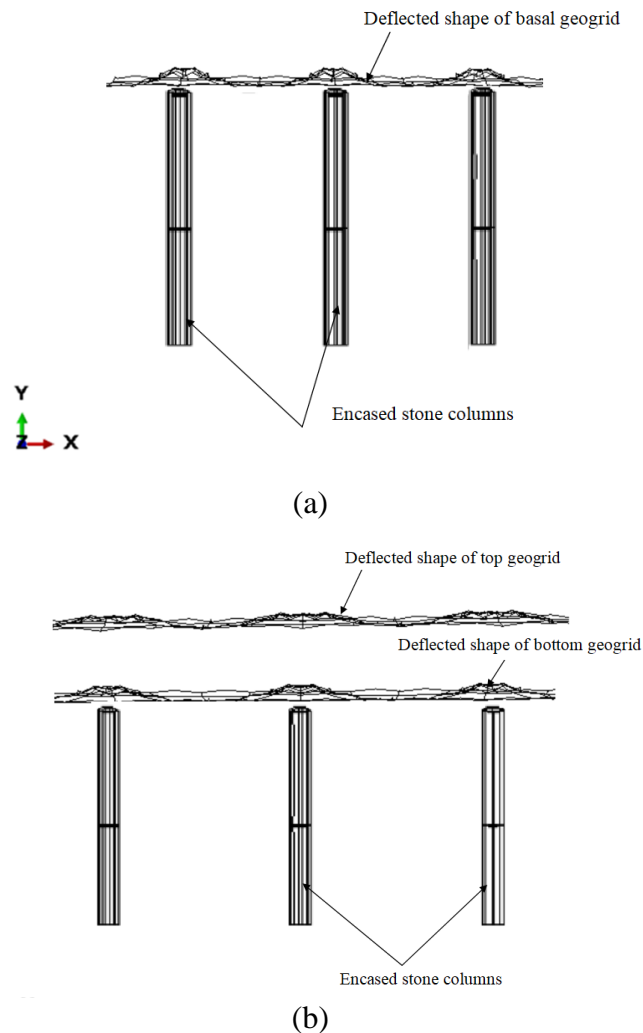
Fig. 6.8 Deflected shape of bottom geogrid (a) single layer and (b) two-layer
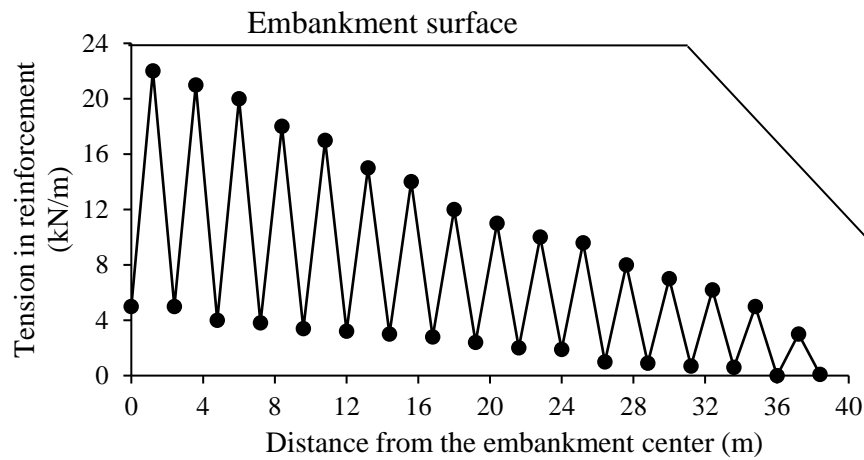
(a)
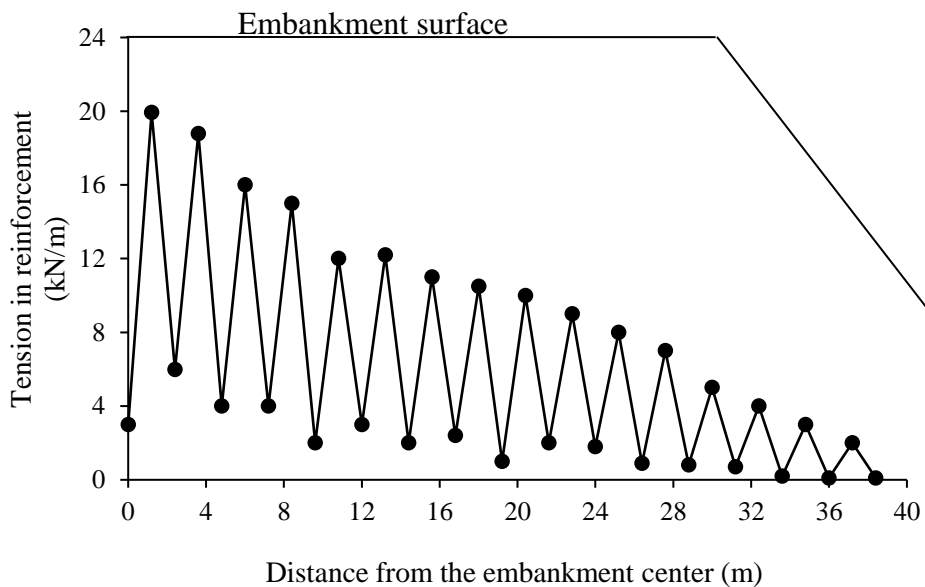


(b)

Fig. 6.9 Reinforcement tension in the bottom layer along the width of the embankment (a) one layer and (b) two-layer

Relatively lower tension was observed in the bottom layer of the two-layer system compared to one layer. This is because of the lower stiffness value of basal geogrid in a two-layer system. Maximum tension in the reinforcement layer developed towards the center of the embankment. As one move towards the edge of the embankment, the reinforcement force shows considerable reduction. This decrease is attributed to the fact that the provision of reinforcement at the embankment base provides considerable restraint against the lateral flow of foundation soil and adds to

slope stability. The maximum tension occurred at the corner of the stone column and gave values of 22 kN/m (*single layer*) and 19.8 kN/m (*two-layer*), respectively.

## 6.7   SOIL ARCHING

The arching can be visible by plotting horizontal stresses in the embankment fill since the horizontal stresses along the arch is constant (Wijerathna and Liyanapathirana 2020). Figs. 6.10, 6.11(a) & (b) show the arch-shaped stress contours formed in a 6 m high embankment for GESC, GESC + One basal layer, and GESC+ Two basal layers, respectively.
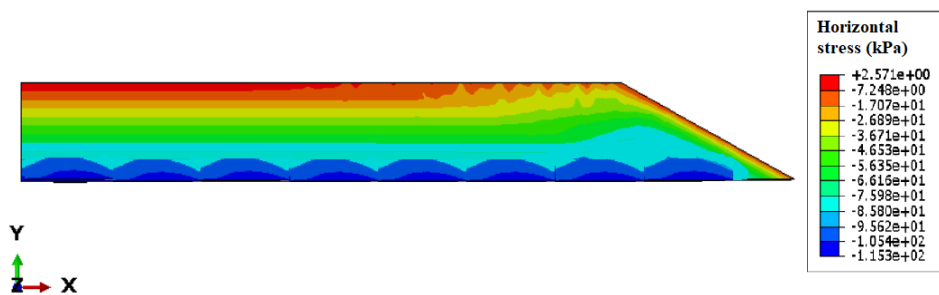


Fig. 6.10 Horizontal stress contours for GESC supported embankment

The figures showed that arching was more in GESC supported embankment without any basal layer. Comparing the case of basal layers, in GESC + One basal layer, the arching height is more than GESC +Two basal layers. This supports the observation that the stress transferred due to soil arching is less when the number of basal layers was more (Section 5.5.1).

Significant portions of embankment load were transferred to columns through soil arching, resulting in lesser stresses in foundation soil. The vertical stress distribution along the embankment fill was found at the mid-span of column spacing, as shown in Fig. 6.12. The vertical stresses exhibited an increasing trend from the embankment top. After reaching a certain depth at the bottom, it starts to decrease near the embankment base. Due to soil arching, the embankment load transferred to the foundation soil is reduced as more load is transferred to the columns. The reduced embankment load coming to the foundation soil is transferred between columns as a vertical line load. The soil arching increases with the embankment height as the differential settlement increases with increased embankment loading (Fig. 6.12). Also, for a height of 6 m, the vertical stresses observed in the embankment fill at the end of

consolidation are more than the stresses developed at the end of construction. The increase is because the differential settlement within the embankment fill increases with foundation soil consolidation, increasing the arching effect.



( a )



(b)
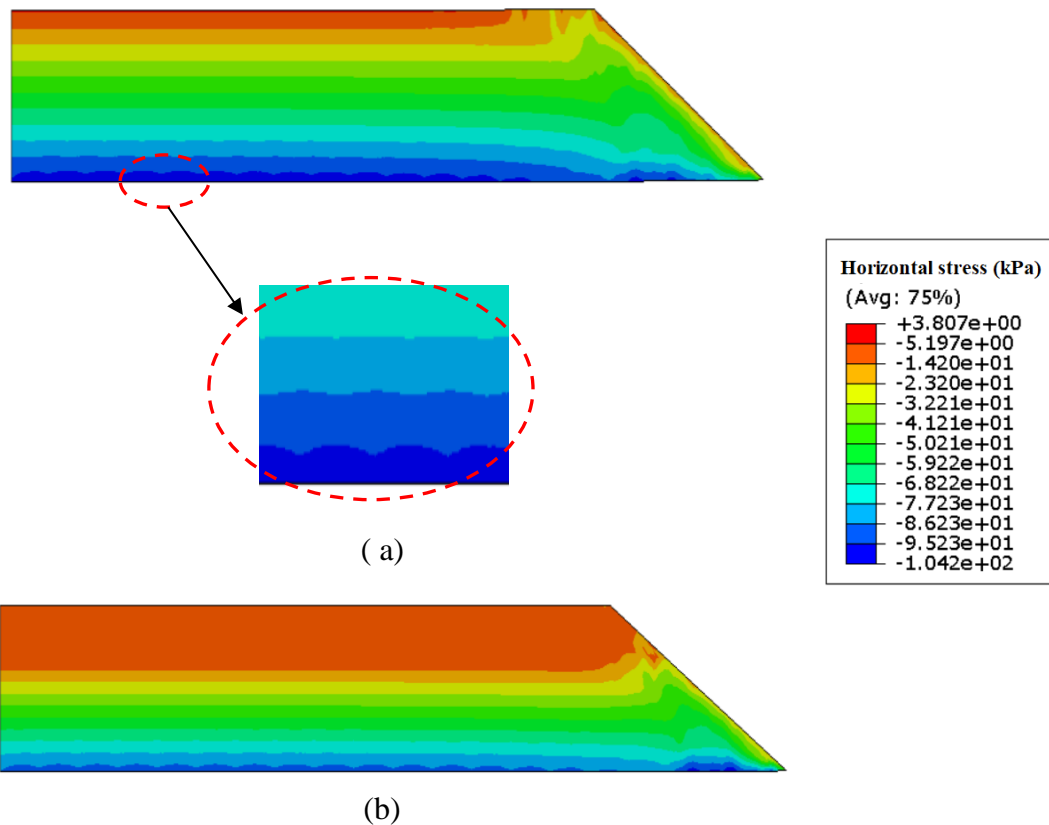
Fig. 6.11 Horizontal stress contours for (a) GESC+ One basal layer and (b) GESC + two basal layers

In the case of single basal geogrid, the vertical stress started decreasing at the height of 2 m from the embankment base. This stress redistribution in the embankment fill indicates that a small amount of soil arching occurred when a single layer of geogrid was placed at the embankment base above the encased stone columns. From Fig. 6.12 (a), it is clear that the arches are not developed in the case of a 2 m fill, and it is visible for a 4 m fill. When two basal geogrids are provided at the embankment base, a considerable reduction in differential settlement occurred in the embankment fill, and thus soil arching effect reduces considerably. The vertical stress distribution along the embankment fill (Fig. 6.12 (b)) supports this observation. The stresses started to decrease at the height of 0.75 m from the embankment base. This indicates that the

height of arches formed was reduced, and the load transfer by soil arching became lesser compared to the case of a single basal layer.



(a)



(b)
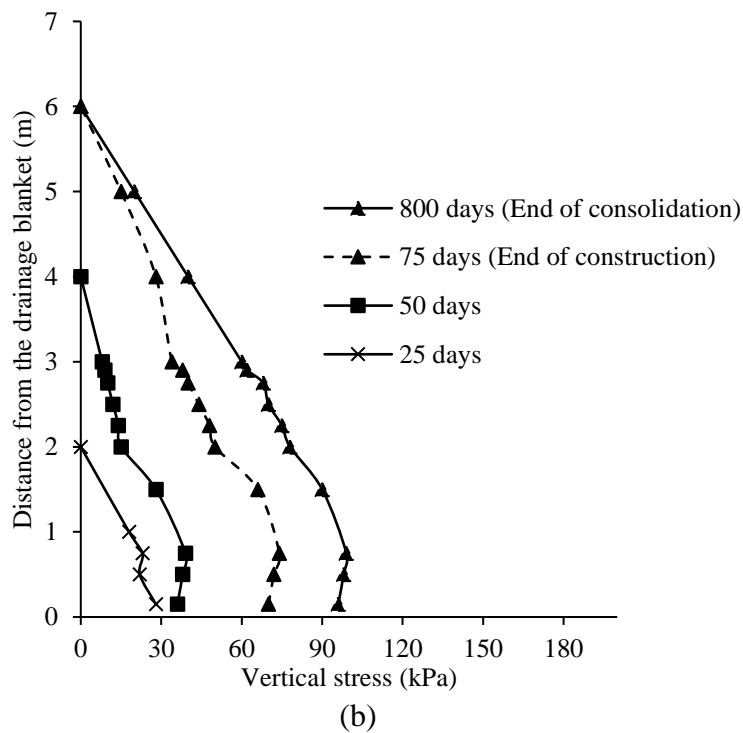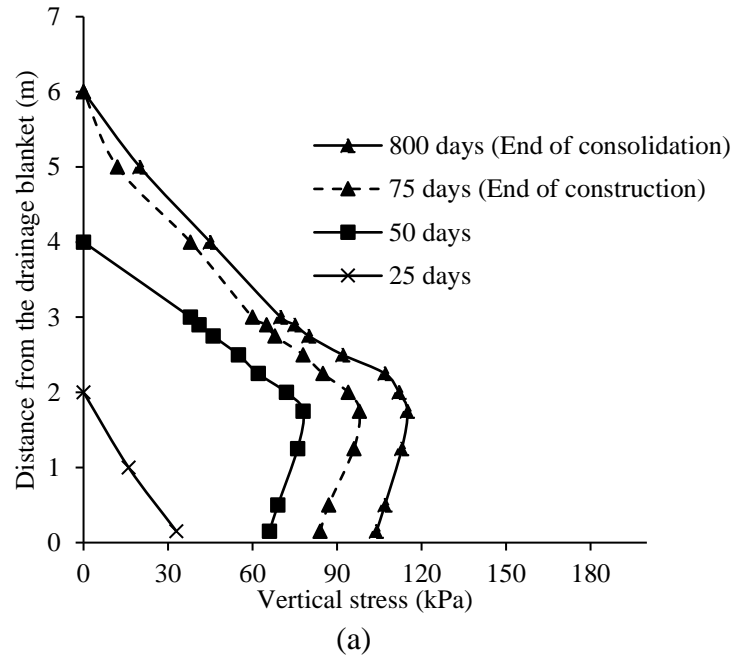
Fig. 6.12 Vertical stress distribution in the embankment fill for (a) GESC+ One basal layer and (b) GESC+ Two basal layers

## 6.8 COMPARISON OF NUMERICAL RESULTS WITH DESIGN CODE RECOMMENDATIONS

The numerical results were compared with the results obtained from the different design codes for the pile-supported embankments. Literature showed a dearth of studies on geogrid reinforced encased stone column supported embankments. Therefore, the stone column's stiffness was assumed to be very high for the comparison purpose, equivalent to a concrete pile. Most of the design methods considered the key load transfer mechanism as arching for pile-supported embankments. The finite element results immediately after construction were used to compare the values estimated by different empirical methods. The amount of embankment load transferred to columnar structures, geosynthetic layer, and foundation soil was found out. The details of various design methods considered in this work are given below.

- ***Terzaghi's Method (1943)***

Based on the trap door experiment Terzaghi (1943) developed an arching theory for the design of pile-supported embankment (Fig. 6.13). The vertical pressure at the base of the soil layer was everywhere equal to the overburden pressure initially. Gradual lowering of a strip of support beneath the soil layer caused the yielding of the overlying material. The yielding material tends to settle, and this movement was opposed by the shear resistance along the boundaries between the moving and the stationary mass of sand. Consequently, the total pressure on the yielding strip was reduced while the load on the adjacent supports increased.
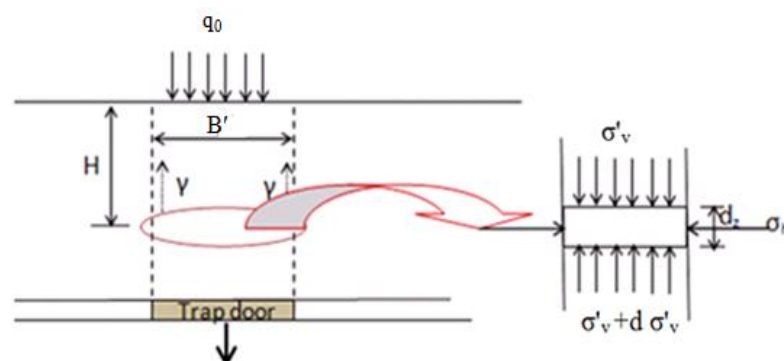


Fig. 6.13 Development of arching (Terzaghi 1943)

Vertical stress at the top surface is,

$$\sigma'_v = \gamma H + q_0 \tag{6.1}$$

where, $\sigma'_v$ = Vertical stress acting on the soil strip considered

$\gamma$ = Unit weight of the soil

$H$ = Thickness of soil above the small area considered

$q_0$ = Surcharge acting at the surface of the soil

The corresponding normal stress on the vertical surface of sliding is given by,

$$\sigma_h = K_0 \sigma'_v \tag{6.2}$$

where $\sigma_h$ is the horizontal stress acting on the strip, and $K_0$ is the earth pressure coefficient at rest.

Assuming the soil as cohesionless; the shear strength of the soil is given by,

$$S = \sigma_h \tan \phi \tag{6.3}$$

Resisting the movement of the soil element due to the applied stress and the weight of the element itself is the soil layer underlying this element and the shear strength of the soil adjacent to the element acting on both sides of the element. When the element is in equilibrium, the summation of the vertical forces must equal zero. Therefore, the vertical equilibrium can be expressed as,

$$\frac{d\sigma'_v}{dz} = \gamma - K_0 \sigma_v \frac{\tan \phi}{B'} \tag{6.4}$$

where $B'$ = width of the strip

Applying the boundary condition $\sigma'_v = q$ at z=0, the differential equation can be solved as follows,

$$\sigma'_v = \frac{\gamma B'}{K_0 \tan \phi} \left( 1 - e^{\frac{-K_0 \tan \phi z}{B'}} \right) + q e^{\frac{-K_0 \tan \phi z}{B'}} \tag{6.5}$$

The main problem with this method is that the coefficient of earth pressures $K_0$ is not known, and it may vary through the depth of the sliding surface. In Terzaghi's method, it is assumed that vertical and horizontal stress equates to principal stresses. Russell *et al.* (2003) proposed that $K_0$ could be conservatively taken as 0.5. Potts and Zdravkovic (2008) proposed that $K_0$ = 1.0 gave good correspondence with plane strain

finite element results. Stress Reduction Ratio ( $S_{3D}$ ) was developed by Russell and Pierpoint (1997) to compare the various design methods. It is defined as the ratio of the average vertical stress acting on the reinforcement to the overburden pressure due to the embankment fill. Based on Terzaghi's theory, the stress reduction ratio is given as,

$$S_{3D} = \frac{(s^2 - a^2)}{4aHK_0 \tan(\phi)} (1 - e)^{\frac{-4aHK_0 \tan(\phi)}{s^2 - a^2}}$$ (6.6)

where $s$ is the pile center-center spacing, and a is the width/diameter of the pile, $H$ is the embankment height, $K_0$ is the lateral earth pressure coefficient at rest, $\phi$ is the friction angle of embankment fill.

The tensile force in the geosynthetic reinforcement was found out using the formula given by Russell and Pierpoint (1997)

$$T = \frac{S_{3D} \gamma H (S^2 - a^2)}{4a} \sqrt{1 + \frac{1}{6\varepsilon}}$$ (6.7)

where $\gamma$ is the unit weight of embankment fill, and $\varepsilon$ is the design strain of reinforcement (5%).

- ***Guido et al. (1987)***

This method is based on the laboratory plate load tests carried out on geogrid reinforced sand in a confined rigid box. Guido et al. (1987) assumed triangular-shaped arches in the embankment fill with an internal angle of 45°. The geosynthetic layer carried the weight of soil below the arch, which is not supported by the piles. The total load ( $\sigma_s$ ) supported by the geosynthetic layer and the tension (*T*) in the reinforcement were given as,

$$\sigma_s = 0.525 \gamma H$$ (6.8)

$$T = \frac{\sigma_s}{2 \sin \delta}$$ (6.9)

Where $\delta$ is the angle of friction between geosynthetic and soil, $\gamma$ is the unit weight of embankment fill.

The vertical stress action on the column $\sigma_s$ is given by,

$$\sigma_p = \frac{\gamma H[s - 0.525(s-a)]}{a} \tag{6.10}$$

Thus, stress reduction ratio $(S_{3D})$ obtained as,

$$S_{3D} = \frac{(s-a)}{H3\sqrt{2}} \tag{6.11}$$

The Guido method did not consider the effect of subsoil support, stiffness of geosynthetic material, the elastic modulus of the pile, and embankment fill properties.

- *Low et al. (1994)*

Hewlett and Randolph (1988) presented theoretical methods to compute the portion of embankment load, which is applied to the foundation soils and the columns through soil arching based on the limit state of soil in the hemispherical domed region over piles. Later, the method was modified by Low et al. (1994). Low et al. (1994) proposed equations and charts for calculating the tension in the geosynthetic layer and stress reduction in the soft ground-based on laboratory tests. The shape of the arches was assumed as semi-cylindrical between pile walls, and the thickness was taken equal to half the width of the pile walls. The method considered the effect of subsoil support and stiffness of the geosynthetic layer.

The vertical stress on the column $(\sigma_p)$ and vertical stress on the geosynthetic layer $(\sigma_s)$ was given as,

$$\sigma_p = \frac{s(\gamma H) - P_0(s-a)}{a} \tag{6.12}$$

$$\sigma_s = \frac{[\gamma(s-a)(K_p - 1)}{2(K_p - 2)} + \left[\frac{(s-a)}{s}\right]^{(K_p - 1)} \left[\gamma H - \frac{\gamma s}{2}\left(1 + \frac{1}{(K_p - 2)}\right)\right] \tag{6.13}$$

where $P_0$ is the assumed uniform pressure applied on the geosynthetic layer, $K_p$ is the passive earth pressure coefficient.

The tension in the reinforcement ($T$) was calculated by assuming circular deflection of geosynthetic with a radius '$R$' and subtended angle of $2\theta$ at the center of the arc. The maximum vertical displacement of the foundation soil midway between the pile caps was denoted as '$t$'.

$$T = J\varepsilon \tag{6.14}$$

where $J$ is the tensile stiffness of the geosynthetic and $\varepsilon$ is the axial strain, which is given by,

$$\varepsilon = \frac{\theta - \sin\theta}{\sin\theta} \tag{6.15}$$

$$R = \frac{s-D}{2\sin\theta} \tag{6.16}$$

Considering the vertical equilibrium of forces, the reinforcement tension ($T$) is calculated as,

$$\frac{T}{R} = P_0 = \sigma_{s-}\left(\frac{tE_s}{h_1}\right) \tag{6.17}$$

here $E_s$ is the elastic modulus of the foundation soil, and $h_1$ is the depth of the foundation soil. A trial and error procedure is used with different values of 't' to get $\theta$ and $R$ values. The tension in the geosynthetic was calculated with equations (6.14) and (6.17) separately with the obtained values until the results were the same. That '$t$' value is used to calculate the stress reduction ratio.

$$S_{3D} = \frac{\sigma_s - \left(\dfrac{tE_s}{h_1}\right)}{\gamma H} \tag{6.18}$$

- **_Abusharar et al. (2009)_**

Abusharar et al. (2009) proposed a new design method for geosynthetic reinforced piled embankment by considering the arching effect on embankment fill similar to Low et al. (1994). The main differences with the Low et al. (1994) method were the inclusion of a uniform surcharge and consideration of the effect of the skin friction mechanism. The tension in the geosynthetic layer was modified as,

$$T = (4\beta^2 J) + \frac{1}{4}(s-a)\lambda_3 \tan\phi'\left[\sigma_s + \left(\frac{tE_s}{h_1}\right)\right] \tag{6.19}$$

where $\beta$ is $\left[t/(s-D)\right]$, $\lambda_3$ is a dimensionless parameter varying between 0.7 and 0.9 depending on the type of geosynthetic. In this study, $\lambda_3$ is taken as 0.8. $\beta$ can be solved by using the equation, $a\beta^3 + b\beta^2 + c\beta + d = 0$;

where, $a = 32h_1 J + 4(sa)^2 E_s$

$$b = 2(s-a)^2 \lambda_3 E_s \tan \phi' - 4(s-a)h_1\sigma_s$$

$$c = 2(s-a)\lambda_3 D\sigma_s \tan \phi'(s-a)^2 E_s$$

$$d = -(s-a)h_1\sigma_s$$

Geosynthetic tension was calculated by using the obtained $\beta$. The $S_{3D}$ value was obtained using equation (6.18).

- ***BS 8006 (2010)***

BS8006 (2010) "Code of practice for strengthened – reinforced soil and other fills" is the British Standard used to design embankments with reinforced soil foundations on poor ground. This is the most widely used method and is very conservative. Based on Marston's (1913) formula for positive projecting conduits, Jones et al. (1990) developed an empirical relationship (Eq 6.19) for the ratio of average vertical stress acting on the pile caps to the average vertical stress acting across the base of the embankment.

$$\frac{P_c}{\sigma_v} = \left(\frac{aa_c}{H}\right)^2 \tag{6.20}$$

where,

$P_c$ =Arched vertical stress per unit length at the top of the conduit/pile

$\sigma_v$ =Average vertical stress per unit length at the top of the conduit/pile

$a$ = width of pile cap

$a_c$ =Arching Coefficient

$H$ = embankment height

Later this formula was adopted by BS8006 for the design of piled embankments. BS8006 (2010) gives empirical equations for arching coefficient $a_c$ as follows,

End bearing piles, $\quad a_c = 1.95\dfrac{H}{a} - 0.18$

Friction piles, $\quad\quad a_c = 1.5\dfrac{H}{a} - 0.07$

BS8006 (2010) considers two cases to find the vertical stress at the embankment base. The two cases are:

(a) *Partial arching*: When the embankment height was below the critical height $1.4(s-a)$, arching is not fully developed, as shown in Fig. 6.14.
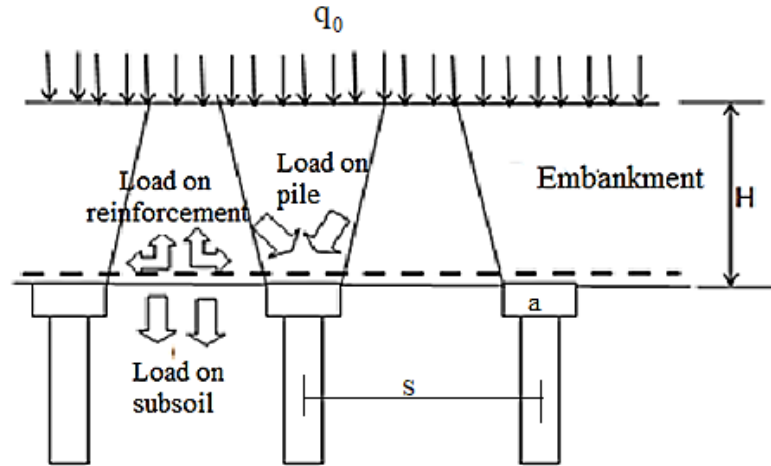


Fig. 6.14 Partial soil arching

For partial arching, the equations for the line load acting on the reinforcement (Eq 6.21) and the Stress Reduction Ratio, $S_{3D}$ (Eq 6.22), are given as:

i.e., $0.7(s-a) \le H \le 1.4(s-a)$

$$W_{Tn} = \frac{s(\gamma H + q_0)}{(s^2 - a^2)}\left[s^2 - a^2\left(\frac{p'_c}{\sigma'_v}\right)\right] \tag{6.21}$$

$$S_{3D} = \frac{2s(\gamma H + q_0)(s-a)}{(s^2 - a^2)\gamma H}\left[s^2 - a^2\left(\frac{p'_c}{\gamma H}\right)\right] \tag{6.22}$$

(b) *Full arching*: When the embankment height is more than the critical height, full arches are developed, and the height of the embankment above the arching height plays no role in the forces developed in the reinforcement layer, as is clear from Fig. 6.15.

175
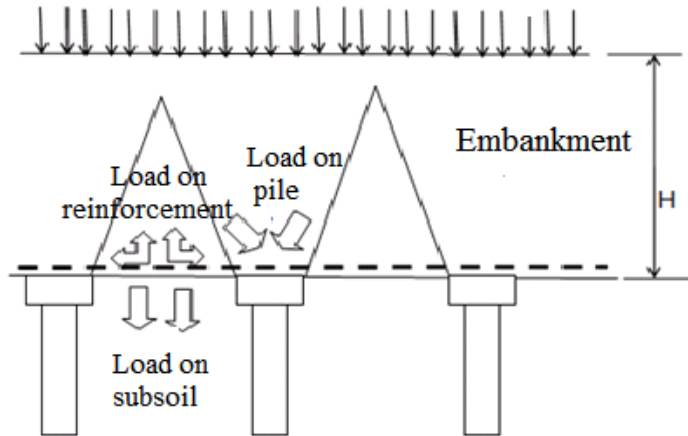
Fig. 6.15 Full soil arching

For full arching, the equations for the line load acting on the reinforcement (Eqn 6.23) and the Stress Reduction Ratio $S_{3D}$ (Eq 6.24) is given as,

$$W_{Tn} = \frac{1.4s\gamma(s-a)}{(s^2-a^2)}\left[s^2 - a^2\left(\frac{p'_c}{\sigma'_v}\right)\right]$$

(6.23)

i.e., $H > 1.4(s-a)$

$$S_{3D} = \frac{16s}{(s+a)^2 H}\left[s^2 - a^2\left(\frac{p'_c}{\gamma H}\right)\right]$$

(6.24)

According to BS8006, no embankment load is carried by the subsoil. So, the effect of subsoil support is nowhere considered in the design equations. The geosynthetic reinforcement supports the embankment load, which is not transferred to the columns, and this load distribution is assumed to be uniform. The deflection of the reinforcement is assumed a catenary described by the equation $y = \cosh(x)$. In this method, the effect of pile modulus, geosynthetic stiffness, and embankment fill properties was also not considered.

Van Eekelen et al. (2011) proposed a few modifications in BS8006 to calculate the load on the geosynthetic layer. More realistic values of stress reduction ratio and geosynthetic tensile forces were obtained using the new equations. The distributed load on the reinforcement $(W_{Tn})$ was obtained for partial and full arching as follows,

176

(i) Partial arching

$$W_{Tn} = \frac{\gamma H}{2(s-a)} \left[ s^2 - a^2 \left( \frac{\sigma_p}{\gamma H} \right) \right]$$

(6.25 a)

(ii) Full arching

$$W_{Tn} = 0.7\gamma \left[ s^2 - a^2 \left( \frac{\sigma_p}{\gamma H} \right) \right]$$

(6.25 b)

The tensile force in the geosynthetic reinforcement per meter run ($T$) was calculated by the following equation,

$$T = \frac{W_{Tn}(s-a)}{2a} \sqrt{1 + \frac{1}{6\varepsilon}}$$

(6.26)

Where $\varepsilon$ is the strain in the reinforcement.

The vertical stress on the stone column and basal geogrid, tension developed on the geogrid, Stress Reduction Ratio, and Stress Concentration Ratio was found out from numerical analyses. The results were compared with the available design methods for column-supported embankments.

## 6.8.1 Comparison of Stress Reduction Ratio $\left( S_{3D} \right)$

The stress reduction ratio values obtained from each design method at the end of embankment construction were compared with the value from the finite element analysis. The numerical results and the analytical results follow the same trend for the Stress Reduction Ratios at different embankment heights. The $S_{3D}$ value decreases with the increase in embankment height. The shear resistance in the fill is large enough to develop arching and transfer more embankment load to the pile top. From Fig. 6.16, it is clear that, out of the various design methods considered, methods proposed by Guido et al. (1987), Low et al. (1994), and Abusharar et al. (2009) significantly under-predicted the Stress Reduction Ratio. For the methods of Low et al. (1994) and Abusharar et al. (2009), the elastic modulus of foundation soil ($E_s$) is considered for the stress reduction ratio calculation, and the variation of 't' and the increase in the term ($tE_s/h_1$) results in lesser stress reduction ratio. In the case of stone column supported embankment, the load transferred due to arching is less, which increased the stress

reduction ratio. The method proposed by Abusharar et al. (2009) gives results close to that of Low et al. (1994) since it is developed with a slight modification of the Low et al. (1994) method. Terzaghi (1943) and BS8006 (2010) methods exhibited a closer range of $S_{3D}$ values for low-height embankments to the value obtained from the full 3-dimensional analyses. 3D column analyses underpredicted the $S_{3D}$ values by around 15% compared to full 3-dimensional analyses (Fig. 6.16).
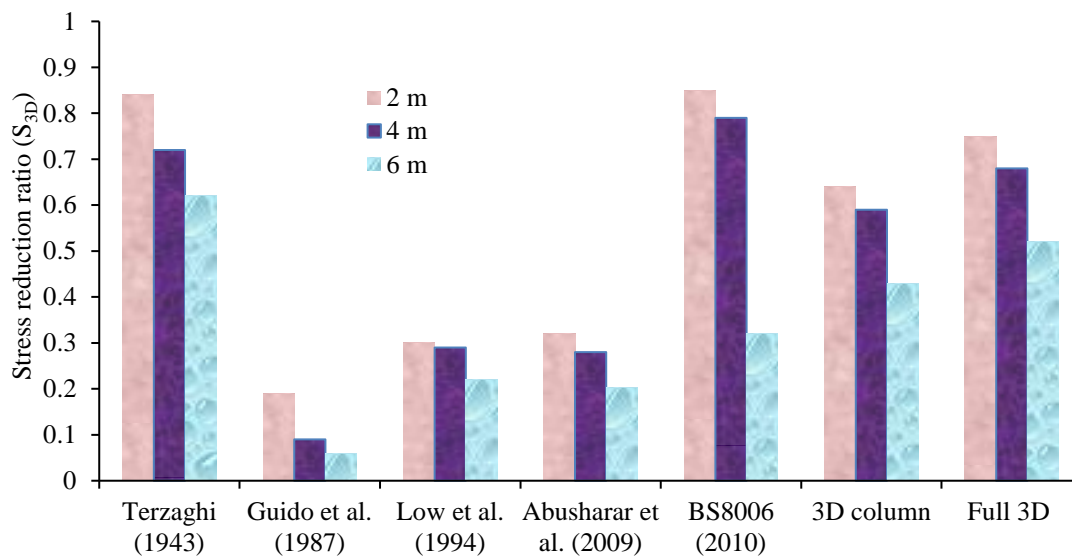


Fig. 6.16 Variation of stress reduction ratio with embankment height

## 6.8.2 Variation of Geosynthetic Tension with Embankment Height

The tensile force in the geosynthetic reinforcement for different embankment heights was found out using the developed 3D column and full 3-dimensional models. The results obtained at the end of construction were compared with the available design methods. The tensile force in the reinforcement was found to be increasing with the embankment height. The higher value of tensile force results in a higher vertical component of tension in the geogrid layer, increasing the embankment load transfer to the stone columns.

BS8006 (2010) shows a slight reduction in the tensile forces after reaching the full arching height, and the reinforcement forces remain constant with an increase in the embankment height. Out of the different design methods considered, Terzaghi (1943) and BS8006 (2010) highly over-predict the tension in the reinforcement. In BS

8006 (2010), the area coverage ratio, which is the ratio between the plane area subjected to the vertical stress to the area between adjacent columns, is taken as a double orthogonal layer (Fig 6.17) which leads to the calculation of higher tensile loads in the reinforcement.
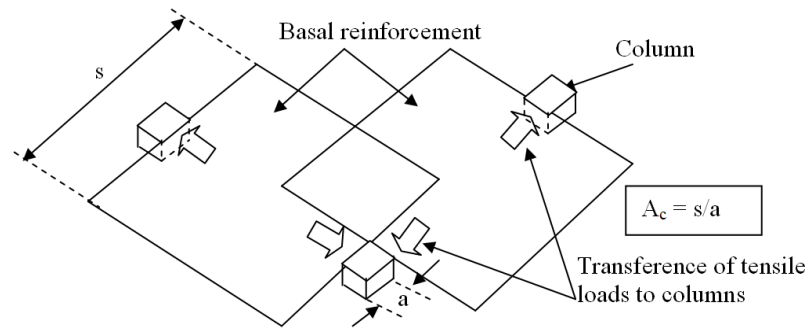


Fig. 6.17 Double-layer coverage in BS8006 (2010) (After Lawson 2012)

These highly conservative results lead to an uneconomical design. 3D column model gives lesser tensile forces compared to the full 3-dimensional model. The presence of vertical boundaries in the 3D column model leads to the reduction in the reinforcement forces. Guido et al.'s (1987) method shows good agreement with results from full 3-dimensional analyses (Fig. 6.18).
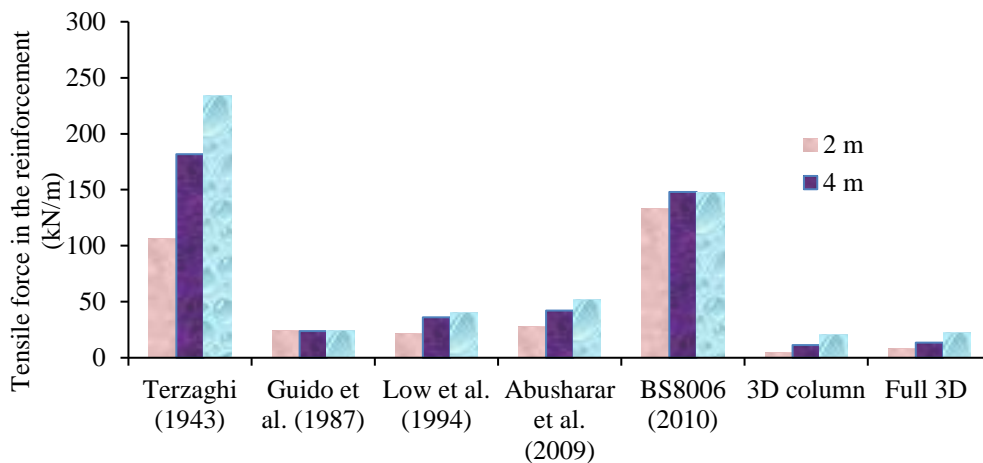


Fig. 6.18 Variation of geosynthetic tension with embankment height

### 6.8.3 Comparison Based on Stress Concentration Ratio (SCR)

Vertical stress acting on the top of the stone column (middle) and the geogrid layer were found using a full 3-dimensional model, and the results were compared with the

results obtained from available design methods. From these values of vertical stresses, the stress concentration ratio was calculated. BS8006 and Guido et al. (1987) do not consider the reaction of soft ground on the reinforcement, i.e., this method considers the subsoil support as zero. The calculated vertical stress in the geogrid layer is more, and thus the stress concentration ratio is under-predicted. The method by Low et al. (1994) shows good agreement with the numerical analysis results for an embankment height of 6 m (Fig. 6.19) since the method considered the effect of subsoil support and stiffness of the geogrid layer.
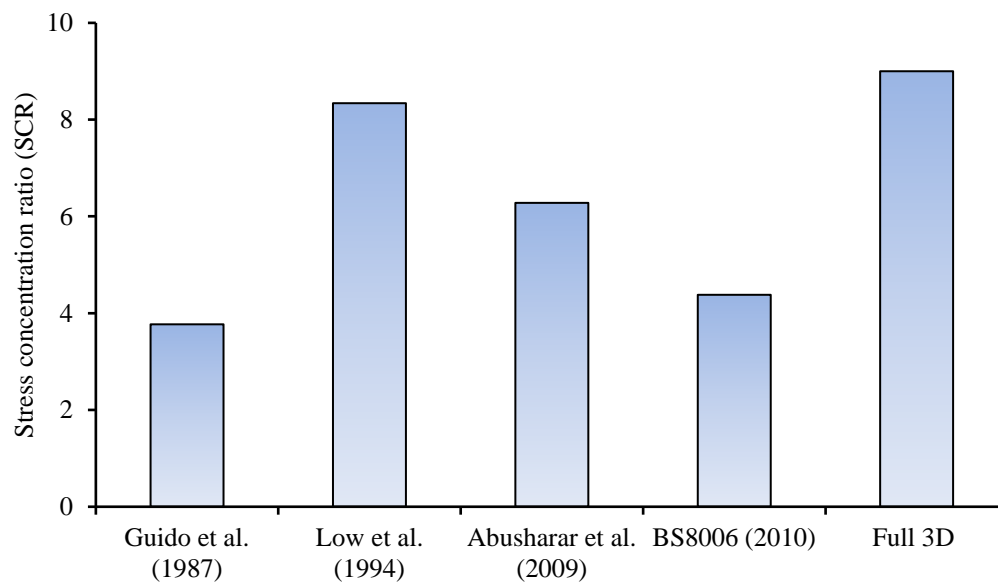


Fig. 6.19 Stress concentration ratio from different design methods

# CHAPTER 7

# SUMMARY AND CONCLUSIONS

## 7.1 SUMMARY

The stone columns are identified as an ideal ground improvement method to support flexible structures such as oil storage tanks, road embankments, etc. The axial load capacities of stone columns are improved by encasing them with suitable geosynthetic material. The technique of enhancing the performance of encased stone columns by providing a geosynthetic layer above the stone columns has been examined in this thesis. These geosynthetic encased stone columns with a basal reinforcement layer were studied through experimental and numerical investigations.

The load-settlement and bulging behavior of stone columns in lithomargic clay has been investigated using experimental and finite element analyses. Studies considered three types of stone columns: ordinary stone column (OSC), geogrid encased stone column (GESC), and geogrid encased stone column with a horizontal layer of geogrid in the middle of the drainage layer. Experiments were carried out for single as well as a group of columns. In group column tests, the same area replacement ratio (15%) was kept by replacing the single column with a group of smaller diameter columns. The trends obtained in the laboratory tests are in good agreement with the results from numerical investigations.

The effectiveness of single basal geogrid layer, double geogrid layers, and geocell-sand mattress as a load transfer platform (LTP) in encased stone column supported embankment was also evaluated using the developed numerical models. The interaction between the geocell wall and infill material is successfully modeled using the finite element program ABAQUS. By considering the limitations of the equivalent composite approach, the infill soil and geocell are modeled separately using two different constitutive models. Parametric studies were also carried out to find the influence of various parameters on the time-dependent behavior of the geosynthetic reinforced encased stone column supported embankment.

The first chapter of this thesis has introduced the concept and necessity of ground improvement techniques such as stone columns and geocell. Also, based on the present scenario, the objectives were formulated. The second chapter of this thesis has reviewed the literature on geocell reinforced soil and encased stone columns and identified the research gap that supports the present work's objectives. The third chapter has discussed the finite element scheme used and numerical models employed in this research work. The validation of numerical models with respect to the published literature was also included. The fourth chapter has described the various laboratory tests performed to understand the behavior of single stone columns and the group of stone columns installed in the lithomargic clay layer. The time-dependent behavior of geosynthetic reinforced encased stone column supported embankment was analyzed using axisymmetric, 3D column models, and the results are presented in the fifth chapter. The sixth chapter contains the full three-dimensional analysis results of different reinforcement cases.

## 7.2   CONCLUSIONS

The major conclusions that can be drawn from this research work are as follows.

1. The experimental investigations found that the improvement in load-carrying capacity of lithomargic clay reinforced by an ordinary stone column was 39%. However, with a geogrid encased stone column, the improvement was 169%. By providing a horizontal layer of geogrid at the embankment base and a geogrid encased stone column, the improvement was 198%.

2. Experimental as well as numerical studies showed that the column configuration affects the performance of the overall system. From a load-carrying capacity point of view, for the same area ratio, a group of ordinary stone columns with smaller diameters will be more advantageous than a single column of large diameter.

3. Significant improvement in Stress Concentration Ratio (SCR) was observed for a group of encased stone columns with basal geogrid layer compared to OSCs and GESCs. The SCR for OSC group, GESC group, and GESC with basal geogrid layer was between 2.5 to 4, 3.19 to 3.65, and 4.56 to 7.02, respectively. Along with the depth, a sudden decrease in SCR was observed

just below the column head, and the SCR value increased with a further increase in depth.

4. The provision of a basal geogrid layer and the geogrid encased stone column showed a significant increase in the improvement factor (IF) compared to the ordinary stone column, and geosynthetic encased stone column. The numerical value of IF for OSC, GESC, and GESC with basal geogrid was 1.38, 2.69, and 2.98, respectively.

5. For a geosynthetic encased stone column, the maximum bulging diameter was reduced by 38%, and the maximum bulging depth was increased by 50% as that of the ordinary stone column. For GESC along with basal geogrid, these values were 82% and 50%, respectively. Group of stone columns with the same area ratio of 15% as a single column exhibited lesser lateral bulging than a single column for all three cases. The depth corresponding to the maximum bulging for the group of stone columns remained unchanged in all the cases.

6. Time-dependent variation in the stress concentration ratio (SCR) and ground surface settlement for embankments supported on ordinary stone columns (OSC), encased stone columns (GESC), encased stone columns with basal geogrids (GESC+ One basal layer), and encased stone columns with geocell-sand mattress (GESC+GEOCELL) were studied by using developed unit cell models. The analysis results showed that SCR increases with time and becomes constant after achieving full consolidation. In the case of GESC, an improvement of 26% was observed for the stress concentration ratio (end of consolidation) compared to OSC. By providing a single basal geogrid layer, the improvement was 52%, and for two basal layers, the improvement was 63%. The geocell layer on top of the geogrid encased stone column (GESC+GEOCELL) showed an improvement of 85%.

7. The geocell-sand mattress reduced the vertical settlement of foundation soil due to the embankment construction by 80%. The reduction in the vertical settlement was 78% and 79% for single and two basal geogrids, respectively. The basal geogrids and geocell-sand mattress decreased the bulging of the stone columns, and the maximum bulging was visible at a depth of 3.5 D in both cases, where D is the diameter of stone columns. For a geogrid encased

stone column, the corresponding zone is 3D. A 69% reduction in the lateral bulging occurred in GESC compared to OSC when a single basal layer was placed. The reduction is 52% and 54% for two basal layers and geocell, respectively. When the geocell-sand mattress was used instead of two layers of geogrid, almost 80% of the stone column bulging occurred by the end of the embankment construction.

8. The tensile stress distribution in the geocells was analyzed, and it was observed that the stresses are non-uniformly distributed in the geocell pockets. Therefore, the maximum tensile force was mobilized at the geocell mid-height. The mobilized tensile strength provided an additional confinement effect to the infill soil and considerably enhanced the overall system's performance.

9. Among the three different infill materials analyzed for geocell, the aggregates were the best-suited in terms of Stress Concentration Ratio (SCR) and vertical settlement. The mobilized tensile force in geocell due to embankment loading was maximum for aggregates and minimum for quarry dust.

10. The developed numerical model considers the actual shape of geocell and the interaction between the geocell wall and the infill soil to overcome the limitations of the equivalent composite approach (ECA). Since the ECA overestimates the Stress Concentration Ratio and bearing capacity, the present 3-dimensional model economizes the design of geocell reinforced embankments.

11. Semicircular-shaped arches can be pictured from the horizontal stress distribution in the embankment fill in GESC supported embankment. The presence of reinforcement layers above the stone column reduces the soil arching. As a result, the maximum height of the arch for GESC+GEOCELL was only half of that with pile-supported embankments with basal reinforcement.

12. From the numerical results, multiple layers of geosynthetic can be replaced by a single layer of geocell, considered to be a superior form of reinforcement because of the three-dimensional confinement offered to the infill material. The numerical results supported the idea that encased stone columns with geocells

at the embankment base can perform similar to a geosynthetic reinforced piled embankment system, which is costlier but very efficient.

13. Compared to an unreinforced embankment, 87% reduction in lateral deformation near the toe was observed for GESC+ One basal layer at the end of consolidation, and 90% reduction in the lateral deformation was obtained when two layers of geogrids (stiffness equivalent to that of a single layer) was provided at the base. The decrease is attributed to the reinforcement layers resisting the shear failure in the foundation soil. This shows that reinforcing the embankment base provides considerable restraint against the lateral flow of foundation soil, adding to slope stability.

14. In two basal geogrids, the tensile force at the top layer was less compared to the bottom layer. A slight decrease in the tensile stresses was observed in GESC+ Two basal layers compared to GESC+ One basal layer because of the lower modulus value of basal geogrid in two-layer systems. Maximum tension in the geogrid layer developed towards the center of the embankment. As one move towards the edge of the embankment, the reinforcement force shows considerable reduction. The maximum tension occurred at the corner of the stone column and gave 22 kN/m (one layer) and 19.8 kN/m (two-layer), respectively.

15. Stress Reduction Ratio ($S_{3D}$) variation with embankment height from different empirical methods and 3-dimensional analyses for GESC+ One basal layer follows the same trend. Among the various design methods, Guido et al. (1987), Low et al. (1994), and Abusharar et al. (2009) significantly under-predicts the Stress Reduction Ratio. On the other hand, Terzaghi's (1943) and BS 8006 (2010) methods exhibited a closer range of S3D values for low height embankments from the full 3-dimensional model.

16. Terzaghi's (1943) and BS 8006 (2010) methods highly over-predict the tensile force in the reinforcement. These highly conservative results can lead to an uneconomical design. On the other hand, the 3D column model gives lesser tensile forces compared to full 3-dimensional analyses. Compared to other methods, Guido et al. (1987) show good agreement with full 3-dimensional analysis results for geogrid tensile force.

## 7.3   SCOPE FOR FURTHER RESEARCH

One of the limitations of the present work is the lack of large-scale tests and field tests, giving more accurate and viable solutions to predict the behavior of encased stone column supported embankments with basal reinforcement. In the future, the numerical work can be extended to explore the system's response under dynamic loading.

# REFERENCES

[1]     ABAQUS. (2016). ABAQUS Analysis User's Manual. Dassault Systems Simulia Corp., Providence RI.

[2]     Abusharar, S. W., Zheng, J. J., Chen, B. G. and Yin, J. H. (2009). "A simplified method for analysis of a piled embankment reinforced with geosynthetics". *Geotextiles and Geomembranes,* 27(1), 39–52.

[3]     Alawaji, H. A. (2001). "Settlement and bearing capacity of geogrid reinforced sand over collapsible soil". *Geotextiles and Geomembranes,* 19(2), 75–88.

[4]     Alexiew, D., Brokemper, D. and Lothspeich, S. (2005). *"*Geotextile Encased Columns (GEC): load capacity, geotextile selection and pre-design graphs". *Contemporary Issues in Foundation Engineering*, GSP 131, 1-14.

[5]     Ambily, A. P. and Gandhi, S. R. (2007). "Behavior of Stone Columns Based on Experimental and FEM Analysis". *Journal of Geotechnical and Geoenvironmental Engineering*, 133, 405–415.

[6]     Andrews, A., Gawu, S. K. Y., Momade, Z., and Momade, F. W. Y. (2014). "Genesis, properties and industrial applications of bauxitic lithomargic clay". *Clays and Clay Minerals: Geological Origin, Mechanical Properties and Industrial Applications*.

[7]     Arulrajah, A., Abdullah, A. and Bouzza, A. (2009). "Ground improvement technique for railway embankments". *Ground Improvement,* 162 (1), 3-14.

[8]     ASTM, D4595. (2011). "Standard test method for tensile properties of geotextiles by the wide-width strip method". *In American Society for Testing and Materials*.

[9]     Barksdale, R.D. and Bachus, R. C. (1983). "Design and construction of stone columns". *Federal highway administration*, RD-83/026.

[10]    Basudhar, P. K., Saha, S. and Deb, K. (2007). "Circular footings resting on geotextile reinforced sand bed". *Geotextiles and Geomembranes,* 25(6), 377–384.

[11]    Bathe, K. J. (2006) "Formulation of the Finite Element Method", Chapter 4 pp-229

[12] Bathurst, R.J. and Karpurapu, R. (1993). "Large-scale triaxial compression testing of geocell-reinforced granular soils". *Geotechnical Testing Journal,* 16(3), 296-303.

[13] Bathrust, R.J. and Knight, M. A. (1998). "Analysis of geocell reinforced soil covers over large span conduits". *Computers and Geotechnics*, 22(3/4), 205–219.

[14] Benmebarek, S., Djeridi, S., Benmebarek, N. and Belounar, L. (2017). "Improvement of bearing capacity of strip footing on reinforced sand". *International Journal of Geotechnical Engineering*. 1-9.

[15] Bhasi, A. and Rajagopal, K. (2015). "Geosynthetic-reinforced piled embankments: comparison of numerical and analytical methods". *International Journal of Geomechanics*, 15(5), 1–12.

[16] Biabani, M. M., Ngo, N. T. and Indraratna, B. (2016a). "Modelling of geocell reinforced subballast subjected to cyclic loading". *Geotextiles and Geomembranes*, 44, 489–503.

[17] Biabani, M. M., Indraratna, B. and Ngo, N. T. (2016b). "Performance evaluation of railway subballast stabilised with geocell based on pull-out testing". *Geotextiles and Geomembranes*, 44(4), 579–591.

[18] Binquet, J. and Lee, K.L. (1975). "Bearing capacity tests on reinforced earth slabs", *Journal of Geotechnical Engineering Division*, *ASCE*, 101 (GT12), 1241-1255

[19] Biot, M. A. (1941). "General theory of three-dimensional consolidation". *Journal of Applied Physics*, 12(2), 155–164.

[20] Biswas, A., Krishna, A. M. and Dash, S. K. (2016). "Behavior of geosynthetic reinforced soil foundation systems supported on stiff clay subgrade". *International Journal of Geomechanics*, 16(5), 1-15.

[21] Bouazza, A., Zornberg, J. G. and Adam, D. (2002). "Geosynthetics in waste containment facilities: recent advances", *Geosynthetics - 7 ICG -* Delmas ISBN 90 5809 523 1.

[22] Boyle, S. and Robertson, K. (2007). "Geocell geogrid and reinforced-soil restoration of eroded steep slopes". *Geosynthetics ,*25(2), 20–26.

[23] Bowles, J. E. (1988). "Foundation analysis and design". 5<sup>th</sup> ed Foundation analysis and design. Mc Graw Hill International Editions, Singapore.

[24] BS 8006 (2010). Code of practice for strengthened/reinforced soils and other fills. British Standard Institution, London.

[25] Bush, D. I., Jenner, C. G. and Bassett, R. H. (1990). "The design and construction of geocell foundation mattresses supporting embankments over soft grounds". *Geotextiles and Geomembranes*, 9(1), 83–98.

[26] Carroll Jr, R.G. and Curtis, V.C. (1990). "Geogrid connections". *Geotextiles and Geomembranes,* 9(4-6), 515-530.

[27] Castro, J. (2017). "Groups of encased stone columns: Influence of column length and arrangement". *Geotextiles and Geomembranes*, 45(2), 68–80.

[28] Castro, J. and Karstunen, M. (2010). "Numerical simulations of stone column installation". *Canadian Geotechnical Journal*, 47(10), 1127–1138.

[29] Chen, J. F., Li, L. Y., Xue, J. F. and Feng, S. Z. (2015). "Failure mechanism of geosynthetic-encased stone columns in soft soils under embankment". *Geotextiles and Geomembranes*, 43(5), 424–431.

[30] Chen, R. H., Wu, C. P., Huang, F. C. and Shen, C. W. (2013). "Numerical analysis of geocell-reinforced retaining structures". *Geotextiles and Geomembranes*, 39, 51–62.

[31] Cheng, X., Chen, W., Jing, W., Yin, C. and Shi, A. (2015). "Influence of area replacement ratio on settlement and stability of oil storage tank composite foundation treated with compaction piles". *Electronic Journal of Geotechnical Engineering*, 20(11), 4665–4678.

[32] Collin, J. G., Han, J. and Huang, J. (2005). "Geosynthetic reinforced column support embankment design guidelines". *Proceedings of the North America Geosynthetics Society Conference*, North American Geosynthetics Society, Albany, NY, 1–15.

[33] Daniel, D. E. and Bowders, J. J. (1996). "Waste containment by geosynthetics". *Proceedings of 2nd International Congress on Environmental Geotechnics*, Osaka 2: 49-66

[34] Darshan, C. S., Nayak. S. and Preetham. H. K. (2017). "Influence of granulated blast furnace slag and cement on the strength properties of lithomargic clay". *Indian Geotechnical Journal*. 47. 10.1007/s40098-017-0228-8.

[35] Das, A. K. and Deb, K. (2018). "Experimental and 3D numerical study on time-dependent behavior of stone column-supported embankments". *International Journal of Geomechanics*, 18(4).

[36] Dash, S. K. (2012). "Effect of geocell type on load-carrying mechanisms of geocell-reinforced sand foundations". *International Journal of Geomechanics*, 12(5), 537–548.

[37] Dash, S. K. and Bora, M. C. (2013). "Improved performance of soft clay foundations using stone columns and geocell-sand mattress". *Geotextiles and Geomembranes*, 41, 26–35.

[38] Dash, S. K., Rajagopal, K. and Krishnaswamy, N. R. (2001a). "Strip footing on geocell reinforced sand beds with additional planar reinforcement". *Geotextiles and Geomembranes*, 19(8), 529–538.

[39] Dash, S. K., Krishnaswamy, N. R and Rajagopal, K. (2001b). "Bearing capacity of strip footings supported on geocell-reinforced sand". *Geotextiles and Geomembranes,* 19, 235–256.

[40] Dash, S. K., Rajagopal, K. and Krishnaswamy, N. R. (2004). "Performance of different geosynthetic reinforcement materials in sand foundations". *Geosynthetics International,* 11,1.

[41] Dash, S. K., Rajagopal, K. and Krishnaswamy, N. R. (2007). "Behaviour of geocell-reinforced sand beds under strip loading". *Canadian Geotechnical Journal*, 44(7), 905–916.

[42] Dash, S. K., Sireesh, S. and Sitharam, T. G. (2003). "Model studies on circular footing supported on geocell reinforced sand underlain by soft clay". *Geotextiles and Geomembranes*, 21(4), 197–219.

[43] Davarifard, S. and Tafreshi, M. (2015). "Plate load tests of multi-layered geocell reinforced bed considering embedment depth of footing". *Procedia Earth Planet Science,* 15,105–110.

[44]    Deb, K. (2010). "A mathematical model to study the soil arching effect in stone column-supported embankment resting on soft soil". *Applied Mathematical Modelling*. 34(12), 3871–3883.

[45]    Deb, K. (2008). "Modeling of granular bed-stone column-improved soft soil". *International Journal of Numerical and Analytical methods in Geomechanics*, 32, 1267-1288.

[46]    Deb, K. and Behera, A. (2017). "Rate of consolidation of stone column-improved ground considering change in permeability and compressibility during consolidation". *Applied Mathematical Modelling*, *48*, 548–566.

[47]    Deb, K. and Mohapatra, S. R. (2013). "Analysis of stone column-supported geosynthetic-reinforced embankments", 37, 2943-2960

[48]    Debnath, P. and Dey, A. K. (2017). "Bearing capacity of geogrid reinforced sand over encased stone columns in soft clay". *Geotextiles and Geomembranes*, 45(6), 653–664.

[49]    Desai, C. and Siriwardane, H.J. (1984). "Constitutive laws for engineering materials", Prentice-Hall: Upper Saddle River, NJ, USA,

[50]    Dhane, G., Kumar, D. and Priyadarshee, A. (2015). "Geocell: An emerging technique of soil reinforcement in civil engineering field", *IOSR Journal of Mechanical and Civil Engineering*, 59-63.

[51]    Duncan, J. M. and Chang, C. Y. (1970). "Non-linear analysis of stress and strain in soils". *Journal of Soil Mechanics and Foundation Division*, 96, 1629–1653.

[52]    Emersleben, A. and Meyer, N. (2008). "Bearing capacity improvement of gravel base layers in road constructions using geocell". *IACMAG 1–6 October*, Goa, India

[53]    Emersleben, A. and Meyer, N. (2011). "Use of geocell reinforced load transfer platforms over vertical columns". *In Geotechnical Special Publication*, 3255–3265.

[54]    Fattah, M. Y., Zabar, B. S. and Hassan, H. A. (2015). "Soil arching analysis in embankments on soft clays reinforced by stone columns". *Structural Engineering and Mechanics*, 56(4), 507–534.

[55]    Fattah, M. Y., Zabar, B. S. and Hassan, H. A. (2016). "Experimental analysis of embankment on ordinary and encased stone columns". *International Journal of Geomechanics*, 16 (4), 04015102.

[56]    Giroud, J. P. and Cazzuffi, D. A. (1989). "Uses of geosynthetics for environmental control". *Proceedings of 12th international conference on soil mechanics and foundation engineering*, vol 4. Rio de Janeiro, Brazil, pp 3119–3125.

[57]    Gniel, J. and Bouazza, A. (2009). "Improvement of soft soils using geogrid encased stone columns". *Geotextiles and Geomembranes*, 27(3), 167–175.

[58]    Greenwood, D. A. (1970). "Mechanical improvement of soils below ground surfaces". *Proceedings of Conference on Ground Engineering, Institute of Civil Engineers*, London, pp. 11–22.

[59]    Greenwood, D. A. and Kirsch, K. (1983). "Specialist ground treatment by vibratory and dynamics methods". *In: Proceedings, international conference on piling and ground treatment*, Thomas Telford, London, 17–45.

[60]    Guido, V. A., Knueppel, J. D. and Sweeny, M. A. (1987). "Plate loading tests on geogrid-reinforced earth slabs". *Proceedings of geosynthetic conference*, New Orleans, pp 216–225.

[61]    Gupta, P. and Somnath, B. (1994). "Bearing capacity improvement using geogrids". *Journal of Civil Engineering and Construction*, 7, 12–13.

[62]    Hamidi, M. and Lajevardi, S. H. (2018). "Experimental study on the load-carrying capacity of single stone columns". *International Journal of Geosynthetics and Ground Engineering,* 4, 26.

[63]    Han, J. and Gabr, M. (2002). "Numerical analysis of geosynthetic-reinforced and pile-supported earth platforms over soft soil". *Journal of Geotechnical and Geoenvironmental Engineering*, 128(1), 44–53.

[64]    Han, J., Yang, X., Leshchinsky, D. and Parsons, R. (2008). "Behavior of geocell-reinforced sand under a vertical load". *Transportation Research Record: Journal of the Transportation Research Board*, 2045, 95–101.

[65]    Hegde, A. and Sitharam, T. G. (2013). "Experimental and numerical studies on footings supported on geocell reinforced sand and clay beds". *International Journal of Geotechnical Engineering*, 7(4), 346–354.

[66]     Hegde, A. and Sitharam, T. G. (2015a). "3-Dimensional numerical modelling of geocell reinforced sand beds". *Geotextiles and Geomembranes*, 43(2), 171–181.

[67]     Hegde, A. and Sitharam, T. G. (2015b). "3-Dimensional numerical analysis of geocell reinforced soft clay beds by considering the actual geometry of geocell pockets". *Canadian Geotechnical Journal*, 52(9), 1396–1407.

[68]     Hegde, A. and T. G. Sitharam. (2015c). "Effect of infill materials on the performance of geocell reinforced soft clay beds". *Geomechanics and Geoengineering*, 10 (3), 163–173.

[69]     Hegde, A. and Sitharam, T. G. (2017). "Experiment and 3D-numerical studies on soft clay bed reinforced with different types of cellular confinement systems". *Transporation Geotechnics*, 10, 73–84.

[70]     Hendricker, A.T., Fredianelli, K.H., Kavazanjiam, E. and McKelvey, J. A. (1998). "Reinforcement requirements at a hazardous waste site". *Proceedings of the 6th international conference on geosynthetics*, Atlanta. pp 465–468.

[71]     Henkel, D. J. and Gilbert, G.D. (1952). "The effect of the rubber membrane on the measured triaxial compression strength of clay samples". *Geotechnique,* 3(1), 20–29.

[72]     Hewlett, W. J. and Randolph, M. F. (1988). "Analysis of piled embankments". *Ground Engineering*, 21(3), 12–18.

[73]     Hughes, J. M. O. and Withers, N. J. (1975). "Reinforcing of soft cohesive soils with stone columns". *Ground Engineering*, 42–49.

[74]     IGS (2018). Guide to the specification of geosynthetics

[75]     Indraratna, B., Balasubramanlam, A. S., and Balachandran, S. (1992). "Performance of test embankment constructed to failure on soft marine clay." *Journal of Geotechnical Engineering*, 118(1), 12–33.

[76]     Indraratna, B., Khabbaz, H., Salim, W. and Christie, D. (2006). "Geotechnical properties of ballast and the role of geosynthetics in rail track stabilization". *Ground Improvement*, 10(3), 91–101.

[77]     Indraratna, B., Nimbalkar, S. and Neville, T. (2013). "Performance assessment of reinforced ballasted rail track". *Ground Improvement,* 167, 24–34.

[78] Indraratna, B., Biabani, M. M. and Nimbalkar, S. (2015). "Behaviour of geocell-reinforced subballast subjected to cyclic loading in plane-strain condition". *Journal of Geotechnical and Geoenvironmental Engineering,* 141(1):04014081.

[79] IS: 15284-2003 Indian standard code of practice for design and construction for ground improvement-guidelines. Part 1: Stone columns, India

[80] Jenner, C.G., Bush, D.I. and Bassett, R.H. (1988). "The use of slip line fields to assess the improvement in bearing capacity in bearing capacity of soft ground given by a cellular foundation mattress installed at the base of an embankment". *Proceedings of International Geotechnical System*, Balkema, Rotterdam, Netherlands. pp 209–214.

[81] Johnson, J. E. (1982). "Bridge and Tidal Waters. Municipal Engineer", 109:104-107.

[82] Johnson, M. W. and McLay, R. W. (1968). "Convergence of the finite element method in the theory of elasticity". *Journal of Applied Mechanics*, 35(2), 274–278. doi:10.1115/1.3601191

[83] Jones, C. J. F. P. (1996). "Earth reinforcement and soil structures". *Thomas Telford Publication, London.*

[84] Jones, C. J. F. P., Lawson, C. R. and Ayres, D. J. (1990). "Geotextile reinforced piled embankments". *In: Hoedt D (ed) Geotextiles, geomembranes and related products*. Balkema, Rotterdam, pp 155–160

[85] Keykhosropur, L. and Imam, R. (2012). "3D numerical analyses of geosynthetic encased stone columns". *Geotextiles and Geomembranes*, 35, 61–68.

[86] Khabbazian, M., Kaliakin, V. N. and Meehan, C. L. (2010). "Numerical study of the effect of geosynthetic encasement on the behaviour of granular columns". *Geosynthetics International*, 17(3), 132–143.

[87] Koerner, R. M. (1990). "Preservation of the environment via geosynthetic containment systems". *Proceedings of 4th international conference on geosynthetics*, The Hague, 3, 975–988.

[88] Koerner, R. M. (1998). "Designing with geosynthetics". Prentice Hall, New Jersey.

[89]    Latha, G. M. (2000). "Investigations on the behaviour of geocell supported embankments". Ph.D Thesis, Indian Institute of Technology Madras, Chennai, India

[90]    Latha, G. M. (2011). "Design of geocell reinforcement for supporting embankments on soft ground". *Geomechanics and Engineering*, 3(2), 117–130.

[91]    Latha, G. M., Dash, S. K. and Rajagopal, K. (2008) "Equivalent continuum simulations of geocell reinforced sand beds supporting strip footings". *Geotechnical and Geological Engineering*, 26, 387–398.

[92]    Latha, G. M., Dash, S. K. and Rajagopal, K. (2009). "Numerical simulation of the behavior of geocell reinforced sand foundations". *International Journal of Geomechanics*, 9(4), 143–152.

[93]    Latha, G. M. and Manju, G. S. (2016). "Seismic response of geocell retaining walls through shaking table tests". *International Journal of Geosynthetics and Ground Engineering*, 2, 7.

[94]    Latha, G. M. and Rajagopal, K. (2007). "Parametric finite element analyses of geocell-supported embankments". *Canadian Geotechnical Journal*, 44(8), 917–927.

[95]    Latha, G.M., Rajagopal, K. and Krishnaswamy, N. R. (2006). "Experimental and theoretical investigations on geocell supported embankments". *International Journal of Geomechanics*, 6(1), 30–35.

[96]    Latha, G. M. and Somwanshi, A. (2009). "Effect of reinforcement form on the bearing capacity of square footing on sand". *Geotextiles and Geomembranes,* 27, 409–422.

[97]    Lawson, C.R. (2012). "Role of modeling in the development of design methods for basal reinforced piled embankments". *Proceedings of Euro Fuge 2012*, Delft, Netherland.

[98]    Lekshmi, S., Prabhu, S. S., Ramesh, P. and Babu, G. L. S. (2016). "Behavior of geocell-reinforced granular base under repeated loading". *Transportation Geotechnics*, 9, 17–30.

[99]    Leshchinsky, B. and Ling, H. I. (2012). "Numerical modelling of behaviour of railway ballasted structure with geocell confinement". *Geotextiles and Geomembranes*, 36, 33–43.

[100] Ling, H. I., Leshchinsky, D., Wang, J. P., Mohri, Y. and Rosen, A. (2009). "Seismic response of geocell retaining walls: experimental studies". *Journal of Geotechnical and Geoenvironmental Engineering, ASCE,* 135, 515–552.

[101] Liu, H. L., Ng, C. W. W. and Fei, K. (2007). "Performance of a geogrid-reinforced and pile-supported highway embankment over soft clay: Case study." *Journal of Geotechnical and Geoenvironmental engineering*, 133 (12), 1483–1493.

[102] Lo, S. R., Zhang, R. and Mak, J. (2010). "Geosynthetic-encased stone columns in soft clay: A numerical study". *Geotextiles and Geomembranes*, 28(3), 292–302.

[103] Low, B. K., Tang, S. K. and Choa, V. (1994). "Arching in piled embankments". *Electronic Journal of Geotechnical Engineering*, 120(11), 1917–1938.

[104] Malarvizhi, S.N. and Ilamparuthi, K. (2004). "Load versus settlement of clay bed stabilized with stone and reinforced stone columns", *Proceedings of the 3rd Asian Regional Conference on Geosynthetics*, GEOASIA, Seoul, Korea, 322-329.

[105] Malarvizhi, S.N. and Ilamparuthi, K. (2008) "Behaviour of geogrid encased stone column and stone column stabilized soft clay bed". *Physical Modelling in Geotechnics,* 1489-1494.

[106] Mandal, J.N. and Gupta, P. (1994). "Stability of geocell reinforced soil". *Construction and Building Materials*, 8, 55-62.

[107] Marston, A. and Anderson, A. O. (1913). "The theory of loads on pipes in ditches and tests of cement and clay drain tile and sewer pipe". Bulletin No.3, Iowa State University Engineering Experiment Station, Ames, Iowa.

[108] Mazumder, T., Rolaniya, A. K. and Ayothiraman, R. (2018). "Experimental study on behaviour of encased stone column with tyre chips as aggregates". *Geosynthetics International*, 25 (3), 259–270.

[109] Mc Kelvey, D., Sivakumar, V., Bell, A. and Graham, J. (2004). "Modelling vibrated stone columns in soft clay". *In: Proceedings of the institute of civil engineers geotechnical engineering*, Vol. 157, Issue GE3, pp 137–149.

[110] McNulty, J. W. (1965). "An Experimental study of arching in sand". Rep. No. I-674, U.S. Army Engineer Waterways Experiment Station, Corps of Engineers,

Vicksburg, Miss., 170.

[111] Mehdipour, I., Ghazavi, M. and Moayed, R. Z. (2013). "Numerical study on stability analysis of geocell reinforced slopes by considering the bending effect". *Geotextiles and Geomembranes*, 37: 23–34.

[112] Mehmet, R. K. (2017). "Settlement Behavior of Reinforced Embankments Supported by Encased Columns". *International Journal of New Technology and Research*, 3(4), 22-25.

[113] Melosh, R. J. (1961). "A stiffness matrix for the analysis of thin plates in bending", *Journal of the Aerospace Sciences*, 28(1), 34–42. doi:10.2514/8.8850

[114] Mhaiskar, S. Y. and Mandal, J. N. (1996). "Investigations on soft clay subgrade strengthening using geocells". *Construction and Building Materials*, 10(4), 281–286.

[115] Mitchell, J. K. (1981). "Soil improvement—state of the art report". *Proceeding in 10th International Conference on Soil Mechanics and Foundation Engineering,* 4, 509–565

[116] Mitchell, J. K. and Huber, T. R. (1985). "Performance of a stone column foundation". *Journal of Geotechnical Engineering*, 111(2), 205–223.

[117] Mitchell, J. K., Kao, T. C. and Kavazanijiam, E. (1979). "Analysis of grid cell reinforced pavement bases". Technical report GL-79-8, U.S. Army waterways experiment station, Vicksburg.

[118] Momade, Z. and Gawu, S.K.Y. (2009). "Geochemical and mineralogical characteristics of lithomargic clay types from awaso bauxite deposit, Ghana: Implications for possible industrial utilization". *Journal of Science and Technology*, 29 (2), 96-106.

[119] Murugesan, S. and Rajagopal, K. (2007). "Model tests on geosynthetic-encased stone columns". *Geosynthetics International*, 14(6), 346–354.

[120] Murugesan, S. and Rajagopal, K. (2009). "Studies on the behavior of single and group of geosynthetic encased stone columns." *Journal of Geotechnical and Geoenvironmental Engineering*, 136(1),129-139.

[121] Nayak, S., Dheerendra Babu, M. R., Shivashankar, R., and James, N. (2014) "Performance of granular columns in dispersive soils". *Proceedings of the Institution of Civil Engineers - Geotechnical Engineering,* 167(1), 72–82.

[122] Nayak, S., and Sarvade, P. G. (2012). "Effect of Cement and Quarry Dust on Shear Strength and Hydraulic Characteristics of Lithomargic Clay". *Geotechnical and Geological Engineering,* 30(2), 419–430.

[123] Nassaji, F. and Asakereh, A. (2013). "Effect of granular bed on behaviour of stone column improved ground". *International Journal of Science and Engineering Invest*igation, 2(23), 67–71.

[124] Ng, K.S and Tan, S.A. (2015) "Stress Transfer Mechanism in 2D and 3D Unit Cell Models for Stone Column Improved Ground". *International Journal of Geosynthetics and Ground Engineering*, 1(1).

[125] Pancar, E.B. (2016). "Geosynthetic reinforcement of pavement subgrade with optimum and high-water content". *International Journal of Engineering Trends and Technology,* 38 (1).

[126] Pokharel, S. K., Han, J., Leshchinsky, D., Parsons, R. L. and Halahmi, I. (2010). "Investigation of factors influencing behavior of single geocell-reinforced bases under static loading". *Geotextiles and Geomembranes*, 28(6), 570–578.

[127] Pokharel, S. K., Martin, I., Norouzi, M. and Breault, M. (2015). "Validation of geocell design for unpaved roads". *Proceedings of Geosynthetics*, 15–18 February 2015, Portland, Oregon

[128] Potts, V. J. and Zdravković, L. (2008). "Finite Element Analysis of Arching Behaviour in Soils". *The 12th International Conference of International Association for Computer Methods and Advances in Geomechanics (IACMAG)*, 3642-3649.

[129] Rai, M. (2010). "Geocell-sand mattress overlying soft clay subgrade: Behaviour under circular loading". *PhD thesis,* IIT Guwahati, India

[130] Raithel, M. and Kempfert H.G. (2000). "Calculation models for dam foundations with geosynthetic coated sand columns", *Proceedings of International Conference on Geotechnical & Geological Engineering. GeoEng*, Melbourne, 347-352.

[131] Rajagopal, K., Krishnaswamy, N. R. and Latha, G. M. (1999). "Behaviour of sand confined with single and multiple geocells". *Geotextiles and Geomembranes*, 17,171–184.

[132] Rajagopal, K., Krishnaswamy, N. R. and Latha, G. M. (2001). "Finite element analysis of embankments supported on geocell layer using composite model". *Proceedings of 10$^{th}$ international conference on computer methods and advances in geomechanics*, Arizona, USA

[133] Rajagopal, K., Chandramouli, S., Parayil, A. and Iniyan, K. (2014). "Studies on geosynthetic reinforced road pavement structures". *International Journal of Geotechnical Engineering*, 8(3), 287–298.

[134] Ramesh, H. and Nanda, H. S. (2007). "Strength behaviour of shedi soil treated with fly ashes". *13th ARC*, Kolkata, pp 893-896.

[135] Ramesh, H., Nanda, H. S. and Manoj, K. (2011). "Effect of soaking on the strength behaviour of shedi soil treated with NFA". *Proceedings of Indian Geotechnical Conference, December 15-17.*

[136] Rawat, A., Rakesh, R. R. and Mandal, J. N. (2010). "Effect of glassgrid geocell inclusion on flexural behavior of cover soil for low level radioactive waste disposal facility", *6$^{th}$ International Congress on Environmental Geotechnics*, New Delhi, India.

[137] Rea, C. and Mitchell, J.K. (1978). "Sand reinforcement using paper grid cells". Reprint 3130, *ASCE spring convention and exhibit*, 24-28.

[138] Roscoe, K.H. and Burland, J.B. (1968). "On the generalised stress–strain behaviour of wet clay". *J. Heyman F.A. Leckie (Eds) Engineering Plasticity*, Cambridge Univ. Press Cambridge 535–609

[139] Rowe, R. K. (1998). "Geosynthetics and the minimization of contaminant migration through barrier systems beneath solid waste". *Proceedings 6th International Conference on Geosynthetics*, Atlanta 1: 27-102.

[140] Rowe, R. K. and Soderman, K. L. (1985). "Geotextile reinforcement of embankments on peat". *Geotextiles and Geomembranes,* 2(4), 277–298.

[141] Russell, G., Guney, O., Robert, E. and Wanda, C. (2003). "Seismically induced lateral earth pressures on a cantilever retaining wall". Technical Council on Life line Earthquake Engineering Monograph. 946-955.

[142] Russell, D. and Pierpoint, N. (1997). "An assessment of design methods for piled embankments." *Ground Engineering*, 30(10), 39–44.

[143] Sanjei, C. and De Silva, L.I.N. (2016). "Numerical modelling of the behaviour of model shallow foundations on geocell reinforced sand". *Moratuwa Engineering Research Conferance (MERCon)*, Moratuwa-Sri Lanka, 5- 6 April 2016, 216-222.

[144] Selçuk, L and Kayabali, K. (2015). "The design of stone column applications to protect against soil liquefaction". *International Journal of Geotechnical Engineering*, 9(3), 279 288.

[145] Shahu, J. T., Hayashi, S. and Madhav, M. R. (2000). "Analysis of soft ground reinforced by non-homogeneous granular pile-mat system". *Lowland Technology*, 2(2), 71-82.

[146] Shankar, A. U. and Suresha, S.N. (2006). "Strength behaviour of geogrid reinforced shedi soil subgrade and aggregate system". *Road Materials and Pavement Design,* 7(3), 313–330.

[147] Shankar, A. U., Chandrashekhar, A. and Prakash, B. H. (2012). "Experimental investigation on lithomargic clay stabilized with sand and coir". *In: Indian Highways, Indian Roads Congress*, 40, 21-31.

[148] Simac, M.R. (1990). "Connection for Geogrid system". *Geotextiles and Geomembrane,* 27, 89-98.

[149] Sireesh, S., Sitharam, T. G. and Dash, S. K. (2009). "Bearing capacity of circular footing on geocell-sand mattress overlying clay bed with void". *Geotextiles and Geomembranes*, 27(2), 89–98.

[150] Sireesh, S., Sailesh, P., Sitharam, T. G. and Puppala, A. J. (2013). "Numerical analysis of geocell reinforced ballast overlying soft clay subgrades". *Geomechanics and Eng*ineering 5(3), 263–281.

[151] Sitharam, T. G. and Hegde, A. (2013). "Design and construction of geocell foundation to support the embankment on settled red mud". *Geotextiles and Geomembranes*, 41, 55–63.

[152] Sitharam, T. G. and Sireesh, S. (2004). "Model studies of embedded circular footing on geogrid reinforced sand beds". *Ground Improvement,* 8(2), 69–75.

[153] Sitharam, T. G. and Sireesh, S. (2005). "Behaviour of embedded footings supported on geocell reinforced foundation beds". *Geotechnical Testing Journal ASTM,* 28 (5), 452– 463.

[154] Sitharam, T. G. and Sireesh, S. (2006). "Effects of base geogrid on geocell-reinforced foundation beds". *International journal of Geomechanics and Geoengineering*, 1(3), 207–216.

[155] Sitharam, T. G., Sireesh, S. and Dash, S. K. (2007). "Performance of surface footing on geocell-reinforced soft clay beds". *Geotechnical and Geological Engineering,* 25(5), 509–524.

[156] Skempton, A.W. and Bjerrum, L. (1957). "A Contribution to the Settlement Analysis of Foundations on Clay". *Géotechnique*, 7, 168-178.

[157] Song, F., Liu, H., Yang, B. and Zhao, J. (2019). "Large-scale triaxial compression tests of geocell-reinforced sand". *Geosynthetics International,* 1, 29.

[158] SP 36 (Part 1) – 1987 of the Indian Standard (IS)

[159] Soude, M., Chevalier, B., Grediac, M., Talon, A. and Gourves, R. (2013). "Experimental and numerical investigation of the response of geocell reinforced walls to horizontal localized impact". *Geotextiles and Geomembranes,* 39, 39-50.

[160] Tafreshi, S. N. M. and Dawson, A. R. (2010). "Comparison of bearing capacity of a strip footing on sand with geocell and with planar forms of geotextile reinforcement". *Geotextiles and Geomembranes,* 28(1), 72–84.

[161] Tafreshi, S. N. M., Khalaj, O. and Dawson, A. R. (2013). "Pilot-scale load tests of a combined multilayered geocell and rubber-reinforced foundation". *Geosynthetics International,* 20(3), 143–161.

[162] Tafreshi, S. N. M., Khalaj, O., Dawson, A. R. and Masek, B. (2015) "Repeated load response of soil reinforced by two layers of geocell". *Procedia Earth and Planetary Science*, 15, 99-104.

[163] Tang, X., and Yang, M. (2013). "Investigation of flexural behavior of geocell reinforcement using three-layered beam model testing." *Geotechnical and Geological Engineering,* 31(2), 753–765.

[164] Terzaghi, K. (1925). "Principles of soil mechanics: I—Phenomena of cohesion of clays," Engineering News-Record, Vol. 95, No. 19, pp. 742-746.

[165] Terzaghi, K. (1943). "Theoretical soil mechanics". Wiley, New York.

[166] Thakur, J. K. and Han, J. (2012). "Performance of geocell- reinforced recycled asphalt pavement (RAP) bases over weak subgrade under cyclic plate loading". *Geotextiles and Geomembranes,* 35, 14-24.

[167] Thomas, B. C., Shivashankar, R., Jacob, S., and Varghese, M. S. (2019). "Erosion studies on lithomargic clays". *Indian Geotechnical Journal.* doi:10.1007/s40098-019-00364-8.

[168] Ti, K. S., Gue See, S., Huat, B. B., Noorzaei, J. and Saleh, M. (2009). "A review of basic soil constitutive models for geotechnical application". *Electronic Journal of Geotechnical Engineering*,14,18.

[169] Van Eekelen, S. J. M., Bezuijen, A. and Van Tol, A. F. (2011). "Analysis and modification of the British Standard BS8006 for the design of piled embankments". *Geotextiles and Geomembranes,* 29, 345–359.

[170] Van Impe, W.Y. (1985) Soil improvement techniques and their evolution. Balkema, Rotterdam

[171] Vermeer, P. A. and Verruijt, A. (1981). "An accuracy condition for consolidation by finite elements". *International Journal for Numerical and Analytical Methods in Geomechanics*, 5(1), 1–14.

[172] Vidal, H. (1969). "The principle of reinforced earth". Highway Research Record, 282, Washington DC.

[173] Webster, S. L. and Watkins, J. E. (1977). "Investigation of construction techniques for tactical bridge approach roads across soft ground". Technical Report S-77-1, U.S. Army Engineer Waterways Experiment Station, Vicksburg, MS

[174] Webster, S. L. (1979). "Investigation of beach sand traffic ability enhancement using sand-grid confinement and membrane reinforcement concepts. Technical Report GL- 79-20. US Army Corps of Engineers, Vicksburg, MS

[175] Wijerathna, M. and Liyanapathirana, D. S. (2020). "Load transfer mechanism in geosynthetic reinforced column-supported embankments". *Geosynthetics International*, 27(3), 236-248.

[176] Yadav, M., Agnihotri, A.K., Priyadarshee, A. and Dhane, G. (2014). "Application of geocells in reinforcement of soil: A review". *Journal of Civil Engineering and Environment Technology*, 60 – 64.

[177] Yang, X., Han, J., Parsons, R. L. and Leshchinsky, D. (2010). "Three-dimensional numerical modeling of single geocell-reinforced sand". *Frontiers of Architecture and Civil Engineering in China*, 4(2), 233–240.

[178] Yoo, C. and Kim, S.B. (2009). "Numerical modeling of geosynthetic encased stone column-reinforced ground". *Geosynthetics International*, 16(3), 116–126.

[179] Yoo, C. (2010). "Performance of geosynthetic-encased stone columns in embankment construction: numerical investigation". *Journal of Geotechnical and Geoenvironmental Engineering*, 136(8), 1148–1160.

[180] Zhang, L. and Zhao, M. (2014). "Deformation Analysis of Geotextile-Encased Stone Columns". *International Journal of Geomechanics*, 1532-3641/04014053(10).

[181] Zhang, L., Zhao, M., Shi, C. and Zhao, H. (2010). "Bearing capacity of geocell reinforcement in embankment engineering". *Geotextiles and Geomembranes*, 28 (5), 475–482.

[182] Zhao, L. and Karim, M. A. (2018). "Use of Geosynthetic materials in solid waste landfill design: A review of geosynthetic related stability issues". *Annals of Civil and Environmental Engineering*, DOI: 10.29328/journal.acee.1001010.

[183] Zhao, M.H., Zhang, L., Zou, X. J. and Zhao, H. (2009). "Research progress in two direction composite foundation formed by geocell reinforced mattress and gravel piles". *Chinese Journal of Highway Transportation*, 22 (1), 1–10.

[184] Zheng, B. G., Chen, Y.E., Lu, S.W., Abusharar and Yin, J. H. (2009) "The performance of an embankment on soft ground reinforced with geosynthetics and pile walls". *Geosynthetics International,* 16(3), 173-182.

[185] Zhou, H. and Wen, X. (2008). Model studies on geogrid- or geocell-reinforced sand cushion on soft soil. *Geotextiles and Geomembranes*, 26(3), 231–238.

[186] Zornberg, J.G. and Christopher, B.R. (1999). "Geosynthetics. Chapter 27", *The Handbook of Groundwater Engineering*, Jacques W. Delleur (Editor-in-Chief), CRC Press, Inc., Boca Raton, Florida.

# PUBLICATIONS

## INTERNATIONAL JOURNALS

1. Nayak, S., Vibhoosha, M. P. and Bhasi, A. (2019). "Effect of column configuration on the performance of encased stone columns with basal geogrid installed in lithomargic clay". *International Journal of Geosynthetics and Ground Engineering*, 5(4), 1-19. DOI: 10.1007/s40891-019-0181-y

2. Vibhoosha, M. P., Bhasi. A. and Nayak. S. (2021). "Analysis of geocell-reinforced stone column-supported embankment considering soil-structure interaction". *Transportation Infrastructure Geotechnology*. DOI: 10.1007/s40515-021-00158-7

3. Vibhoosha, M. P., Bhasi. A. and Nayak. S. (2021). "A Review on the Design, Applications and Numerical Modeling of Geocell Reinforced Soil". *Geotechnical and Geological Engineering,* 1-23. DOI: 10.1007/s10706-021-01774-3

4. Vibhoosha, M. P., Anjana Bhasi., Sitaram Nayak. "3D Modeling of Geocell-Reinforced Encased Stone Column- Supported Embankments Incorporating Soil-Geocell Interactions". Geomechanics and Geoengineering: An International Journal (Under Review-(TGEO-2021-0093) )

## BOOK CHAPTERS

1. Vibhoosha. M. P., Bhasi A. and Nayak S. (2020). "Effect of geosynthetic stiffness on the behaviour of encased stone columns installed in lithomargic clay". *Advances in Computer Methods and Geomechanics,* Springer, DOI: 10.1007/978-981-15-0886-8

2. Vibhoosha. M. P., Bhasi A. and Nayak S. (2020). "Effect of column configuration on the behaviour of stone column supported ground". *Green Buildings and Sustainable Engineering*. Springer Transactions in Civil and Environmental Engineering. Springer, DOI: 10.1007/978-981-15-1063-2

## INTERNATIONAL CONFERENCES

1. Vibhoosha, M.P. and Anjana Bhasi (2017). "Settlement behaviour of embankments supported by columnar structures". *Proceedings of 4th International Conference on Modeling and Simulation in Civil Engineering,* TKM College of Engineering, Kollam.

2. Vibhoosha, M.P., Anjana Bhasi and Sitaram Nayak (2019). "Effect of column configuration on the behaviour of stone column supported ground". *Proceedings of International conference on Green Buildings and Sustainable Engineering (GBSE 2019),* Rajagiri School of Engineering & Technology Rajagiri Valley, Kakkanad.

3. Vibhoosha, M.P., Anjana Bhasi and Sitaram Nayak (2019). "Effect of geosynthetic stiffness on the behaviour of encased stone columns installed in lithomargic clay". *Proceedings of International Symposium of International Association for Computer Methods and Advances in Geomechanics,* Indian Institute of Technology Gandhinagar.

4. Vibhoosha, M.P. and Anjana Bhasi (2019). "Analysis of geocell reinforced stone column supported embankments considering 3d structure of geocell". *Symposium on Recent Advances in Sustainable Geotechnics IGS Kanpur Chapter.* 17-20 October 2019, IIT Kanpur, India

5. Vibhoosha, M.P. and Anjana Bhasi (2020). "Three dimensional modeling of Geocell using membrane elements by considering the actual curvature". *International Conference on Computational Sciences- Modeling, Computing and Soft computing (CSMCS 2020),* 10-12 September 2020, NIT Calicut. *AIP Conference Proceedings,* 2336 (1), 050009. DOI: 10.1063/5.0045934

# CURRICULUM VITAE

1. NAME                 : VIBHOOSHA. M. P.

2. DATE OF BIRTH    : 10 May 1990

3. EDUCATIONAL QUALIFICATIONS

| | |
|---|---|
| Degree | : Bachelor of Technology (B.Tech) |
| Specialization | : Civil Engineering |
| Institute | : Government College of Engineering, Kannur, Kerala |
| Year | : 2011 |

| | |
|---|---|
| Degree | : Master of Engineering Technology (M. Tech) |
| Specialization | : Environmental Geotechnology |
| Institute | : National Institute of Technology Calicut (NITC) |
| Year | : 2014 |

| | |
|---|---|
| Degree | : Doctor of Philosophy (Ph. D) |
| Specialization | : Geotechnical Engineering |
| Institute | : National Institute of Technology Karnataka, Surathkal, India |

4. CONTACT          : Mobile: +91 9495475119
                            Email: vibhoosha@gmail.com

5. WORK EXPERIENCE

- Worked as Project Associate at IIT Madras in the NIOT project 'Studies on Geosynthetics' for seven months (Dec-2011 to July-2012).

- Worked as an Assistant Professor at CET Payyannur, Kerala, for four months (Jun to Nov 2014).

- Worked as a Design Engineer in UR Ground Engineering Pvt Ltd, Chennai (Nov-2014 to March- 2016).